DEVELOPMENT AND IMPLEMENTATION OF CONFIGURATIONAL FORCES BASED CONSTITUTIVE PHASE FIELD MODELS FOR SHAPE MEMORY ALLOYS

A Dissertation

by

BABATUNDE OMOGBOLAHAN AGBOOLA

Submitted to the Office of Graduate and Professional Studies of
Texas A&M University
in partial fulfillment of the requirements for the degree of

DOCTOR OF PHILOSOPHY

Chair of Committee,	Dimitris.C. Lagoudas
Committee Members,	Jay. R. Walton
	Junuthula.N. Reddy
	Amine A. Benzerga
	Raymundo Arroyave
Head of Department,	Rodney Bowersox

August 2015

Major Subject: Aerospace Engineering

ABSTRACT

Continuum thermodynamic constitutive phase field models are developed to simulate the rate dependent, thermomechanical response and precipitate formation in shape memory alloys (SMAs). The two models are based on the application of the balance of configurational forces, a scalar order parameter (a phase field) and atomic concentration to extend standard continuum thermodynamics approach. Constitutive field equations that capture the kinetics of solid-solid martensitic phase transition in SMA and the diffusion mediated precipitate formation in an elastic solid are developed. The coupled set of thermodynamically consistent field equations results from balance of configuration forces, balance of linear momentum, balance of energy and balance of atomic species mass. The field equations capture the kinetics of phase transition, deformation and elastic wave, heat transfer and atomic diffusion respectively. The first model is thermomechanical and is used to simulate the macroscopic response of SMA such as pseudoelasticity; transformation induced pseudo-creep, stress relaxation as well as the effect of cooling rate on mechanical and thermally induced phase transformation of SMA. The second model couples diffusion with elasticity to simulate growth and coarsening of precipitate and experimentally observed concentration depletion near the precipitates Results of the simulations of the macroscopic SMA response are in very good agreement with experimental observation. Simulations suggest that rate dependent and complex thermomechanical response of SMA are due to the interaction of an inherent time scale (as well as length scale) of phase transformation, introduced through the balance of configurational forces, with other time scales. This work contributes to improved SMA

modeling, scientific understanding and design. In particular, for aerospace application under stringent requirement and severe environmental conditions. Contribution of fundamental use of balance of configurational forces to extend continuum thermodynamic modeling is demonstrated.

DEDICATION

Humbly dedicated to the only begotten Son of God-Jesu Kristi ti Nasareti-who is my savior and Lord (olugbala ati Oluwa mi) and to the closest people he has brought into my life for divine stewardship in His infinite mercy-my wife Elizabeth Oyenike Agboola, my son Toluwani David Agboola and my daughter Ayanfeoluwa Achsah Agboola

ACKNOWLEDGEMENTS

Obtaining a PhD degree is a climax of many years of official student life until now. However, these achievements and the quality of this work will not be possible without the investment of many great people that God has brought into my life. Therefore, my first thanks goes to God and father of my Lord Jesus Christ who died to redeem me unto divine adoption as a son of God. Second, I will like to thank both my parents and my wives' parent as well as our siblings. I can not but mention the investment of my mum and dad who labored to ensure I get quality education and christian heritage. Words can not quantify how much I am grateful for your parenthood. Special thanks goes to my wife and children for their support throughout my study.

I want to thank all of my teachers from my nursery school days up till my PhD education. You are all wonderful teachers. Consequently, I will like to say thank you to Prof. Dimitris C. Lagoudas for advising my PhD Work. Dr. Benzerga's meticulous approach to teaching continuum mechanics is invaluable. In the same vein, I must say very clearly that without Prof. Jay. R. Walton's in-depth, methodical and thorough teaching of the mathematical foundation of continuum mechanics; this work will not be of the quality it is. Thank you so much Prof. Walton. I want to thank Dr. Arroyave for his contribution as a committee member for this PhD work. It is a privilege to have Prof. Reddy in any PhD committee and mine is not an exception. Everything I know in finite element is connected to his ingenuity in contributing to the development of this numerical approach. I must say a big thank you to Prof. Walter Bradley for standing by me when the going was getting tough. His recommendation and support until I was able to finish my PhD work is invaluable.

I also want to say thank you to Dr. David A. Jack for being a friend and encouragement throughout my study at TAMU after serving as my advisor for Masters degree at Baylor University.

Finally, I will like to thank all of my friends at Texas A and M University in particular Oluwafemi Oyedokun who was there to listen to my dry run whenever I had presentation. Thanks to all of my other friends at the department of Aerospace Engineering, members of Center for intelligent Multifunctional Materials and Structures (CiMMS) (formerly Texas Institute for Intelligent Materials and Structures (TiiMS)) as well as SmartLab members.

TABLE OF CONTENTS

Page

LIST OF FIGURES

FIGURE Page

LIST OF TABLES

TABLE Page

1. INTRODUCTION AND LITERATURE REVIEW

Very few materials possess such a rich combination of complexity and promise of use as shape memory alloys (SMA). A major challenge to the use of SMAs is that they are very hard to work with due to complex thermomechanical response. Therefore their use as structural and active components in the form of wires, rods, spring and in other forms have necessitated very active experimental and theoretical research in many field of engineering [1]. It has been reported that so many papers, patents and inventions have resulted from prevalent research on SMA across the globe [1]. However, there is still need for improved experimental and theoretical study of SMA to enhance their scientific understanding and industrial use. Therefore, this work is a contribution toward improved understand and use SMAs within existing industrial applications and to open insight into new ground to harness the potential of SMAs based on improved theoretically aided scientific understanding. Like any engineering materials, the relationship among processing, structure, properties and performance of SMA is what result in their macroscopic properties. SMAs undergo solid-solid reversible, thermomechanical hysteretic phase transformation, which result in their characteristic complex macroscopic response. SMAs are choice material when high work density is needed although their use if often limited due to lower actuation frequency and bandwidth.

1.1 Introduction to Shape Memory Alloys and Their Phase Transformation Behavior

Two basic type of transformation, in terms of atomic motion, is known in the material science community, these include diffusional and diffusionless transformation. Diffusional or "civilian" transformation involves long range motion of atomic species

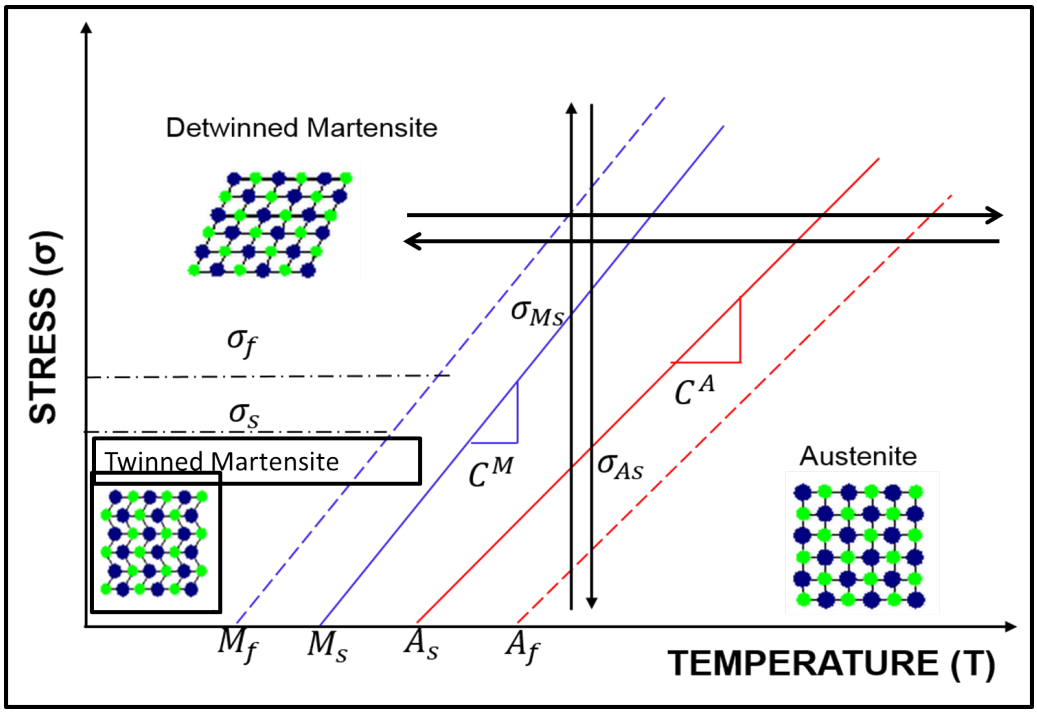

Figure 1.1: Typical phase diagram for SMA showing pseudoelastic and constant load thermally induced phase transformaion paths

relative to their initial neighboring atoms. On the other hand, diffusionless phase transformation proceeds in a manner such that atoms retain their relative position to adjacent atoms as they undergoing "military" rearrangement [2]. A review on phase transformation can be seen in Olson and Owen (1992). SMAs along with some multifunctional materials such as ferroelectric, ferromagnetic and high temperature superconducting ceramic alloys among others undergo a diffusionless phase transition. SMA can exist and co-exist in two solid states (i.e. austenite and martensite) with each phase differing in their crystal structure. Each phase is stable (or preferred) under suitable condition of stress and temperature. Austenite is the phase that is stable at high-temperature phase while martensite is the phase that is stable at low temperature. Since a particular phase is preferred under condition of stress

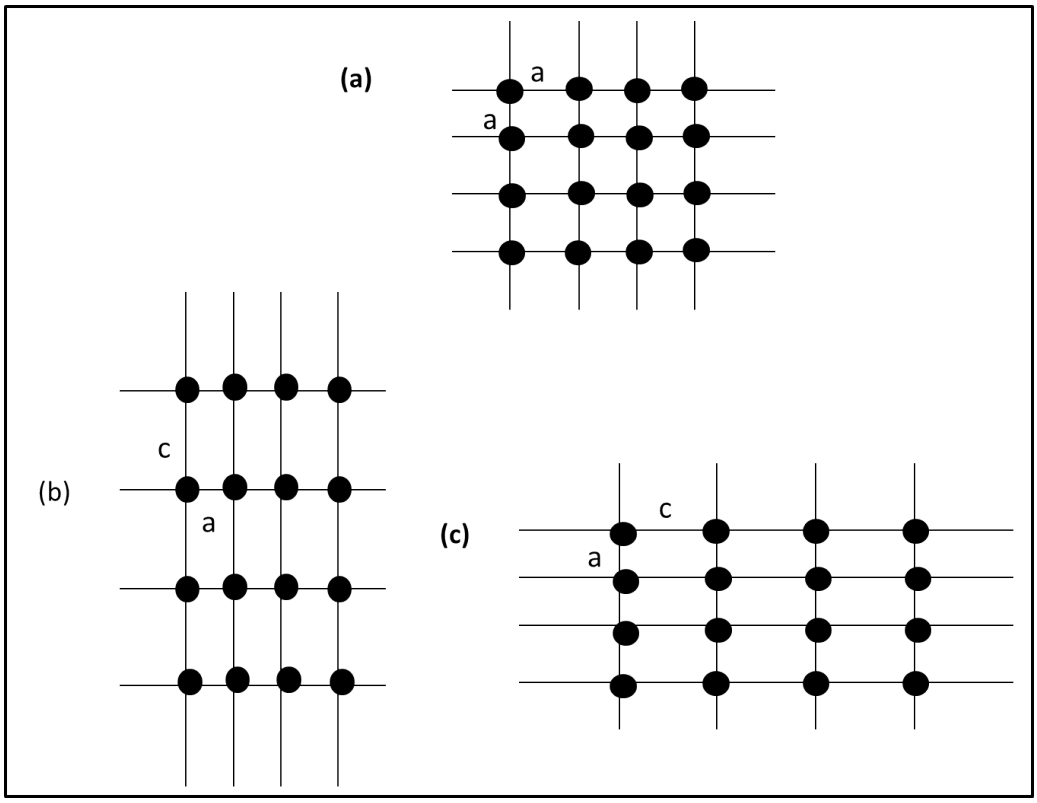

Figure 1.2: Schematic of martensitic phase transformation from high symmetry phase to lower symmetry phase

and temperature, thermodynamically, it is possible for SMA to transform between the two phases as the mechanical and thermal condition changes. The region of stability of each phase is often represented in the stress-temperature phase diagram for engineering purposes (see figure 1.1). As mentioned earlier and as the name suggests, SMA possess characteristic shape memory behavior. The shape memory observed in SMA is a manifestation of martensitic transformation. Martensitic transformation is a structural phase change that is diffusionless, displacive and discontinuous. Thermodynamically, it is a first order crystalline phase transformation. In this kind of transformation, the molecular or lattice structure of SMA changes abruptly at particular temperature. Introduction to martensitic transformation can be found in

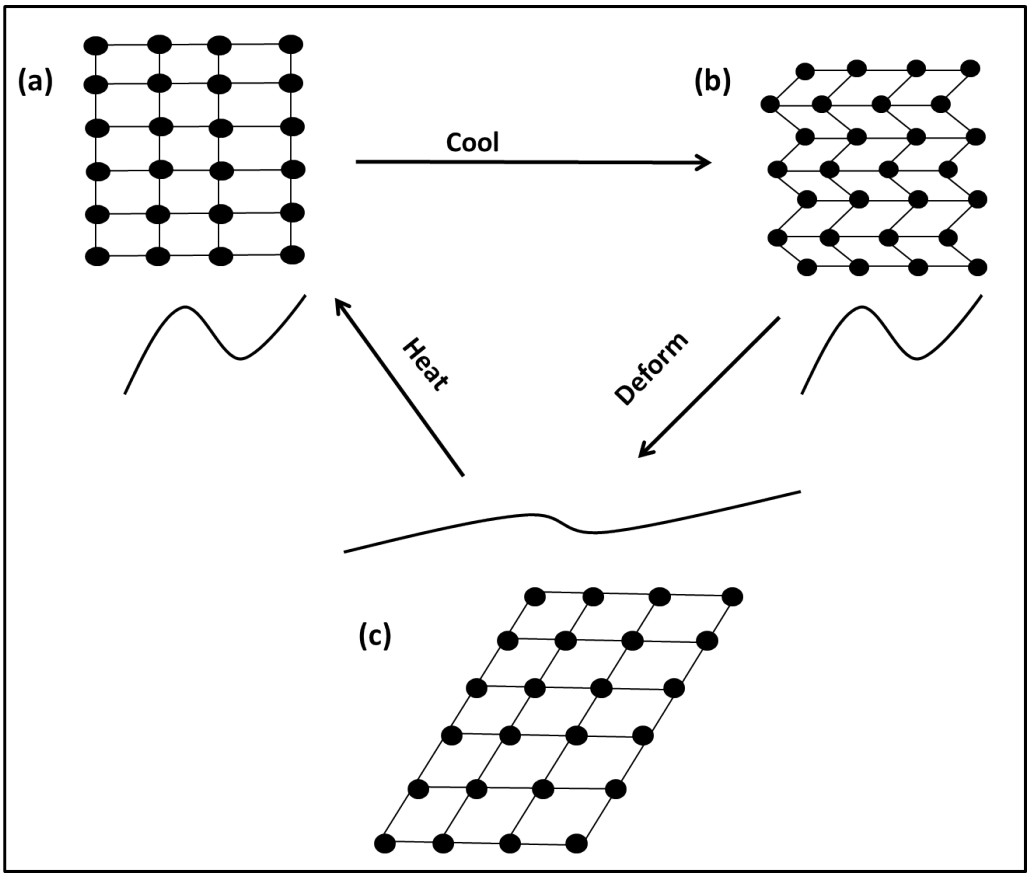

Figure 1.3: Schematic representation of microstructural change during shape memory effect (SME)

the work of Schetky,while a detailed discussion of microstructural and metallurgical description of SMA can be found in the work of Battacharya [3] and Otsuka and Wren. Martensitic transformation in SMA can be illustrated with a schematic diagram as shown in figure 1.2. Of all the different SMA compositions, NiTi SMAs have enjoyed the most wide-spread use because they are the most technologically and commercially useful SMAs. These alloys have received intense scientific attention ever since their discovery in 1963. Second to NiTi among the commercially available SMA is Cu-Zn-Al alloys which is a Cu-based shape memory alloys (SMAs) and they have been studied since 1970 by L. Delaey. Cu-Zn-Al Alloy have been

shown to exhibit some superior properties next to NiTi such as high ductility, lower cost, good resistance to inter-granular fracture and excellent electrical and thermal conductivity

To describe the behavior of typical SMA, figure 1.2a is a 2-D schematic representation of an austenite phase that is assumed to arrange in a square lattice, which at a critical temperature undergoes an abrupt change to form different variant of martensite (figure 1.2 b and c) that are arranged in rectangular lattice. This abrupt change does not involve any change in the relative position of the atoms although significant distortion of the unit cell is observed. The above representative transformation will be observed at some critical temperature (M_s) (often called martensite start) upon cooling of an SMA component. Once reheated, the SMA rectangular structure reverts back to the square lattice (austenite) structure (see figure 1.2a) at another critical temperature (called austenite start A_s), which points to the fact that martensitic transformation in SMA is crystallographically reversible and hysteretic. Martensitic transformation is again a displacive (no diffusion) and first order transformation (it involve abrupt changes in lattice parameter). When a single or polycrystalline SMA is cooled from a high temperature (where austenite is the stable phase), a particular critical temperature is reached where a portion of the lattice suddenly transform into a structure that is energetically preferred at the lower temperature (which is martensitic structure). The sudden appearance of the new phase is called nucleation in the material science literature. The small portion that is transformed begins to grow, into the other parts of the SMA that are still of the high temperature stable structure. As the new structure grows or accrete over the existing ones (other nucleation sites may still occur). It is known that as the temperature continues to decrease below this critical temperature (M_s), martensite nucleates and the interface between the two phases (which is a phase boundary) be-

gins to propagate into the existing structure that is stable at the high temperature. So, phase transformation is essentially a propagation of phase boundary of a nucleated second phase into initially stable phase. The high temperature stable phase is transformed into the low temperature stable phase (martensite) as material points cross the moving front. During heating, the entire material would have transformed at an austenite finish temperature (A_f). Similarly, during cooling the entire material would have transformed at a martensite finish temperature M_f. One thing to note, however, is that the reversible phase transformation in SMA is accompanied by hysteresis (manifested by a difference between the critical transformation temperature during heating and cooling),which may range from a few to hundreds of degrees Celsius for different SMA compositions. *The primary mechanism behind this dissipative behavior is the phase transformation itself.* The reversible solid to solid phase transformation can occur under mechanical loading and thermal stimulus. The size and other characteristic features of the hysteresis depend on the loading rates as well as the temperature at which the test takes place. Ability to model these features is important to aid the design of SMA for use in engineering applications. In terms of the microstructure, because of the difference between the high symmetry of the austenite phase and the low symmetry of the martensite, SMA transforms from austenite to martensite by forming multiple variants in difference region of a typical SMA device or components. The reason is explained by the propensity of the SMA crystal to form independent nucleation events and transform into different shapes by taking on combination of different energetically favored variants. *The transformation process explained earlier is for an idealized two-phase SMA wherein variants of martensite are indistinguishable.* The real mechanism though involves the formation of several variants of martensite when, say, an SMA wire is cooled from the austenite phase to below a critical temperature M_s. Below this temperature, different region

of the SMA transform into variants of martensite in such a way to form twins such that there is no net macroscopic change of the wire. Such an arrangement is called *"self-accommodated"* martensite as it accommodate the deformation imposed by each variants. (See figure 1.3b). Self-accommodated martensite results because of the material's propensity to maintain equilibrium by minimizing the energy of the system. Upon deformation of the detwinned martensite, the deformation imposed by an externally applied load could be accommodated by either rearranging the variants or distorting the crystal. However, based on energetic reason, the material prefers to rearrange the variants to detwinned martensite. The explanation is that it does not cost energy to rearrange variants from one to another, since each variant possess the same energy having been formed from the same parent phase. Therefore, the material can change its shape at no energy cost. On the other hand, distortion of the crystal will cost energy so the material would not prefer this mode. When the load is removed, the material retains its shape as there is no energetic reason to do otherwise since the energy of the variants are the same for both detwinned and twinned martensite. Upon heating the material to a temperature A_s all the variants transform back to austenite as this phase is energetically favored. Therefore, the shape memory characteristic of SMA is result of multiple low energy state below M_s and one low energy state above A_s.

1.2 Characteristic Macroscopic Phenomena of Engineering Significance in SMA

As noted earlier, SMA transform between two solid-state phases to produce macroscopic deformation. SMAs can recover seeming permanent strains when subjected to particular thermo-mechanical inputs. The shape recovery is driven by the reversible martensitic transformation between solid-state phases that take place in SMAs during thermal and/or mechanical loadings. The transformation results in

two remarkable macroscopic phenomena (i.e. the shape memory effects (SME) and pseudoelasticity). These properties can be harnessed using different loading path in stress-temperature space. The SME is characterized by a recovery of permanent deformation, induced by loading at a low temperature, when the SMA is heated. Another way to harness the shape memory property is through thermally induced phase transition, whereby the SMA is cooled under stress to a temperature sufficient to transform the material into a martensite phase. The transformation can be under constant or varying load. Subsequent heating will recover the seeming permanent strain that was generated. Pseudoelasticity on the other hand describe the recovery of large inelastic strain, generated based on mechanical loading of SMA at a sufficiently high temperature where austenite is the stable phase, when the load is removed. Engineering use of SMA relies on three major response based on transformation path of an SMA as represented by the phase diagram (figure 1.1). They are described in a little more details next.

1.2.1 Shape Memory Effect

As described in figure 1.3, SME in SMA describes the ability of an SMA to recover seeming permanent strain induced after initial cooling below M_s and to temperature at which self-accommodated martensite is stable (see figure 1.1). This seeming permanent deformation which is retained upon removal of load at lower temperature is recovered after reheating the SMA to temperature above that which austenite is the stable phase. To further explain this phenomenon from the microstructural point of view, consider an SMA wire that is initially in the high temperature (where austenite is stable) figure 1.3a. If the SMA is cooled, at a critical temperature, the austenite transform to martensite. However, because of the difference in typical symmetry of austenite (higher) and martensite (lower), different variants are formed in different

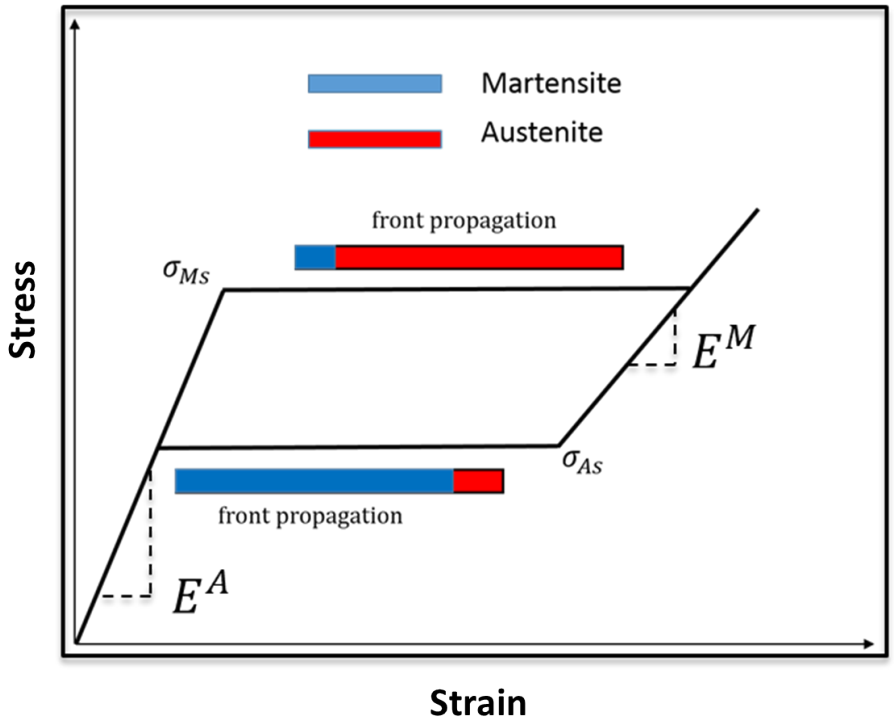

Figure 1.4: Schematic of pseudoelastic stress-strain response under force controlled loading

region of the SMA wire. These different variants, with the intent to minimize energy at lower temperature and stress, tend to arrange themselves in such a manner that no net macroscopic change in shape is observed by the SMA. Upon application of mechanical load at the lower temperature and stress state where self-accommodated martensite is preferred, as the stress increases to a particular critical stress σ_s the SMA accommodates the distortion by rearranging the different variants that was initially formed (see figure 1.1). The energetic argument behind how SMA deform is explained by the fact that the materials prefers to remain in the state with the least energy under given conditions. So when the load is applied, the SMA rearrange the variants (detwin) rather than distort the crystal lattice. The distortion of crystal

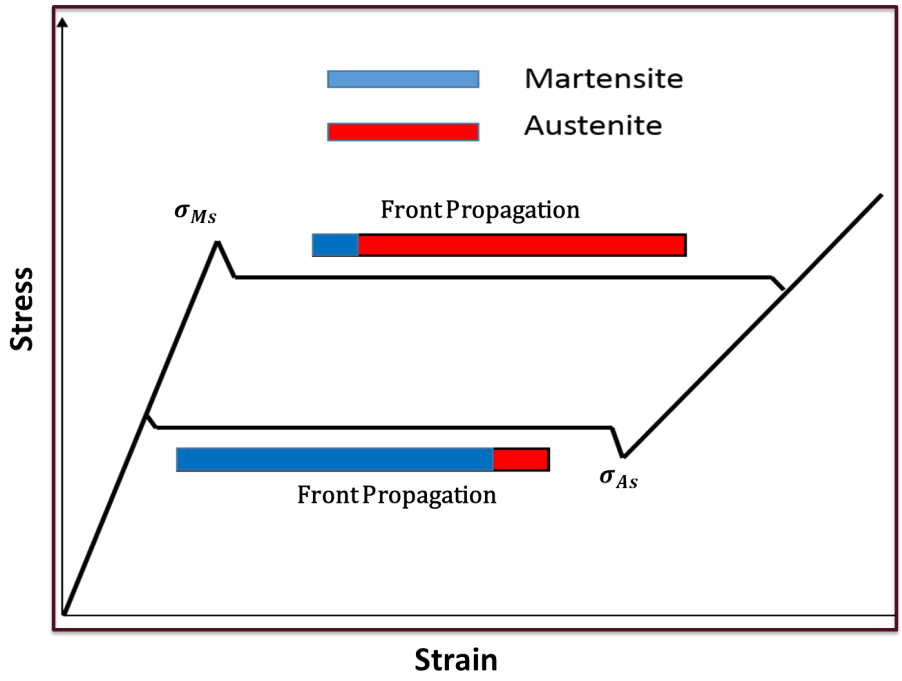

Figure 1.5: Schematic of pseudoelastic stress-strain response under displacement controlled loading

lattice cost energy) but the reorientation does not (see figure 1.3) since all variants comes from the same parents, thereby possessing the same energy. Now, upon removal of the load, the SMA retains its macroscopic deformation by maintaining the deformed or detwinned microstructure because the energy of the "*reoriented*" or detwinned martensite variants and the self-accommodated martensite are the same (being made of variants whose energy are not different). Now, upon subsequent heating of the SMA A_s all the variants transforms back to the lower energy state (austenite) and initial configuration thereby recovering the imposed seeming permanent deformation at lower temperature.

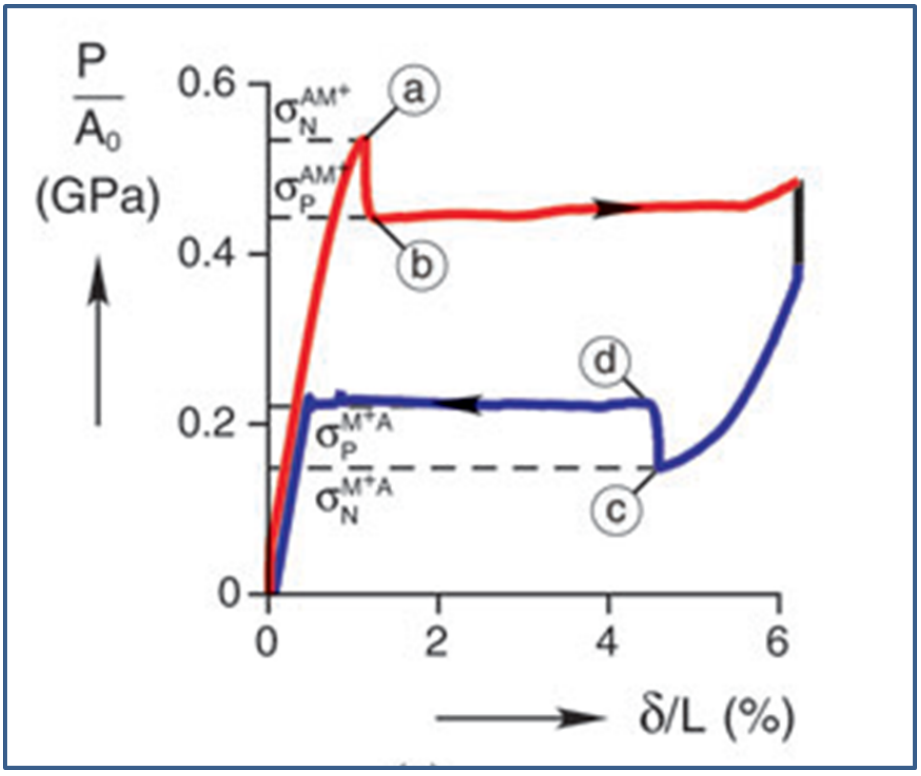

Figure 1.6: Experimental results motivation for strain softening due to material instability and difference in Nucleation and propagation stress (Churchill et al [6])

1.2.2 Pseudoelasticity

The phenomenon of pseudoelasticity or supereleasticity is displayed by most SMA. The stress-strain response as represented in figure 1.4. Classical view of the phenomenon involves large recoverable strain beyond the elastic response of SMA. To describe the phenomena of pseudoelasticity, consider an SMA wire that is at a temperature above which austenite is the only stable phase, if mechanical load is applied without externally imposed temperature change, the material responding in an elastic manner (figure 1.4). When a critical stress level is reached, the material begins to transform from austenite to martensite resulting in large deformation (figure 1.4). After the material is completely transformed to martensite, the ma-

terial now begins to respond in an elastic manner in the martensite phase. Upon unloading of the wire, once it reaches the critical unloading stress level at point, the large deformation is recovered at an almost constant stress level if the loading rate is slow enough to neglect inertial effect. The ability of pseudoelastic SMA wire to recover large deformation is the reason why it is often called superelastic. For NiTi wire, strain ranging from $5 - 8\%$ can be recovered. The underlying crystallographic mechanism for the pseudoelastic response of SMA is to the stability of microstructure at different stress and temperature state. So, when an SMA wire is initially in the austenite phase, it deforms the austenite in an elastic manner. Once the critical load is reached, stress-induced martensite is favored energetically. As portion of the SMA wire begins to transform, the large strain is produced. Once the entire wire is transformed to stress-induced martensite, the material then responds in an elastic manner in the martensite phase. Upon removal of the load, the elastic strain is recovered in the martensite phase until a critical load below which austenite is energetically favored. Since the stress-induced martensite is at a higher energy state than the austenite phase at lower stress for a constant temperature, the crystal structure begins to transform to austenite as stress induced martensite becomes unstable with unloading. At this point, the large deformation resulting due to austenite-martensite transformation is recovered. It has been observed experimentally that the pseudoelastic response differs for displacement controlled loading in that there is an observed difference in the critical stress for nucleation of a new martensite phase and the stress for propagation because of material instability[4, 5, 6]. The same behavior is observed during unloading of the SMA (see figures 1.5 and 1.6)

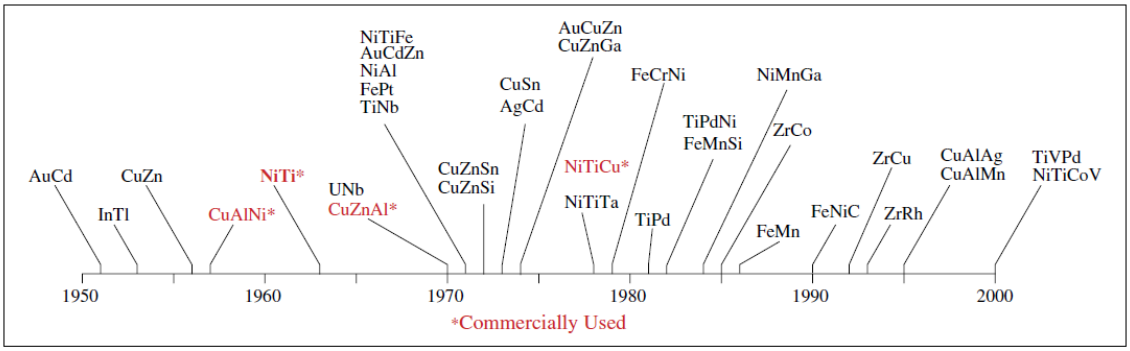

Figure 1.7: A diagram of the history of SMA (Shaw et al[7])

1.2.3 Thermally Induced Phase Transformation under Constant Load

In addition to pseudoelasticity and the shape memory effect (SME), there is another manifestation of the shape memory behavior of SMA, it is the thermally induced phase transformation under constant load. In this case the SMA is subjected to a constant load at a temperature above A_f where austenite is the only stable phase. Upon cooling under constant load, the SMA transform from the austenitic structure to a detwinned martensite once the temperature drops below M_s and stress is above σ_s in figure 1.1. Different region of the SMA transforms and the transformation fronts begins to propagate until the entire material is transformed. Upon reheating to above A_s, the SMA transform back to austenite by nucleating austenite within the detwinned martensitic material. This reversible transformation results in generation of transformation strain and its recovery upon reheating accompanied by hysteresis. This transformation path is used for tensile or compressively loaded SMA actuators. Regardless of whether the SMA is loaded in tension or compression, the transformation temperature increases with the magnitude of the applied load in a somewhat linear manner or at least very close to linear. This is represented in the figure 1.1

1.3 Brief History of SMA

The discovery of shape memory alloys date back to the mid-1900s to late 1900s. Most SMA contains precious metals and can be used either in the single crystal or polycrystalline form, which do not lend them to practical use in commercial applications. Among the many SMA available, Cu-based alloys such as CuAlZn and NiTi (Nitinol) are the most widely used SMA. NiTiNOL has the most widespread use among others because of its best shape memory and pseudoelastic properties. Nitinol was first discovered in the 1960s in the Naval Ordinance Laboratory where the name -NOL was coined. Some other ternary alloys of NiTi are being developed for high temperature use such as NiTiPt, NiTiNb, NiTiPd and NiTiHf. Figure 1.7 is a timeline showing the historical development of SMA

1.4 Application of Shape Memory Alloys

SMAs are now used in a large number of structural and functional applications in the fields of aeronautical and aerospace engineering, biomedical, robotic, micro-electromechanical (MEMS) devices and structural engineering etc. A detailed review of the application of SMAs is given in a recent publication by Jani et al[1] . These applications ranges from large scale (seismic, vibration damping civil structures) as rods and beams to lower scale MEMS applications as micro-wire, micro-beams, micro-tubes, thin films etc. SMAs are being increasingly studied, designed, and optimized in several fields of science. Due to the improved properties of Cu-Zn-Al, they have been used industrially as hydraulic couplings, anti-seismic dampers, fastening devices; as active elements in the form of helical springs, wires, strips, sheets.

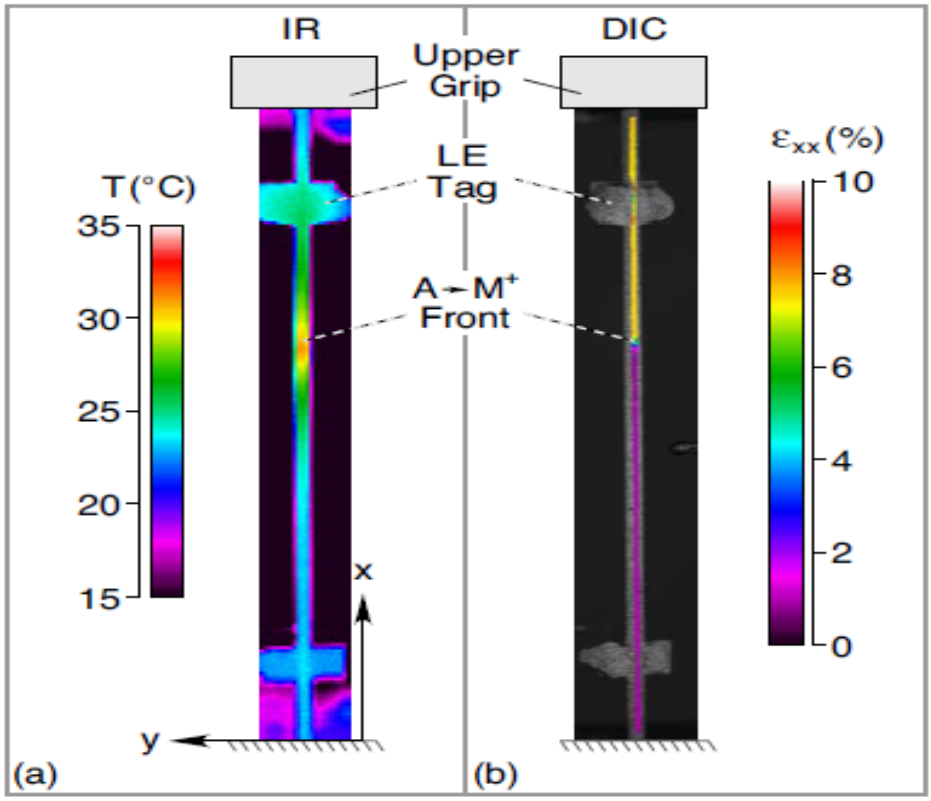

Figure 1.8: Experimental results motivation for latent heat and moving front (Reedlunn et al [8])

1.4.1 Potential Applications

SMA are being researched and considered for use in biomimetic unmanned undersea vehicles, requiring dynamic response [10]. NiTi SMA actuators are commercially available mainly in wire form . The two main types of commercially available NiTi wires are (1) Flexinol and (2) Biometal fiber, and they have demonstrated in various applications. Flexinol has been demonstrated for use in robot-eye systems [11], prosthetic hands [12, 13] and robotic manipulators[14]. Luchetti et al [15] demonstrated an anti-glare rear-view mirror based on SMA actuation for automobile applications.

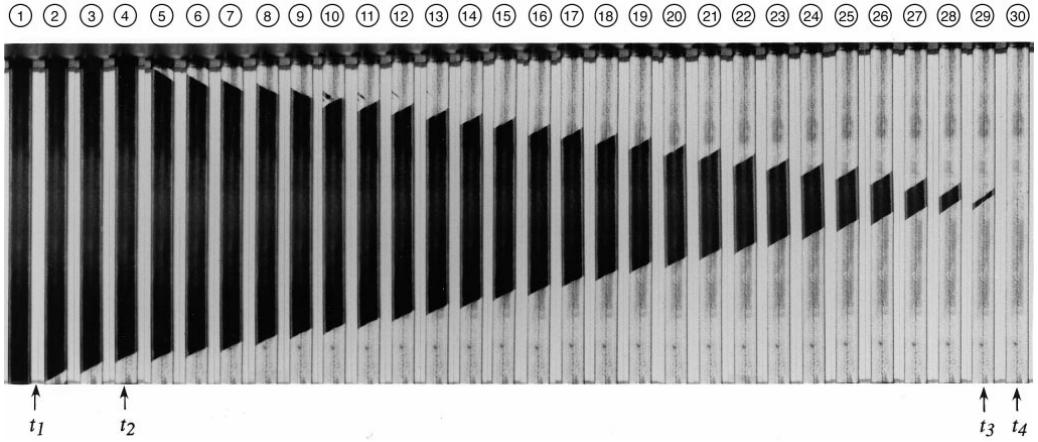

Figure 1.9: Two dimensional SMA Thin Strip Experimental results showing Luders Band-Like Formation (Shaw and Kyriakides 1998 [9])

SMA is being considered for use in expressive humanoid face that is capable of showing real time facial expressions (see Tadesse and Jani et al [1] for details). Other potential future application of aerospace significance might be in deployable space antenna and tensegrity structures

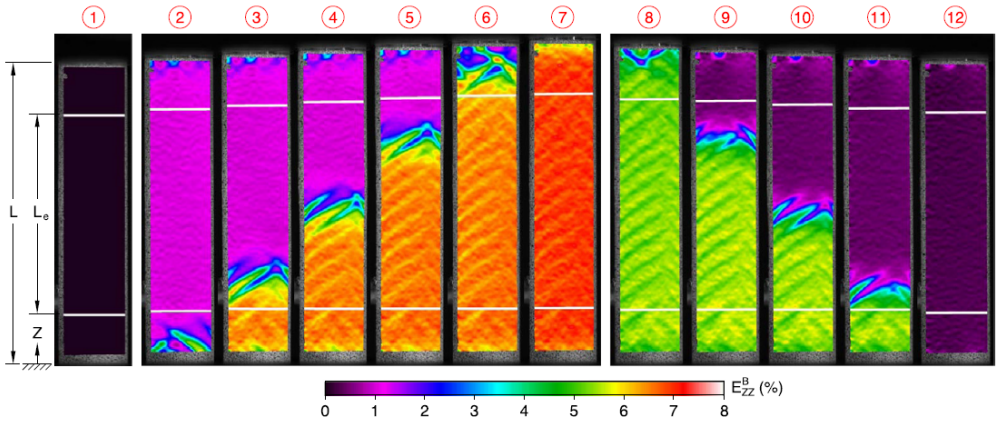

Figure 1.10: Two dimensional SMA Thin walled Tube Experimental results showing Luders Band-Like Formation (Reedlunn et al 2014 [8])

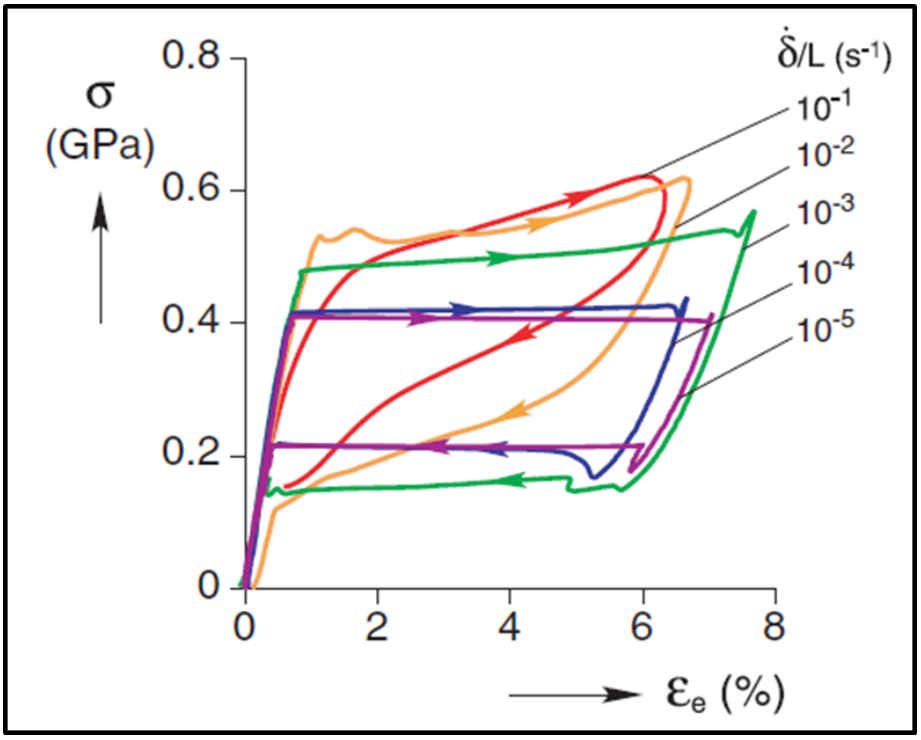

Figure 1.11: Experimental results motivation for rate dependent response (churchill et al [20])

1.5 Introduction on Experimentation and Characterization of SMA

As research towards design, optimization and application of SMAs increases, experiments have been performed under load, displacement and temperature control. Many works have been carried out in literature to investigate the thermomechanical response of martensitic materials. The goal of such experiments is to characterize the macroscopic response of SMA. According to Abeyaratne and knowles, based on loading type, the experiments type can be grouped into: uniaxial tensile loading experiments, multi-axial loading experiments, and high-rate experiments.[16]

Uniaxial tensile loading experiments: Quasi-static (slow in the sense that inertia is negligible) tensile loading and unloading of SMA bars have been reported in the

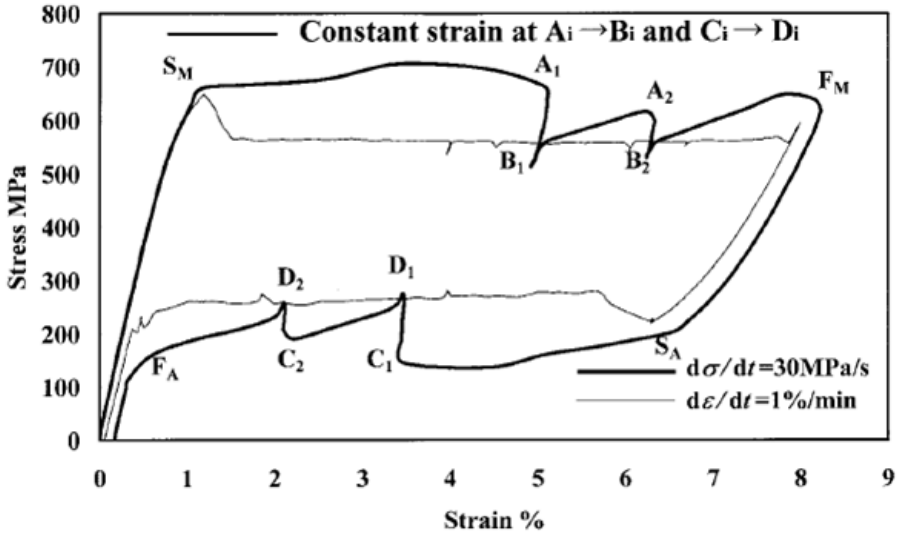

Figure 1.12: Experimental results motivation for stress relaxation (Matsui et al [30])

literature, of which NiTi SMA has been the most technologically important. Some of the works that have been carried out includes the works of Krishnan and Brown [17], Gao and Brinson [18], Shaw and kyriakides[4], and Leo et al[19]. Depending on the loading rate and ambient medium, the response of SMA will differ and exhibit localized heating and cooling of the material. It has been observed for very slow cooling at about $10^{-4}s^{-1}$, that the process behind the response of NiTi SMA is isothermal and as the loading rate increases localized heating and cooling at the phase boundary occurs (see figure 1.8). Many other characteristic features result from the complex interaction being the mechanical, thermal and phase transition condition of SMA. For example under quasi-static loading rate, polycrystalline SMA wires, strips and tubes have been observed to exhibit stress peak (during loading) and stress valley (during unloading) which are followed by steady-state propagation stress plateaus [4, 9, 21, 22, 23]. The inhomogeneous inelastic strain generated during

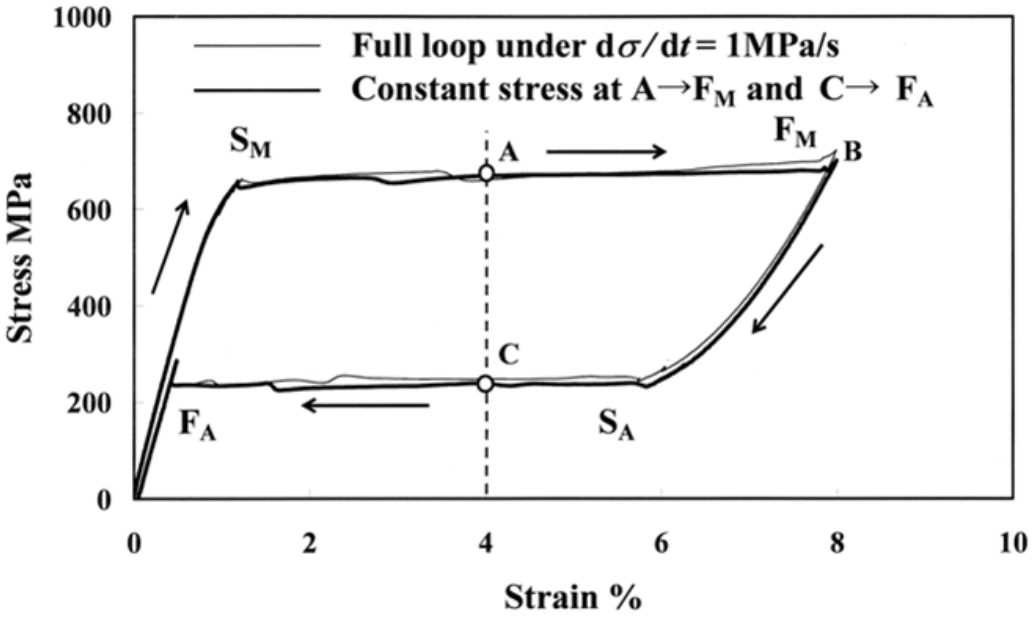

Figure 1.13: Experimental results motivation for creep at 1MPa/s loading (Matsui et al [30])

pseudoelastic loading has been reported to be due to the nucleation and propagation of single or several fully transformed martensite bands, exhibiting Luders band like features that is well known in plasticity, depending on the thermal condition (see figures 1.8, 1.9 and 1.10). In general the features reported in experiments [4, 9, 21, 22, 23, 24, 25, 26, 27] are said to be due to complex interaction between mechanical work, heat production, the prevailing heat transfer conditions and the loading rate [28, 29]. Rate dependency in SMA response has been reported, which includes observed strain and stress rate dependent stress-strain response (see figure 1.11), the pseudo-viscoelastic response (where SMAs behave like classical viscoelastic material as they exhibit transformation induced creep and stress relaxation at low temperature).[30, 31] (see figures 1.12, 1.13, 1.14). A couple of experiments and accompanying models have also been carried out to harness the thermally induced transformation of SMA (see [32, 33, 34, 35]. Unlike the uniaxial tensile loading,

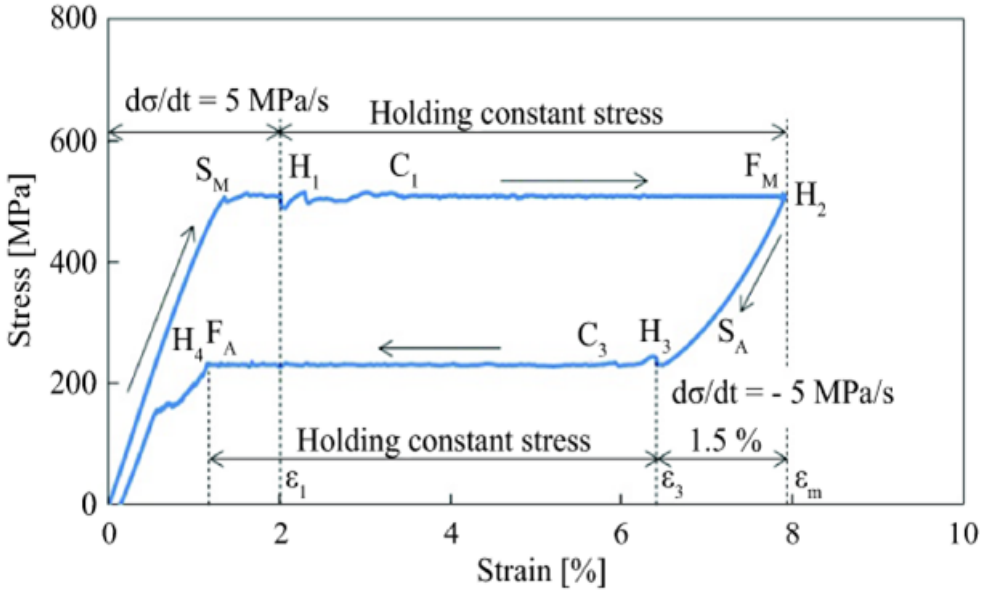

Figure 1.14: Experimental results motivation for creep 5MPa/s loading (Takeda et al 2013 [37])

experiments under multi-axial loading are fewer in the literature[16] . Other category of experiments is the loading of SMA under high strain rate such as their responsne to shock and Impact-loading[16, 36] . One major goal of this type of experiment is to determine the impact speed and how they affect the speed of phase transformation.

Characterization and testing of SMA, which are useful for improved understanding of SMA for design as well as to develop better models, can be very tricky for the uninitiated. Recently, for the characterization of SMA wire, a series of papers was published to avoid the pitfalls and learn the trick for characterization and testing of SMA. The difficulty in SMA characterization and testing is due to their extreme sensitivity to environmental and testing conditions. Unlike many other conventional metallic alloys, there is no standardized testing and correct materials property tables yet for testing SMA because of its complex nonlinear, hysteretic, and extremely temperature dependent behavior. This complexity makes SMA standardization to

require more work. The work in this dissertation is a contribution towards addressing these need using computational modeling and analysis. The transformation temperatures for start and finish of austenite and martensite, often determined by the tangent to the peak of the exothermic and endothermic region of SMA DSC thermogram as seen in figure 1.15, as well as the difference between the start and finish temperatures are important factors in characterizing SMA

A lot of study have been carried out on SMAs since their discovery , but this work will mostly focus on simulation of result for NiTi SMA because of the abundance of commercial usage. Harnessing of pseudoelastic response of SMA for commercial application necessitate their testing and characterization. Testing of SMA results in characteristic stress-strain response and temperature field under thermo-mechanical loading path. These response have great sensitivity to loading rates (see figure 1.11 and ambient medium due to interaction between the thermal state of the material and the environment. The tests can be carried out under force or displacement control and the measurement are carried out using several local and full field temperature and strain measurement such as extensometer Digital Image Correlation (DIC) and infrared images and thermography. Some of the observed characteristics features and behavior of SMA pseudoelastic response of SMA will be itemized in details in chapter 3. Since most SMA used are non-stoichiometric, their properties and responses such as transformation temperature and crystal structure will depend on the composition. It often desirable to form precipitate in SMA to increase it resistance to plastic deformation as it result in higher yield strength.

1.5.1 Introduction of Precipitation and Influence on SMA Response

In addition to macroscopic response of SMA, their microstructure is often manipulated by metallurgist to get desired macroscopic improvement. One often ma-

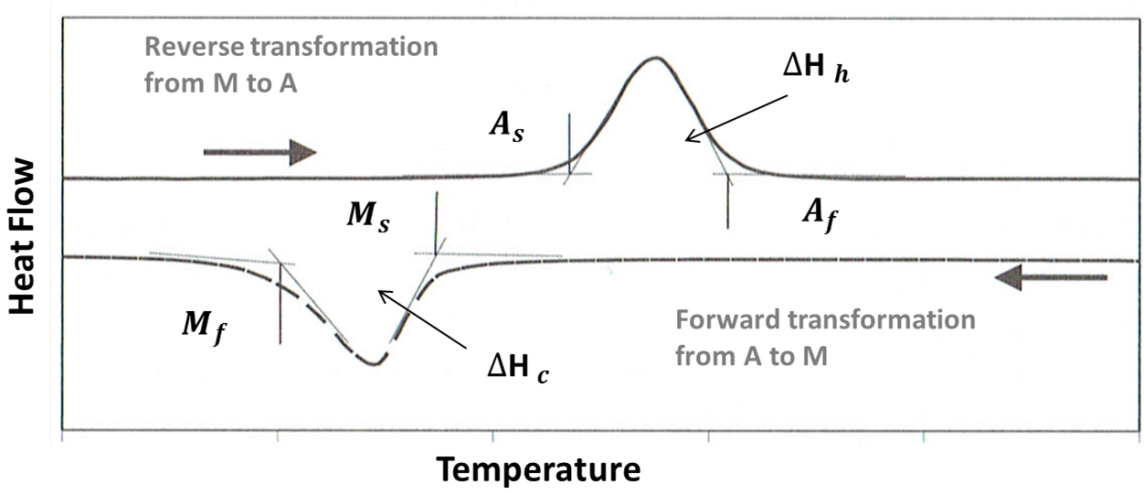

Figure 1.15: Typical differential scanning calorimetry (DSC) result for one Stage transformation from austenite to martensite and vice versa show typical way to measure transformation temperatures and enthalpy of transformation (ΔH)related to the latent heat

nipulated microstructural feature is precipitate formation. Shape memory alloys, including the high temperature ones, are often aged to form fine precipitates [38, 39, 40, 41, 42, 43, 44, 45, 46]. Particularly, fine Ni_4Ti_3 precipitates have been reported to enhance strength of the austenite and limit the degree of plastic deformation during martensitic transformation of NiTi. However precipitate formation alters the path, transformation temperature and nature of deformation (e.g. degree of homogeneity of the deformation in NiTi single crystal) in NiTi shape memory alloys[38, 39, 40]. The martensitic transformation temperature of shape memory alloy (e.g. NiTi) can be altered by controlling size and density of Ni_4Ti_3 precipitates. Also the martensite start temperature is also very sensitive to nickel concentration both in the bulk and around the precipitate [40]. To observe these features, high accuracy and spatial resolution of the experiments technique is required.

1.6 Introduction to SMA Modeling

In order to aid in the design of SMA based device and components, models have been developed. However, the development of models that focus on engineering applications have remain a relevant challenge and it has experienced a very slow progress over the last couple of years. Review of the available models can be found in Birman [47], Lagoudas et al. [48], Patoor et al [49] and Paiva and Savi[50]. Of all the different approaches, the continuum modeling is suitable for engineering use. One major reason is the ease of implementation in finite element packages, particularly for complex geometries. A modeling approach of SMA that is related to this work is continuum two-phase modeling of SMA. Studies of the equilibrium of a two phase elastic bar composed of a material with inhomogeneity, thereby comprise of non-monotonic stress-strain response, was first studied by Ericksen (1975). The two phase material is described by a strain-energy function that has two local minima. Modeling of solid-solid phase transformation has been carried out afterwards using several approaches. Phase front based modeling of SMA could be categorized under this general continuum approaches for modeling two-phase materials. Works on the subject of solid-solid phase transformation can be divided into two main parts. The first approach use the principle of energy minimization of which the recent book by Bhattacharya [3] and the article by James and Hanes did provide very comprehensive discussion on this approach. On the other hand the second categories of study on solid-solid phase transformation are related to the time dependent response of continuum body under different thermo-mechanical loading processes. These methods seek to understand the evolution of microstructure of materials at the microscale. At the macroscale, the hysteretic macroscopic response of the material is the main concern. Regardless of the details, it is desired to characterize and model the dissipation in

SMA that is known to come solely from phase transformation. Among the continuum modeling that are in the literature, there are three categories (1) phenomenological [51, 52, 53, 54, 55, 56, 57, 58, 59, 60, 61, 62, 63, 64, 65] (2) micromechanical [66, 67, 68, 69, 70] and (3) phase front-based continuum models.[71, 72, 73, 74]. The micromechanics-based models utilize information about the microstructure of the SMA to predict the macroscopic response. Modeling of SMAs using this approach is still an active area of research. Their disadvantage is that they require substantial computational effort to analyze component response at the macroscopic scale. Phenomenological models, on the other hand, do not directly capture material behavior at the microscopic level, but consider energy potentials defined over homogenized material volumes and employ methods similar to those of classical plasticity to capture bulk behavior [74]. These approach trade microscopic accuracy for global computational efficiency as they are calibrated by parameters measured at the macroscale through experimental observation. The third approach which is of importance to this work is the phase front approach and will be discussed in details in the next sub-section. Unlike the categorization above, Jaeger et al recently categorized SMA models at the length scale of continuum thermodynamics. Based on this categorization, the different route for constitutive equations from literature was categorized into three, namely: empirical models, plasticity models, and energy-based models. Empirical models use ansatz functions, fitted to measurements in the state space. Plasticity models are models that rooted in classical theory of plasticity. Energy base models are models that are more physically sophisticated and are based on the free energy description of the material.[75]

1.6.1 Continuum Phase Front Approaches

The new modeling approach develop for SMA in this work can be categorized under phase front based modeling (encompassing continuum phase field models) In 1991 Abeyaratne and Knowles treated the dynamics of phase transformations in elastic bars [71]. They studied the compatibility of the field equations and jump conditions of the one-dimensional theory of such bars. They included two additional constitutive requirements: a kinetic relation controlling the rate at which the phase transition takes place and a nucleation criterion for the initiation of the phase transition. A special elastic material with a piecewise-linear, non-monotonic stress-strain relation was considered, and the Riemann problem was analyzed for the material. For a large class of initial data, they found that the kinetic relation and the nucleation criterion together single out a unique solution to the problem from among the infinitely many solutions that satisfy the entropy jump condition at all strain discontinuities. .In the year that followed, they studied a 1-D thermo-elastic solid capable of undergoing either mechanically- or thermally- induced phase transitions. They constructed a Helmholtz free energy, a kinetic relation and a nucleation criterion for the 1-D solid. They studied the hysteretic macroscopic response predicted by the model in the case of quasi-static processes involving stress cycling at constant temperature, thermal cycling at constant stress or a combination of mechanical and thermal loading that gives rise to the shape-memory effect. They noted that their predictions compared qualitatively with experimental results. In the later part of 1992[72], they published another work that reviewed their recent studies on the nucleation and kinetics of propagating phase boundaries in an elastic bar and related them to various admissibility criteria. Like what was done in their earlier work, they discussed how the field equations and jump conditions of the quasi-static theory of such a bar must be

supplemented with additional constitutive information pertaining to the initiation and evolution of phase boundaries. They discussed the relation between their approach based on nucleation and kinetics as well as three admissibility criteria. They reported incorporation of inertial effects, and found that in the context of the Riemann problem that, as long as phase boundary velocities are subsonic, the theory again needs - and has room for - a nucleation criterion and a kinetic relation. The objective of that work was to provide a unified review of the work they had carried out earlier. In 1993[71], they reported a 1-D continuum model for shape memory Alloys. The study carried out in the paper, generalized their earlier model. In the paper, they constructed an explicit constitutive model that is capable of describing the thermo-mechanical response of a shape memory alloy. The model consisted of a Helmholtz free-energy function, a kinetic relation and a nucleation criterion. They associated the free energy with a three-well potential energy function; the kinetic relation was based on thermal activation theory; and the nucleation was assumed to occur at a critical value of the appropriate energy barrier. They examined predictions of the model in various quasi-static thermo-mechanical loadings and compared it with experimental observations. Rosakis and Knowles in 1997[76] explored the implications of relinquishing the assumption of monotonicity of the kinetic relation in the purely mechanical setting of tensile bars modeled as one-dimensional elastic solids capable of changing phase. They noted that for a class of non-monotonic kinetic relations, models of their kind permit stick-slip motions of a phase boundary, as observed in certain experiments. In 1997, they considered a 1-D quasi-static displacement-controlled loading through one stress cycle of a shape-memory tensile modeled as a 1-D, two-phase elastic solid. They used the model to explore the effect of various qualitatively different types of kinetic relations on associated hysteresis loops. They showed that a nonhomogeneous kinetic relation intended to model the

effect of micro-obstacles on interface motion also leads to irregular interface motion and a serrated stress-elongation curve at all elongation rates in the case considered. An approach that can be categorized under the phase front based modeling of SMA is the phase-field model. The phase-field model however can model microstructure that is more complex. The model developed in this work combines the strength of the phase-front approach and the phenomenological model in continuum thermodynamic phase field approach.

1.6.2 Phase Field Modeling

Improved control of microstructural design and macroscopic hysteretic response of SMA for various application, and simulation of SMA precipitate formation requires improved modeling. A detailed general review of microstructure based phase-field method is reviewed by Chen [77] and Emmerich[78].

1.6.2.1 Microstructure Modeling Using Phase Field Approach

In phase field approach, a microstructure is described by using a set of conserved and /or non-conserved field variables that are continuous across the interfacial regions separating the neighboring phases or structure. The temporal and spatial evolution of such field variables is described by applying the Cahn-Hilliard (C-H) nonlinear diffusion equation and the time dependent Ginzburg-Landau (Allen-Cahn) relaxation equations [77] and Emmerich[78]. The beauty of this method is that it can predict the evolution of complex microstructure and arbitrary morphology without keeping track of the interface(s) once the thermodynamic and kinetic data are available. Formulation of free energy density function and subsequently the free energy of specific physics system are foundational to all phase field models with phase field models only differing in the components of the free energy [77] and Emmerich[78].

1.6.2.2 Macroscopic Phase Field Models

The phase-field approach model for the thermo-mechanical model reported in this work can be categorized under macroscopic continuum type. One of the earliest works on macroscopic phase-field that is still being used and modified today is that of Falk[79, 80, 81] and Barsch [82, 83]. The works are based on Landau theory. Review on Landau and Ginzburg-Landau theory of SMA modeling are reviewed in the article by Mamivand et al [84]. Falk in 1990 [81], presented a phenomenological model free energy function based on Landaus theory. He proposed a free-energy expansion of sixth order in a single shear strain component. The model accounted for the shape memory effect in alloys due to a first order martensitic phase transitions. T reported the mechanical and thermodynamic consequences of the model (such as stress-strain curves, elastic constants, and the heat of the phase transition). The author reported that their model is the simplest function which qualitatively yields the experimental results on shape memory alloys. They compared the result of their model with experiments. He also proposed a 1-D static Ginzburg-Landau theory for the martensitic phase transitions in shape memory alloys. Falk calculated from the equilibrium conditions the structure of static domain walls of martensite-martensite as well as of martensite-austenite type. In the same year, Falk discussed how the landau theory evolved from being initially appropriate for describing second order phase transition to its improvement to first order phase transition by Devonshire. Challenges that ensue upon appropriating the landau theory for first order phase transition and the consideration for overcoming them was discussed. Falk noted that in the case of martensitic phase transition, Landau theory may be used as a starting point to obtain deeper insight into phenomena such as soft modes, nucleation, and the role of lattice defect. In 1990, Falk and Konopka [81]reported a modified Landau

theory in which the free energy of the crystal depends on the temperature and on the full strain tensor. It is reemphasized here that earlier works have been carried out to model SMA behavior considering transformation based on evolving phase boundary. Abeyaratne and Knowles [71, 72, 85] pioneered this approach, and it is based on the seminal work of Ericksen for a two phase material [86]. Their approach however is limited since it is based on a sharp interface, which requires explicit tracking of the phase boundary. Other similar but static approach, looking at deformation from the lattice scale up thereby emphasizing microstructure of martensite, is that of Bhattacharya and his co-workers [3, 87, 88, 89]. In keeping with the microstructural features of SMA, phase field modeling based on the theory of Landau, Devonshire and Ginzburg- Landau has also enjoyed widespread research. A detailed review of the state of the art in phase field modeling is given in by Mamivand et al [84]. Others have also made attempt to develop a phase front-like models to capture the macroscopic localization and propagation of instability in SMAs [9, 21, 90, 91] using constitutive approach. Some other 1-D purely mechanical approach and 3-D models exist [90, 92]. A couple of non-isothermal models exist, which are not constitutive in their evolution equation development. [93, 94, 95]. Other recent phase field models that is based on earlier work of Falk and Krumhansl is that of Dhote et al , Levitas and co-workers have also carried out very recent work to further include strain energy to the classical Landau-Devonshire theory. This work in this dissertation, in general, moves the modeling of first-order macroscopic phase transformation in a positive direction using an extension of standard continuum thermodynamics.

1.7 Research Goal and Objective

As it has been discussed up to this point, there is a dare need for models in the SMA communities that can be used to reliably model the macroscopic response of

SMAs. The research reported in this dissertation has two main objectives, which is to develop a constitutive model for SMA based on propagating boundary between austenite and martensite as observed in experiment (see figures 1.8, 1.9 and 1.10). A predictive and more reliable model that is suitable for engineering use for the design of SMA is sought, particularly as the SMA becomes thinner in dimension. The model is intended to provide explanation to challenging experimentally observed phenomenon in SMA that influences their engineering use. The model developed in this work will be used to simulate and explain basic scientific questions related to SMA's macroscopic rate dependent response. Effort is made to develop a more reliable and predictive model that can be used to simulate some of the challenging experimental features that are relevant to the design of SMA components and structures. Two main engineering problems that this work addresses are (i) The Apparent Rate Dependent Response of SMA: the rate dependent response include the loading rate dependent response of SMA , the seeming intrinsic rate dependency in SMA response manifesting in the stress-relaxation, pseudo-creep under mechanical loading; cooling and heating rate dependent SMA response. Essentially, the scientific questions is that is there really an inherent rate dependency in the response of SMA apart from those derived from the strong thermo-mechanical coupling?. Can explanation and improved modeling be achieved that account for the rate dependent response based on the mechanism of propagation of transformation front.

(ii) Effect of microstructural features such as precipitate on SMA macroscopic response - It has also been observed as described in the earlier discussion that precipitates formation during aging of SMA has impact on the macroscopic transformation temperatures as well as the hysteresis of SMA. So, as a first step in the direction of more detailed work, this dissertation also attempt to develop and implement a model that describe in a qualitative manner the essential feature of precipitate formation in

SMA that can later be improved for detailed simulation of precipitate microstructure formation in shape memory alloys based on processing parameters.

1.8 Underlying Hypothesis and Influence on Methodology

In the light of the objective of this work, a hypothesis is made based on the underlying mechanism of martensitic transformation as known from material science. Martensitic transformation being a discontinuous first order phase transformation occurs by nucleation and transformation front evolution. Experimental observation of formation of macroscopic propagating domain of martensite for thin specimen also confirms this mechanism. Upon careful study of these experimentally observed complex thermomechanical response of SMA and the classical approach for constitutive modeling of SMA and their limitation, I propose that a different time scale of transformation front evolution is needed to correctly modeling and correctly capture prevalent macroscopic response of phase transition in SMA. The time scale is in addition to the time scale resulting from heat transfer, mechanical deformation or wave propagation. This different time scale is presumed inherent to the SMA phase boundary propagation, resulting in rate dependent response shown from experimental results described earlier. The observation leading to my hypothesis is that SMA rate dependent response is due to the interaction between different phenomena associated with other time scales and that of phase transformation. In keeping with this observation and the hypothesis, a time scale is introduced through the introduction of a new balance law in addition the balance law of linear momentum and energy that introduces the time scales of heat transfer and wave propagation. This new balance law will introduce time scales for phase transition and length scale intrinsic to SMA transformation mechanism. As will be elucidated under the modeling section, the length scale comes from the width of the interface being taken as diffuse and this is

captured by a gradient energy coefficient. The time scale is embedded in a kinetic coefficient (a dynamic viscosity like parameter) which is a measure of the resistance of the material to phase transformation. This time scale and length scales are derived through a non-dimensionalization of the coupled system of equation. In this work, since this modeling work is motivated by the afore mentioned engineering design, relevant features of SMAs, SMA macroscopic response is modeled to be a result of nucleation and propagation of fully austenite and fully martensite transformation front or domain boundary. Although models already exist for the simulating SMAs response, there is however a need for a thermodynamically consistent rate dependent constitutive continuum based SMA model. A model that overcomes the limitation of the phenomenological and the phase front model are desired. In particular, for the design of SMA for aerospace application where stringent requirement (such as combination of sensing and actuation) and thermomechanical coupling are inevitable, a reliable and yet efficient model is needed. The model reported in this work is intended to comprise all these relevant features necessary to simulate SMAs for application design. The effect of latent heat during transformation on the pseudoelastic response of SMAs and the complex interaction between mechanical deformations, kinetic of phase transition are addressed. In summary, the models developed in this work are based on extension of continuum thermodynamics to model the dynamics of SMA transformation front in a thermodynamically consistent manner. Therefore, physically admissible experimental observations are simulated.

1.9 Layout of Dissertation

To achieve the goals of this research several steps were taken and will be thoroughly described in this dissertation. This dissertation comprises six chapters.

Chapter 1 Introduces SMA and the present state of the art in SMA characteriza-

tion and application as well as review on the modeling of SMA including the phase field approach

Chapter 2 describes the modeling theory and approach used to simulate the prevalent and new challenging experimental results. Furthermore, constitutive modeling and the resulting field equations are explained in details both for the thermo-mechanical response as well as the elasto-diffusion coupling for precipitate modeling. Calibration of the model as well as non-dimensionalization of the model is discussed. Finally, the field equations resulting from the model are stated. In chapter 3, numerical implementation and simulation of the thermo-mechanical model is described in detail with analysis and discussion of the results from mechanical loading of SMA. Detailed result of key experimentally observed, but challenging, features are simulated by the model for forward transformation under pseudoelastic loading path; transformation induced relaxation and creep as well as parametric study of relevant model parameters. In chapter 4 numerical implementation, analysis and discussions of the thermo-mechanical response of SMA is discussed for actuation or load biased thermally induced phase transformation. The effect of cooling rate on SMA response is discussed. Proposed experimental works and simulation that should be carried to further aid in SMA design based on simulation results under thermally induced phase transformation are also highlighted In chapter 5, implementations and numerical simulation of precipitate growth is presented and discussed. Simulation of concentration depletion in the neighborhood of precipitate is described. Simulated result for both 2-D and 3-D precipitate growth and effect of elastic inhomogeneity and anisotropy. Result will be simulated for single and multiple precipitate with equilibrium morphology described. In Chapter 6 Conclusions and future works with recommendation is made for the research. In the conclusion, key scientific contributions are mentioned. Future work and recommendations are also highlighted.

2. MODELING APPROACH: CONFIGURATIONAL FORCES BASED PHASE FIELD APPROACH (CFPA)

Central to the theory upon which the model developed in this work is based is the notion of configurational forces. The work on configurational forces dates back to the 50s. One result of the seminal work of Peach and Koehler (1950)[96], Herring(1951) [97] and Eshelby (1951,1970 and 1975)[98, 99, 100] on lattice defect is that additional configurational forces may be needed to describe phenomena associated with a continuum material itself. Their approaches have been based on a constitutive framework whereby the configurational forces are restricted to particular class of material. Recently, a completely difference paradigm to configurational forces introduced by Gurtin and struthers(1990)[101] and later developed by Fried and Gurtin , which was written in Gurtin (2000) [102] uses the perspective of invariance under change in observer to conclude that a configurational force balance should join the standard (Newtonian) force balance as a *basic* law of continuum physics. What this paradigm means is that independent of constitutive assumptions, the configurational force balance (like other balance laws) when placed within a thermodynamic framework allow one to use the now standard procedures of continuum thermodynamics to develop suitable constitutive theories. The approach for modeling SMA used in this research is based on the theory proposed by Gurtin (2000) [102] resulting from several works he did along with other colleagues. Particularly, the micro-forces resulting from the normal balance of configurational forces, yet consistent with the general frame work of configurational forces. These set of works are an attempt by these researchers to extend continuum mechanics to treat moving boundaries in materials and metallurgy. Since the hypothesis, based on observations, I made for modeling SMA both

for the thermomechanical and precipitates problem involves phase boundary motion-it seem natural to use this approach to fundamentally model phase transformation. This chapter describes the theory and the application to model thermomechanical macroscopic response of SMA and diffusion of atomic species within an elastic solid to model coherent precipitate growth in SMA. In this approach, following Gurtin, I derive a kinetic equation similar to that of Ginzburg and Landau in a methodical way that is consistent with the fundamental law of thermodynamics. Therefore, consistent with the state of modeling in non-linear continuum mechanics, I separate between balance laws (which generally holds for all materials) and constitutive equations which are restricted to specific class of materials (in this case thermoelastic solids undergoing phase transformation, of which SMA is one of them). In addition to the standard balance laws of thermodynamics, the new balance law for "micro-forces" which are essentially configurational forces is introduced. A separate configurational balance law must be introduced since a new kinematic descriptor (the order parameter) is introduced to capture the kinematics of interface evolution, which is the mechanism of transformation in SMAs.

2.1 Fundamental Approach to The Use of Configurational Forces

The monograph written by Gurtin (2000) [102] introduced, in a rational manner, the notion of configurational forces which is central to the kinetic equations developed in this work. Gurtin proposed a new view point in continuum modeling of materials. The concept of configurational forces was introduced within a classical context with their use in diverse areas of moving boundary involving dissipation such as phase transition and fracture. I belief in the new view point introduced by Gurtin (2000) [102] as potential extension of classical continuum thermodynamics to model moving boundaries. The theory is based on unification of the notion of

forces. Gurtin argues in his treatise that the crude notion of forces as "push" and "pull", rather than a mathematical construct, has obscured the generalization of the notion of forces to dissipative mechanism in materials. He argued that central to continuum mechanics is the notion of forces, which is simply a mathematical concept Essentially, Gurtin argued that although the notion of forces seem obvious to all because of the way it has been thought of as pushes and pulls which has aided teaching, the notion of forces is not necessarily well understood as can be seen in the set of scientific literature following Newton. To give a scientific thought to those who would quickly challenge the notion of configurational forces used in this work as capricious introduction of "physical laws" , it should be noted that several scientists in the past have alluded to the fact that the notion of force is not necessarily clear. Below are some quotations from some earlier scientist on the notion of forces taken from Gurtin (2000)[102]. Pierce stated that force is the great conception which, developed in the early part of the seventeenth century from the idea of a cause, and constantly improved upon since, has shown us how to explain all the changes of motion which bodies experience, and how to think about physical phenomena; which has given birth to modern science. D'Alembert spoke of forces as obscure metaphysical being, capable of nothing but spreading darkness over science clear by itself. Jammer paraphrased remarks of Maupertius, stating that we speak of forces only to conceal our ignorance. According to Carnot force is an obscure metaphysical notion. Now, having noted the mathematical character of the idea of forces, the following quotations are also necessary words for though to those challenged by the idea of introducing configurational forces. To address the possible reluctance in accepting a separate balance for configurational forces, it should be noted that a balance law for moments was not part of Newtonian mechanics. Indeed, a balance law of moments-first stated explicitly by Euler (1776) almost a century after the appearance of New-

tons Principia. Furthermore Truesdell and Touplin stated that it should be, but unfortunately it is not, unnecessary to comment that the laws of Newton are ..[not] sufficiently general to serve as a foundation of continuum mechanics.

The notion of configurational forces has been alluded to by works as early has the work of Eshelby (who according to Maugin) is the father of the theory of configurational forces often term materials , accretive, or chemical forces. Gibbs introduced this concept when he was discussing multiphase equilibria. Standard (Newtonian) forces describe the response of materials to deformation and these forces are consistent with the balance of linear and angular momentum. However, Gurtin noted that the works of Eshelby, Gibbs and Cahn does reduced the notion of configurational forces to a subsidiary status since the theories on statics are derived from variation arguments making the generalization to dynamics to be derived from manipulation of the standard balance of linear momentum. This different view point and perspectives is used in this work. The idea of configurational forces is an attempt to model the dynamics of solid to solid phase transformation in SMAs. A summary of the perspective of configurational forces used in this work are highlighted

- Force is primitive and not derived unlike the variational arguments which follows from the earlier work by Gibbs that is central to material science where forces is not primitive but derived. Gurtin noted that it seem inappropriate to use the variational argument put forth by Gibbs in his masterpiece to situations involving dissipation

- the idea of configurational forces should be viewed as basic objects consistent with their own force balance. This perspective was proved by Gurtin to be true by deriving the standard balance of linear and angular momentum from the same concept of invariance under change in observers

- At every points of a body, two distinct systems of forces are in operation. This idea is the reason why configurational forces have been seen as merely a derived quantity.

- The concept which unifies the notion of forces is generalized by a fundamental framework for the notion of configurational forces and classical forces.

- Variational form of balance laws are not considered as basic, but rather as consequence of more classically formulated balances. So, variational approach will be put aside for this new notion which is treated as being more basic. This reasoning is derived from the argument put forth by Gurtin that (i) The principle of virtual work is physically well-grounded because it has virtual velocities as the test functions. However variational form of other balance laws such as energy seems devoid of meaning because the associated physical test function does not have any obvious physical interpretation. (ii) An a priori notion of stress is required in principle of virtual work but classical formulation of balances may be based on more fundamental notion of traction, then stress becomes a derived quantity via Cauchys theorem.

- Invariance of working under changes in spatial observer results in the *standard* force balance

- Invariance of working under changes in material observer yields an additional balance for configurational forces. According to Gurtin, and for pedagogy, force balances are postulated as consequences of invariance mainly because the concept of configurational forces is non-intuitive.

At this point I will like to state again that this approach is based on the unification of the notion of forces to solve phenomena related to materials processes that

involve dissipative mechanisms. *The unifying concept of the notion of force is "The rate at which work is performed", or simply, The working or power expenditure". This notion can be roughly stated that "to each independent kinematic descriptor an associated system of forces is assigned and to each density of forces, whether it be surface traction or body forces a work conjugate generalized velocity, which is the rate of change of the kinematic descriptor.* Essentially, the underlying continuum theory is the unification of the notion of forces as causalities to motions either as deformation or velocity. The concept which unifies the notion of forces both in the Newtonian and the configurational sense is the working or the rate at which work is being performed by these forces. The idea is that the density of working is the product of a generalized velocity with a density of force whether in physical space or material manifold. The theory is based on the belief that generalized forces are conjugate to kinematic descriptors. These kinematic descriptors are field variables that serve to capture independent kinematic processes that are prevalent in a material system if it involves energy or dissipation. In summary, the basic unifying concept is stated as density of working is the product of force density and generalized velocities. In order to buttress the validity of this fundamental concept that unifies the notion of forces, a basic question needs to be asked and answered. The question is to ask what makes a kinematic quantity independent thereby needing a distinctly different kinematic descriptor. The answer is the need for an independent observer to measure its generalized velocity. The essential origin of this approach to determine independent kinematic quantities is the invariance in thermodynamics to change in observer, which yields the mechanical balance laws. To further understand this idea, it should be noted that statical theory based variational treatments allows independent kinematical quantities to be varied independently to yield a corresponding Euler-Lagrange balance but there has been no similar variational treat-

ment process in dynamics to encompass the general form of dissipation. Therefore, the use of independent observer (like independent varying of kinematic quantities) which necessitates the need for independent kinematic quantities provides a general and rational basis for determining mechanical balance laws.*In the light of these arguments, the need for a separate observer to view motion taking place in the reference configuration necessitates the need for configurational forces essentially.*

2.2 Some Important Definition and Nature of Configurational Forces

Configurational forces are related to the integrity of a bodys material structure and perform work in the transfer of material and the evolution of material structure such as defects and phase interfaces. Another researcher that has given a description of the notion of configurational forces is Cahn, who noted that *the creation of surfaces involves configurational forces while stretching the surface involves standard forces* Configurational forces act within the reference configuration and perform work in the transfer of material and in the evolution of structural defects. Standard forces are different from configurational forces because of the presence of internal configurational forces. Internal configurational forces are intimately connected to the material structure of the body **B**. As classical in continuum mechanics, it is convenient to represent a body **B** with a region of space it might occupy, which might change from time to time. However, the theories of the notion of configurational forces, as used in this work, consider this representation as somewhat misleading. It is taken that a more encompassing view of a body is " a set B of material point **X** together with a collection of possible configurations, where a configuration of **B** is a one-to-one mapping that assign to each material point **X** a point $X = \mu(\mathbf{X})$ of Eucleadian space. Therefore, to each configuration $\mu(\mathbf{X})$, there is a corresponding distribution of material and an associated system of configurational forces. The internal configurational

force is viewed as a force needed to hold in place the material at X when the configuration is μ, or better still to hold X in place in that configuration μ. *Therefore a body in continuum mechanics is now constituted by internal configurational forces as part of the complete system-material points plus region of space.* Another key reason for configurational forces is the need to determine kinetics of phenomena at smaller length scales. Gurtin (1996) noted that standard or deformational forces in continua relates to macroscopic length scales while configurational, accretive forces are associated with phenomena operating at lower length scales and relates to the microscopic atomic configuration (or densities or arrangements) of atoms. Therefore the disparate length scales brought about the need for configurational (micro) force balance. This author believes, along with Gurtin(1996),that if we represent atomic kinematics by an order parameter, then in consonance with the dissipative nature of this kinematic process, it seems right and reasonable to macroscopically characterize inter-atomic forces by fields that perform work when the order parameter undergoes changes. In order to support the generalization of the use of configurational forces with the standard (Newtonian) force notion, whereby configurational forces are treated as primitive objects and stress a derived field, three nontraditional kinematic notions to capture the physics related to the transfer of materials. The three notions are (i) parts P(t) that migrates through the reference configuration $\mathbf{B}$; (ii) Materials observers that view the reference configuration and measure, e.g., velocities associated with migrating parts; these observers are used independently of the classical spatial observers that view motion of $\mathbf{B}$; (iii) time-dependent changes in reference configuration. Therefore based on these new ideas, a new form of the second law of thermodynamics was introduced by Gurtin, whereby the working resulting from both configurational and standard forces are accounted for in an implicit manner for a flow of energy across the boundary of a migrating part $\partial P(t)$ as it migrates. It

is important to note here that configurational stresses are not the same as residual stresses . Here I use the standard second law augmented with the contribution from the workings of the configurational forces in addition to the working of the standard (Newtonian) forces as well as the form of the second law proposed by Gurtin

2.2.1 Understanding Configurational Forces within Framework of Classical Continuum Mechanics

In classical continuum mechanics, bodies have one distinct physical properties, they occupy regions of Euclidean space E, which is their configuration. It is known that although a given body will occupy different regions at different times, and no one of these regions can be intrinsically associated with the body. What is classically done, for convenience, is to choose one of such region, say, $\mathbf{B}$ as reference. In this same context to each configuration of a body $\mathbf{B}$, there correspond a distribution of material and internal configurational forces that acts to hold the body in place in that configuration. Consequently, internal configurational forces characterize the materials resistance to structural changes. To better understand the role of internal forces, note the difference between the body's reference configuration and the deformed (actual) configurations assumed by the body during a motion. In the deformed configuration, the body moves in manner dictated by the standard (Newtonian) forces acting on it. *These standard forces result from interaction of separate part of the body* and interaction of the body with its environment. Therefore there are no internal forces. On the other hand, the mathematical foundation of a continuum body upon which we talk about deformation and motion assume that the body is not free to move in the reference configuration which brought about the basic presumption of the theory of configurational forces. The presumption is that in addition to distribution of materials, there are internal configurational forces that pin,

in place, the material points of the body thereby maintaining its internal structure. Therefore, whenever there is a structural change in the material, these forces becomes determinate and expends power as a result of structural changes. It is important to note at this point that, in the case where there is no change in material structure, the configurational system of forces falls into the category of indeterminate forces such as those associated with pressure in an incompressible fluid and the stress in a rigid body. Take for example a rigid body, since there are not motion (in the sense of deformation), the forces due to interaction of different part of the body are superfluous and will generally not be found in the local form of the second law of thermodynamics or energy balance for that matter. Therefore, in the case where there are no structural changes such as defect motion, moving phase interfaces, the internal configurational forces are indeterminate. In such a situation, although the configurational forces act at every continuum point along with the standard forces, they are superfluous. However, if there is materials structural changes (identified by a motion in reference configuration), the internal configurational forces will have a constitutive specification. The general rule is that all bulk material and all material structures such as free surfaces and interfaces have associated internal configurational forces, with such forces indeterminate when and only when the associated structures are fixed in the material.

2.3 Application of Configurational Forces to Phase Transformation

Based on the theory described above, in order to capture the phenomena of phase transformation which we understand to belong to the material manifold, in addition to the Newtonian forces which act in physical space, configurational forces are introduced (which are analogous to the Newtonian forces). *A material manifold is the set of points building up the material, whether discrete or continuous.* To sim-

plify this concept, I simply say that configurational forces relate to the materials while the standard deformational forces relates to the deformation of the material. Fundamental to the usage of this configurational forces theory in this work is the combination with the phase field theory described in the *Chapter*1. What I mean is that this model although based on standard continuum approach for two phase material, deviates from the Gibbs idea of an interface as being sharp to a postulation of a diffuse interface. (See schematic in figure 2.1). In classical continuum modeling of two phase materials, field quantities and their gradients normally becomes discontinuous across the interface. Once the interface is taken to be diffuse as used in this work, each of the continuum field variables will be continuous across the interface with no jump discontinuity in the field as the diffuse interface is characterized by the gradient of the order parameter. The order parameter is then coupled to other field variables to ensure their continuity across the interface. Essentially, the interface is no longer a discontinuous surface but now an integral part of continuum point with associated determinate configurational forces that result in interface kinetics. In the thermomechanical phase field model of this work, an order parameter is taken to be the kinematic variable which serves to identify the state (in the sense of phase) of a material point. In this work, a scalar order parameter is used to capture the macroscopic representation of austenite and martensite across a (diffuse) transformation front. In this case the configurational force is conjugate to the rate at which the order parameter η changes and therefore expend power whenever the austenite-martensite interface (or transformation front) moves. Therefore, like the balance of linear momentum accounts for equilibrium of forces associated with strain or displacement as the kinematic descriptor of deformation, it seem right that there should be an analogous balance of forces to ensure equilibrium of forces associated with the order parameter as a kinematic descriptor of macroscopic manifestation of

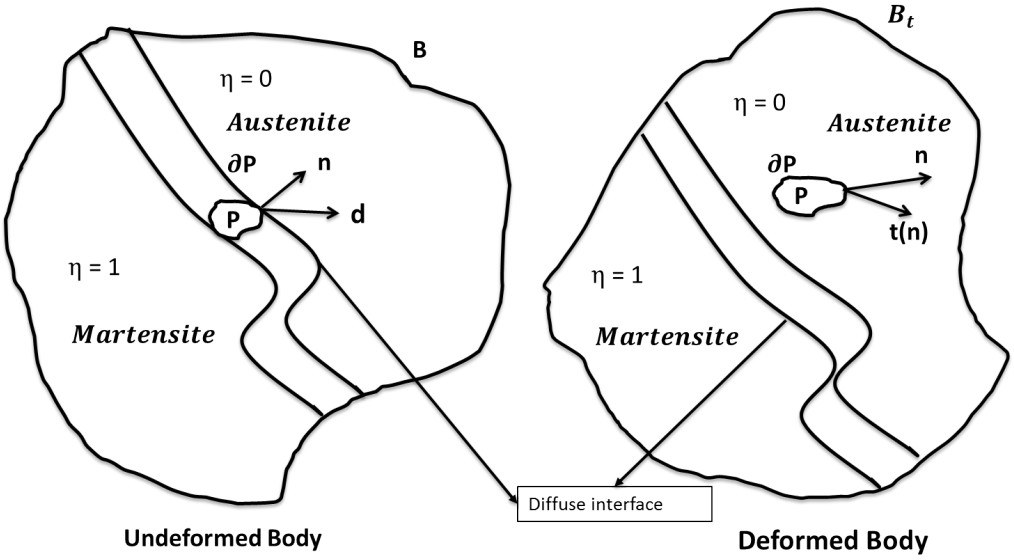

Figure 2.1: Schematics of continuum phase field approach showing classical reference and deformed configuration of a continuum body augmented with postulated diffuse interface

material microscopic phenomena of evolution of austenite-martensite interface. To model the thermomechanical response of SMA, the velocity used in the phase field description is scalar rather than vector. Therefore, for consistency, the system of configurational forces will contain scalar internal and external configurational forces while the stress will be a vector. What it means is that regardless of the spatial direction of the structure that is evolving the behavior is the same in all three directions. The appendix in the work of Fried and Gurtin contain proof that unifies the scalar microforces as consistent with general vector configurational forces, which is basic to the concept. The theory used in this work is extendable to multiple variants in SMA- which for NiTi is 24 martensite variants. That will not be ventured into here but will be a subject of future research. Similarly, a normalized concentration field is used to identify precipitate and matrix phases.

2.4 Model Development

Development of a phase field model with coupled thermomechanical phenomena for predicting transformation in SMA is presented. The derivation of the model developed in this work is be based on standard rational continuum thermodynamic approach which distinguishes between (1) kinematics (2) balance laws and (3) material constitutive class.

In classical continuum mechanics, different types of material behavior or constitutive class are distinguished based on the following general assumptions[103] (i) Kinematics assumption- possible deformation the body may undergo (ii) form of the stress tensor (iii) constitutive equation relating stress to motion.

2.4.1 Kinematics

A shape memory alloys is considered as a body **B** identified with the region of space it occupies in a fixed uniform reference configuration $\mu(\mathbf{X})$along with SMA austenitic materials distribution. I take the stress-free configuration of the austenitic phase as the reference configuration from which deformation can be described under applied loads. In this configuration, the SMA contains distributed internal configurational forces that pins the materials in place in that configuration. The referential position of material points $\mathbf{X} \in B$. Parts P are subsets or bounded subregion of B. The motion of B, $\mathbf{y}$, associate with each material points $\mathbf{X}$ and time t is defined by

$$\boldsymbol{y(X,t)} = \mathbf{X} + \mathbf{u}(\mathbf{X}, t) \tag{2.1}$$

The position of an SMA material point in the deformed, actual or current configuration in relation to the position of the same material point in the reference configuration is given by the displacement vector field, $\mathbf{u}$(**X**,t). We define a measure of

the deformation of neighboring materials points in terms of the *deformation gradient tensor* which is defined as

$$\boldsymbol{F} = \mathbf{I} + \nabla \mathbf{u}, \tag{2.2}$$

subject to J = det$\mathbf{F}$ >0. I base my derivation on finite deformation using a reference, material or Langrangian derivatives. It should be noted that the strain observed in a shape memory alloys relatively small. This observation leads to a later infinitesimal displacement gradient assumption, leading to infinitesimal strain theory. In such a case the difference between reference and deformed configuration becomes negligible i.e. $\mathbf{F} \longrightarrow \mathbf{I}$. The derivative is therefore carried out for a fixed $\mathbf{X}$. In general, a complete large deformation and rotation theory will comprise the deformation gradient $\mathbf{F}$ and the total deformation will be given as $\mathbf{F} = \mathbf{F}^t\mathbf{F}^e$. Where $\mathbf{F}^t$ represent the transformation part of the deformation gradient and $\mathbf{F}^e$ is the elastic part of the deformation gradient. However, such an assumption is relaxed in the presentation here along the line to the use of Green-Lagrange strain measure. The Green-Lagrange or the Green-St. Venant strain tensor which is defined as

$$\boldsymbol{E} = \frac{1}{2}(\mathbf{F}^T\mathbf{F} - \mathbf{I}). \tag{2.3}$$

Later infinitesimal strain assumption will be made such that

$$\boldsymbol{E} = \frac{1}{2}\left(\nabla \mathbf{u} + \nabla \mathbf{u}^T + \nabla \mathbf{u}^T \nabla \mathbf{u}\right) \approx \epsilon = \frac{1}{2}\left(\nabla \mathbf{u} + \nabla \mathbf{u}^T\right), \tag{2.4}$$

where ϵ is the linearized lagrance strain as the dislplacement gradient becomes small.

Another variable that relates to interface kinematics is η, which is called order parameter. In addition to the displacement field which relates to the deformation,

another kinematic descriptor of the full thermomechanical theory for material undergoing phase transformation used in this work is a scalar order parameter (η). The purpose of the scalar order parameter in this work is to identify the state in terms of phase of every continuum point in the material. The order parameter takes on a value of 1 for one phase and a value of zero for the other phase (see figure 2.1). In addition to the scalar order parameter, the diffuse interface is characterized by the gradient of the order parameter ($\nabla\eta$). So, in general there are two basic kinematic variable-displacement ($\mathbf{u}$) and the order parameter (η). Similarly, for the atomic diffusion, the order parameter used is concentration (c) of diffusing species, which is a conserved order parameter, therefore necessitating additional mass balance as will be discussed shortly. The concentration gradient ∇c is also used to characterize the diffuse interface as well.

2.4.2 Stress Measures Employed in Modeling

Like many solids, SMA usually possesses stress-free reference configurations from which deformation and strain can be measured and constitutive equations developed. So, a referential stress measure is used to develop the model, SMA being a solid. There are measures of stress in the reference configuration that is of interest to the model development. The first stress measure is the first Piola Kirchhoff ($1stPK$) stress defined as

$$\mathbf{P} = J\sigma\mathbf{F}^{-T}, \tag{2.5}$$

where J = det($\mathbf{F}$), the determinant of the deformation gradient. $\mathbf{P}$ represents the stress measured per unit reference area in the reference body. The second stress measure of interest, which is also defined per unit reference area in the reference

body is the second Piola Kirchhoff ($2^{nd}PK$)stress defined as

$$\mathbf{S} = \mathbf{F}^{-1}\mathbf{P}, \tag{2.6}$$

where σ is the Cauchy stress tensor defined per unit deformed area in the deformed configuration. In the energy balance that will be discussed shortly and for the sake of objectivity of constitutive equation, certain power conjugate pair of stress and strain measures are appropriate. For the three stress measures of interest to the modeling in this work, the following three power conjugate pair is stated. For the Cauchy stress σ, the power expended within a part of a continuum body (Stress power) is p

$$p = \sigma : \mathbf{D} \tag{2.7}$$

where $\mathbf{D}$ is the stretching or rate of strain. While for the $1^{st}PK$ stress measure $\mathbf{P}$, the stress power

$$p = J^{-1}\mathbf{P} : \dot{\mathbf{F}}, \tag{2.8}$$

and for the $2^{nd}PK$ stress, the stress power is

$$p = J^{-1}\mathbf{S} : \dot{\mathbf{E}} \tag{2.9}$$

As stated earlier, this pairing must be maintained for the constitutive equation to be invariant under change in observer. The reason is because each of the conjugate pairs has the same transformation properties.

2.4.3 Transformation Properties of Kinematic Field and Stress Measures

As stated earlier, the power conjugate pair has the same transformation properties. The transformation properties of relevant field are stated below. For the

kinematic fields, we have

$$\mathbf{F}^* = \mathbf{Q}\mathbf{F} \tag{2.10}$$

$$\mathbf{E}^* = \mathbf{E} \tag{2.11}$$

$$\mathbf{D}^* = \mathbf{Q}\mathbf{D}\mathbf{Q}^T \tag{2.12}$$

Where $\mathbf{Q}$ is the frame rotation, which is proper orthogonal tensor valued function of time alone.

$$\mathbf{P}^* = \mathbf{Q}\mathbf{P} \tag{2.13}$$

$$\mathbf{S}^* = \mathbf{S} \tag{2.14}$$

$$\sigma^* = \mathbf{Q}\sigma\mathbf{Q}^T \tag{2.15}$$

Based on the transformation of the stress and strain measures above, we can note that $\mathbf{D}$ is frame-indifferent as it transform like a tensor that it is. $\mathbf{E}$ is invariant while $\mathbf{F}$ is neither. The same properties hold for the conjugate stress measures respectively.

2.4.4 Definition of the Derivatives Used in the Model Development

In continuum mechanics there are two time derivatives, namely Lagragian and Eulerian or Material and Spatial derivatives. So given an field ω, it is written that the material time-derivative is

$$\frac{D\omega}{Dt} = \dot{\omega}(\mathbf{X}, t) = \frac{\partial \omega(\mathbf{X}, t)}{\partial t} \tag{2.16}$$

holding $\mathbf{X}$ fixed. The second derivative is the spatial derivative given as

$$\omega^{'}(\mathbf{X}, t) = \frac{\partial \omega(\mathbf{X}, t)}{\partial t} \tag{2.17}$$

holding $\mathbf{x}$, a spatial point, fixed. At this point, however, it is important to define that all derivatives are all Lagrangian (i.e. Material derivative) and ∇ is the gradient and Div or $\nabla \cdot ()$ is the divergence with respect to the material point $\mathbf{X}$. So $\dot{\overline{()}}$ is the derivative w.r.t to time t, holding the material point $\mathbf{X}$ fixed. The Material and spatial derivatives are related through the relationship for a scalar field

$$\dot{\omega} = \omega^{'} + \mathbf{v} \cdot grad\omega. \tag{2.18}$$

Where $grad$ is a spatial gradient. And for a vector field it is

$$\dot{\mathbf{g}} = \mathbf{g}^{'} + (grad\mathbf{g})\mathbf{v} \tag{2.19}$$

2.5 Fundamental Balance Laws of Continuum Thermodynamics

There are a balance laws that should hold at every point. They are discussed in this section and are used in the derivation of the constitutive model for SMAs presented in this work. These laws are axioms of continuum thermodynamics. The derivation is based on global balance laws for a part P of the body B. Using the requirement that the underlying regions be arbitrary, local balance laws in the form of partial differential equations are developed. Unlike classical continuum thermodynamics where discontinuity in field, velocities and deformation gradient are modeled by jump conditions, the order parameter gradient is used to ensure the fields are continuous.

2.5.1 Balance of Mass

The balance of mass is the statement that during motion, the mass of a continuum body never changes. So the mass is fixed or constant. Let P_t be a spatial region that convects with the body $\mathbf{B}$ so that $\mathrm{P}_t = \mathbf{y}(P)$ for some material region P. The

balance of mass mathematically in a nutshell is the requirement that

$$\overline{\int_{P_t} \rho dV}^{\cdot} = 0 \tag{2.20}$$

and a consequence, the local form can be derived as

$$\rho_o = J\rho \tag{2.21}$$

where ρ_0 is the density of in the reference configuration and ρ is the density in the deformed configuration.

2.5.2 Balance of Configurational (micro) Forces

The theory used requires that additional balance law for a system of configurational forces should be added. This system of forces includes in general a second order Stress tensor $\mathbf{C}$ analogous to Eshelby stress tensor, a vector internal force $\mathbf{p}$ and a vector external force $\mathbf{g}$, whereby the new kinematic descriptor in general will be a vector field like displacement based on the Newtonian forces. However, for the present use of the configurational system of forces, a scalar order parameter is used which necessitate the use of a scalar internal and external configurational force as well as vector stress measure per unit length to ensure consistency of the conjugate pairs. For details on how this order parameter related configurational forces are derived (see chapter 9 of Gurtin (2000)[102], Appendix of Fried and Gurtin 1994 and Gurtin (1996)). In this CFPA which utilize a scalar order parameter, configurational (micro)force systems accompanies the work done due to changes in the order parameter(η) . The forces are (1) a Configurational (micro) Stress ($\mathbf{d}$) vector. (2) a scalar internal configurational (micro) body force (p) ; and (3) a scalar external configurational (micro) body force (g) The configurational (micro) force balance

equation is

$$\int_{\partial P} \mathbf{d} \cdot \mathbf{n} dA + \int_{P} (p + g) dV = 0. \tag{2.22}$$

Where P is an arbitrary subregion of the reference body B The above global form of the configurational (micro) force balance, upon application of divergence theorem, results in the local form given as

$$\nabla \cdot \mathbf{d} + p + g = 0 \tag{2.23}$$

p is a dissipative forces (it is of such nature that energy is lost from a system when motion takes place. Of course energy is in general conserved but it is lost from the degrees of freedom of interest into heat). Also, in the context of the material (in this case for SMA), p is likened to forces exerted by the lattice on the atoms (to hold them in place) in their configuration, and therefore are intrinsic to the part (P). In order to properly understand the physical meaning of the configurational forces in the context of martensitic phase transformation, consider the configuration of a body as a lattice or network together with atoms that moves, microscopically relative to the lattice. Attention is focused on configuration (or arrangement) of atoms which are characterized by the order parameter. In the case of SMA, a configuration that is cubic (being austenite) is encoded by an order parameter value of zero in its continuum description; otherwise it has a value of 1 for martensite. The change in the order parameter being characteristic of the interface between the austenitic and martensitic domains and is represented by a gradient of the order parameter. Macroscopically, the effect of the microscopic phenomena of phase transformation is manifested through power expenditure or working as material transforms from one phase to another across the interface.

2.5.3 Balance of Atomic Species Mass

In addition to the standard balance of mass, which for incompressibility assumption reduces to constant density, there is another mass balance which relates to the diffusion of atomic species. This balance of mass is the requirement that the mass or number concentration (c)(a measure of density) of atomic species satisfy the following equation

$$\overline{\int_P c dV}^{\cdot} = -\int_{\partial P} \mathbf{J} \cdot \mathbf{n} dA + \int_P h dV, \tag{2.24}$$

where $\mathbf{J}$ is a vectorial species flux and h is a species supply. Note that $\overline{\int_p c}^{\cdot} dV = \int_p \dot{c} dV$. Upon application of the divergence theorem to term involving the species flux in equation 2.24,the localized form of the species mass balance becomes

$$\dot{c} = -\nabla \cdot \mathbf{J} + h \tag{2.25}$$

2.5.4 Balance of Linear and Angular Momentum

The balance laws associated with these standard (Newtonian) forces are the balance of linear and angular momentum. The balance of linear momentum is given as

$$\int_{\partial P} \mathbf{P}\mathbf{n} dA + \int_P \mathbf{b} dV = \overline{\int_P \rho \dot{\mathbf{y}}}^{\cdot} dV \tag{2.26}$$

The above global form of the balance of linear momentum, upon application of divergence theorem, results in the local form given as

$$\nabla \cdot \mathbf{P} + \mathbf{b} = \rho_0 \ddot{\mathbf{u}} \tag{2.27}$$

The global form of the balance of angular momentum is written as

$$\int_{\partial P} \mathbf{y} \times \mathbf{P}\mathbf{n} dA + \int_P \mathbf{y} \times \mathbf{b} dV = \overline{\int_P \mathbf{y} \times \rho \dot{\mathbf{y}} dV}^{\cdot} \tag{2.28}$$

which result in the local balance

$$\mathbf{P}\mathbf{F}^T = \mathbf{F}\mathbf{P}^T \tag{2.29}$$

By using the relationship between the first and second Piola Kirchhoff (PK) stress the balance of angular momentum for the second PK stress is

$$\mathbf{S} = \mathbf{S}^T \tag{2.30}$$

2.5.5 Balance of Energy

So far, the balance laws we described are based on two distinct system of forces: a configurational (micro) force system consisting of a stress **d**, an internal force p and an external force g which are subject to the balance law in Equation (2.23). The other standard (Newtonian) forces system consist of a stress **P** and a body forcre **b**,subject to Equation (2.27). The configurational (micro) force system works against changes in the order parameter while the working of **P** and **b** is given by the relation

$$W_0(P) = \int_{\partial P} \mathbf{P}\mathbf{n} \cdot \dot{\mathbf{y}} dA + \int_P \mathbf{b} \cdot \dot{\mathbf{y}} dV \tag{2.31}$$

The first postulate of continuum thermodynamics states that the time rate of change of the total energy (kinetic plus internal) of a continuum body is equal to the rate at which external mechanical work is done by surface and body forces and the thermal energy entering the boundary surface by heat flux and the heat sources. Essentially,

the time rate of change of total energy is a result of working and heating of the body. However, since there is an introduction of configurational forces, and for any arbitrary volume including the diffuse interface, there will be a contribution of working or power expenditure associated with the configurational forces. Although heating due to configurational forces is essentially a part of this theory, it will be neglected for now. The integrand of

$$\int_{\partial P} \mathbf{d}\cdot\mathbf{n}\dot{\eta}dA \tag{2.32}$$

$$\int_{P} p\dot{\eta}dV \tag{2.33}$$

$$\int_{P} g\dot{\eta}dV \tag{2.34}$$

are respectively (1) the working across ∂P by the configuration or lattice exterior to the part $\mathbf{P}$, but neighboring $\mathbf{P}$. (2) working on the atoms of P by the lattice as atoms are reordered when transformation takes place across the front (3) Working on the atoms of P by sources external to the continuum body Recall that based on the underlying theory, these forces are indeterminate for parts that do not lie at the evolving diffuse interface although the forces are present at every continuum point. Therefore in order for the parts used in energy balance to be arbitrary, the working due to configurational forces external to the part has to account for power expenditure due to the order parameter and these forces. In view of these two force systems, heat flux $\mathbf{q}$, absolute temperature (T) and the heat supply (r) per unit mass; the energy balance, which is the first postulate of thermodynamics is written in global form as

$$\dot{\int_{\partial P}(\rho\epsilon+\frac{1}{2}\rho|\mathbf{y}|^2}dV = \int_{\partial P}(\mathbf{P}\mathbf{n}\cdot\dot{\mathbf{y}}+(\mathbf{d}\cdot\mathbf{n})\dot{\eta}-\mathbf{q}\cdot\mathbf{n})dA+\int_{P}(\mathbf{b}\cdot\dot{\mathbf{y}}+\rho r+g\dot{\eta})dV. \tag{2.35}$$

The conventional power balance is given as [103, 104]

$$\int_{\partial P} \mathbf{P}\mathbf{n} \cdot \dot{\mathbf{y}} dA + \int_{\partial P} \mathbf{b} \cdot \dot{\mathbf{y}} dV = \int_P \mathbf{P} \cdot \dot{\mathbf{F}} dV + \overline{\int_P (\frac{1}{2}\rho|\dot{\mathbf{y}}|^2 dV} \tag{2.36}$$

Notice that because p is internal to the part, it doesn't enter into the energy balance-which is essentially based on contributions from external surface and body forces. By using divergence theorem on the configurational stress term,the conventional power balance equation 2.35 and equation (2.23),equation 2.36 becomes

$$\rho\dot{\epsilon} = -\nabla \cdot \mathbf{q} + \rho r + \mathbf{P} \cdot \dot{\mathbf{F}} + \mathbf{d} \cdot \dot{\nabla}\eta - p \cdot \dot{\eta}. \tag{2.37}$$

A linearized strain formulation is also derived that uses the balance of linear momentum and in the energy balance to get the local form. Now, since lagrange strain is to be used, the power conjugate pair of interest from now on is $\mathbf{S} \cdot \dot{\mathbf{E}}$. This imples that

$$\rho\dot{\epsilon} = -\nabla \cdot \mathbf{q} + \rho r + \mathbf{S} : \dot{\mathbf{E}} + \mathbf{d} \cdot \dot{\nabla}\eta - p\dot{\eta}. \tag{2.38}$$

2.5.6 Entropy Inequality: Second Law of Thermodynamics

Every admissible thermodynamic process must obey the entropy inequality at each time and for all material point in the body. The entropy inequality states that the rate of increase of entropy s in a fixed part (P) of a material is not less that the influx of entropy $\mathbf{q}/T$, across the surface of the part plus the entropy supply within the volume. It is mathematically expressed as

$$\frac{d}{dt}\int_P \rho s dV \geq -\int_{\partial P} \frac{\mathbf{q}}{T} \cdot \mathbf{n} dA + \int_P \rho \frac{r}{T} dV. \tag{2.39}$$

Where s is entropy per unit mass. By applying divergence theorem, and the quotient rule, the local form is

$$\rho\dot{s} \geq -\nabla \cdot \left(\frac{\mathbf{q}}{T}\right) + \frac{\rho r}{T} \tag{2.40}$$

Replace ρr in Equation (2.40) by its expression from Equation (2.38) and using the Legendre transformation

$$G = \epsilon - \frac{1}{\rho}\mathbf{S} \cdot \mathbf{E} - Ts \tag{2.41}$$

and using Equation(2.23)the entropy inequality becomes

$$-\rho\dot{G} - \rho\dot{T}s - \mathbf{E} \cdot \dot{\mathbf{S}} - p\dot{\eta} + \mathbf{d} \cdot \dot{\nabla}\eta - \frac{\mathbf{q}}{T} \cdot \nabla T \geq 0 \tag{2.42}$$

In addition, to capture dissipation in the atomic diffusion in an elastic solid, another form of the second law of thermodynamics is used. This imbalance of free energy is based on that embodies the intuitive notion that, for dissipative processes,*not all conventional power expended on a convecting spatial region can be converted into changes in the net free energy- and kinetic energy of the region, because a portion of that power must go into dissipation.* Such an imbalance is simply a mechanical manifestation of the first two laws of thermodynamics. In order to account for coupling of species diffusion with elastic deformation, such a balance is a mechanical version of the two laws of thermodynamics and accounts for working, not only due to Newtonian forces but also for that of the energy flow due to species transport, which is characterized through the chemical potentials, which are viewed as primitive quantities. For purely mechanical theory, basic to the theory of configurational forces is a mechanical form of the second law of thermodynamics for both stationary and migrating part. This form of the second law is based on free energy imbalance

and stated below

$$\overline{\int_P \psi dV}^{\cdot} \geq -\int_{\partial P} \mathbf{P}\mathbf{n}\cdot\dot{\mathbf{u}}dA + \int_P \mathbf{b}\cdot\dot{\mathbf{u}}dV - \int_{\partial P} \mu\mathbf{J}\cdot\mathbf{n}dA + \int_P \mu h dV + \int_{\partial P} (\mathbf{d}\cdot\mathbf{n})\dot{c}dA + \int_P g\dot{c} \tag{2.43}$$

Upon application of divergence theorem on the boundary terms, the configurational (micro) forces balance and using the fact the volume is arbitrary; the local form of the free-energy imbalance is given as

$$\dot{\psi} - \mathbf{P}\cdot\dot{\mathbf{F}} + (p-\mu) - \mathbf{d}\cdot\nabla\dot{c} + \mathbf{J}\cdot\nabla\mu \leq 0 \tag{2.44}$$

2.5.7 Summary of of Fundamental Thermodynamics Equations of This Work

The basic equation for the thermomechanical and species diffusion modeling are given below. Notice the addition of configurational forces.

$$\rho_0 = J\rho \tag{2.45}$$

$$\nabla\cdot\mathbf{d} + p + g = 0 \tag{2.46}$$

$$\dot{c} = -\nabla\cdot\mathbf{J} + h \tag{2.47}$$

$$\nabla\cdot\mathbf{P} + \mathbf{b} = \rho\ddot{\mathbf{u}} \tag{2.48}$$

$$\nabla\cdot\mathbf{S} + \mathbf{b} = \rho\ddot{\mathbf{u}} \tag{2.49}$$

$$\mathbf{P}\mathbf{F}^T = \mathbf{F}\mathbf{P}^T \tag{2.50}$$

$$\mathbf{S} = \mathbf{S}^T \tag{2.51}$$

$$-\rho\dot{G} - \rho\dot{T}s - \mathbf{E}\cdot\dot{\mathbf{S}} - p\dot{\eta} + \mathbf{d}\cdot\dot{\nabla}\eta - \frac{\mathbf{q}}{T}\cdot\nabla T \geq 0 \tag{2.52}$$

$$\dot{\psi} - \mathbf{P}\cdot\dot{\mathbf{F}} + (p-\mu) - \mathbf{d}\cdot\nabla\dot{c} + \mathbf{J}\cdot\nabla\mu \leq 0 \tag{2.53}$$

2.6 Thermomechanical Constitutive Modeling of Shape Memory Alloy

The following section describe constitutive model for SMA such that are thermodynamically consistent, such that all physically admissible thermomechanical process on SMA can be simulated. I employ a rational procedure that dates back to the likes of Coleman and Benard, Walter Noll and Truesdell which has been further used in detailed by Gurtin. My model is guided by features and variable observed from experimental results as described in the introduction section of this dissertation

2.6.1 Thermomechanical Constitutive Assumptions

The class of material describe here although later specified to shape memory alloys satisfy the following assumption of material class of

- the dynamic process is isochoric, so the constitute class is for incompressible material, therefore the density is constant
- Material is phase transforming under thermomechanical stimulus
- The strain measure can be additively decomposed into elastic transformation and thermal expansion part.

Therefore, the Green-Lagrange strain is taken to be separable in the sense of additive decomposition into elastic and a transformation. Using this decomposition, it is expected that large rotation will be captured.

$$\mathbf{E} = \mathbf{E}^e + \mathbf{E}_t(\eta) + \alpha_t(\eta)(T - T_0) \tag{2.54}$$

where $\mathbf{E}_t := \mathbf{E}^t \varpi(\eta)$, and $\mathbf{E}^t$ is the transformaton strain at thermodynamic equilibrium in the martensite phase.

2.6.2 Derivation of Constitutive Function for Thermomechanical Response of SMA

I now make the following anzats that the independent variable of our constitutive model are $[\mathbf{S}, \eta, \nabla\eta, \dot{\eta}, \mathbf{E}^t, T, \mathbf{z}]$. Where $\mathbf{z} = \nabla T$. $\mathbf{E}^t$ is the lagrangian transformation strain tensor. $\mathbf{S}$, T and $\mathbf{z}$ are basic to thermo-elastic theory. So by extension to model dynamics of solid-solid phase transformation that involve thermo-mechical process using continuum phase field approach, η is introduce to identify the phase present, $\nabla\eta$ is introduced to characterize the interfacial structure; $\dot{\eta}$ is introduced based on the hypothesis of an intrinsic rate dependence due to interface motion. While $\mathbf{E}^t$ is the Lagrangian transformation strain accompanying martensitic phase transformation. Now, I assume that the constitutive behavior of material points is characterized by the following response functions when the independent variables are known:

$$G = \hat{G}(\mathbf{S}, \eta, \nabla\eta, \dot{\eta}, \mathbf{E}^t, T, \mathbf{z}) \tag{2.55}$$

$$s = \hat{s}(\mathbf{S}, \eta, \nabla\eta, \dot{\eta}, \mathbf{E}^t, T, \mathbf{z}) \tag{2.56}$$

$$\mathbf{q} = \hat{\mathbf{q}}(\mathbf{S}, \eta, \nabla\eta, \dot{\eta}, \mathbf{E}^t, T, \mathbf{z}) \tag{2.57}$$

$$\mathbf{E} = \hat{\mathbf{E}}(\mathbf{S}, \eta, \nabla\eta, \dot{\eta}, \mathbf{E}^t, T, \mathbf{z}) \tag{2.58}$$

$$\mathbf{d} = \hat{\mathbf{d}}(\mathbf{S}, \eta, \nabla\eta, \dot{\eta}, \mathbf{E}^t, T, \mathbf{z}) \tag{2.59}$$

$$p = \hat{p}(\mathbf{S}, \eta, \nabla\eta, \dot{\eta}, \mathbf{E}^t, T, \mathbf{z}) \tag{2.60}$$

I based my method on Truesdell principle of equipresence. In this principle, Truesdell postulated that a quantity or independent variable that is present in one constitutive equation should be so present in all except if its presence does contradict some law of physics or rule of invariance. Inclusion of $\dot{\eta}$ in the response function of Gas well is jus-

tified by the need to ensure compatibility of every constitutive response function with the second law of thermodynamics and this is based on the Truesdell equipresence principle. As will be shown later it is proven that in order for the thermodynamics process in SMA to be consistent with the second law of thermodynamics, $\dot{\eta}$ should not be found in the free energy but in the internal configurational force p or the heat flux $\mathbf{q}$ Now, using chain rule

$$\dot{G} = \frac{\partial \hat{G}}{\partial S} \cdot \dot{\mathbf{S}} + \frac{\partial \hat{G}}{\partial T} \cdot \dot{T} + \frac{\partial \hat{G}}{\partial \eta} \cdot \dot{\eta} + \frac{\partial \hat{G}}{\partial \dot{\eta}} \cdot \ddot{\eta} + \frac{\partial \hat{G}}{\partial \nabla \eta} \cdot \dot{\nabla \eta} + \frac{\partial \hat{G}}{\partial \mathbf{E}^t} \cdot \dot{\mathbf{E}}^t + \frac{\partial \hat{G}}{\partial \mathbf{z}} \cdot \dot{\mathbf{z}}, \quad (2.61)$$

by insertion of $\dot{G}$ into Equation(2.42) and using Coleman-Noll procedure the following restrictions are placed on the constitutive response functions.

$$\mathbf{E} = -\rho \frac{\partial \hat{G}}{\partial \mathbf{S}}, \quad (2.62)$$

$$\mathbf{d} = \rho \frac{\partial \hat{G}}{\partial \nabla \eta}, \quad (2.63)$$

$$s = -\frac{\partial \hat{G}}{\partial T}, \quad (2.64)$$

$$-\mathbf{q} \cdot \mathbf{z}, \geq 0, \quad (2.65)$$

and that the response functions of the constitutive fields should only depend on the following independent variables

$$G = \hat{G}(\mathbf{S}, \eta, \nabla \eta, \mathbf{E}^t, T), \quad (2.66)$$

$$s = \hat{s}(\mathbf{S}, \eta, \nabla \eta, \mathbf{E}^t, T), \quad (2.67)$$

$$\mathbf{q} = \hat{\mathbf{q}}(\mathbf{S}, \eta, \dot{\eta}, \nabla \eta, \mathbf{E}^t, T, \mathbf{z}), \quad (2.68)$$

$$\mathbf{E} = \hat{\mathbf{E}}(\mathbf{S}, \eta, \nabla \eta, \mathbf{E}^t, T), \quad (2.69)$$

$$\mathbf{d} = \hat{\mathbf{d}}(\mathbf{S}, \eta, \nabla \eta, \mathbf{E}^t, T), \quad (2.70)$$

$$p = \hat{p}(\mathbf{S}, \eta, \dot{\eta}, \nabla\eta, \mathbf{E}^t, T, \mathbf{z}), \tag{2.71}$$

for the model to be thermodynamically consistent. The Coleman-Noll procedure is based on the premise that for all admissible processes, the second law must be satisfied regardless of how difficult it is to produce such process in the laboratory. As noted by Gurtin, the Coleman-Noll procedure has the same goal as variational procedures. Their goal is to ensure a properly invariant theory that is consistent with fundamental laws under the broadest given circumstances. The Coleman-Noll procedure is based on the premise that all conceivable or admissible processes, regardless of how hard it is to produce such process in the laboratory, should satisfy the second law of thermodynamics. The rational application of this procedure requires external forces and supplies that may be assigned arbitrarily to ensure satisfaction of the underlying balances in all processes. This may seem artificial, but it is no more artificial than theories based on virtual work, a paradigm that requires arbitrary variations, which are not guaranteed to be consistent with the resulting evolution equations, granted a constitutive description. The Coleman-Noll procedure makes explicit the external fields needed to support the "virtual processes" used, and in so doing ensures that these external fields, whether virtual or not, enter he theory in a thermodynamically consistent manner. As can be seen in the response functions, the intrinsic rate dependence and the temperature gradient can only enter the constitutive model through either the heat flux $\mathbf{q}$ or the internal configurational force p. There is nothing that suggests that the heat flux depends on the rate of the order parameter or the transformation rate, however, the internal configurational force being intrinsic to the material itself may manifest the inherent rate dependency more so that it relates to interface motion. So base on my hypothesis, the intrinsic rate dependency is introduced using the internal configurational force p. The reduced form

of the dissipation rate depends on the transformation strain as seen in the equation below

$$-(p\dot{\eta} + \rho\frac{\partial\hat{G}}{\partial\eta}\dot{\eta} + \rho\frac{\partial\hat{G}}{\partial\mathbf{E}^t} : \dot{\mathbf{E}}^t) \geq 0. \tag{2.72}$$

Now, since the order parameter is the sole kinematic descriptor which characterizes phase transformation and consequently dissipation, the inelastic strain or transformation strain $\mathbf{E}^t$ evolution is related to the order parameter rate according to the following equation

$$\dot{\mathbf{E}}^t = \Lambda\dot{\eta}, \tag{2.73}$$

$$\Lambda = \sqrt{\frac{3}{2}}\left[H\frac{\mathbf{S}^{'}}{\left\|\mathbf{S}^{'}\right\|}\right], \tag{2.74}$$

$$\mathbf{S}^{'} = \mathbf{S} - \frac{1}{3}tr(\mathbf{S}), \tag{2.75}$$

$$\left\|\mathbf{S}^{'}\right\| = \sqrt{\mathbf{S}^{'} : \mathbf{S}^{'}}. \tag{2.76}$$

The above equation is used to eliminate the transformation strain from the dissipation so that the order parameter (η) is the sole kinematic contributor to dissipation during thermomechanical response of SMA. The particular expression for the proportionality tensor Λ is motivated by three reasons (1) The model is developed to ensure that the transformation strain is stress driven (2) Experimental observation showed the formation of Luder's like band which is not plasticity. So taken expression that is based on deviatoric stress measure is necessary (3) the expression has been used in the internal state variable theory of phenomenological modeling of SMA using the maximum rate of transformation dissipation [58]. The transformation strain is eliminated from the reduced form of the second law of thermodynamics after restriction has been placed by the second law of thermodynamics. Now the following inequality holds for all $[\mathbf{S}, \eta, \nabla\eta, \dot{\eta}, \mathbf{E}^t, T, \mathbf{z}]$

$$-\pi_{dis}(\mathbf{S},\eta,\nabla\eta,\dot{\eta},\mathbf{E}^t,T)\dot{\eta}\geq 0, \tag{2.77}$$

$$\pi_{dis}=p+\rho\frac{\partial\hat{G}}{\partial\eta}+\rho\frac{\partial\hat{G}}{\partial\mathbf{E}^t}:\Lambda \tag{2.78}$$

$$-(p+\rho\frac{\partial\hat{G}}{\partial\eta}+\rho\frac{\partial\hat{G}}{\partial\mathbf{E}^t}:\Lambda)\dot{\eta}\geq 0. \tag{2.79}$$

Granted smoothness, the most general form of π_{dis} consistent with Equation(2.77) is

$$\pi_{dis}=-\tau\dot{\eta}, \tag{2.80}$$

where $\tau(\mathbf{S},\eta,\dot{\eta},\nabla\eta,\mathbf{E}^t,T,\mathbf{z})\geq 0$. In general τ is function of $[\mathbf{S},\eta,\dot{\eta},\nabla\eta,\mathbf{E}^t,T,\mathbf{z}]$, in which case is a generalization of the constant τ used for simulation for the response of the SMA in this work. A constant τ represent a Linear kinetic relation between the generalized flux $\dot{\eta}$ and its thermodynamic force conjugate π_{dis} similar to that utilized by Abeyartne and knowles. In this case π_{dis} represents the primary agent responsible for entropy production (dissipation) due to phase transformation. Essentially, π_{dis} is a "driving force" at the boundary of the phases while $\dot{\eta}$ is like the velocity of the interface which represents that rate at which material transform from a high energy state to a lower energy state depending on the stress-temperature conditions. Therefore equation 2.80 is a kinetic law for the change in the order parameter and it captures the motion of the interface which is considered diffuse. This motion of the interface represents progress of phase transformation. According to the 1st and second of equation 2.77 there are two contribution to the internal force: a contribution $\rho\frac{\partial G}{\partial\eta}+\rho\frac{\partial G}{\partial\mathbf{E}^t}\cdot\Lambda$ arising from change in the free energy and a dissipative contribution $\pi_{dis}=-\tau\dot{\eta}$. Now using $\mathbf{d}=\rho\frac{\partial G}{\partial\nabla\eta}$, the second of equations 2.77 and 2.80,in equations (2.23) gives the equation of evolution of order parameter as stated

in equation 2.81. The evolution equation of the order parameter when τ is taken to be constant is essentially a linear kinetic law following classical non-equilibrium, irreversible thermodynamics. The evolution equation provides the kinetic law that characterizes the evolution of the austenite and martensite phases.

$$\tau\dot{\eta} = \rho\nabla \cdot \left(\frac{\partial G}{\partial \nabla\eta}\right) - \rho\frac{\partial G}{\partial \eta} - \rho\frac{\partial G}{\partial \mathbf{E}^t} : \Lambda(\mathbf{S}') + g \tag{2.81}$$

The above equation in conjunction with a free energy of the form

$$G = G(\mathbf{S}, \eta, \nabla\eta, \mathbf{E}^t, T) = G^M(\mathbf{S}, \eta, \mathbf{E}^t) + G^{Th}(T) + \frac{1}{2}\lambda\left|\nabla\eta\right|^2, \tag{2.82}$$

is a necessary precondition to fully model the time evolution of SMA macroscopic phase transition. Where $\mathbf{S}$' is the deviatoric part of the second PK stress tensor. λ, the gradient energy per unit mass, is scalar because the interfacial energy is assumed isotropic. The final field equation that is yet undetermined is that of the heat flux $\mathbf{q}$. From the restriction placed by the second law of thermodynamics using the Coleman-Noll procedure, it was noted that the heat flux $\mathbf{q}$ must satisfy the inequality $\hat{\mathbf{q}}(\mathbf{S}, \eta, \dot{\eta}, \nabla\eta, \mathbf{E}^t, T, \mathbf{z}) \cdot \mathbf{z} \geq 0$ for the value of its arguments. Now if we assume that $\mathbf{q}$ is a linear function of $\mathbf{z}$, then the most general form of the constitutive equation for

$$\mathbf{q} = -\mathbf{K}(\mathbf{S}, \eta, \nabla\eta, \mathbf{E}^t, T, \mathbf{z})\mathbf{z} \tag{2.83}$$

where $\mathbf{K}$ is the conductivity tensor that is semi-definite. Now, if the conductivity tensor is taken to be isotropic, then $\mathbf{K} = k\mathbf{I}$. Therefore the heat flux constitutive equation becomes the Fourier law

$$\mathbf{q} = -\kappa\nabla T \tag{2.84}$$

2.6.3 Gibbs Free Energy Formulation

Now, free energy of the following form is proposed in keeping with the restriction imposed by the second law of thermodynamics for the field variables.

$$G = -\frac{1}{\rho}\mathbf{S} : \left[\frac{1}{2}S(\eta)\mathbf{S} + \alpha_t\left(T - T_o\right) + \mathbf{E}^t\varpi(\eta)\right] + c(\eta)\left[(T - T_o) - T\ln(\frac{T}{T_o})\right] \\ -s_o(\eta)T + \epsilon_o(\eta) + \frac{1}{2}\lambda\left|\nabla\eta\right|^2 \quad (2.85)$$

However, assuming the strain due to thermal expansion is negligible and the heat capacity is constant, we have

$$G = -\frac{1}{2\rho}\mathbf{S} : S(\eta)\mathbf{S} - \frac{1}{\rho}\mathbf{S} : \mathbf{E}^t\varpi(\eta) + c\left[(T - T_o) - T\ln(\frac{T}{T_o})\right] - s_o(\eta)T + \epsilon_o(\eta) + \frac{1}{2}\lambda\left|\nabla\eta\right|^2 \quad (2.86)$$

The above free energy is proposed based on the need for the function to not violate basic thermodynamics, the kinematic assumption (decomposition of strain) and the restriction placed on the free energy and the field variables by the second law of thermodynamics. To confirm this we realize that the above free energy satisfy the requirement that $G = \hat{G}(\mathbf{S}, \eta, \nabla\eta, \mathbf{E}^t, T)$ and there is neither dependency on $\dot{\eta}$ nor ∇T. Similarly

$$\mathbf{E} = -\rho\frac{\partial\hat{G}}{\partial\mathbf{S}} = S(\eta)\mathbf{S} + \mathbf{E}^t\varpi(\eta) \quad (2.87)$$

$$\mathbf{d} = \rho\frac{\partial\hat{G}}{\partial\nabla\eta} = \rho\lambda\nabla\eta \quad (2.88)$$

$$s = -\frac{\partial\hat{G}}{\partial T} = c\ln\frac{T}{T_0} + s_0(\eta) \quad (2.89)$$

All the above three equation are expected, based on both thermodynamics and unit consistency reasons for a measure of total strain that is decomposed into an elastic

and an inelastic (only present in martensite), a configurational stress vector as well as entropy. Which means that the form of the free energy proposed ensures thermodynamic consistency of the field variables. Now, the following interpolation of the properties of the SMA between the two phases austenite and martensite are proposed.

$$S = S^A + (S^M - S^A)m(\eta) \tag{2.90}$$

$$s_o = s_o^A + (s_o^M - s_o^A)f(\eta) \tag{2.91}$$

$$\epsilon_o = \epsilon_o^A + (\epsilon_o^M - \epsilon_o^A)\kappa(\eta) \tag{2.92}$$

$$\alpha_t = \alpha_t^A + (\alpha_t^M - \alpha_t^A)b(\eta) \tag{2.93}$$

$$c = c^A + (c^M - c^A)a(\eta) \tag{2.94}$$

Where

$$m(\eta) = m_1\eta^3 + m_2\eta^4 + m_3\eta^5 \tag{2.95}$$

$$\varpi(\eta) = \gamma_o\eta + \gamma_1\eta^2 \tag{2.96}$$

$$\gamma(\eta) = \eta\varpi(\eta) \tag{2.97}$$

$$\kappa(\eta) = \kappa_o\eta^2 + \kappa_1\eta^3 + \kappa_2\eta^4 \tag{2.98}$$

$$f(\eta) = f_o\eta^2 + f_1\eta^3 + f_2\eta^4 \tag{2.99}$$

$$b(\eta) = b_o\eta^2 + b_1\eta^3 + b_2\eta^4 \tag{2.100}$$

$$a(\eta) = a_o\eta^2 + a_1\eta^3 + a_2\eta^4. \tag{2.101}$$

The polynomials are essentially 2-3-4 polynomials, whose coefficients are determined to ensure that the thermo-chemical part of the free energy is double well (as classically used in phase field models). The calibration to make the polynomials double well is

the need to ensure that at stress-temperature conditions corresponding to different region of stability of each phase (as represented on the stress-temperature phase diagram) and the well of the energy is minimum. The strain energy comprise of a transition of elastic properties from austenite to martensite within region of their stability

2.6.4 Thermomechanical 3-D Field Equations

The three field equations of the thermo-mechanical macroscopic continuum phase field models are essentially the balances laws of configurational forces, linear momentum and energy that has been restricted by the second law of thermodynamics such that admissible process are captured by the model. The only additional condition needed to have a complete equation is nucleation criterion, which in this work is not considered. But the nucleus is seeded based on the stress-temperature phase diagram boundary of stability of the two phases. In general the field equations based on the three balance laws are

$$\nabla \cdot \left[\rho \frac{\partial G}{\partial \nabla \eta}\right] - \tau\dot{\eta} - \left(\frac{\partial G}{\partial \nabla \eta}\right) - \rho \frac{\partial G}{\partial \mathbf{E}^t} : \Lambda(\mathbf{S}') + g = 0 \tag{2.102}$$

$$\nabla \cdot \left[\rho \frac{\partial G}{\partial \mathbf{E}}\right] + \mathbf{b} - \rho\ddot{\mathbf{u}} = 0 \tag{2.103}$$

$$-\nabla\cdot\kappa\nabla T + \rho c\dot{T} - \left[\mathbf{S} : \Lambda\varpi(\eta) + \mathbf{S} : \mathbf{E}^t \frac{d\varpi}{d\eta} + \frac{1}{2}\mathbf{S} : \Delta\boldsymbol{S} : \mathbf{S}\frac{dm}{d\eta} - \rho\Delta\epsilon_o \frac{d\kappa}{d\eta} - p\right]\dot{\eta} - \rho r = 0. \tag{2.104}$$

which can be written as the field equations for the variables $\mathbf{u}$, T and η becomes

$$\tau\dot{\eta} = \frac{1}{2}\mathbf{S} : \Delta S : \mathbf{S}\frac{dm}{d\eta} + \mathbf{S} : \mathbf{E}^t \frac{d\varpi}{d\eta} + \rho\Delta s_o T\frac{df}{d\eta} - \rho\Delta\epsilon_o \frac{d\kappa}{d\eta} + \mathbf{S} : \Lambda\varpi + \rho\lambda\nabla^2\eta \tag{2.105}$$

which solves for the evolution of the order parameter field

$$\rho\ddot{\mathbf{u}} = \nabla \cdot \mathbf{S} + \mathbf{b} = \nabla \cdot \left[C(\eta) \left[\mathbf{E} - \mathbf{E}^t \varpi(\eta) \right] \right] \tag{2.106}$$

solves for the evolution of the displacement field, and

$$\rho c \dot{T} = -\nabla \cdot \mathbf{q} + \left[\mathbf{S} : \Lambda \varpi(\eta) + \mathbf{S} : \mathbf{E}^t \frac{d\varpi}{d\eta} + \frac{1}{2} \mathbf{S} : \Delta \boldsymbol{S} : \mathbf{S} \frac{dm}{d\eta} - \rho \Delta \epsilon_o \frac{d\kappa}{d\eta} - p \right] \dot{\eta} + \rho r \tag{2.107}$$

describes the evolution of the temperature field.

2.7 Model for Thermomechanical Response for Linear Elastic Phases

The above model derived using finite strain measures can be derived using infinitesimal strain. In that case the displacement gradient is small and there is negligible difference between the deformed and reference configuration. Therefore the strain measure becomes the linearized Lagrange strain or the infinitesimal strain ϵ and the stress measure becomes the Cauchy stress σ. Therefore, the constitutive restrictions becomes

$$\epsilon = -\rho \frac{\partial \hat{G}}{\sigma} \tag{2.108}$$

$$\mathbf{d} = \rho \frac{\partial \hat{G}}{\partial \nabla \eta} \tag{2.109}$$

$$s = -\frac{\partial \hat{G}}{\partial T} \tag{2.110}$$

The linear constitutive restrictions then required that

$$G = \hat{G}(\sigma, \eta, \nabla\eta, \epsilon^t, T) \tag{2.111}$$

$$s = \hat{s}(\sigma, \eta, \nabla\eta, \epsilon^t, T) \tag{2.112}$$

$$\mathbf{q} = \hat{\mathbf{q}}(\sigma, \eta, \dot{\eta}, \nabla\eta, \epsilon^t, T, \mathbf{z}) \tag{2.113}$$

$$\mathbf{E} \ = \hat{\epsilon}(\sigma, \eta, \nabla\eta, \epsilon^t, T) \tag{2.114}$$

$$\mathbf{d} = \ \hat{\mathbf{d}}(\sigma, \eta, \nabla\eta, \epsilon^t, T) \tag{2.115}$$

$$p = \hat{p}(\sigma, \eta, \dot{\eta}, \nabla\eta, \epsilon^t, T) \tag{2.116}$$

The transformation or inelastic strain evolution becomes

$$\dot{\epsilon^t} = \mathbf{\Lambda}\dot{\eta}, \tag{2.117}$$

$$\Lambda = \frac{3}{2}\left[H\frac{\sigma^{'}}{\bar{\sigma}^{'}}\right], \tag{2.118}$$

$$\sigma^{'} = \sigma - \frac{1}{3}tr(\sigma)\mathbf{I}, \tag{2.119}$$

$$\bar{\sigma}^{'} = \sqrt{\frac{3}{2}\left\|\sigma'\right\|^2}. \tag{2.120}$$

Consequently,

$$\tau\dot{\eta} = \rho\nabla\cdot\left(\frac{\partial G}{\partial\nabla\eta}\right) - \rho\frac{\partial G}{\partial\eta} - \rho\frac{\partial G}{\partial\epsilon^t} : \Lambda(\sigma') + g \tag{2.121}$$

The free energy can now be written as

$$G = -\frac{1}{2\rho}\sigma : S(\eta)\sigma - \frac{1}{\rho}\sigma : \epsilon^t\varpi(\eta) + c\left[(T - T_o) - T\ln(\frac{T}{T_o})\right] - s_o(\eta)T + \epsilon_o(\eta) + \frac{1}{2}\lambda\left|\nabla\eta\right|^2 \tag{2.122}$$

λ is scalar because the interfacial energy is assumed isotropic.

2.7.1 Linearized Field Equations

Now the linearized field equations for linear elastic phases are

$$\tau\dot{\eta} = \frac{1}{2}\sigma : \Delta S : \sigma\frac{dm}{d\eta} + \sigma : \epsilon^t\frac{d\varpi}{d\eta} + \rho\Delta s_o T\frac{df}{d\eta} - \rho\Delta\epsilon_o\frac{d\kappa}{d\eta} + \sigma : \Lambda\varpi + \rho\lambda\nabla^2\eta \tag{2.123}$$

$$\rho\ddot{\mathbf{u}} = \nabla\cdot\sigma + \mathbf{b} = \nabla\cdot\left[C(\eta)\left[\epsilon - \epsilon^t\varpi(\eta)\right]\right] + \mathbf{b} \tag{2.124}$$

$$\rho c\dot{T} = -\nabla \cdot \mathbf{q} + \left[\sigma : \Lambda\varpi(\eta) + \sigma : \epsilon^t \frac{d\varpi}{d\eta} + \frac{1}{2}\sigma : \Delta S : \sigma \frac{dm}{d\eta} - \rho\Delta\epsilon_o \frac{d\kappa}{d\eta} - p\right]\dot{\eta} + \rho r \tag{2.125}$$

Again, these field equations are simply the thermodynamically restricted balance of configurational forces, linear momentum and energy this is to ensure that the coupled field equation simulates all admissible thermomechanical processes during the thermomechanical loading of SMA.

2.7.2 1-D Simplification of Constitutive and Field Equation

SMA is mostly available and used industrially in wire form in which the relevant physics can be mathematically represented in 1-D form, therefore the current model is simplified into 1-D which will be used to simulate SMA wire as an axisymmetric rod experiencing only field variation only in the longitudinal direction. Now, simplifying the Gibbs free energy formulation for the linear elastic phases to 1-D becomes

$$G = -\frac{1}{2\rho}\sigma^2 S(\eta) - \frac{1}{\rho}\sigma H\gamma(\eta) + c\left[(T - T_o) - T\ln(\frac{T}{T_o})\right] - s_o(\eta)T + \epsilon_o(\eta) + \frac{1}{2}\lambda\left(\frac{\partial\eta}{\partial x}\right)^2 \tag{2.126}$$

and the field equations, assuming quasi-static loading, are

$$\tau\dot{\eta} = \frac{\sigma^2}{2}\left(\frac{1}{E^M} - \frac{1}{E^A}\right)\frac{dm}{d\eta} + \sigma H\frac{d\gamma}{d\eta} + \rho\Delta s_o T\frac{df}{d\eta} - \rho\Delta\epsilon_o\frac{d\kappa}{d\eta} + \rho\lambda\frac{\partial^2\eta}{\partial x^2}, \tag{2.127}$$

$$\frac{\partial}{\partial x}\left[E(\eta)\left(\frac{\partial u}{\partial x} - H\gamma\right)\right] + b_x = \rho\ddot{u} \tag{2.128}$$

and

$$\rho c\dot{T} = k\frac{\partial^2 T}{\partial x^2} + \left[\frac{\sigma^2}{2}\left(\frac{1}{E^M} - \frac{1}{E^A}\right)\frac{dm}{d\eta} + \sigma H\frac{d\gamma}{d\eta} - \rho\Delta\epsilon_o\frac{d\kappa}{d\eta} - p\right]\dot{\eta} + \rho r \tag{2.129}$$

Simplifying the thermomechanical coupled equation to 1-D, a fundamental assumption is made that the SMA specimen in consideration (e.g. a wire), is insulated at the surface and therefore there is no flux of heat within the rod at that surface. What this means is that there is no temperature gradient in the y and z direction for Cartesian co-ordinate or r and θ direction for cylindrical co-ordinate. The assumption of 1-D for a rod that is 3-D by taking the wire to be insulated surface in reality is really not true. The insulation assumption takes away the heat transfer at the surface, which after all remains part of the problem. Therefore, there is the need to somehow reintroduce this heat transfer into the mathematical description of the problem. One way this can be done is to assume or pretend that the amount of heat transfer occurring at the surface of the rod is, in fact, occurring as a loss of heat or heat sink from the system, uniformly distributed throughout the cross section of the rod. Addition of distributed heat sink restores the heat transfer at the surface approximately and the heat transfer at the surface is counted mathematically as consumption per unit volume term in the energy balance equation. The distributed heat sink will replace the source term ρr in equation (2.129). So at a position x where the temperature is $T(x)$ and for a slab of thickness Δx, the heat loss is

$$\left(\frac{heattransfer}{volume}\right) = \frac{(heatflux) * (surfacearea)}{volume} \tag{2.130}$$

where P is the length of the perimeter of the rod and A its cross-sectional area. For a circular rod $P = \pi d$ and $A = \pi(d/2)^2$. Therefore the field equation for temperature is now given as

$$\rho c\dot{T} = k\frac{\partial^2 T}{\partial x^2} + \left[\frac{\sigma^2}{2}\left(\frac{1}{E^M} - \frac{1}{E^A}\right)\frac{dm}{d\eta} + \sigma H\frac{d\gamma}{d\eta} - \rho\Delta\epsilon_o\frac{d\kappa}{d\eta} - p\right]\dot{\eta} - \frac{hPR(T(x,t) - T_\infty)}{A} \tag{2.131}$$

where h is the heat transfer coefficient and d is the diameter in the case of a rod and PR is the perimeter of the rod . Equation 2.131 now simplify to

$$\rho c\dot{T} = k\frac{\partial^2 T}{\partial x^2} + \left[\frac{\sigma^2}{2}\left(\frac{1}{E^M} - \frac{1}{E^A}\right)\frac{dm}{d\eta} + \sigma H\frac{d\gamma}{d\eta} - \rho\Delta\epsilon_o\frac{d\kappa}{d\eta} - p\right]\dot{\eta} - \frac{4h(T(x,t) - T_\infty)}{d} \tag{2.132}$$

. The one dimensional form of the balance of linear momentum under quasi-static loading assumption becomes

$$\frac{\partial}{\partial x}\left[E(\eta)\left(\frac{\partial u}{\partial x} - H\gamma\right)\right] = 0 \tag{2.133}$$

2.7.3 Non-Dimensionalization of Field Equations

The 1-D model is recast into the dimensionless form to generate non-dimensional field equations for the order parameter, dimensionless temperature and dimensionless displacement (and consequently stress). The dimensionless form of the equation for quasi-static (in the sense that inertia is negligible) results in five non-dimensional parameters of the model, all of which will be stated shortly. In addition, possible expressions to determine the two parameters that are introduced due to the kinetic law resulting from the configurational forces balance are also stated. The resulting dimensionless field equations are

$$\upsilon\frac{\partial\eta}{\partial t^*} = \beta\bar{\sigma}^2 m^{'} + \varphi H\bar{\sigma}\gamma^{'} + \mu f^{'}\theta - \zeta\kappa^{'} + \frac{\partial^2\eta}{\partial\chi^2} \tag{2.134}$$

$$\phi\frac{\partial\theta}{\partial t^*} = \varsigma\frac{\partial^2\theta}{\partial\chi^2} + \left\{\beta\bar{\sigma}m^{'} + \varphi H\bar{\sigma}\gamma^{'} - \zeta k^{'} + \frac{\partial^2\eta}{\partial\chi^2}\right\}\frac{\partial\eta}{\partial t^*} + \psi \tag{2.135}$$

$$\frac{\partial^2\bar{u}}{\partial t^{*2}} = \aleph\left(\frac{\partial}{\partial\chi}\left[\frac{E(\eta)}{E_c}\left(\frac{\partial\overline{u}}{\partial\chi} - H\gamma\right)\right] + b_x\right) \tag{2.136}$$

Now the dimensionless parameters that originally fall out of the dimensionless equations are

$$\upsilon = \frac{\tau x_c^2}{\Lambda t_c} \tag{2.137}$$

$$\beta = \frac{E_c^2 x_c^2 \Delta S}{\Lambda} \tag{2.138}$$

$$\varphi = \frac{x_c^2 E_c}{\Lambda} \tag{2.139}$$

$$\mu = \frac{\rho \Delta s_0 T_c x_c^2}{\Lambda} \tag{2.140}$$

$$\zeta = \frac{\rho \Delta \epsilon_0 x_c^2}{\Lambda} \tag{2.141}$$

$$\phi = \frac{T_c c x_c^2}{\Lambda} \tag{2.142}$$

$$\varsigma = \frac{k T_c t_c}{\Lambda} \tag{2.143}$$

$$\psi = \frac{\rho r x_c^2 t_c}{\Lambda} \tag{2.144}$$

$$\aleph = \frac{E_c t_c^2}{\rho x_c^2} \tag{2.145}$$

Now, for the non-dimensionalization, characteristic or intrinsic properties such characteristic time, length, modulus and temperature of the model are used to normalize the fields. The normalized form of these fields are given as

$$\chi = \frac{x}{x_c} \tag{2.146}$$

$$t^* = \frac{t}{t_c} \tag{2.147}$$

$$\bar{\sigma} = \frac{\sigma}{E_c} \tag{2.148}$$

$$\theta = \frac{T}{T_c}. \tag{2.149}$$

Now,if υ, β, μ and ζ are all set to unity, we can derive the characteristic properties which are intrinsic as

$$x_c = \sqrt{\frac{\rho\lambda}{\rho\Delta\epsilon_0}} \tag{2.150}$$

The characteristic length based on this equation is essentially the square root of the ratio of the gradient energy coefficient of the reference internal energy, which is related to the latent heat of transformation.

$$t_c = \frac{\tau}{\rho\Delta\epsilon_0} \tag{2.151}$$

The characteristic time is essentially the ratio of the dynamic viscosity" or kinetic coefficient to that of the reference internal energy, which is related to the latent heat of transformation..

$$E_c = \sqrt{\frac{\rho\Delta\epsilon_0}{\Delta S}} (2.152)$$

The intrinsic modulus of the problem is essentially the square root of the ratio of the change in reference internal energy, which is related to the latent heat of transformation to the compliance difference between austenite and martensite.

$$T_c = \frac{\Delta\epsilon_0}{\Delta s_0} \tag{2.153}$$

While the characteristic temperature is the ratio of the change in reference internal energy and change in reference entropy per unit mass.

$$\Delta S = \frac{1}{E^M} - \frac{1}{E^A} \tag{2.154}$$

Notice that $\rho\lambda$ relates to length scale and intrinsic modulus. τ relates to time scale from equation 2.151. After the earlier stated parameter have been set to unity, the

non-dimensional field equations becomes In this case we have

$$\frac{\partial \eta}{\partial t^*} = \bar{\sigma}^2 m^{'} + \varphi H \bar{\sigma} \gamma^{'} + f^{'} \theta - \kappa^{'} + \frac{\partial^2 \eta}{\partial \chi^2} \tag{2.155}$$

$$\phi \frac{\partial \theta}{\partial t^*} = \varsigma \frac{\partial^2 \theta}{\partial \chi^2} + \left\{ \bar{\sigma}^2 m^{'} + \varphi H \bar{\sigma} \gamma^{'} - k^{'} + \frac{\partial^2 \eta}{\partial \chi^2} \right\} \frac{\partial \eta}{\partial t^*} + \psi \tag{2.156}$$

$$\frac{\partial^2 \bar{u}}{\partial t^{*2}} = \aleph \left(\frac{\partial}{\partial \chi} \left[\frac{E(\eta)}{E_c} \left(\frac{\partial \overline{u}}{\partial \chi} - H \gamma \right) \right] + b_x \right) \tag{2.157}$$

and for quasi-static case the balance of linear momentum becomes

$$\frac{\partial}{\partial \chi} \left[\frac{E(\eta)}{E_c} \left(\frac{\partial \overline{u}}{\partial \chi} - H \gamma \right) \right] = 0 \tag{2.158}$$

In this case we have only five non-dimensional parameters φ, ς and ψ and ϕ and $\aleph$. These parameters are

$$\varphi^2 = \frac{1}{\rho \Delta \epsilon_0 \Delta S} \tag{2.159}$$

$$\phi = \frac{c}{\Delta s_0} \tag{2.160}$$

$$\varsigma = \frac{k \tau}{\Lambda \rho \Delta s_0} \tag{2.161}$$

$$\psi = \frac{\rho r \tau}{(\rho \Delta \epsilon_0)^2} \tag{2.162}$$

which actually in terms of the approximation made to lateral convection becomes

$$\psi = \frac{-4h(T - T_\infty)\tau}{d(\rho \Delta \epsilon_0)^2} \tag{2.163}$$

Upon inserting the expression for characteristic length (x_c), time (t_c) and modulus (E_c) based on the model parameter calibrated from experiment. The expression

becomes

$$\aleph = \frac{\tau^2}{\rho^2 \lambda} * \varphi \tag{2.164}$$

$$\aleph^2 = \frac{\tau^4}{\rho^4 \lambda^2} * \varphi^2 \tag{2.165}$$

Alternatively, we can choose appropriate choice for x_c, t_c , E_c and T_c rather than using the intrinsic dimensionless numbers. Possible choices are certain length scale in the problem, e.g. length of specimen, grain size e.t.c., and thermal time constant which is ratio of square of some system dimension such as length or diameter and that of thermal diffusivity. For temperature, we can choose the equilibrium temperature and for intrinsic modulus, we can choose modulus of austenite being the reference material state. For example I am planning to choose the following to non-dimensionalize with.

$$x_c = L, \tag{2.166}$$

$$t_c = \frac{L^2}{\alpha}, \tag{2.167}$$

$$E_c = E^A, \tag{2.168}$$

$$T_c = \frac{A_s + M_s}{2}. \tag{2.169}$$

where L is the specimen length or diameter or certain length dimension ,$\alpha = \frac{k}{\rho c}$ is thermal diffusivity. If these dimensionless parameters are used, we have

$$\upsilon = \frac{\alpha \tau}{\Lambda} \tag{2.170}$$

$$\beta = \frac{E_A^2 L^2 \Delta S}{\Lambda} \tag{2.171}$$

$$\varphi = \frac{L^2 E_A}{\Lambda} \tag{2.172}$$

$$\mu = \frac{\rho \Delta s_0 (A_s + M_s) L^2}{2\Lambda} \tag{2.173}$$

$$\zeta = \frac{\rho \Delta \epsilon_0 L^2}{\Lambda} \tag{2.174}$$

$$\phi = \frac{(A_s + M_s) \rho c L^2}{2\Lambda} \tag{2.175}$$

$$\varsigma = \frac{k(A_s + M_s) L^2}{2\alpha\Lambda} \tag{2.176}$$

$$\psi = \frac{\rho r L^4}{\alpha\Lambda} \tag{2.177}$$

2.7.4 Understanding the Meaning of Non-Dimensional Parameters

As noted earlier, there are five non-dimensional parameters that come out of the fully coupled model developed in this work. Each one of them has the meaning of coupling phenomena of conduction, convection, phase transformation and mechanical deformation and wave propagation,labelled as $\varphi^2, \phi, \psi, \varsigma, \aleph$. Each of this parameter has a meaning of relating the different phenomena prevalent in a full structural analysis of an SMA using thermomechanical coupled field equations of this model. These phenomena are heat conduction, heat convection, phase transformation and elastic wave propagation under dynamic (impact) loading. Now each of the non-dimensional parameter gives insight into how the different phenomena are coupled, particularly the times scale. So the first non-dimensional parameter

$$\varphi^2 = \frac{1}{\rho \Delta \epsilon_0 \Delta S} = \frac{1}{E_c^2 \Delta S^2}, \tag{2.178}$$

$$\varphi = \frac{1}{E_c \Delta S} \tag{2.179}$$

seem to relate the modulus of the system. It is the inverse of the product of the intrinsic modulus and the change in compliance of the martensite and austenite.

Therefore the non-dimensional parameter is a measure of the intrinsic compliance of the system scaled by the inverse of difference in elastic compliance of the SMA phases. Now, since the entropy change does not have a ready physical meaning in the model compared to the change in internal energy as it is hard to measure entropy through any experimental means. The second and third non-dimensional parameter actually have physical meaning when the change in entropy parameter is removed by diving both parameters ϕ and ς In order to understand the meaning of the other four non-dimensional parameters coming out of the dimensionless field equations, Note that they are related to the intrinsic properties of SMA that are derived from the coupled system of field equations, it is important to note some important time scale of the different phenomena present in a typical SMA response. These time scales are

$$t_c = \frac{\tau}{\rho \Delta \epsilon_0} \tag{2.180}$$

$$t_{cond} = x_c^2/\alpha \tag{2.181}$$

$$t_{conv} = \frac{d(\rho \Delta \epsilon_0)}{4h(T - T_\infty)} \tag{2.182}$$

$$t_{wp} = \frac{x_c}{\sqrt{E_c/\rho}} \tag{2.183}$$

Where t_c is the time scale of phase transformation, t_{cond} is the well-known time scale of heat conduction, t_{conv} is the time scale for heat convection out of the SMA rod and t_{wp} is the time scale of wave propagation through SMA in the light of the moving transformation front. Notice that t_{wp} carries a similar expression as that of the classical time scale for wave propagation in an homogeneous elastic solid usually written as

$$t = \frac{L}{C_L} \tag{2.184}$$

$$C_L = \sqrt{\frac{\lambda_h + 2\mu_h}{\rho}} \tag{2.185}$$

where λ_h and μ_h are the Lame's constant. Now having defined the time scales, it could be shown that

$$\psi = \frac{-4h(T - T_\infty)\tau}{d(\rho\Delta\epsilon_0)^2} \equiv \frac{Timescale of phase transformation}{Timescale of convection} \tag{2.186}$$

$$\iota = \frac{\phi}{\varsigma} = \frac{x_c^2}{\alpha}\frac{\rho\lambda}{\tau x_c^2} \equiv \frac{Timescale of heat conduction}{Timescale of phase transformation} \tag{2.187}$$

$$\aleph = \left(t_c^2 \frac{E_c}{\rho x_c^2}\right) \equiv \left(\frac{Timescale of phase transformation}{Timescale of wave propagation}\right)^2 \tag{2.188}$$

$\aleph$ is proportional to φ^2 which relates change in compliance of the SMA to the latent heat of transformation.

2.7.5 Calibration to Experiment-Determination of Unknown Model Coefficient in Terms of Experimental Parameters

The condition for austenite and martensite stability is used to calibrate the model so as to obtain a landau type free energy in the sense that at different temperature and stress the condition of stability and instability of austenite and martensite are met at the boundary corresponding to the Clasius Clapeyron slope on the stress-temperature phase diagram ($C^A and C^m$). For vanishing stress, the boundary of martensite stability (upon heating or unloading) is the austenite start temperature (A_s)and the boundary for austenite stability upon cooling or loading is the martensite start temperature (M_s). The equilibrium phase transition temperature is determined by the condition that in both phases the Gibbs free energies are equal. The equilibrium phase transition temperature is determined by the condition that in both phases the Gibbs free energies are equal. This equilibrium temperature is the foremost temperature for phase transition to occur upon heating and cooling. However, super

cooling and super heating leads to hysteresis, hence the reason for the difference between Austenite start temperature and martensite start temperature. Falk assumed the temperature for Austenite start and martensite start based on the equilibrium temperature. However based on standard practice of the stress-temperature phase diagram, and assume linear relationship, A_s and M_s can be determined. The idea behind the calibration of the model is the requirement that at high temperature above the austenite start temperature for zero stress (which is the boundary for the stability of austenite) the free energy function should have a single minimum only at vanishing order parameter (i.e. an order parameter value of zero which correspond to austenite phase) which is the condition for the stability of austenite at T $\geq$A$_s$. While at temperature lower than M_s, the only minimum should correspond to non-vanishing order parameter- which in this case is taken to have a value of 1 for the martensite phase. At intermediate temperature, the free energy is expected to have minima corresponding to both phases (i.e. austenite and martensite). A single free energy applies to both phases and based on the choice of the free energy, it is expected that at $T > T_0$ the martensite phase is metastable and $T < T_0$, the high temperature phase (austenite) is metastable. Essentially, the martensite phase becomes unstable at $T = A_s$ which implies that austenite is the only stable phase at $T \geq A_s$. Similarly, for $T \leq M_s$ for austenite phase. In the present formulation, the calibration is taken to be such that the only a single variant of martensite is favored as the load is high enough to bias the variant. Since the martensitic transformation is a 1st order phase transition, there exists phase equilibrium such that at certain stress and temperature range, both phases may be in equilibrium and therefore may coexist. Below are the final equations for the coefficient of the polynomials introduced to ensure a double

well potential of the free energy as seen in Equations

$$f_0 = \frac{6C_M}{C_A + C_M} \tag{2.189}$$

$$f_1 = \frac{4C_A - 2C_M}{C_A + C_M} \tag{2.190}$$

$$f_2 = \frac{-3(C_A - C_M)}{C_A + C_M} \tag{2.191}$$

$$\kappa_0 = \frac{6C_M M_s}{A_s C_A + C_M M_s} \tag{2.192}$$

$$\kappa_1 = \frac{4A_s C_A - 2C_M M_s}{A_s C_A + C_M M_s} \tag{2.193}$$

$$\kappa_2 = \frac{-3(A_s C_A - C_M M_s)}{A_s C_A + C_M M_s} \tag{2.194}$$

$$\Delta\epsilon_0 = \frac{-(A_s C_A - C_M M_s)H}{2\rho} \tag{2.195}$$

$$\Delta s_0 = \frac{-(C_A + C_M)H}{2\rho} \tag{2.196}$$

In addition there are five additional coefficients that results in just numbers $\gamma_0 = 3$,$\gamma_1 = -2$,$m_1 = 10$,$m_2 = -15$,$m_3 = 6$. Details of the derivation of the above set of equation is given in Appendix A.

2.8 Derivation of Constitutive Response Function for Diffusion in Elastic Solid Modeling of Precipitation in SMA

The approach used to derive this model is essentially not different from that of the last section in essence except that the balance of species mass across the interface is added to the balance laws. Also, the order parameter is now the concentration(c) of diffusing species (which is conserved). **J** is mass flux and h is external species mass

supply. Following an approach similar to that of the thermo-mechanical case, and using the configurational (micro) force balance and the species mass balance, I now make the following anzats that the independent variable of my constitutive model are $[\mathbf{F}, c, \nabla c, \dot{\eta}, \mu, \nabla\mu]$. The concentration is assumed to only change in the matrix and accross the diffuse interface.

I consider that the constitutive behavior of material points is characterized by the following response functions when the independent variables are known:

$$\psi = \hat{\psi}(\mathbf{F}, c, \nabla c, \dot{c}, \mu, \nabla\mu) \tag{2.197}$$

$$\mathbf{J} = \hat{\mathbf{J}}(\mathbf{F}, c, \nabla c, \dot{c}, \mu, \nabla\mu) \tag{2.198}$$

$$\mathbf{d} = \hat{\mathbf{d}}(\mathbf{F}, c, \nabla c, \dot{c}, \mu, \nabla\mu) \tag{2.199}$$

$$\mathbf{P} = \hat{\mathbf{P}}(\mathbf{F}, c, \nabla c, \dot{c}, \mu, \nabla\mu) \tag{2.200}$$

$$p = \hat{p}(\mathbf{F}, c, \nabla c, \dot{c}, \mu, \nabla\mu) \tag{2.201}$$

Notice that in this modeling approach, the chemical potential and its gradient enter in as independent variable, unlike the way it is classically defined as a function of the concentration. Here it enters the constitutive equation along with the concentration and its gradient. Similarly, the strain and stress measure used ensure that the constitutive response be invariant under changes in observer. By using the Coleman-Noll procedure on the dissipation inequality (resulting from the local form of the second law) to place restriction on the constitutive equation, the restricted constitutive equations becomes

$$\psi = \hat{\psi}(\mathbf{F}, c, \nabla c) \tag{2.202}$$

$$\mathbf{J} = \hat{\mathbf{J}}(\mathbf{F}, c, \nabla c, \dot{c}, \mu, \nabla\mu) \tag{2.203}$$

$$\mathbf{d} = \hat{\mathbf{d}}(\mathbf{F}, c, \nabla c) \tag{2.204}$$

$$\mathbf{P} = \hat{\mathbf{P}}(\mathbf{F}, c, \nabla c) \tag{2.205}$$

$$p = \hat{p}(\mathbf{F}, c, \nabla c, \dot{c}, \mu, \nabla \mu) \tag{2.206}$$

and the micro-stress and the 1st PK stress are given as

$$\mathbf{d} = \frac{\partial \hat{\psi}(\mathbf{F}, c, \nabla c)}{\partial \nabla c} \tag{2.207}$$

$$\mathbf{P} = \frac{\partial \hat{\psi}(\mathbf{F}, c, \nabla c)}{\partial \mathbf{F}}. \tag{2.208}$$

Finally, the following inequality comes out as the reduced form of the dissipation and must be satisfied for all $[\mathbf{F}, c, \nabla c, \dot{c}, \mu, \nabla \mu]$

$$\pi_{dis}(\mathbf{F}, c, \nabla c, \dot{c}, \mu, \nabla \mu)\dot{c} + \hat{\mathbf{J}}(\mathbf{F}, c, \nabla c, \dot{c}, \mu, \nabla \mu) \cdot \nabla \mu \leq 0, \tag{2.209}$$

$$\pi_{dis}(\mathbf{F}, c, \nabla c, \dot{c}, \mu, \nabla \mu)\dot{c} = \hat{p}(\mathbf{F}, c, \nabla c, \dot{c}, \mu, \nabla \mu) + \frac{\partial \hat{\psi}(\mathbf{F}, c, \nabla c)}{\partial c} - \mu \tag{2.210}$$

In order for inequality in equation 2.209 to hold all the time, then π_{dis} must have the following expression

$$\pi_{dis}(\mathbf{F}, c, \nabla c, \dot{c}, \mu, \nabla \mu) = -\delta(\mathbf{F}, c, \nabla c, \dot{c}, \mu, \nabla \mu)\dot{c} - \mathbf{b} \cdot \nabla \mu \tag{2.211}$$

$$\hat{\mathbf{J}}(\mathbf{F}, c, \nabla c, \dot{c}, \mu, \nabla \mu) = -\mathbf{a}\dot{c} - \mathbf{M}\nabla \mu, \tag{2.212}$$

where $\mathbf{a} = \hat{\mathbf{a}}(\mathbf{F}, c, \nabla c, \dot{c}, \mu, \nabla \mu)$ and $\mathbf{b} = \hat{\mathbf{b}}(\mathbf{F}, c, \nabla c, \dot{c}, \mu, \nabla \mu)$ are vectors and the existence of a constitutive modulus $\delta(\mathbf{F}, c, \nabla c, \dot{c}, \mu, \nabla \mu)$ (a scalar). By combining this with the configurational (micro) force balance leads to an expression for the

chemical potential, given as

$$\mu - \mathbf{b} \cdot \nabla\mu = \frac{\partial\hat{\psi}(\mathbf{F}, c, \nabla c)}{\partial c} - \nabla \cdot \frac{\partial\hat{\psi}(\mathbf{F}, c, \nabla c)}{\partial \nabla c} + \delta\dot{c} - g \tag{2.213}$$

The above equation simplifies to

$$\mu = \frac{\partial\hat{\psi}(\mathbf{F}, c, \nabla c)}{\partial c} - \nabla \cdot \frac{\partial\hat{\psi}(\mathbf{F}, c, \nabla c)}{\partial \nabla c} + \delta\dot{c} - g \tag{2.214}$$

for isotropic material, in which case $\mathbf{b} = \mathbf{0}$. The kinetic equation for the evolution of the concentration field can now be derived by inserting, equation 2.213 and the second of equation of 2.211 into the balance of diffusing species, equation 2.25. This equation upon assumption of constant δ yield

$$\dot{c} = \nabla \cdot \mathbf{M}\nabla[\frac{\partial\hat{\psi}(\mathbf{F}, c, \nabla c)}{\partial c} - \nabla \cdot \frac{\partial\hat{\psi}(\mathbf{F}, c, \nabla c)}{\partial \nabla c} + \delta\dot{c} - g] + h \tag{2.215}$$

2.8.1 3-D Field Equations for Diffusion in Elastic medium

In general the three field equations of this model including inertia for two phase elastic solid are

$$\dot{c} = \nabla \cdot \mathbf{M}\nabla\mu + h \tag{2.216}$$

$$\nabla \cdot [\frac{\partial\hat{\psi}(\mathbf{F}, c, \nabla c)}{\partial \mathbf{F}}] + \mathbf{b} = \rho\ddot{u} \tag{2.217}$$

$$\mu = \frac{\partial\hat{\psi}(\mathbf{F}, c, \nabla c)}{\partial c} - \nabla \cdot \frac{\partial\hat{\psi}(\mathbf{F}, c, \nabla c)}{\partial \nabla c} + \delta\dot{c} - g \tag{2.218}$$

Notice that the field equations are simply the balance of species mass, the balance of linear momentum and the equation of the chemical potential μ

2.9 Model Form in Linear Elastic Phases

As noted earlier, shape memory alloy are material that do not have very large elastic deformation, therefore the continuum theory can be simplified into that of linear elastic solid by linearization of the finite strain theories to infinitesimal strain and appropriate stress measures. The section will focus on that simplification of the model to linear elastic phase. This is the form of the model that is implemented for the result in this work For diffusion of atomic species in an elastic phase, the strain measure is now the infinitesimal strain tensor. As a result the stress measure also becomes the Cauchy stress σ as often used in linear elasticity, so just like the derivation above, the restricted constitutive equation now becomes

$$\psi = \hat{\psi}(\epsilon, c, \nabla c) \tag{2.219}$$

$$\mathbf{J} = \hat{\mathbf{J}}(\epsilon, c, \nabla c, \dot{c}, \mu, \nabla \mu) \tag{2.220}$$

$$\mathbf{d} = \hat{\mathbf{d}}(\epsilon, c, \nabla c) \tag{2.221}$$

$$\sigma = \hat{\sigma}(\epsilon, c, \nabla c) \tag{2.222}$$

$$p = \hat{p}(\epsilon, c, \nabla c, \dot{c}, \mu, \nabla \mu). \tag{2.223}$$

The micro-stress and cauchy stress are given as

$$\mathbf{d} = \frac{\partial \hat{\psi}(\epsilon, c, \nabla c)}{\partial \nabla c} \tag{2.224}$$

$$\sigma = \frac{\partial \hat{\psi}(\epsilon, c, \nabla c)}{\partial \epsilon}. \tag{2.225}$$

Finally, the following inequality comes out as the reduced form of the dissipation and must be satisfied for all $[\epsilon, c, \nabla c, \dot{c}, \mu, \nabla\mu]$

$$\pi_{dis}(\epsilon, c, \nabla c, \dot{c}, \mu, \nabla\mu)\dot{c} + \hat{\mathbf{J}}(\epsilon, c, \nabla c, \dot{c}, \mu, \nabla\mu) \cdot \nabla\mu \leq 0, \tag{2.226}$$

$$\pi_{dis}(\epsilon, c, \nabla c, \dot{c}, \mu, \nabla\mu)\dot{c} = \hat{p}(\epsilon, c, \nabla c, \dot{c}, \mu, \nabla\mu) + \frac{\partial\hat{\psi}(\epsilon, c, \nabla c)}{\partial c} - \mu \tag{2.227}$$

$$\pi_{dis}(\epsilon, c, \nabla c, \dot{c}, \mu, \nabla\mu)\dot{c} = -\delta(\epsilon, c, \nabla c, \dot{c}, \mu, \nabla\mu)\dot{c} - \mathbf{b} \cdot \nabla\mu \tag{2.228}$$

$$\hat{\mathbf{J}}(\epsilon, c, \nabla c, \dot{c}, \mu, \nabla\mu) = -\mathbf{a}\dot{c} - \mathbf{M}\nabla\mu, \tag{2.229}$$

where $\mathbf{a} = \hat{\mathbf{a}}(\epsilon, c, \nabla c, \dot{c}, \mu, \nabla\mu)$ and $\mathbf{b} = \hat{\mathbf{b}}(\epsilon, c, \nabla c, \dot{c}, \mu, \nabla\mu)$ are vectors and the existense of a constitutive modulus $\delta(\epsilon, c, \nabla c, \dot{c}, \mu, \nabla\mu)$ (a scalar). By combining this with the configurational (micro) force balance leads to an expression for the chemical potential, given as

$$\mu - \mathbf{b} \cdot \nabla\mu = \frac{\partial\hat{\psi}(\epsilon, c, \nabla c)}{\partial c} - \nabla \cdot \frac{\partial\hat{\psi}(\epsilon, c, \nabla c)}{\partial\nabla c} + \delta\dot{c} - g \tag{2.230}$$

The above equation simplifies to

$$\mu = \frac{\partial\hat{\psi}(\epsilon, c, \nabla c)}{\partial c} - \nabla \cdot \frac{\partial\hat{\psi}(\epsilon, c, \nabla c)}{\partial\nabla c} + \delta\dot{c} - g \tag{2.231}$$

2.9.1 3-D Field Equations Diffusion in Linear Elastic Medium

Now the three linear elastic field equations to be solved for the different field variable for the problem including inertia for linear elastic two phase material like SMA are

$$\dot{c} = \nabla \cdot \mathbf{M}\nabla\mu + h \tag{2.232}$$

$$\nabla \cdot [\frac{\partial\hat{\psi}(\epsilon, c, \nabla c)}{\partial\epsilon}] + \mathbf{b} = \rho\ddot{u} \tag{2.233}$$

$$\mu = \frac{\partial \hat{\psi}(\epsilon, c, \nabla c)}{\partial c} - \nabla \cdot \frac{\partial \hat{\psi}(\epsilon, c, \nabla c)}{\partial \nabla c} + \delta \dot{c} - g \tag{2.234}$$

Assuming linear elastic phases, the final form of the free energy and other constitutive fields such as species flux, micro-traction and internal micro force can be derived. Combining them appropriately with the balance of linear and angular momentum, while using isotopic mobility, leads to the following basic equations. The free energy is taken to have the following form

$$\widehat{\psi} = U(c, \epsilon) + f(c) + \frac{1}{2}\kappa \left|\nabla c\right|^2 . \tag{2.235}$$

$U(c, \epsilon)$ is the mechanical strain energy, $f(c)$is the chemical energy that is double well whose wells defines the precipitate and the matrix, and $\frac{1}{2}\kappa \left|\nabla c\right|^2$ represent interfacial energy. The mobility tensor $\mathbf{M}$ is taken to be isotropic, therefore it becomes

$$\mathbf{M} = M\mathbf{I} \tag{2.236}$$

It important to note that for this model the form of the field equation used quasi-static mechanical equilibrium equation, the terms δ and g are set to zero for the current implementation in this work. Therefore the model reduces to the classical Cahn-Hilliard equation for the evolution of the concentration of diffusing species in an elastically stressed solid. Therefore, the relevant equations are

$$\nabla \cdot (\sigma) = \mathbf{0} \tag{2.237}$$

where

$$\sigma = \frac{\partial U(c, \epsilon)}{\partial \epsilon}, \tag{2.238}$$

and

$$\mu = f^{'}(c) + \frac{\partial U(c,\epsilon)}{\partial c} - \kappa \Delta c. \tag{2.239}$$

It is important to note that in the current model the form of equation solved is dimensionless, therefore the concentration is normalized and therefore has a value of zero in the matrix and a value of one in the precipitate. So given, an initial microstructure, the future evolution can be studied by solving the coupled field equations for the phase transition. The coherency strain due to lattice mismatch between the precipitate and the matrix, taken to be dilatational, is given as

$$\varepsilon = \beta \epsilon^t \mathbf{I} \tag{2.240}$$

The stiffness tensor of the precipitate matrix system taken to be interpolated between that of the matrix and precipitate for the normalized concentration, which is one in precipitate and zero in matrix. Therefore the stiffness tensor is given as

$$C(c) = \overline{C} + \hbar(c)\Delta C \tag{2.241}$$

$$\Delta C = C^p - C^m \tag{2.242}$$

$$\hbar(c) = \left\{ c^3 \left(10 - 15c + 6c^2 \right) - \frac{1}{2} \right\} \tag{2.243}$$

$$\overline{C} = \frac{1}{2} \left[C^p - C^m \right] \tag{2.244}$$

where $\hbar(c)$ is an interpolation polynomials. From the micromechanics of an inclusion in a matrix, then, we can see that $\overline{C}$ represents the effective elastic modulus of the macroscopic homogeneous system. If the diffusion source h is zero, then the dimensionless field equation solved for the present models with negligible inertia are

$$\dot{c} = \nabla \cdot \mathbf{M} \nabla \mu, \tag{2.245}$$

$$\mu = 2\Gamma c(1-c)(1-2c) - 2\alpha_c \nabla^2 c + \frac{1}{2}\hbar^{'}(c)\epsilon^e : \nabla C : \epsilon^e - \beta^{'}(c)\epsilon^t C : \epsilon^e, \quad (2.246)$$

$$\nabla \cdot \Big[C(c) \Big[\epsilon - \epsilon^t \beta(c) \Big] \Big] = \mathbf{0} \quad (2.247)$$

The above three field equation has the displacement, concentration and chemical potential as the constitutive fields.

3. NUMERICAL IMPLEMENTATION AND SIMULATION OF PRECIPITATE GROWTH

The discussion in this chapter is motivated by the need to simulate the evolution of precipitate in an elastically stresses solid using the model for diffusion in an elastically stressed solid as described earlier in Chapter 2. In addition, although the results are qualitative in this chapter, they serve to show the breadth of capability and strength of the modeling and implementation approach used; which will be demonstrated to yield more qualitative results in chapter 4 and 5. Capability of a 3-D implementation and simulation of transformation by phase boundary motion is also a consequence of the results.

Development of such capability is particularly useful for precipitate morphology and subsequently SMA microstructure design. SMAs are often aged to developed fine precipitate with the intention of improving their toughness (resistance to dislocation motion) changing the path of transformation as well as to shift the martensitic transformation temperature such as M_s [38, 40, 105]. Fine Ni_4Ti_3 precipitates increase the strength of the austenite and limit the degree of plastic deformation during martensitic transformation under temperature or load cycling. So, the path and M_s of SMA can be altered by controlling the size and density of Ni_4Ti_3. However, the high sensitivity of M_s to Nickel concentration and the small sizes of coherent Ni_4Ti_3 precipitate require experimental method with very high accuracy and spatial resolution in the measurement. Such precision in measurement and consequently cost of equipment imposes a very serious challenge [38, 40]. Therefore, it is desirable to use computational methods to complement the experimental efforts in exploring the influence of fine precipitate on martensitic transformation. In the light of the above

need, qualitative simulations are carried out with the elasto-diffusion model as an attempt towards a more physical result in the future. The results in this chapter is intended to demonstrate the capability of the model to capture qualitative salient features of precipitate formation in an elastically stressed solid which is representative of the formation of finely dispersed Ni_4Ti_3 in NiTi SMA.

It is the goal of this chapter to demonstrate that this model is useful (qualitatively for the present form of free energy) to simulate diffusion controlled precipitate formation in SMAs. The depletion of concentration fields around precipitate, which has been experimentally measured, is well captured. The stress field expected around an inclusion in a matrix (known from micromechanics), the effect of elastic anisotropy and inhomogeneity are all captured qualitatively as well.

It is important to note that the current model is useful only for coherent precipitates. Fully coherent interphases occur when two crystals match perfectly at the interface plane so that the two lattices are continuous across the interface. For a material having a coherent interface, within the bulk of each phase, every atom has an optimum arrangement of nearest neighbors that produces a low energy. However, at the interface there is usually change in composition so that each atom is partly bonded to wrong neighbors across the interface. The interaction increases the energy of the interfacial atoms and leads to a chemical contribution to the interfacial energy. If the distance between atoms of, say, two crystals are identical, there are no strains generated. However, whenever the distance between the atoms in the interfaces is not identical it is possible to maintain coherency by stretching one or both of the two lattices. The resultant lattice distortions are known as the coherency strains which result in coherency stress and coherent strain energy. In SMA coherency strain develop due to composition difference between the austenite B_2 structure and Ni_4Ti_3 phase because the formation of the Ni_4Ti_3 is by Ni atom diffusion, and the atom

of Ni is 149pm and that of Titanium is 176pm with atomic size difference of about 0.8466, the strain energy is expected to be more important than the interfacial energy in determining the equilibrium shape of the precipitate.[2]. So it is important to account for coherency elastic strain energy effect on precipitate morphology.

The strain energy is a product of misfit strain due to compositional difference between the precipitate and matrix. Precipitates with coherent interfaces have a low interfacial energy, but in the presence of misfit, they are associated with coherency strain energy. If the same precipitate has non-coherent interfaces, it will have a higher interfacial energy but the coherency strain energy will be absent.

One major challenge of simulating the formation of precipitate in SMA is the ability to couple, in a transient manner, the concentration of diffusing species and the mechanical field arising from the elastic strain energy due to coherency. In other words, modeling the kinetics of diffusion mediated phase transformation in an elastically stressed solid is been challenging. The presentation in this chapter promises a way to address the challenges. One thing to note from the beginning is that the word equilibrium as used in this chapter is not really a thermodynamic equilibrium in the sense that not change can occur anymore in all thermodynamic fields but a steady state.

3.1 Numerical Implementation in COMSOL Multiphysics

The developed model is implemented in COMSOL Multiphysics as well in 2-D and 3-D. The field equation resulting from the balance of species mass, the balance of configurational forces and the balance of linear momentum discussed in earlier chapter which are a set of PDEs are solved using COMSOL Multiphysics(a commercial finite element code). Two of the coupled PDEs are implemented in the PDE interface of COMSOL. The solid mechanics module in COMSOL is used to solve the

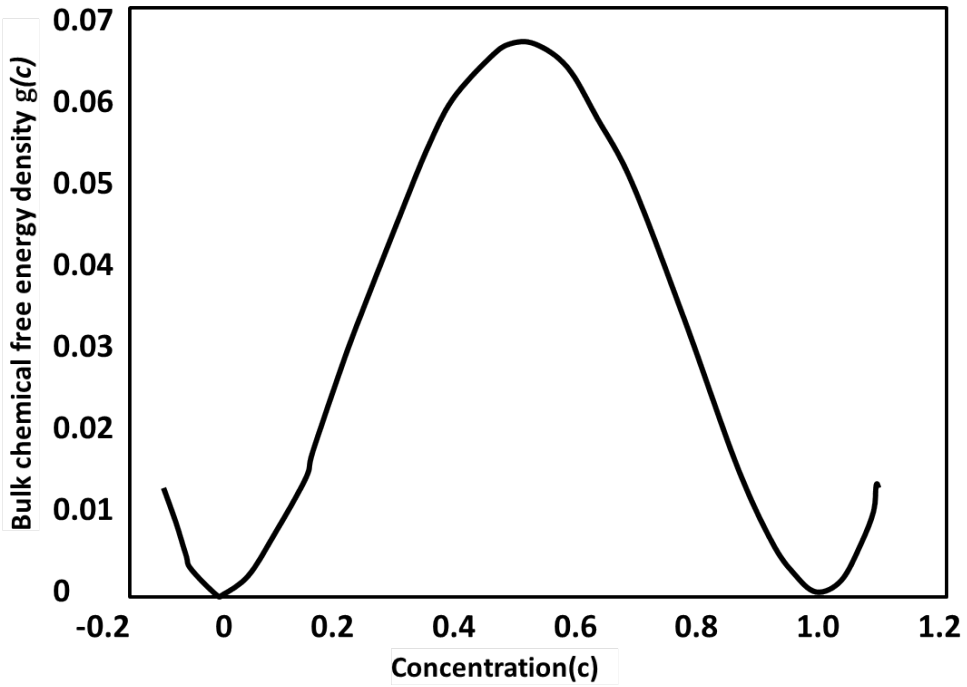

Figure 3.1: Chemical free energy as a function of the normalized concentration field

balance of linear momentum which comprises the coherency strain.

A unit cell of precipitate in a matrix is used with a periodic boundary condition imposed on all the eight sides of the cubic RVE. The precipitate is initially seeded as a circle in 2-D and a sphere in 3-D to represent an isotropic nucleus with isotropic interfacial energy. Once the nucleus is seeded, the three set of coupled PDEs are then solved to evolve the precipitate, which then grows into equilibrium size and shape as dictated by these evolution laws. In order to resolve the sharp gradient of field at the diffuse interface, an adaptive mesh refinement tool, present in COMSOL is used. The adaptive mesh capability ensured that the meshes at the interface during the growth of the precipitate has small enough meshes to properly approximate the geometry and consequently better approximate the underlying physics of the diffuse interface. It is important to note here that the simulations reported in this chapter takes several

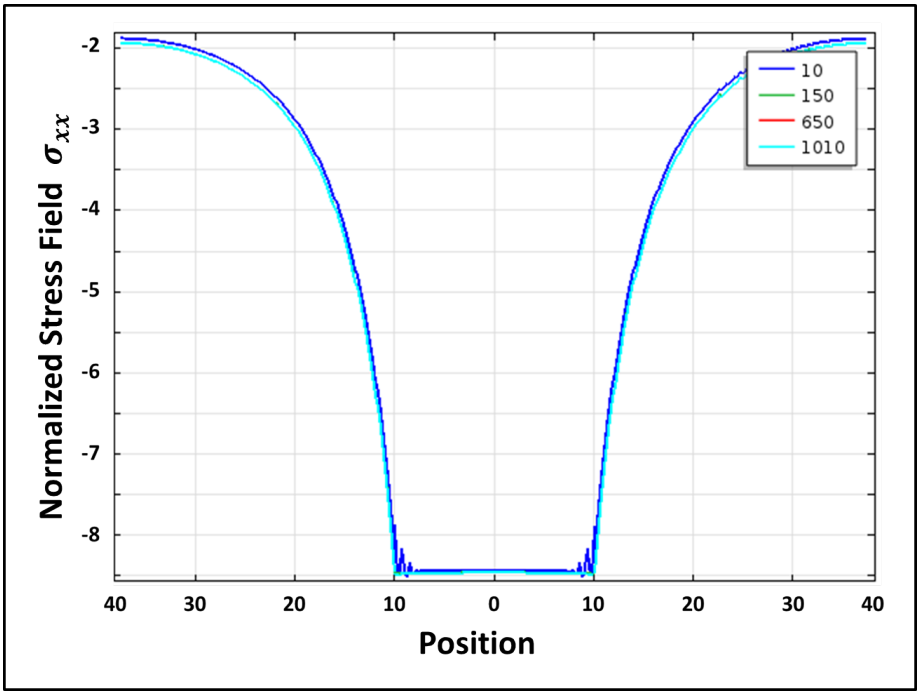

Figure 3.2: Stress field in the x-direction (σ_{xx}) around a coherent precipitate

hours to days to get to equilibrium configuration. In order to capture the minimum of the free energy for the two equilibrium phase (matrix and precipitate), a double well potential is used. Figure 3.1 is a plot of the double well potential which is a very crude approximation of the problem. However, the results are qualitatively representative of the actual problem. Future work should involve incorporation of thermodynamically consistent double well potential based on material parameters as will be demonstrated in chapter and .

3.2 2-D Precipitate Growth Simulation

This section describes the results of the simulations carried out for two dimensional circular precipitate in a matrix. Discussion on the effect of diffusion, precipitate-matrix elastic inhomogeneity, material anisotropy and equilibrium morphology will be described.

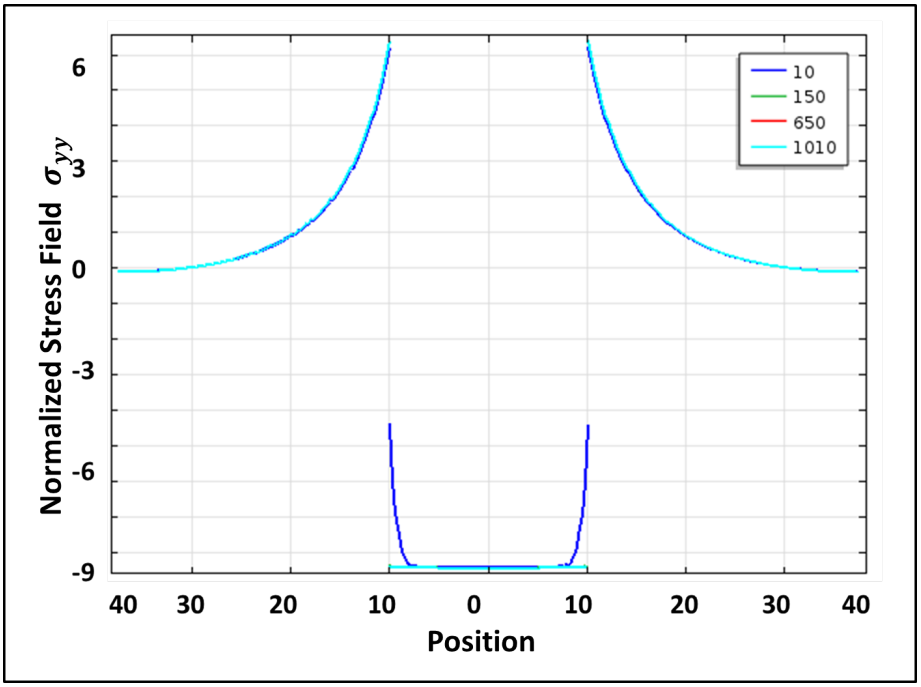

Figure 3.3: Stress field in the y-direction (σ_{yy}) around a coherent precipitate

3.2.1 Diffusion Driven Growth of Inclusion in an Elastic Solid

One of the major contributions of this chapter, as noted earlier, is the implementation of coupled elastic and diffusion field to simulate kinetics of diffusion driven precipitate evolution. In order to verify the implementation, the stress field around an isotropic precipitate in an isotropic matrix is plotted for the axial stress σ_{xx} and the transverse stress σ_{yy}. The results are shown in figures 3.2 and 3.3. The stress field is dimensionless since they are intended to be qualitative and verify the implementation and the ability of the model to capture the expected trend. Comparing the stress field to simulation in earlier works and micromechanics, the implementation is verified as correct. The transverse stress field exhibits a sharp rise at the interface and the decays to value of zero at the far field. The observation is correct because there is no far field stress applied, therefore the rise in stress at the interface decays

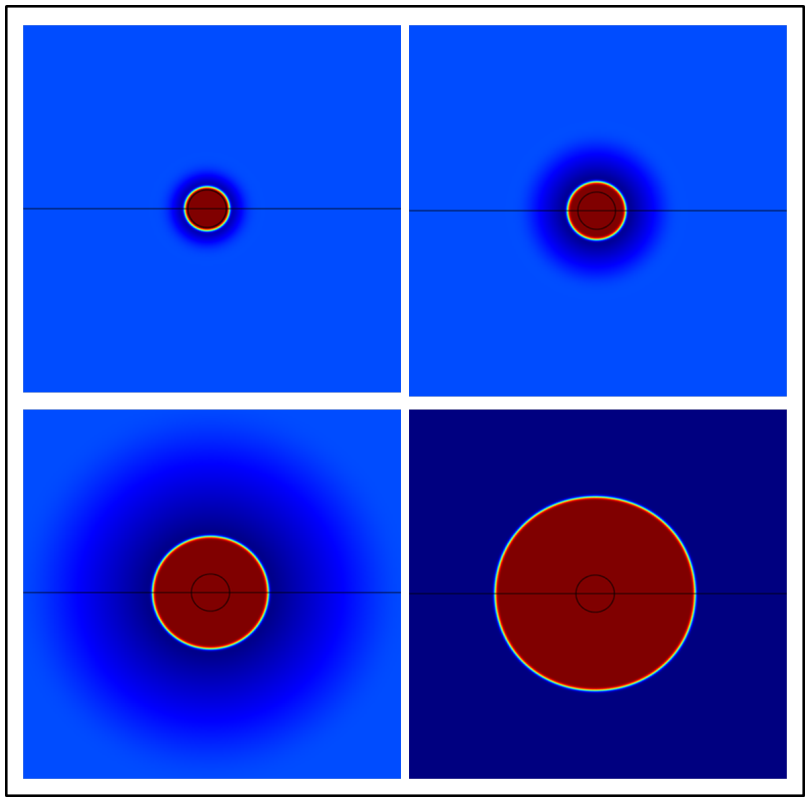

Figure 3.4: Pure diffusion growth of precipitate

as the distance increases form the interface. The axial stress also shows an expected trend of a very high compressive axial stress close to and within the precipitate-matrix interface which becomes less compressive farther from the interface. The trends are also the same as reported by Hu and Chen [106]. The advantage here is that, apart from 3-D implementation that will be discussed shortly, the implementation allows for the simulation of evolution of the precipitate under simultaneous fully coupled diffusion and elastic deformation fields. So, this stress field is the coherency stress that arises from constitutive relation with the coherency strain that result from mismatch at the interface.

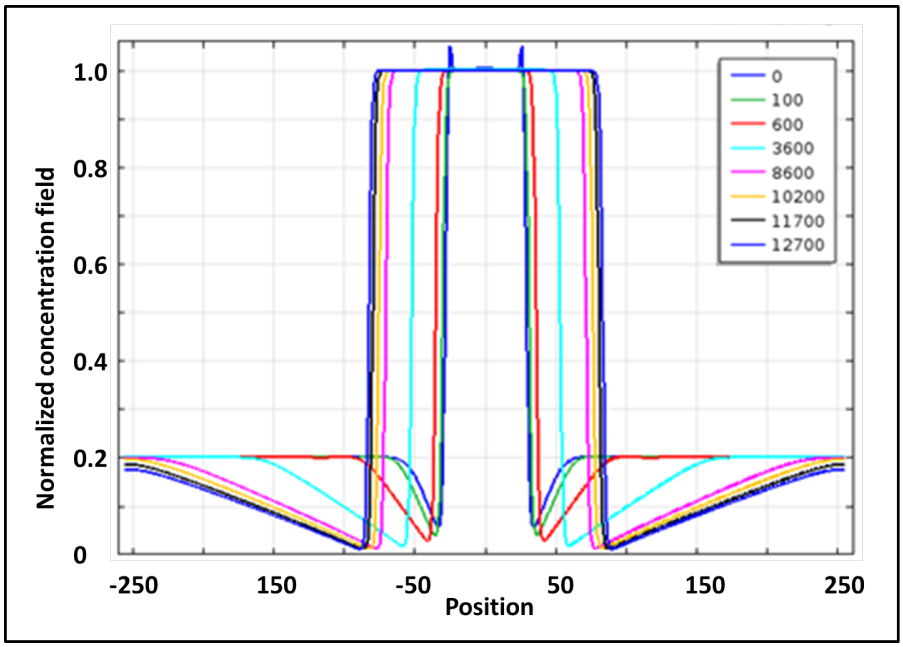

Figure 3.5: Concentration field around a circular precipitate in an isotropic matrix

3.2.2 Discussion on Isotropic 2-D Growth of Single Precipitate

Growth of a circular precipitate without mechanical coupling is presented in figure 3.4. The plot shows how initially a very small circular precipitate grows as diffusion progresses across the interface to enrich the precipitate to form equilibrium circular precipitate. The equilibrium morphology is spherical as the gradient energy coefficient is scalar, representing an isotropic interfacial behavior. A characteristic of precipitate growth during aging of SMA is the depletion of concentration around the precipitate. Figure 3.5 is a normalized concentration field showing depletion of concentration near the precipitate. For the simulation, the matrix has an initial normalized concentration of 0.2 and the precipitate seeded has a normalized concentration of 1. The precipitate is therefore unstable as it lies below the inflexion point of the double well potential. So the precipitate is enriched as the matrix close

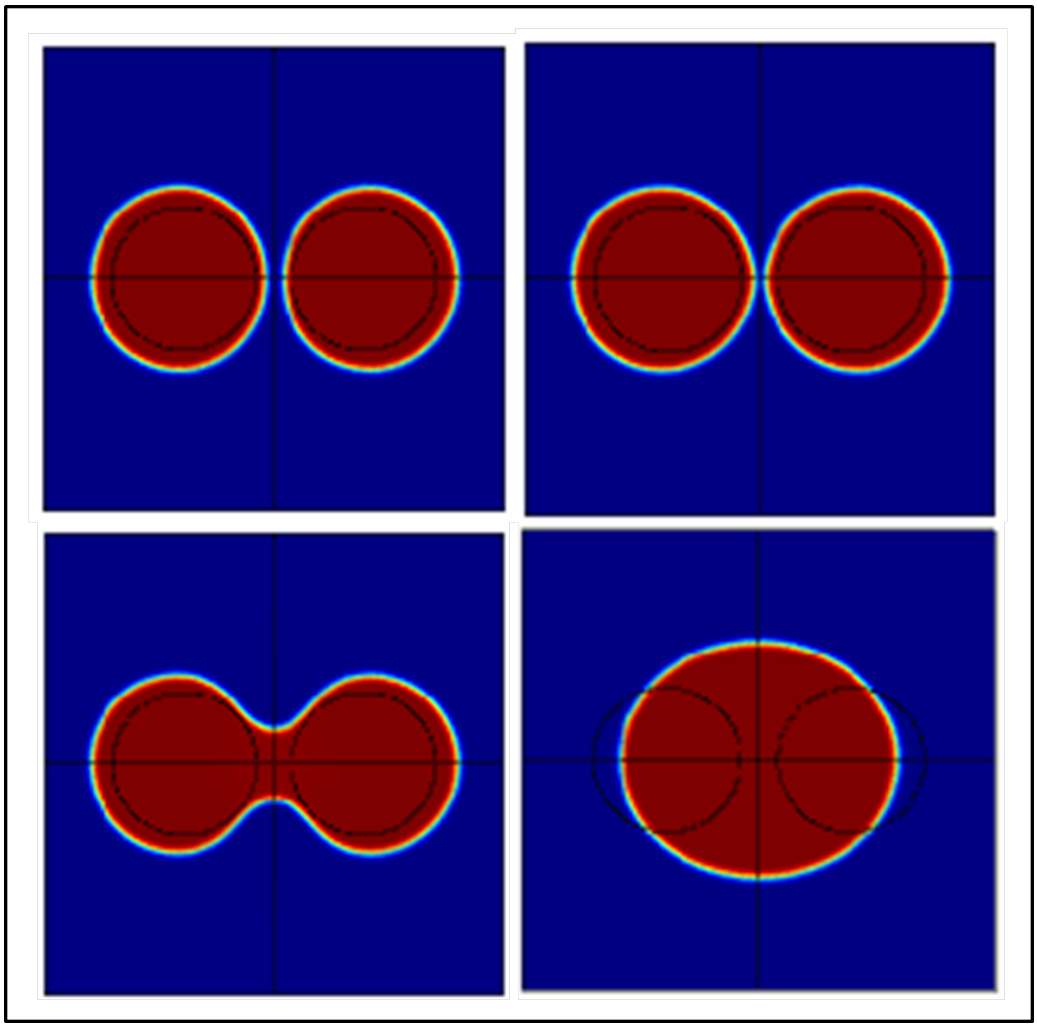

Figure 3.6: Coarsening of precipitate under pure diffusion driven growth of precipitate

to the precipitate is depleted of concentration. Unlike classical Ficks diffusion, the direction of flow of species is not necessarily from high concentration to low concentration but from high chemical potential to low chemical potential. It is important to note that concentration field plots in Figure 3.5 does not include equilibrium concentration field. A t equilibrium, the concentration in the matrix becomes zero. However, note that as transformation progress the concentration is driving towards

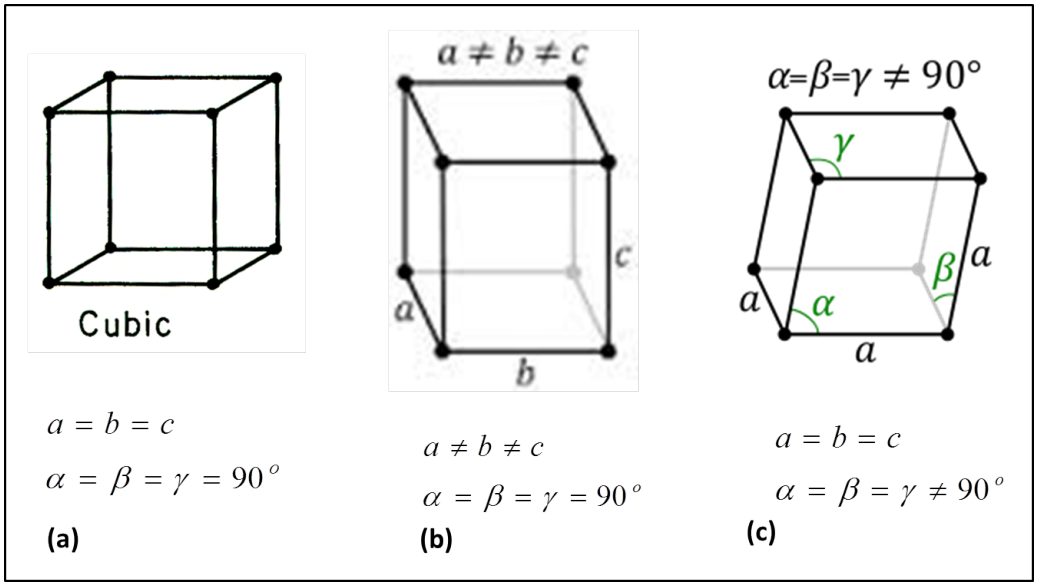

Figure 3.7: Representation of (a) cubic symmetric (b) Orthorhombic symmetric and (c) Rhombohedral symmetric crystals

zero as the slope of the depleted curve changes and becomes less steep. This result also serves to verify the implementation and lends some credibility to the ability of the model to qualitatively capture the physics of precipitate growth.

3.2.3 Discussion on Isotropic 2-D Growth and Coarsening of Two Precipitates

In a typical SMA, during aging, a precipitate nucleates and grows such that they merge with adjacent precipitate resulting in precipitate coarsening. So, the elasto-diffusion model is used to simulate the growth of two precipitate that are within very close proximity to each other. Figure 3.6 shows two precipitate coarsening. The features shown are representative of simulation from other works in the literature such as the work of P.H. Leo et al[107]. This result demonstrates the ability of the model to capture growth of multiple precipitate. It is also important to note that the result in figure 3.6 is representative of the evolution of microstructure under pure diffusion without the effect of coherency strain. Therefore, it is a qualitative

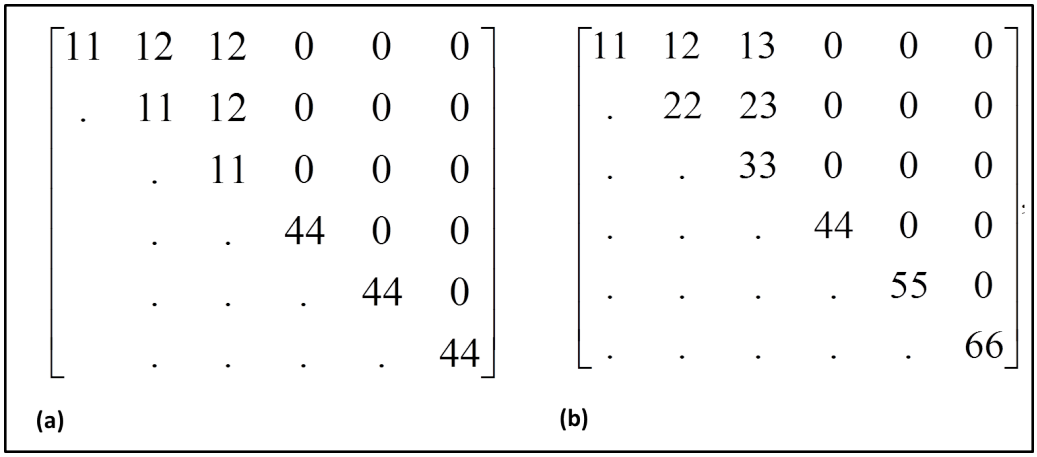

Figure 3.8: Representative stiffness tensor for (a) cubic and (c) orthorhombic symmetric crytal

description at best. However, the predictions follow what is expected.

3.3 Effect of Material Anisotropy

In order to account for the anisotropic elastic behavior of the precipitate and the matrix within which it grows, the elastic stiffness tensor representative of the crystal structure of the precipitate and the matrix is used in the stiffness tensors of the constitutive equation of the mechanical field as described in equation 2.241. Figure 3.7a, b and c are an example for three crystal lattices unit cell for a cubic, orthorhombic and rhombohedra crystals respectively. These different crystals will result in different stiffness tensor. Example of generalized form of representative elastic stiffness tensors for a cubic and orthorhombic crystals are presented in figure 3.8 a and b. These numerical values of the component of the stiffness tensors will be determined by the basic elastic properties of the different material, which for SMA is cubic for austenite matrix. First, the growth of a precipitate with a cubic elastic property in a cubic matrix is simulated using the implemented model within COMSOL. As shown in figure 3.9 the precipitate is seeded to be initially a circle of

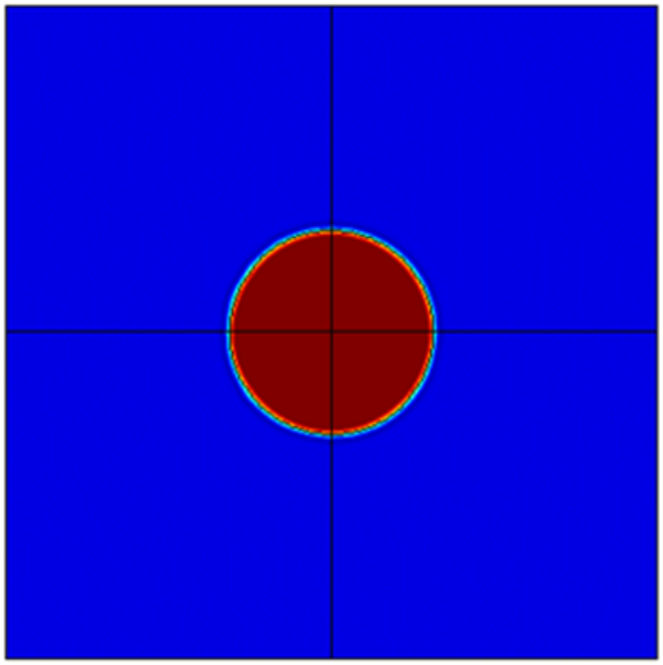

Figure 3.9: Initial size and shape of the precipitate with cubic symmetric in a cubic matrix

radius of about 40 unit in a square matrix RVE of about 200 unit sides. The initial condition is that the precipitate has a normalized concentration with numerical value of 1 and the matrix has a concentration value of 0.2. This will result in a difference in the chemical potential between the two phases. The potential of the precipitate is lower than that of the matrix. The difference in potential then drives the diffusion from matrix to precipitate, which results in the growth of the precipitate. What was observed is that initially the precipitate grows as a circle because its shape was dominated by the interfacial energy which is isotropic. However, after a few time units, the precipitate shape begins to change from circular to a cubic shape. The shape is being determined by the elastic strain energy, which dominates as the precipitate size increases. Notice that because the initial size of the precipitate is relatively bigger, the shape change occurs faster before much growth takes place.

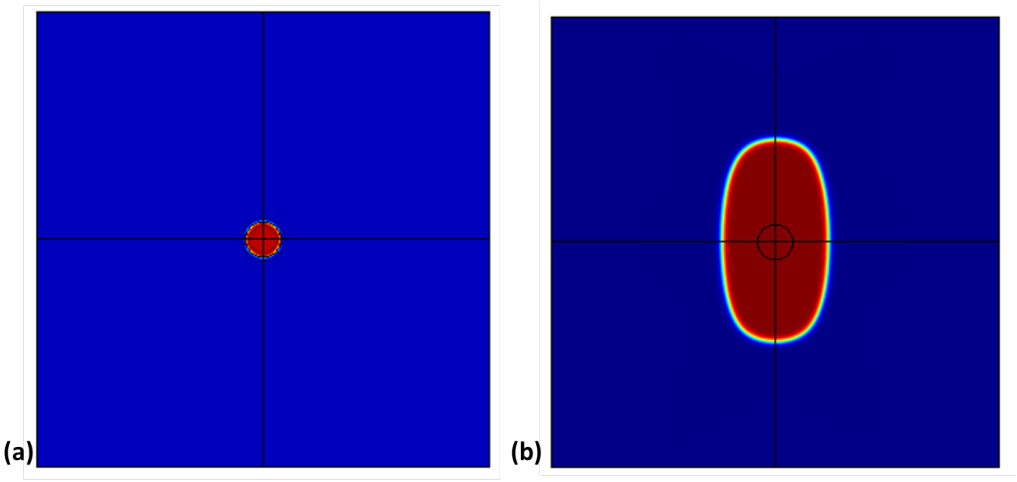

Figure 3.10: Isotropic Equilibrium Size and Shape with coupled problem with Rhombohedra inclusion and Cubic matrix

Figure 3.11 is a picture of the equilibrium shape of the precipitate which is typical of a cubic symmetric inclusion in a cubic matrix[106, 107]. Other simulations that were carried out but not shown here suggests that the equilibrium shape of the precipitate may be slightly different from what is presented in Figure 3.11 for different initial precipitate size. The precipitate often grows much bigger before the strain energy effect begins to dominate and result in shape change. Whatever the case, the set of simulation carried out by this model, of which Figure 3.11 is a representative equilibrium morphology, the equilibrium size and shape depends strongly on the competition between the strain energy and the interfacial energy, which is influenced also by the initial size of the precipitate nucleus. The axial stress field around the precipitate at equilibrium is shown in figure 3.12. If the axial stress field at the center of the precipitate is plotted from left to right, the profile will be observed to be similar to what was reported in figure 3.2. The field demonstrates that there is elastic stress present due to coherency strain energy which results in precipitate shape change. The reported stress field and precipitate morphology shows similarity in shape to

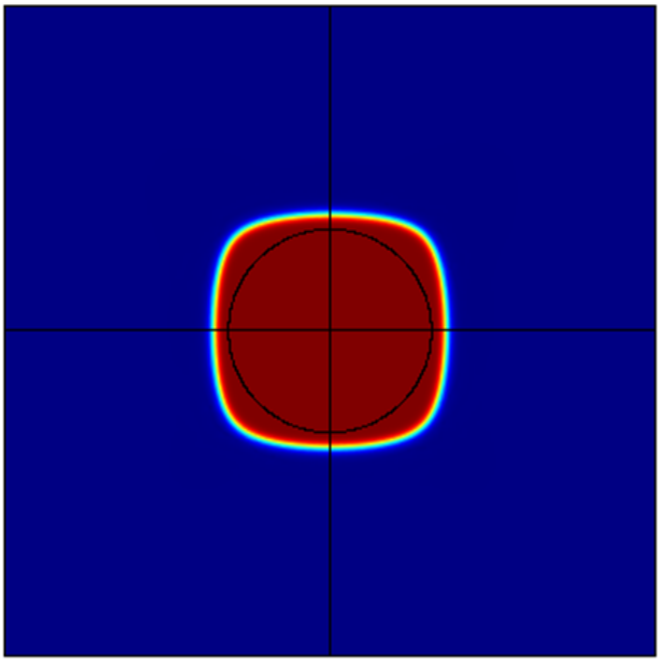

Figure 3.11: Anisotropic elastic property on equilibrium Size and Shape with coupled problem with Cubic inclusion and matrix

demonstrate the direct correlation between the stress field and the precipitate shape. The result therefore verifies the implementation of the model has been fully coupled between mechanical and diffusion fields. To further demonstrate the usefulness of the model and its implementation, a precipitate assigned an orthorhombic stiffness tensor in a cubic matrix is simulated as well. Initially the precipitate is seeded as a circle as well but much smaller than the initial precipitate size for the cubic precipitate of figure 3.9. Notice from figure 3.10a that the precipitate size is smaller, which result in a substantial growth of the precipitate before reaching equilibrium configuration. The observation supports the earlier explanation of the competition between the elastic strain and interfacial energy to determine the size and shape of the precipitate. It is important to note that the final shape of the precipitate in figure 3.10b shows an elongated precipitate with a higher aspect ratio than the equilibrium

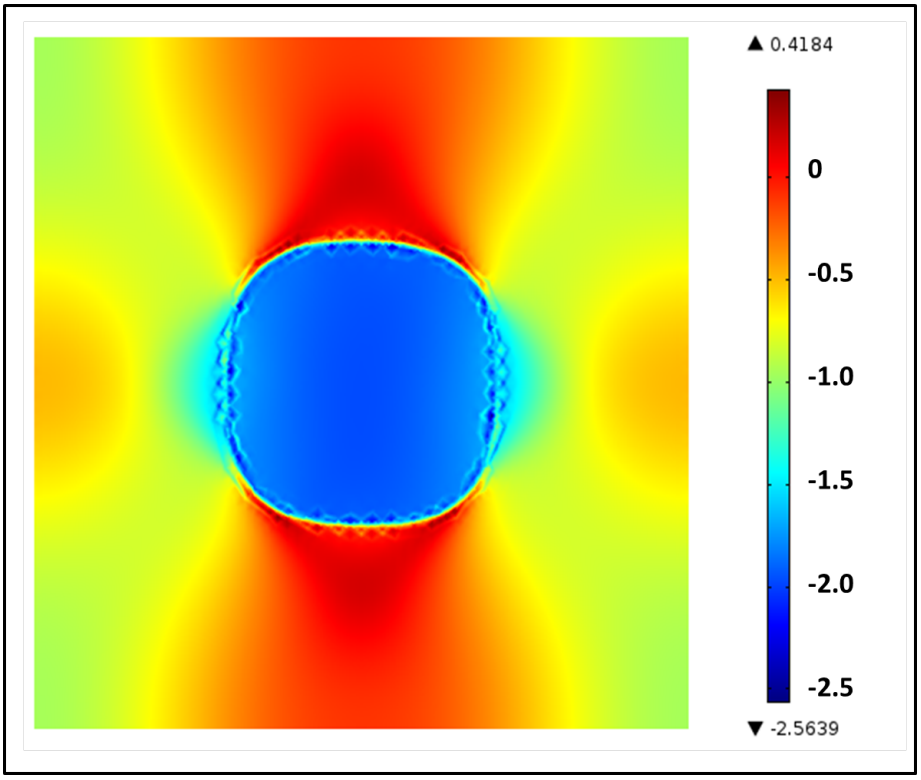

Figure 3.12: Stress field around an equilibrium cubic symmetric precipitate in a cubic symmetric matrix

shape of the cubic symmetric precipitate. It seems that this would make sense if we compare the unit cell of an orthorhombic and cubic crystal. The present simulation will be representative, in a qualitative manner, of an isolated (from the field of other precipitate) precipitate growth in a single crystal.

3.4 3-D Precipitate Growth

It is not only important to demonstrate the capability of the model in 2-D, but also in 3-D because the real microstructure and precipitate formations result in a three dimensional morphology. Therefore, this section is a brief discussion on the qualitative results of precipitate growth and morphology in three dimensions

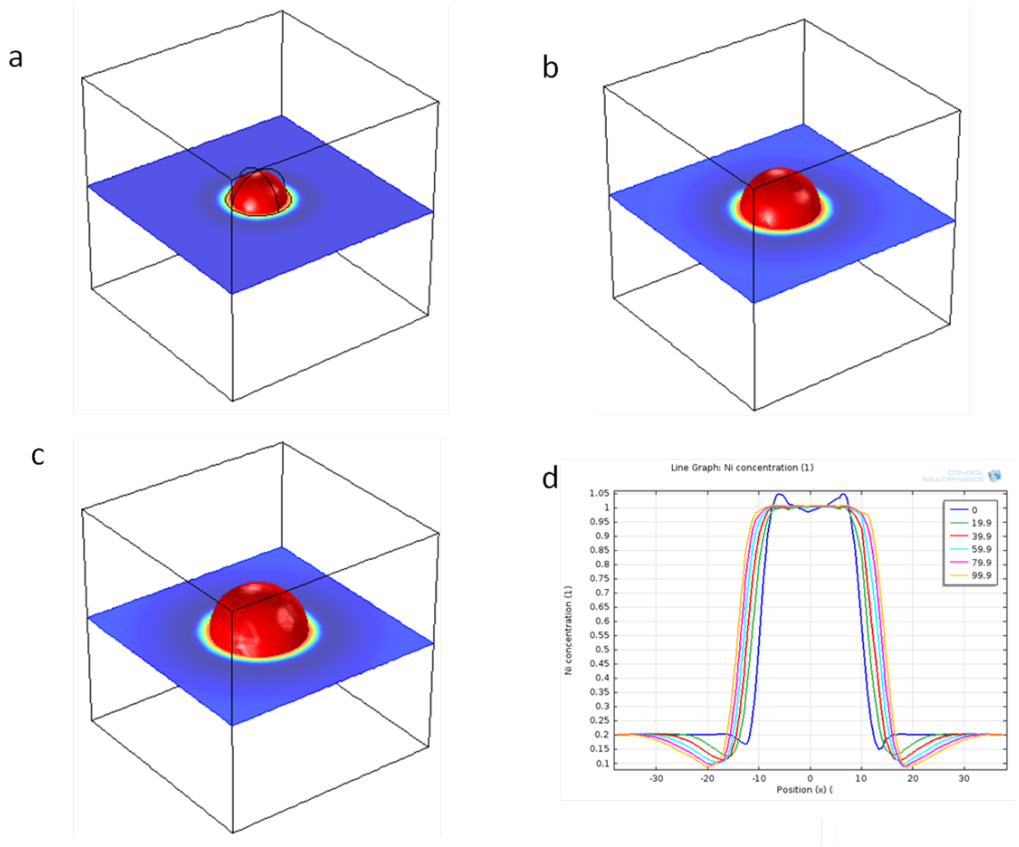

Figure 3.13: Pure diffusion evolution of precipitate

3.4.1 3-D Growth of Elastically Isotropic Precipitate in an Isotropic Matrix

Similar to what has been reported to 2-D growth of precipitate in an elastically stressed solid, 3-D results are reported in this section. An example of the growth of a precipitate in an isotropic matrix is given in figure 3.13. Figure 3.13a shows a precipitate that is initially seeded as a sphere of radius 10 units with a normalized concentration vale of 1 in a matrix of unit cell 80 unit lengths with a concentration value of 0.2 as well. The solution of the model results in the growth of the precipitate to an equilibrium shape that is spherical, which is as shown in figure 3.13b and c. The result is expected since the matrix and the precipitate are isotropic and the interfacial

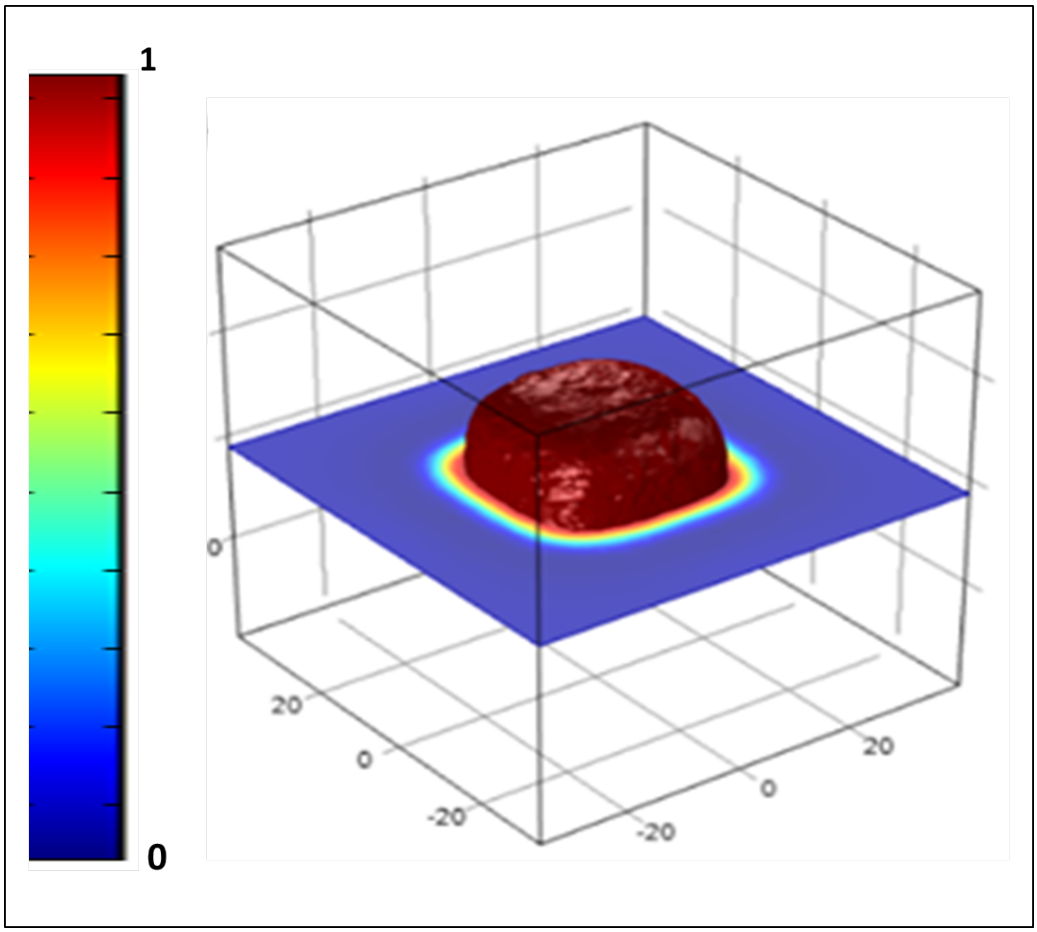

Figure 3.14: Concentration field around an equilibrium shape of cubic symmetric precipitate in a cubic symmetric matrix

energy is also isotropic. Figure 3.13d shows the concentration field on a line drawn across the center of the unit cell of the simulation. It is important to note that the 3-D implementation also shows the concentration depletion that has been reported in experiment during precipitate growth. Ability to capture concentration depletion in 3-D is very interesting because it serves to affirm this modeling approach as suitable for modeling the evolution of concentration field during precipitate growth when SMA is being aged. The concentration field showing difference as the precipitate evolves can be used to design suitable concentration profile that gives the desired Ms for a

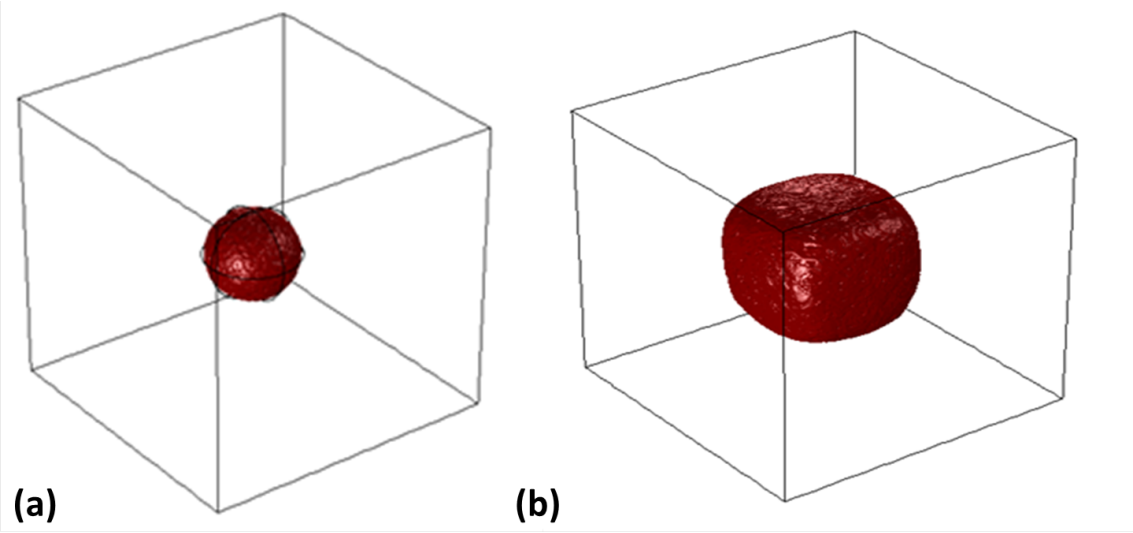

Figure 3.15: 3-D cubic precipitate simulations

typical SMA. In other words a microstructure based SMA design is possible with the phase field model, more so that a methodical approach based on standard continuum thermodynamics is used in this work to include relevant features.

3.4.2 3-D Growth of Cubic Precipitate in a Cubic Matrix

The real SMA material will develop a coherent precipitate that will result in coherency strain energy and anisotropic material effects. Figure 3.14 shows equilibrium morphology of a cubic symmetric precipitate in a cubic matrix. Notice the concentration field around the precipitate shows that the precipitate growth is also diffusion driven in 3-D. The 3-D result verifies the implementation of the model as being fully coupled. Figure 3.15a also shows the initial and equilibrium shape of the same cubic symmetric precipitate in a cubic matrix. The precipitate is initially seeded as a sphere like that of figure 3.13a, but the equilibrium shape of the precipitate is cubic as dictated by the elastic stiffness tensor through the elastic strain energy. The coherency strain which is taken to be dilatational changes the stress

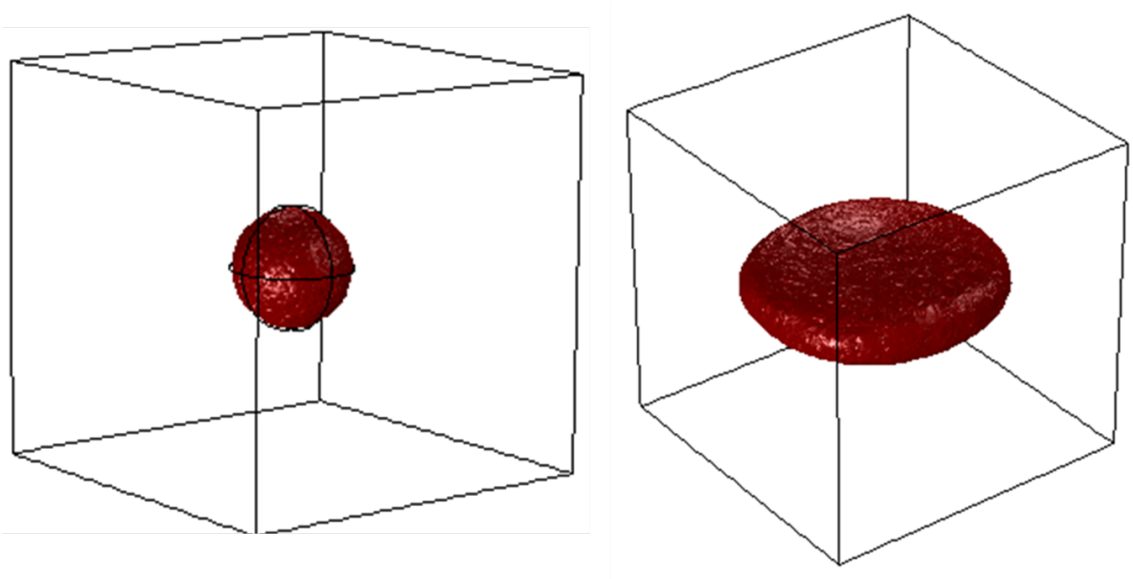

Figure 3.16: 3-D Evolution of cubic-orthorhombic matrix-precipitate from initial to equilibrium configuration

state in the material system as the precipitate evolves and grows thereby causing shape change as the size of the precipitate increases. Just like the 2-D result, the interfacial energy dominates the initial response of the precipitate resulting in initially spherical growth but as the precipitate size increases; the elastic energy begins to dominate causing the shape to change to a cube as seen in Figure 3.15b

3.4.3 3-D Growth of Orthorhombic Precipitate in a Cubic Matrix

To verify that the model and the implementation is properly capturing the influence of elastic stiffness tensor via the strain energy on the precipitate and that the shape change is not going to be always cubic, an orthorhombic precipitate is seeded in a cubic matrix. The initial size is the same as that of figure 3.15a. The initial shape is also spherical as seen in figure 3.16a such that we compare the shape change between a cubic and orthorhombic symmetric matrix without other effect of size coming to play. Figure 3.16b clearly shows a more penny shape like configura-

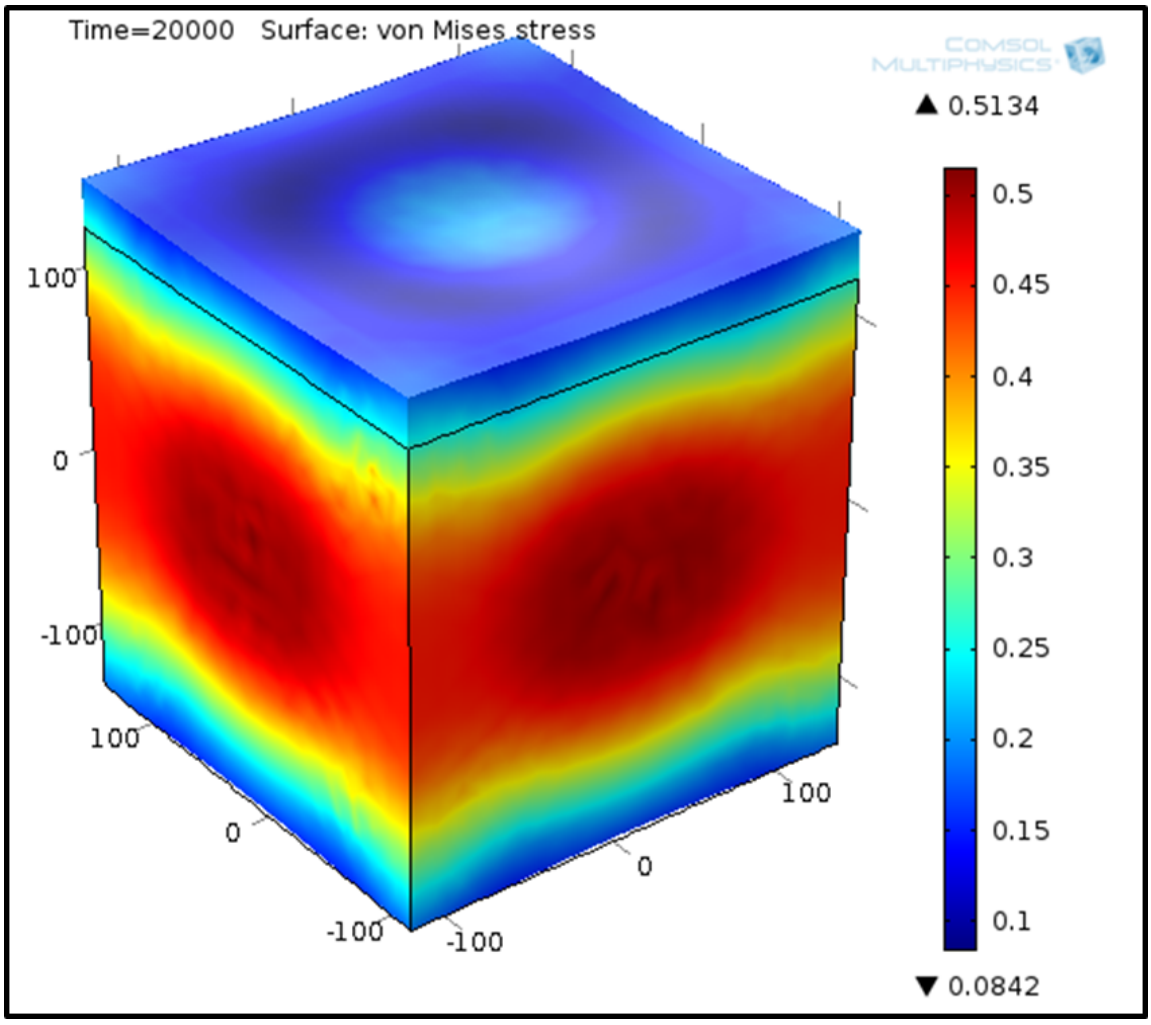

Figure 3.17: Dimensionless Von Misses Stress Field at some point during precipitate growth showing obvious change in the stress field

tion of the equilibrium orthorhombic precipitate as compared to the cubic shape of a cubic symmetric precipitate. Accompanying equivalent von-misses stress is shown in figure 3.17. Qualitatively, the dimensionless stress field shows non-uniform field due to the anisotropy of the matrix and precipitate properties. Therefore, the current model and the 3-D implementation is verified as fully coupled between mechanical and diffusion field, incorporating matrix-precipitate elastic inhomogeneity as well as

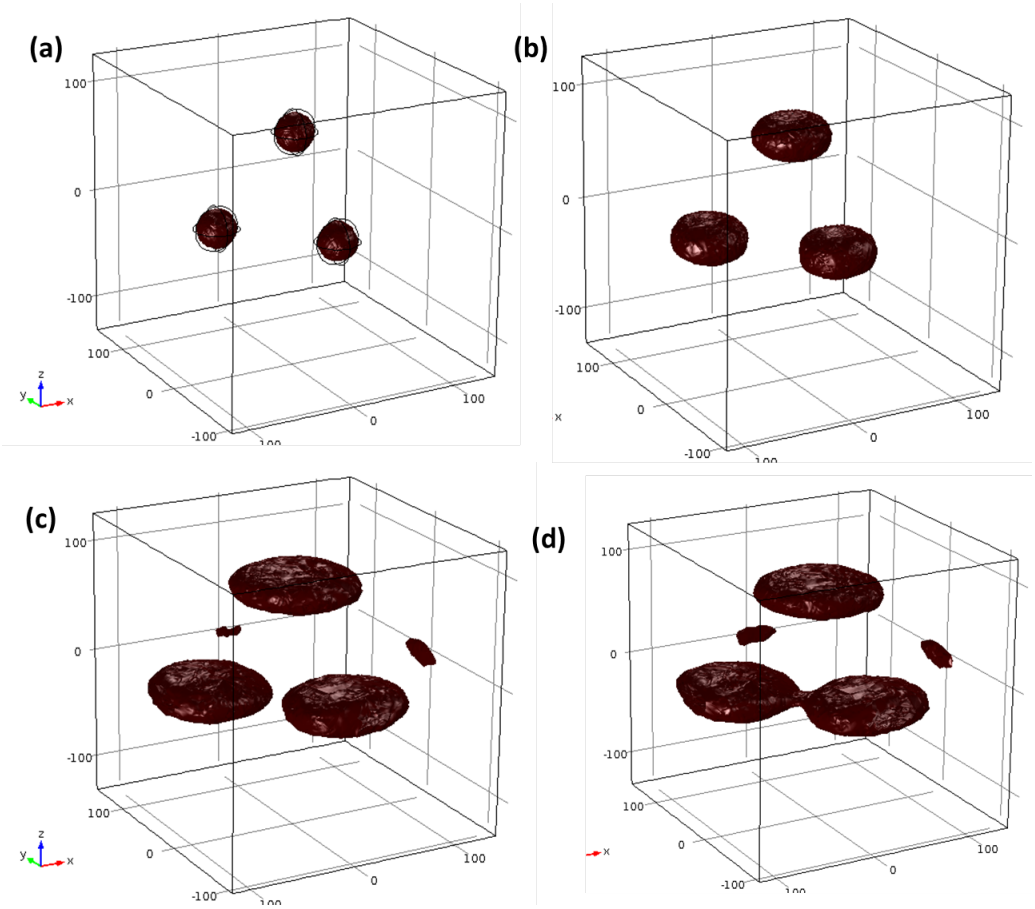

Figure 3.18: Multiple 3-D Evolution of cubic-orthorhombic matrix-precipitate from initial to equilibrium configuration

material anisotropy.

3.4.4 3-D Coarsening of Orthorhombic Precipitate in a Cubic Symmetric Matrix

Now, to sort of complicate the simulation, the coarsening of orthorhombic precipitate in a cubic matrix is simulated. The results as shown in figure 3.18 does clearly shows that the coarsening of precipitate due to diffusion in an elastic field is well captured. From figure 3.18a, three precipitate are seeded with shape and size that is the same as the previous 3-D simulations. The normalized concentration field in the

precipitate, with initial value 1 and the matrix of value 0.2. Notice that after some time as seen in figure 3.18b all three precipitates, at intermediate size, begins to change shape from spherical to that which looks somewhat cubic but elongated and then to a more penny shaped precipitate figure 3.18c and the finally, the three precipitate begins to coarsen as shown in figure 3.18d. It seem also that a new nucleus is formed in other parts of the RVE, however I think this may not be actual material behavior but a possible numerical issue because of the mesh not being refined enough to capture the refined details. Attempt to refine the to be much more finer increased the memory usage so much that the 32MB RAM used runs out of memory. So it is recommended that a super computer be used for simulations such as this and microstructure simulation for the 3-D morphology of multiple precipitate. At this point, the ability of the phase field model reported in this work is demonstrated and the implementation verified to simulate relevant features of precipitate growth and coarsening with the effect of elastic anisotropy and precipitate size demonstrated in a qualitative manner. More quantitative and detailed simulation will be subject of careful numerical study and improvement of the model in the future

4. MECHANICALLY INDUCED PHASE TRANSFORMATION USING CFPA

SMAs properties can be harnessed either by subjecting them to mechanical or thermal stimuli. This chapter is focused on pseudoelastic response of SMA.Particularly during forward transformation from austenite to martensite. Simulation of prevalent, design relevant features of the time dependent stress-strain and thermal response of SMA during forward transformation for a pseudoelastic loading path is simulated using the thermo-mechanical field equations 2.127, 2.132, 2.158 described in Chapter 2. The interest is to demonstrate the capability of the current model to simulate the kinetic of phase transition in SMA under thermomechanical loading paths that produce pseudoelastic response, to examine the possible limitations of the model and new insight it offers for improved design of SMA for engineering application; and to confirm the correctness or otherwise of the hypothesis made and the methodology for developing the model to simulate challenging features of SMA response. In addition, it is desired to draw reasonable scientific conclusions from the results of the simulation.

4.1 Numerical Implementation

This section focus on the numerical implementation of the SMA model. The three field equations arising form the quasi-static balance of linear momentum, configurational forces and energy balances restricted by the second law of thermodynamics is solved within a finite element framework. A commercial finite element solver COMSOL Multiphysics is used. Within the COMSOL Multiphysics a mathematical module exist, which comprise of a PDE interface that consist of common partial differential equations as well as two forms of generalized differential equations. The

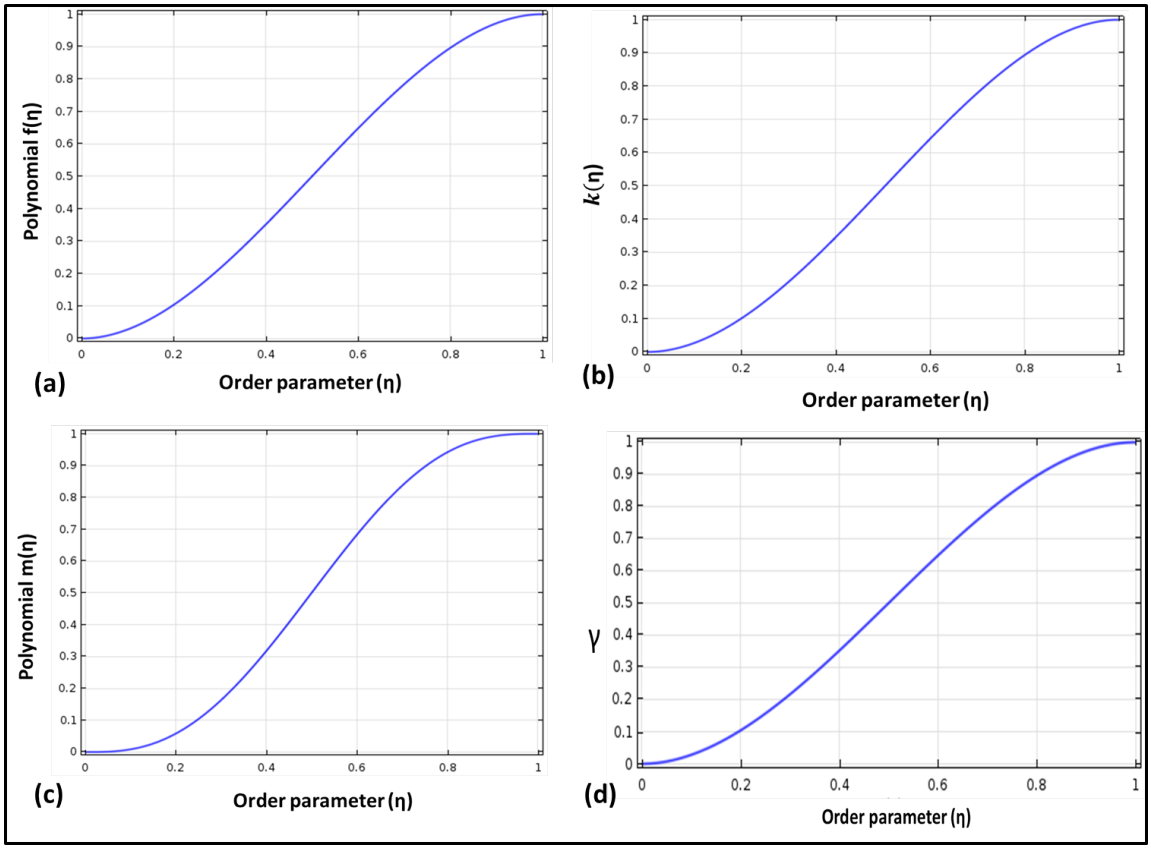

Figure 4.1: The interpolating polynomial functions for parameters in table 4.1

PDE interface becomes very handy because it does allow a custom implementation of differential equations as the case is for this work. There is no need to write a UMAT (user material subroutine). There are three main ways of utilizing the COMSOL generic PDE interface, they are (1) coefficient form (2) general form (3) weak form. Each of the ways has their strengths and weaknesses. For the implementation of the field equations solved in this chapter, the coefficient form of the PDE is used. In this coefficient form, the three PDEs are written to match the coefficients of the PDE. COMSOL is written to accept PDE in this form, even for very highly non-linear PDEs because COMSOL has a fairly sophisticated linear and nonlinear solver. Appropriate initial and boundary conditions can be specified along with the

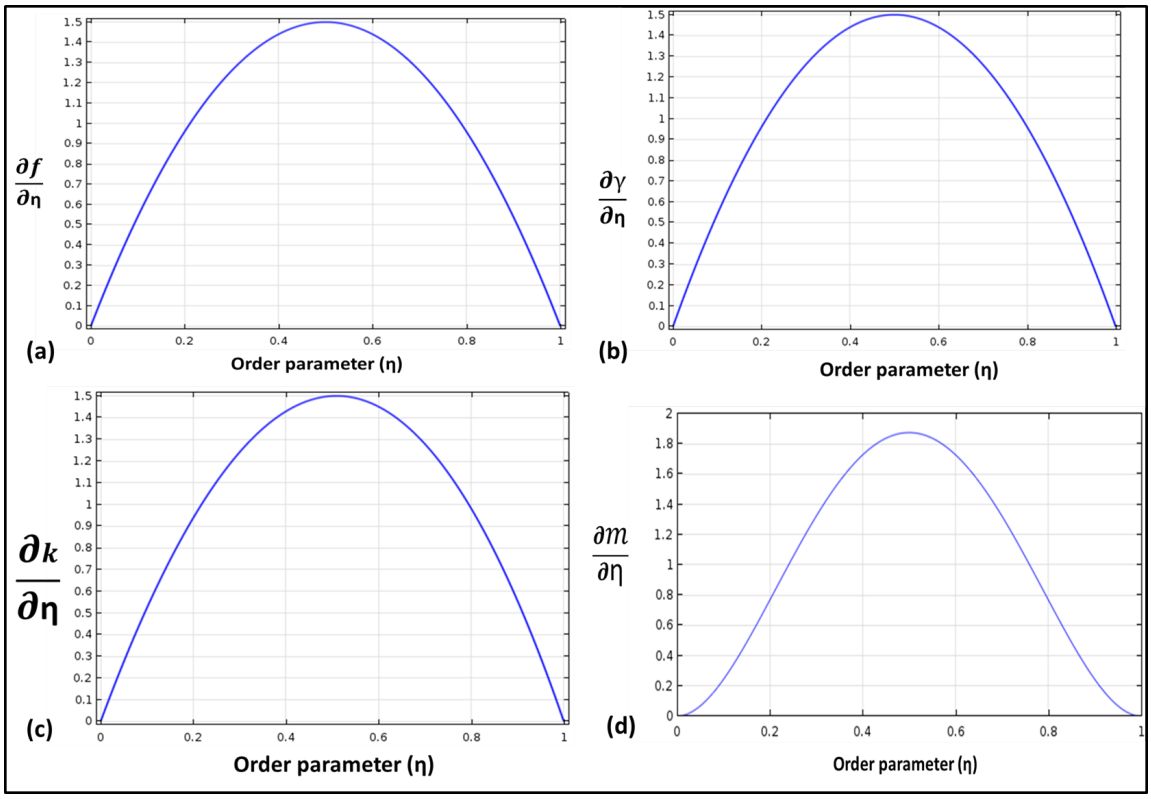

Figure 4.2: Derivative of the interpolating polynomials for parameter values in table 4.1

differential equations in COMSOL so that a well posed problem is given. COMSOL allows for very sophisticated meshing abilities, including adaptive mesh refinement. Also as will be stated clearly shortly, COMSOL gives the flexibility of specifying the type of interpolation function used. Essentially, I am solving three set of PDEs two of which are parabolic nonlinear PDEs and the third one is a elliptic PDE. So, COMSOL Multiphysics (a commercial finite element code) is used to solve three the fully thermomechanical coupled equations simultaneously.

The polynomials in the field equations have been calibrated to the parameter of the particular NiTi SMA being studied. The polynomials has value of 0 when the order parameter is zero so that the phase will have free energy representative

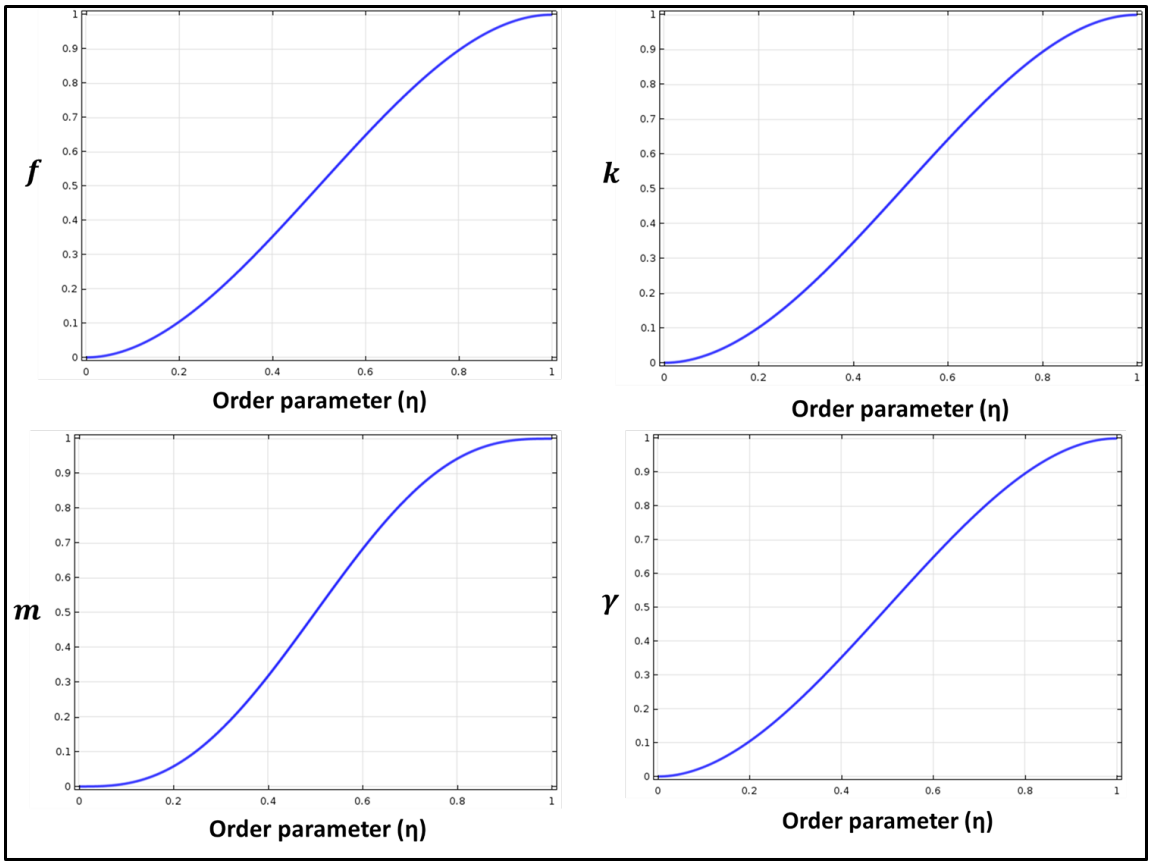

Figure 4.3: The interpolating polynomial functions for parameter in table 4.2

of austenite phase. The polynomials have numerical value of 1 when the order parameter is 1 so that free energy is that of martensite. Essentially at each point an order parameter value of 1 (0) is assigned a free energy value of martensite (austenite). Similarly, their derivative show how the free energy has extremum value at order parameter values of 1 and 0 (i.e. their derivative is zero at the two order parameter values second derivative $\geq$ will ensure a local minimum),representing martensite phase and austenite phase as admissible phases. As seen in figure 4.1a-d and figure 4.2a-d which are for the simulation using parameters in table 4.1. Figure 4.3a-d and figure 4.4a-d are for parameters in table 4.2 as well.

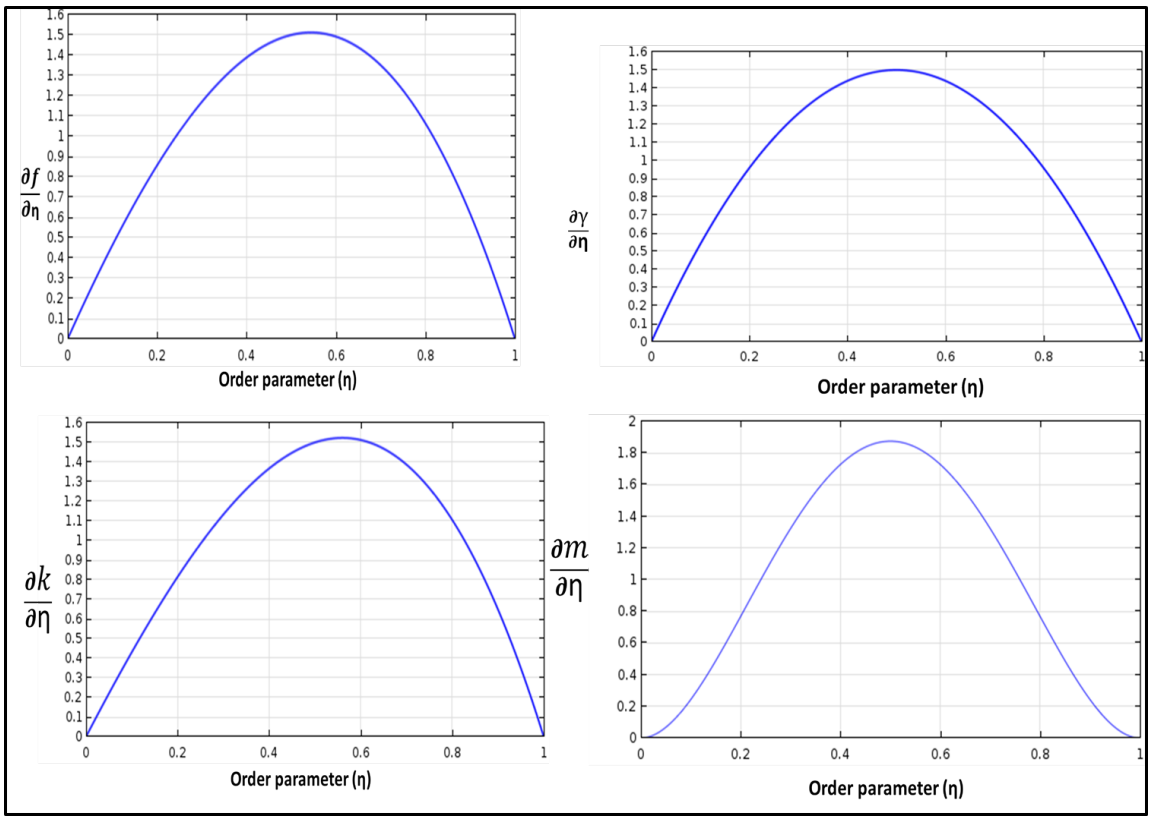

Figure 4.4: Derivative of the interpolating polynomials for parameters values in table 4.2

4.2 Mechanically Induced Phase Transformation-Pseudoelasticity

An SMA wire is simulated as an axisymmetric rod under different strain rates and thermal boundary conditions. Figure 4.5 is a diagram of the president of the initial-boundary value problem(IBVP). Heat transfer is assumed to be negligible radially across the wire such that temperature is constant at each cross section but only vary axially along the wire. The earlier discussed model is used to simulate the kinetic of phase transition, the resulting temperature profile due to heat generation, heat transfer and the stress-strain response under different mechanical loading conditions, rates and thermal ambient conditions. The initial and boundary conditions of the

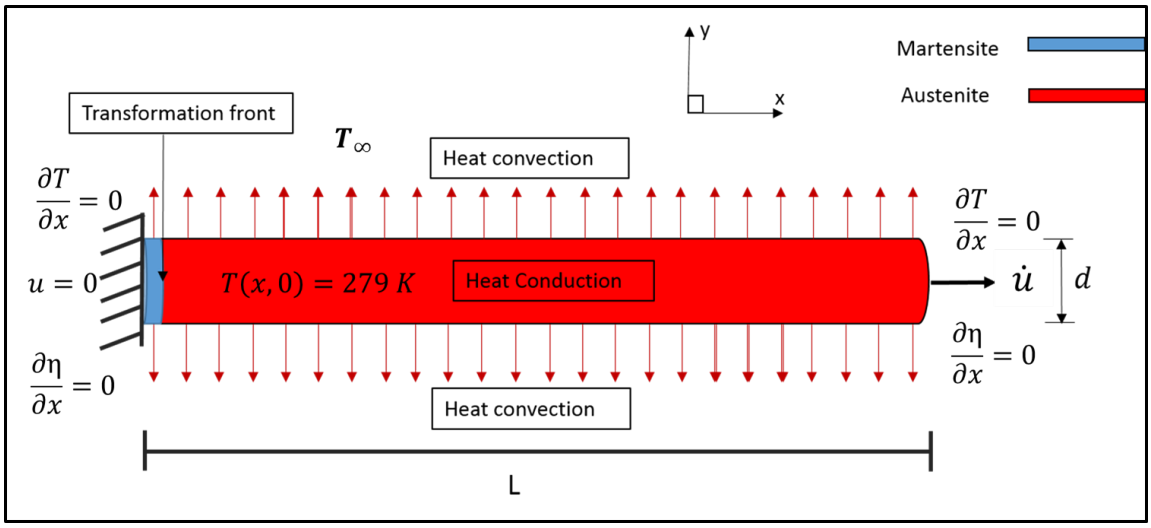

Figure 4.5: Schematics of initial-boundary value problem (IBVP) for displacement controlled loading of SMA rod showing thermal, mechanical and order parameters boundary conditions and intial conditions

coupled PDEs are given below. For the order parameter field equation, the following initial and boundary conditions are imposed

$$\mathbf{n} \cdot \nabla \eta(0,t) = 0, \tag{4.1}$$

$$\mathbf{n} \cdot \nabla \eta(L,t) = 0, \tag{4.2}$$

$$\eta(0 \leq x \leq x_1, t = t_c) = 1, \tag{4.3}$$

$$\eta(x_1 \leq x \leq L, t = t_c) = 0. \tag{4.4}$$

The field equation of displacement, which is the mechanical equilibrium equation, has the following boundary conditions:

$$u(L,t)) = \overline{u}(t), \tag{4.5}$$

$$\mathbf{n} \cdot \mathbf{t}(L,t) = \widetilde{F}(t), \tag{4.6}$$

$$u(0,t) = 0. \tag{4.7}$$

Equation 4.5 is for displacement controlled loading, while the second is for force controlled loading. Now, for the temperature field equation, the initial and boundary conditions are

$$\mathbf{n} \cdot k\nabla T(0,t) = 0, \tag{4.8}$$

$$\mathbf{n} \cdot k\nabla T(L,t) = 0, \tag{4.9}$$

$$\eta(x, t = t_0) = Tin. \tag{4.10}$$

For the finite element model of the problems, a quadratic lagrange interpolation function was chosen for all three field equations in COMSOL Multiphysics. Other types and order of interpolation functions are present in the commercial code up to septic order of the polynomial. The solver used for the field equation is a direct solver MUMPS, other options includes PARDISO, SPOOLES and Dense matrix direct solver. The nonlinear solver uses a Newton's method. A customized user controlled meshing sequence was used to achieve the best approximation of the domain in the light of the physics of the problem. It is important to restate that the mechanical loading condition simulated in the research is for the pseudoelastic response. The goal is so that relevant features of the SMA rate dependent thermomechanical response can be captured. Some of these features include the following

- Sensitivity of stress-strain response to loading rates and related temperature changes due to self-heating and cooling (latent heat)
- Temperature change due to exothermic nature of forward transformation has effect on stress-strain response

- increase in nucleation and propagation stress with ambient temperature
- Difference in stress-strain response depending on whether it is under displacement controlled loading or force controlled loading
- Relaxation and creep due to self-heating and possible viscosity of the material (intrinsic to the material itself). This supposed viscous behavior of SMA necessitate explanation as it is still being debated in the SMA community
- Polycrystalline NiTi strips, wires and tubes deforms under tension by nucleation and growing macroscopic martensite domains that consist of most fully transform grains
- Martensite (austenite) nucleates at a higher(lower) stress level than the stress at which phase transition progresses during forward(reverse) transformation
- Deformation during transformation of NiTi SMA under mechanical load is inhomogeneous comprising of two or more differently deformed regions (phases) connected by a narrow zone with steep deformation gradient (transition front). This observation motivates the use of a two phase, diffuse interface model
- Application of uniform stress with isothermal condition results in only one nucleation front
- under non-isothermal condition, it may be possible that the released (absorbed) heat can cause a local change in temperature and result in thermal hardening (rise in propagation stress). Therefore, the nucleation stress in a cooler region of the specimen may be surmounted resulting in a new nucleation.
- location where two existing front meets is the preferred site for the nucleation during unloading

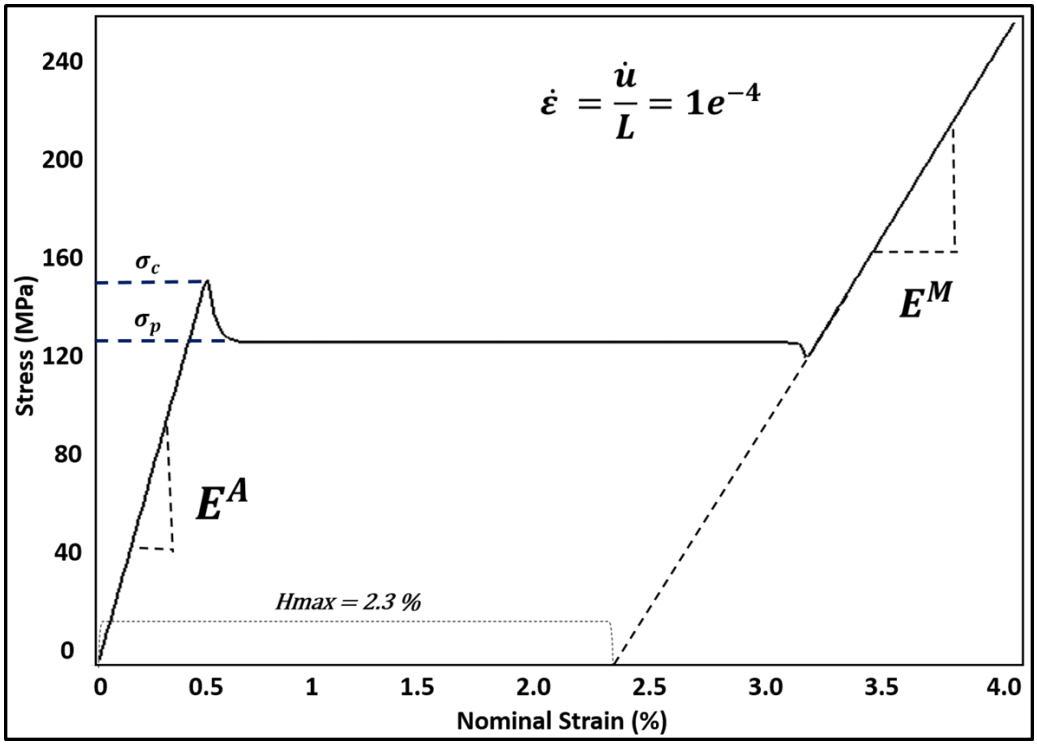

Figure 4.6: Stress-strain response for isothermal (without thermomechanical coupling) condition under $\dot{\epsilon} = 10^{-4}s^{-1}$

- Transition front is nearly at an angle of between $55 - 60°C$ to the loading direction and sometimes have criss-cross pattern

Attempt will be made towards simulating some of the features and the limitation of the model for others will be noted as a possible recommendation for future improvements and simulations

4.2.1 Initial Isothermal Result for Forward Transformation

The simulations reported in this section are based on results for an SMA wire with properties given in table 4.1. The first result to be analyzed is that of an SMA axisymmetric rod in a water ambient medium, which is known to be representative of near isothermal condition. The loading rate was a strain rate of $10^{-4}s^{-1}$. Before,

Table 4.1: Properties for simulation except otherwise stated

Properties	Notation	Value
Martensite Modulus	E^M	15GPa
Austenite Modulus	E^A	33 GPa
Martensite Start Temperature	M_s	242 K
Austensite Start Temperature	A_s	261 K
Kinetic Coefficient	τ	4.08 $\times 10^6 Pas$
Gradient energy coefficient	$\rho\lambda$	1.5 N
clasius clapeyron parameter (austenite)	C^A	4.5 Mpa K^{-1}
clasius clapeyron parameter (Martensite)	C^M	4.5 Mpa K^{-1}
Heat Transfer coefficient in air	h	6.5 $W/m^{-2}K^{-1}$
Heat Transfer coefficient in water	h	890 $W/m^{-2}K^{-1}$

Table 4.2: Properties for simulation

Properties	Notation	Value
Martensite Modulus	E^M	30GPa
Austenite Modulus	E^A	60 GPa
Martensite Start Temperature	M_s	272 .5K
Austensite Start Temperature	A_s	318 K
Kinetic Coefficient	τ	1 $\times 10^7 Pas$
Gradient Energy Coefficient	$\rho\lambda$	5 N
clasius clapeyron parameter (austenite)	C^A	8.8 Mpa K^{-1}
clasius clapeyron parameter (Martensite)	C^M	6.125 Mpa K^{-1}

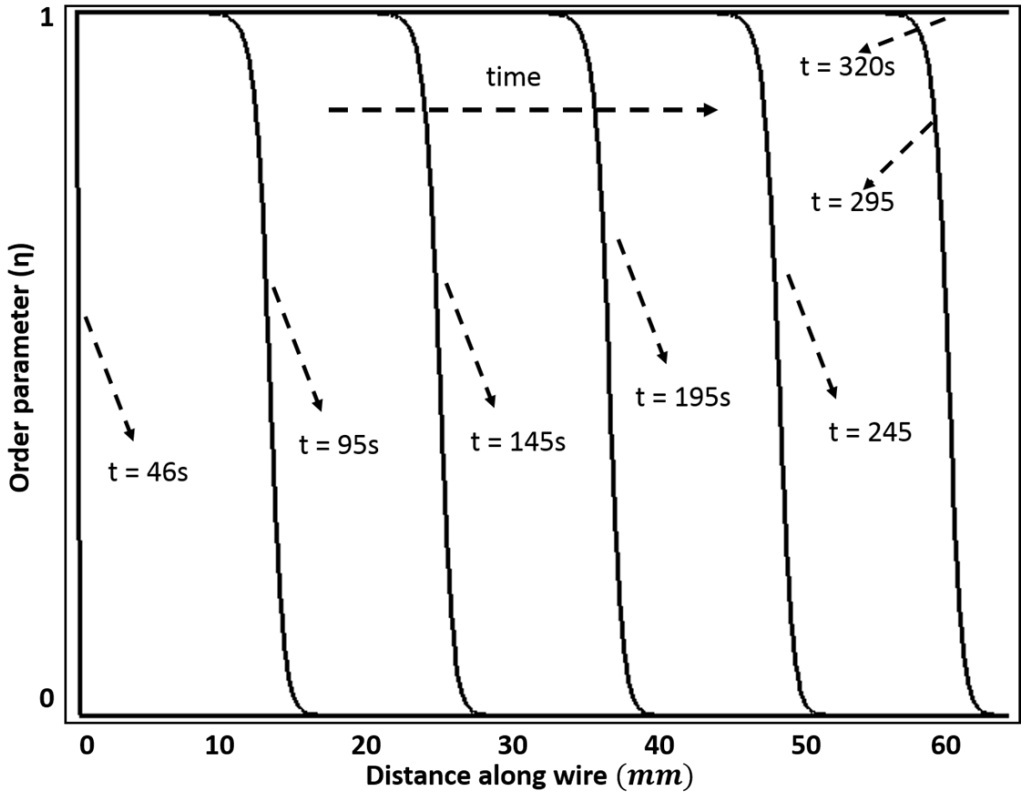

Figure 4.7: Order parameter evolution characterizing phase transformation for isothermal (without thermomechanical coupling) condition (Agboola et al 2014 [108])

the full thermomechanical coupled model was solved; a bench mark to verify that the model is solving the actual physics was carried out. The first simulation is based on the solution of the balance of linear momentum and the balance of configurational forces to solve for the displacement and order parameter field respectively. The balance of energy is not solved in this case. The result of the simulation is given in figure 4.6. The ordinate axis is the stress in MPa, while the abscissa in the plot is the nominal strain defined as $\frac{u}{L}$. u is the axial elongation and L is the length of the rod. Looking at the figure, the observed difference between the nucleation (σ_c)and propagation (σ_p) stress during forward transformation is clearly simulated.

Since this result is for purely isothermal without any thermomechanical coupling (as the temperature field equation was not solved), then the response obviously is not due to thermomechanical coupling but due to mechanical instability of nucleation event and subsequent propagation. The transformation strain generated due to the nucleation event does result in a relaxation of the stress-(i.e. the material softens due to nucleation and propagation of boundary between two phases with different elastic properties). Notice also that the deep in the end of the plateau is also captured by the model. Classically, a trilinear curve is used to represent such material that soften. So, the plateaus stress is often termed the Maxwell stress. In the standard phase front models based on Ericksen seminal work, the Maxwell stress is taken to be the stress value of the line that cuts the trilinear curve into two equal areas. However, in this model the plateau stress results from the solution of the IBVP once the nucleus is seeded. As noted in table 4.1, the maximum transformation strain of this particular NiTi SMA is 0.023 and it is well reproduced by the model. The maximum transformation strain of the result is determined using the line drawn from the elastic curve for pure martensite to the strain axis (see dashed line in the plot). Another important feature of importance in the plot, is that the slope of the homogenous elastic response of the purely austenite phase is different from that of the homogeneous elastic deformation of the purely martensite phase. These slopes also have the numerical values of the prescribed modulus of the austenite and martensite phases in table 4.1. The hypothesis of this model is that the unique features and the macroscopic transformation strain generated in SMA as observed in experiments and shown in figure 1.8 are due to the propagation of a transformation front which introduced a new time scale to the model. The simulation result so far, as first evidence, demonstrates this hypothesis to be true. Figure 4.7 shows the evolution of the order parameter which characterizes phase transition. The ordinate

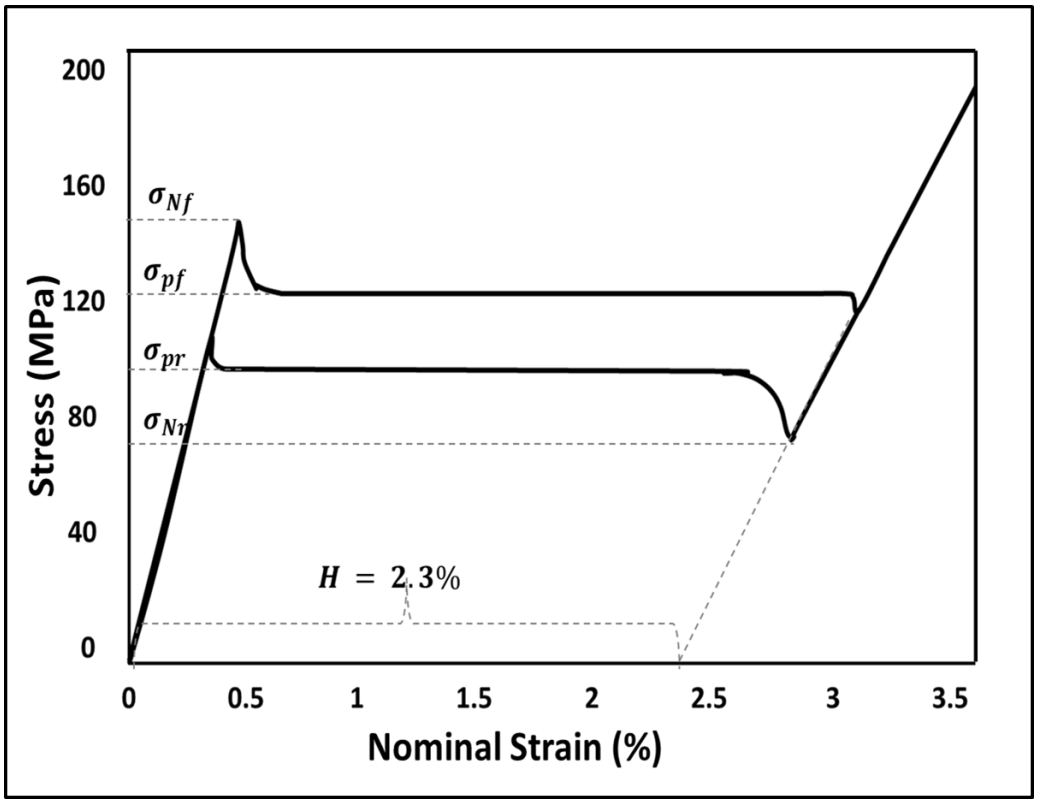

Figure 4.8: Isothermal pseudoelastic stress-strain response under displacement control

of the plot is the order parameter, which has a value of 1 for martensite and 0 for austenite. Transformation from purely austenite (with a martensite nucleus) to a fully martensite phase progresses from left to right. The SMA is loaded and deform in a homogenous elastic manner in a fully austenite phase at a constant displacement rate. At about $46s$, the critical stress σ_c is reached and a seed of martensite of about $0.2mm$ in length is nucleated on the left of the rod. Since at this critical stress, the driving force for phase transformation has reached its critical value, the transformation progresses. At about $320s$, the entire rod has transformed to martensite after which the deformation is purely elastic in martensite phase as stated earlier. So, the order parameter evolution plot serves to show that the transformation

strain in figure 4.6 is a result of the accretion of martensite over the austenite phase with time, which cause strain to accumulate in the specimen. The rod then elongates to the right and the nominal strain is measures as described earlier. The hypothesis of a moving boundary for modeling SMA response is corroborated by these plots.

4.2.2 Full Isothermal Hysteretic Response

In addition to the isothermal forward transformation response simulation, a full isothermal hysteretic response was carried out using the balance of linear momentum and the configurational forces balance. The result is shown in figure 4.8. In this figure also, the ordinate is the stress in MPa and the abscissa is the nominal strain. Notice that apart from he difference in the nucleation $\sigma_{Nf} = 150MPa$ and propagation $\sigma_{pf} = 125MPa$ stress for the forward transformation, there is also a difference in the nucleation $\sigma_{Nr} = 80MPa$ and propagation $\sigma_{pr} = 100MPa$ stress for the reverse transformation due to the recovery of the transformation strain causing the stress to increase beyond the nucleation stress. The magnitude of difference between the nucleation and propagation stress are about $20MPa$. Afterward the nucleation for both forward and reverse transformation, a stress plateau is observed. This observation is very similar to what experiment has shown, where distinct stress plateau is expected for isothermal quasi-static loading of SMA. It is also important to note that the slope of the elastic part of the response both for complete austenite and martensite are fairly the same during loading and unloading. The result demonstrates the ability of the model to simulate the observed experimental feature of SMA response, particularly for thin devices and components. It is also important to state that this features does occur from the solution of the IBVP once the nucleus is seeded at the appropriate critical stress level for transformation to begin as observed on the $\sigma - T$ phase diagram.

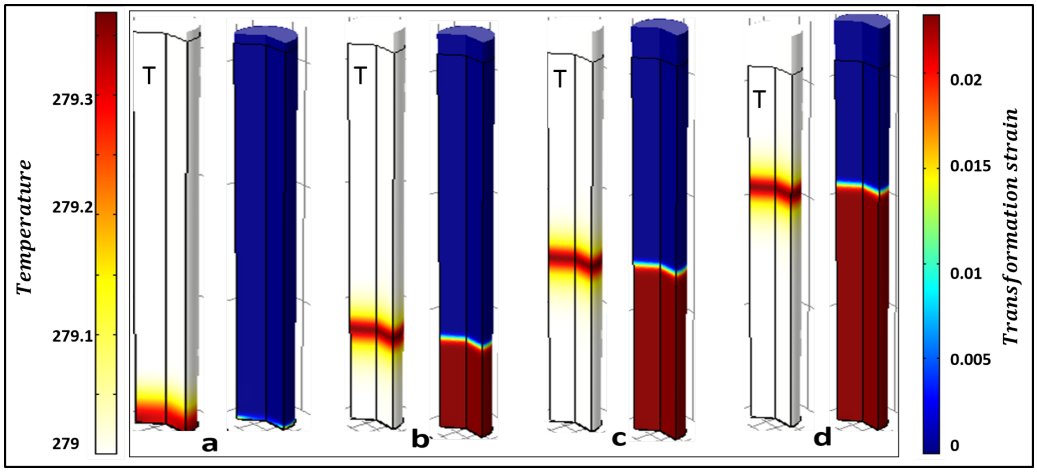

Figure 4.9: Interface evolution and accompanying temperature field due to localized heat release and transfer (Agboola et al 2015 [109])

To determine the gradient energy coefficient $\rho\lambda$ which incoporate the length scale of the problem. The length scale is the distance traveled by the transformation front in one second. BY using the values of $\rho\lambda$ that gives experimentally comparable result

4.2.3 Thermomechanical Coupled Response of SMA for Forward Transformation

The two set of result discussed so far are for purely isothermal loading condition. In this section, focus will be on the fully thermomechanical model. In essence, the simulated result will come from solution field equations 2.127, 2.132and 2.158; coming from the three balance laws of linear momentum, configurational forces and energy. So we expect to have evolution of order parameter, temperature and displacement (consequently stress and strains). Figure 4.9 shows the evolution of phase transformation with local increase in temperature due to exothermic latent heat of the forward transformation. The result for figure 4.9 is for a water ambient medium, which is representative of practical isothermal loading condition. Accumu-

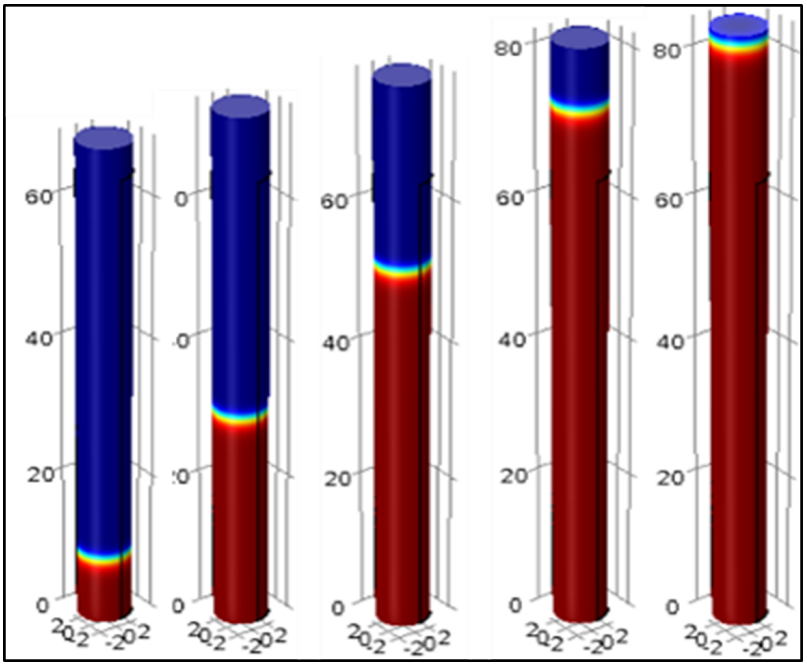

Figure 4.10: Interface evolution showing elongation of SMA rod

lation of strain due to the motion of transformation front is also observed. Notice that the rod elongates as transformation progresses. A better view of the elongation of the rod due to phase transformation is better captured by figure 4.10. The plots in white and labelled T in figure 4.9 are the accompanying temperature fields. It is important to note that the result of the simulation shows a peak in temperature at the interface. Notice that by comparing the white (the temperature field) and colored plots (which represents the transformation strain field), it is obviious that as the transformation front moves from bottom to top in the plots, the peak of the temperature also moves with it. The temperature peak is localized at the interface between a fully austenite and a fully martensite regions. This observation is in keeping with experimental result as depicted in figure 1.8, which served to motivate the underlying hypothesis for this scientific research. The other conclusion from the

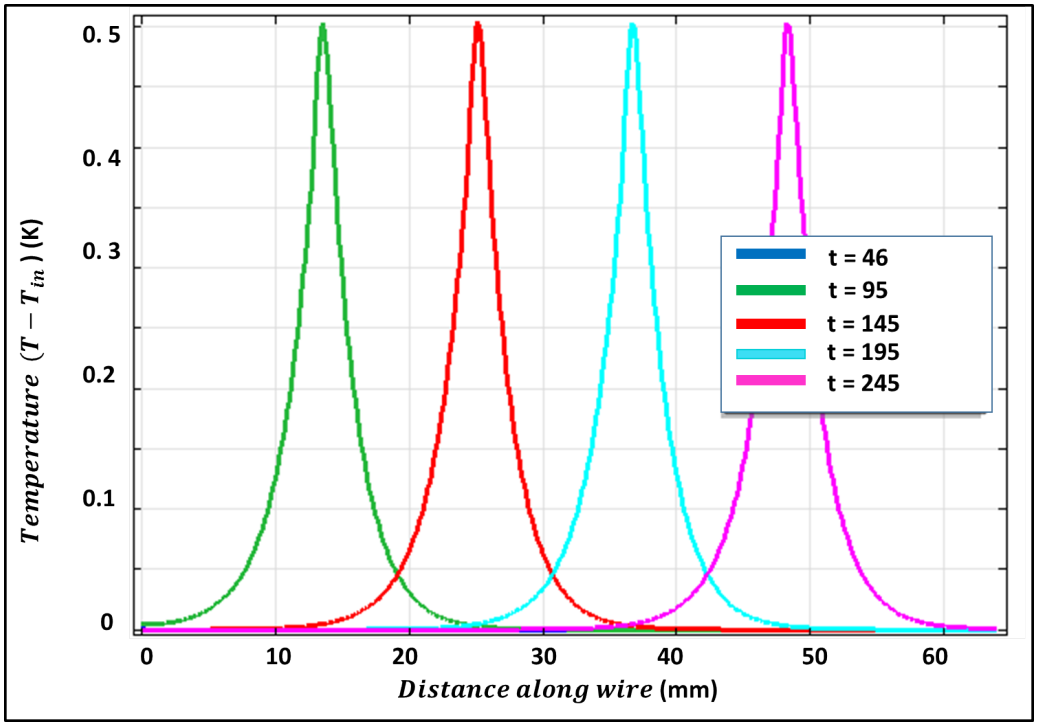

Figure 4.11: Temperature field under water ambient media

plots is that transformation occurs at the interface, which explains why thr rise in temperature is maximum at the interface and the transformation strain in maximum in one region and aproximately zero in the other region, thereby distinguishing between austenite and martensite phases. It is, however, important to note at this point that the transformation front is only visible specimen that are closer to the grain dimension. So the current model is more accurate for thinner specimen but also a good approximation for thicker specimen.

4.2.3.1 Temperature Field

To understand what the model reveal about how different ambient medium changes the temperature field of the thermomechanical results, the temperature field of the SMA loaded in water and air ambient medium as well as adiabatic thermal

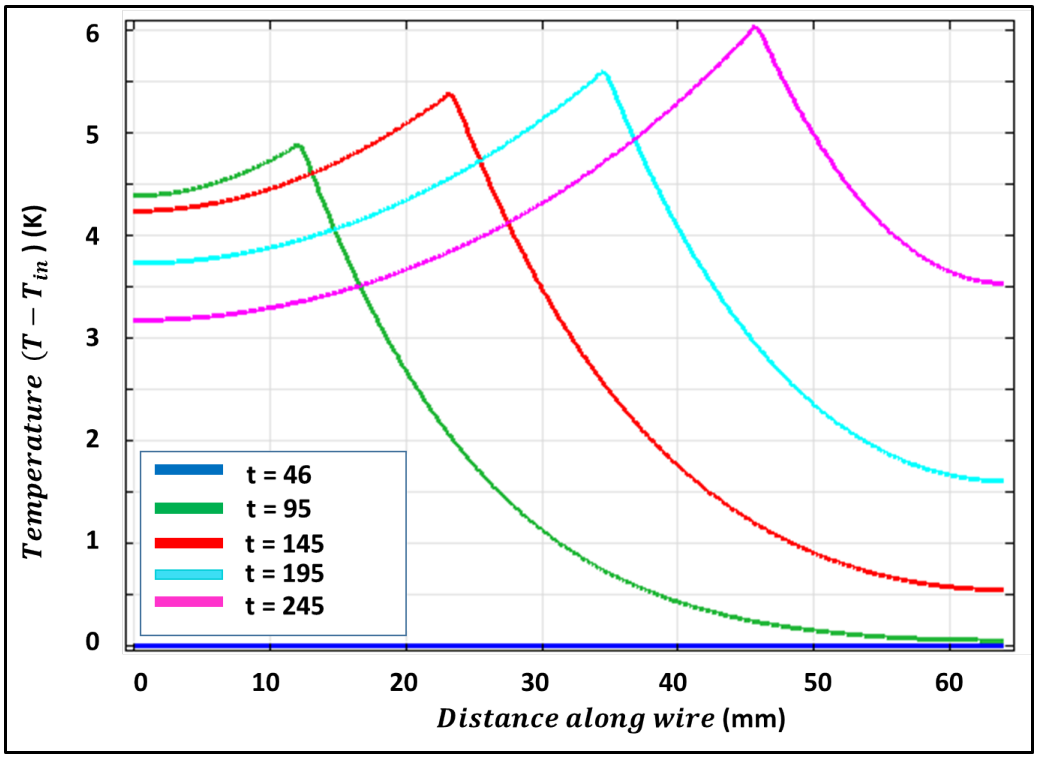

Figure 4.12: Temperature field under air ambient medium

condition is reported in figures 4.11, 4.12 and 4.13 respectively. On the vertical axis, the plot has the difference between the temperature field in the rod and the initial temperature T_{in}, measured in Kelvin (K). On the horizontal axis, the distance along the specimen is plotted. To simulate the different ambient medium, heat transfer coefficient of $h = 890$, $h = 6.5$ and $h = 0$ are used to represent the water, air and adiabatic ambient conditions respectively. This number are not magical, they can be varied to best simulate given SMA results. More importantly, they can be determined from realistic fluid mechanics flow condition depending on ambient media and prevailing flow confitions. Result for water ambient medium, figure 4.11, shows a constant peak in temperature throughout the transformation and has a maximum temperature difference of about 0.5K. As time progresses from 46 s to 245 s on the

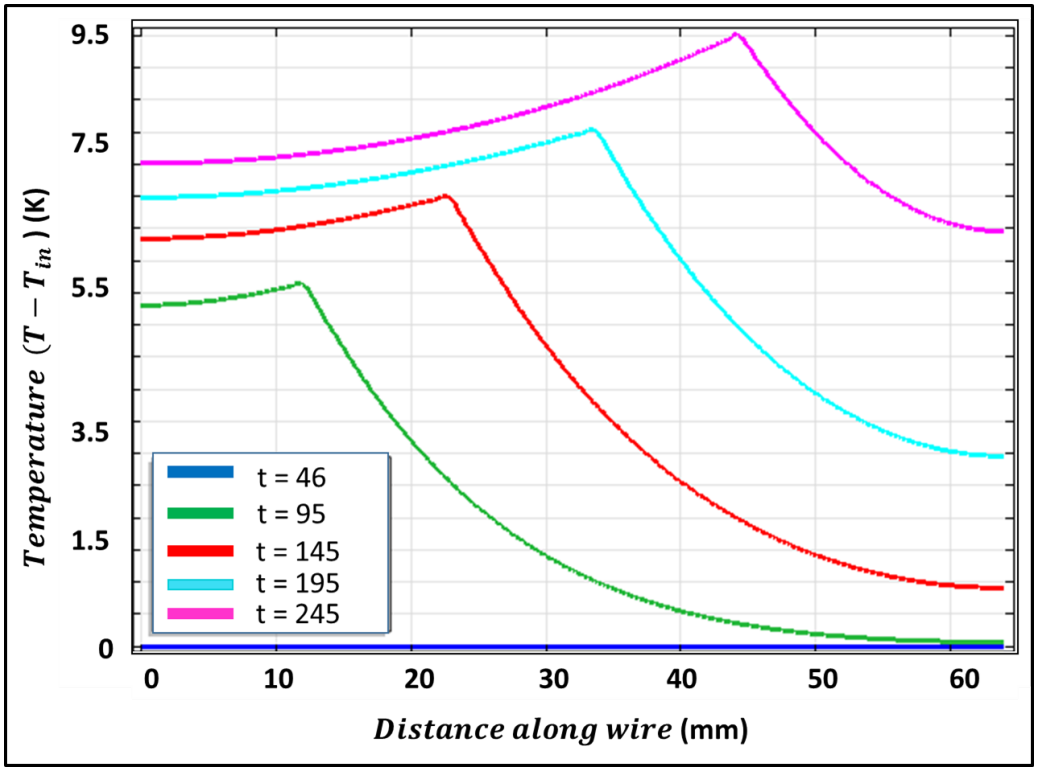

Figure 4.13: Temperature field under adiabatic condition

plot, the peak in temperature at the interface remains the same. These constant peaks suggest that the convection rate dominate the conduction rate.

In air ambient medium, as shown in figure 4.13 the local rise in temperature at the SMA transformation front is higher than that of the case of water ambient medium. It is expected that this is so from the understanding of the physical difference between the heat transfer coefficient of water and air. The temperature field not only show higher temperature change in peak compared to water ambient medium, but also a fairly moderate increase in temperature throughout the rod as transformation progress. The increase in temperature which can be attributed to an increase in the degree of heat conduction in the specimen, where the convection rate is not as dominating as would have been in water ambient medium.

Under adiabatic thermal condition, the heat released into the specimen are not transferred out of the specimen through convection. Therefore, all the heat transfer is due to conduction in the specimen. It is important to note that temperature field at $t = 245s$ is not the maximum temperature difference in adiabatic condition. The maximum is about $14K$ for this NiTi SMA as will be shown later. Since, conduction dominates in adiabatic condition, the peak of temperature difference at the transformation front rises considerably as transformation progresses. Also, remember that the no flux boundary condition is at thE end of the roddoes not allow for heat flux in and out of the specimen. So all the heat transfer is by conduction within the rod, thereby raising the temperature of other parts of the specimen considerably as the transformation progresses. (See figure 4.13)

4.3 Rate Dependent Response due to Coupling Betweeen Environmental and Loading Condition on Pseudoelastic Forward Transformation Response of NiTi SMA

One of the features that have been reported in experiments that characterize the response of SMA, when loaded along a path that result in pseudoelasticity is the difference in the response under different ambient medium. Therefore, to further verify the reliability of the model presented in this work as relevant for SMA design, simulation of the response of NiTi SMA under different ambient medium is carried out. The properties used are indicated in the plots, otherwise they are in table 4.1. The effect of different loading rates for the same ambient medium is also simulated. The observations that are gathered from the plots further demonstrate the reliability of this conttinuum thermodynamics constitutive phase field model and gives credibitity to the underlying hypothesis and theory. In the following subsections, the results are elucidated to convince the reader of the claim.

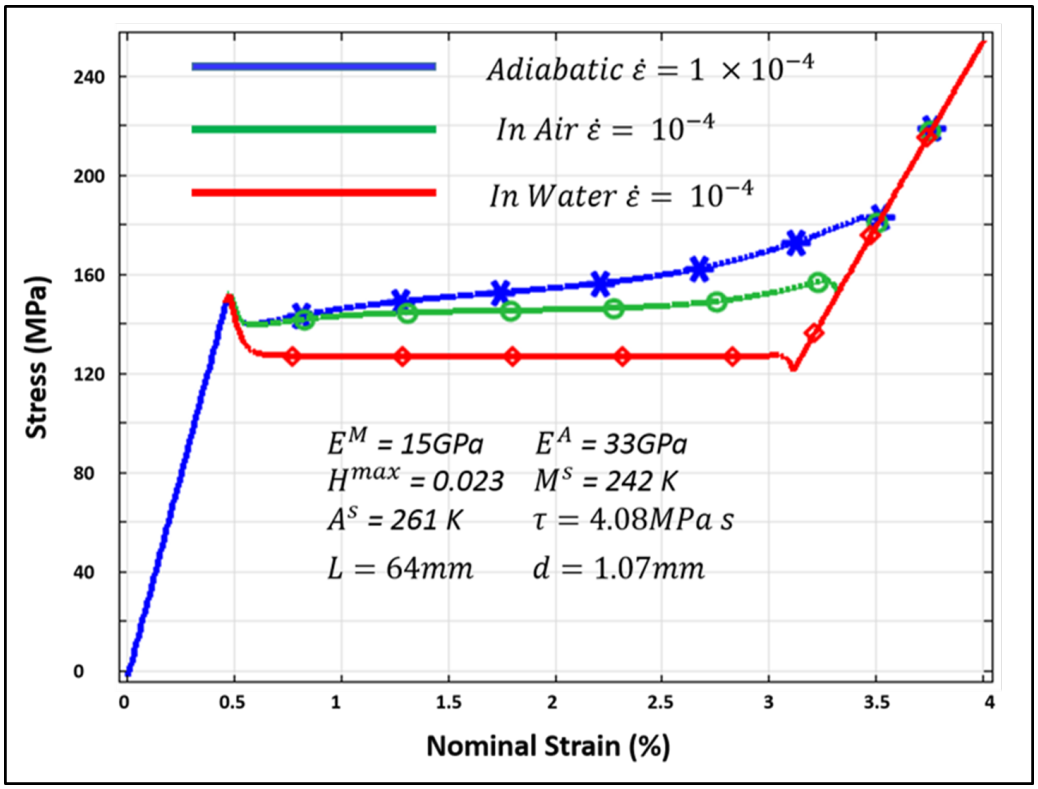

Figure 4.14: Nominal Stress and strain comparison for different ambient medium under the same mechanical loading condition (Agboola et al 2015 [109])

4.3.1 Slow Displacement Controlled Loading of SMA in a Water Environment

Application of SMA under relatively slow loading rate that represents isothermal condition is often taken at a strain rate of about $\dot{\varepsilon} = 10^{-4}s^{-1}$ in water ambient medium. So, to see the ability of the model to simulate this response, result of quasi-static tensile loading of the SMA rod at $\dot{\varepsilon} = 10^{-4}s^{-1}$ within a water ambient medium is reported here. The heat transfer coefficient used is $(h = 890W/(m^2K))$. The result as shown in figure 4.14, comprise results of three ambient medium for the same loading rate. The ordinate axis is the stress and the abscissa axis is the nominal strain. The red color and diamond marker represents the case in water. Notice that the result, which is obtained by solving the full phase transition thermomechanical

field equations, is an exact replica of the result for isothermal condition (see figure 4.6), which was obtained without solving the energy balance for the temperature field. The strong similarity serves to verify the model and the implementation of the full thermo-mechanically coupled models. Just like the earlier result, the result obtained for this simulation is based a nucleation of martensite in austenite at a stress level corresponding to the isothermal critical stress on the stress-temperature phase diagram. After the nucleation, a strain softening is experienced as the stress drops while the strain increases a little due to the transformation strain generated by the martensite domain. After this, a lower rest stress or propagation stress is reached which remains constant throughout the phase transition. The reason is because the ambient medium is considered to be water, the heat is removed throughout the specimen by convection at a faster rate compared to the rate at which heat is being conducted through the material as noted earlier when discussing the temperature field. Therefore only very small peak, localized at the interface, is observed in the temperature field. As a consequence, no thermal hardening is observed since the stress needed to sustain phase transformation remains the same as loading continues. Figure 4.15 shows the accompanying order parameter evolution which is indicative of phase transformation. Notice that the transformation in a water ambient medium is much faster than that of other ambient condition studied. It is important to again note by comparing the temperature field of the water ambient medium as shown in figure 4.16 that the rise in temperature at the interface for the water ambient medium is neglible relative to the other ambient condition. I point this out to show that the result is very consistent with what is expected experimentally for an SMA loaded under water ambient condition for pseudoelastic response of SMA.

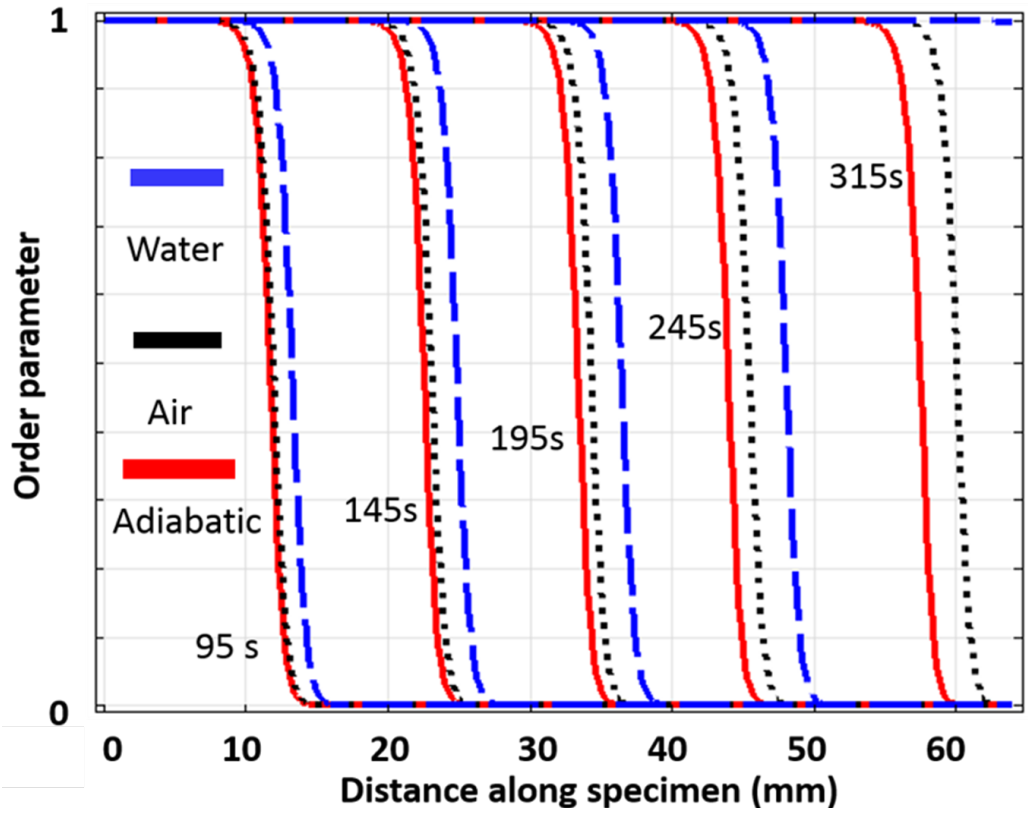

Figure 4.15: Order parameter field comparison for different ambient medium under the same mechanical loading condition (Agboola et al 2015 [109])

4.3.2 Slow Displacement Controlled Loading of SMA in a Air Environment

There are certain applications, if not most, of SMA where the ambient medium is air. In such application, it is desirable to know how the ambient air interacts with the SMA to change its response. So, in order to confirm the ability of the model to simulate such condition, loading at strain rate of $\dot{\varepsilon} = 10^{-4}s^{-1}$ within an air ambient medium is reported here. The heat transfer coefficient used is $h = 6.5W/(m^2K)$. The result as shown in figure 4.14 indicate that unlike the water ambient medium, the air ambient medium (captured by a lower heat transfer coefficient) results in the same initial behavior as the water ambient medium. However as phase transi-

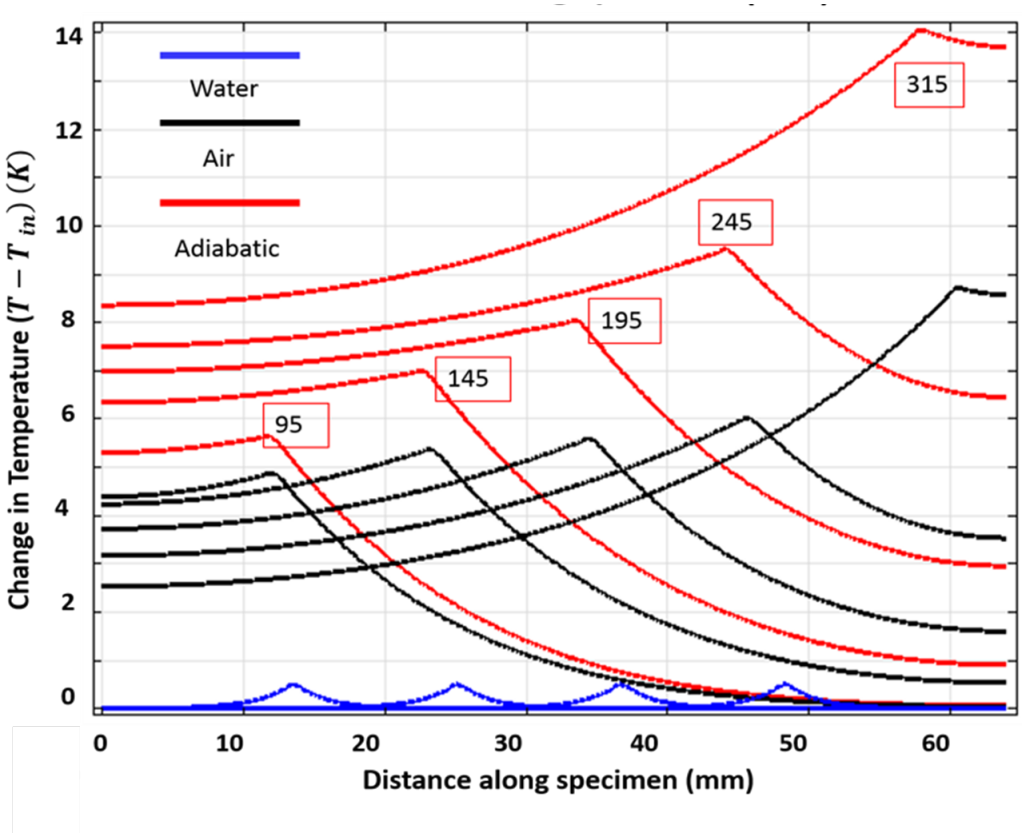

Figure 4.16: Temperature change field for different ambient medium under the same mechanical loading condition. (Agboola et al 2015 [109])

tion continues, thermal hardening is observed as more mechanical work is needed to propagate the phase front due to the rise in temperature. Essentially, a higher stress is needed to keep martensite stable as the temperature rises locally at the interfcace and throughout the SMA rod as heat is being conducted. The relatively higher temperature change at the interface resulting from the exothermic nature of the forward transformation causes thermal hardening. The hardening, which manifested in higher stress magnitude to sustain transformation, increases with further transformation because the heat convection is relatively slower than conduction compared to that of water ambient medium. Therefore, there is moderate conduction

within the rod throughout the phase transition, causing not only the interfacial temperature to rise with further transition but for the temperature of other part of the material to rise as well (see figure 4.16). It is also important to note that the order parameter field for air is much slower than that of water as shown in figure 4.15. Te observation indicates that depending on ambient medium, manifested by difference in cooling rate, the speed of SMA response can vary slightly because of different resistance to transformation. So, the speed of SMA may be controlled by using appropriate cooling medium. The difference between the stress-strain responses of the simulated NiTi SMA for the same quasi-static loading rate shows that the ambient medium in which an SMA is tested is very crucial for their design.

4.3.3 Slow Displacement Controlled Loading of SMA Insulated from the Environment

Although it is rarely the case that an SMA is loaded under an adiabatic condition, it is important to demonstrate that the model does represent the physics of the SMA response under such condition. Therefore, in order to quantify the amount of heat released during the transformation from austenite to martensite, simulation of the loading of the SMA in adiabatic condition is reported. The loading rate is still quasi-static at a strain rate of $\dot{\varepsilon} = 10^{-4}s^{-1}$. The adiabatic condition is simulated by $(h = 0W/(m^2K))$ since no convection is allowed at all by this condition. Therefore, all the exothermic latent heat released into the specimen stays within the specimen-there is no heat flux across the boundary of the material. However, heat conduction dominates due to the temperature gradient between the interface and the rest of the material. Under this condition, there is obvious difference in the stress-strain response of the SMA. More thermal hardening is observed as the stress needed to sustain phase transformation is higher compared to that of water and air as shown

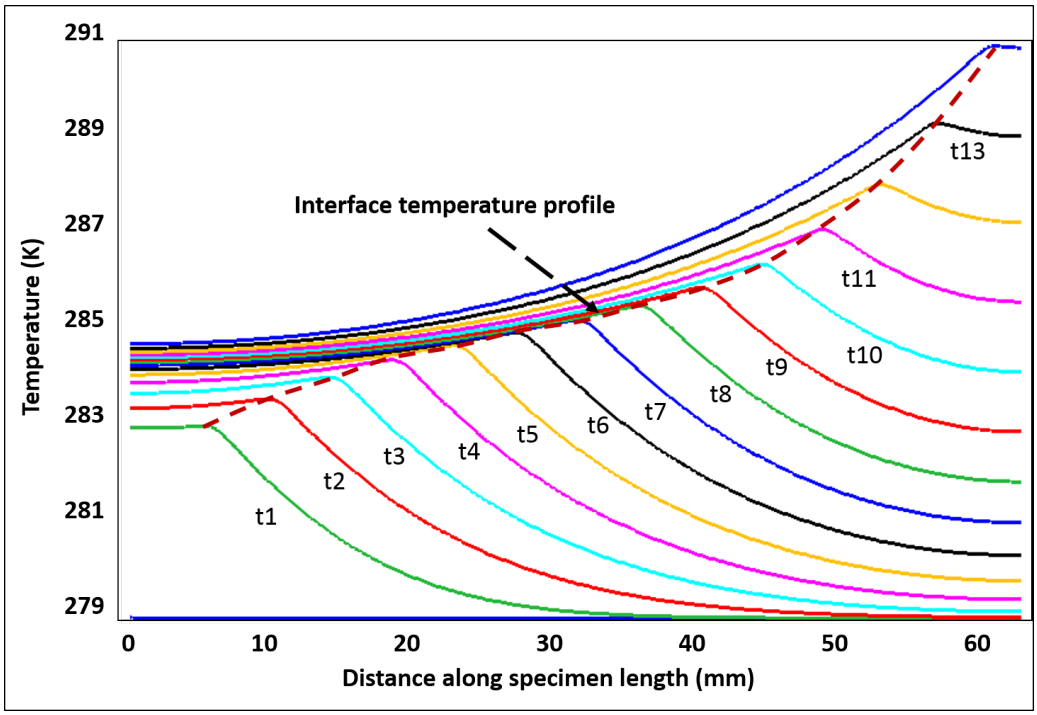

Figure 4.17: Temperature field for constant loading rate in Air. (Agboola et al 2015 [109])

in figure 4.14. Explanation of this higher stress level can be seen in figure 4.16, where not only is the rise in temperature for adiabatic condition locally higher than that of air and water, but also the temperature at parts of the SMA that are not the transformation front. The temperature of the other part of the rod rises considerably. The degree of temperature rise is much higher than that of air and water. The reason for this is because only heat conduction takes place within the SMA rod due the temperature gradient that drives it. Another observation is that the temperature field shows a switch in behavior as time increases. This switch is due to the fact that although heat is rising throughout the specimen by heat conduction, the region closest to the interface experience higher increase per time as compared with the rest of the material. Therefore, initially the left region has higher temperature while

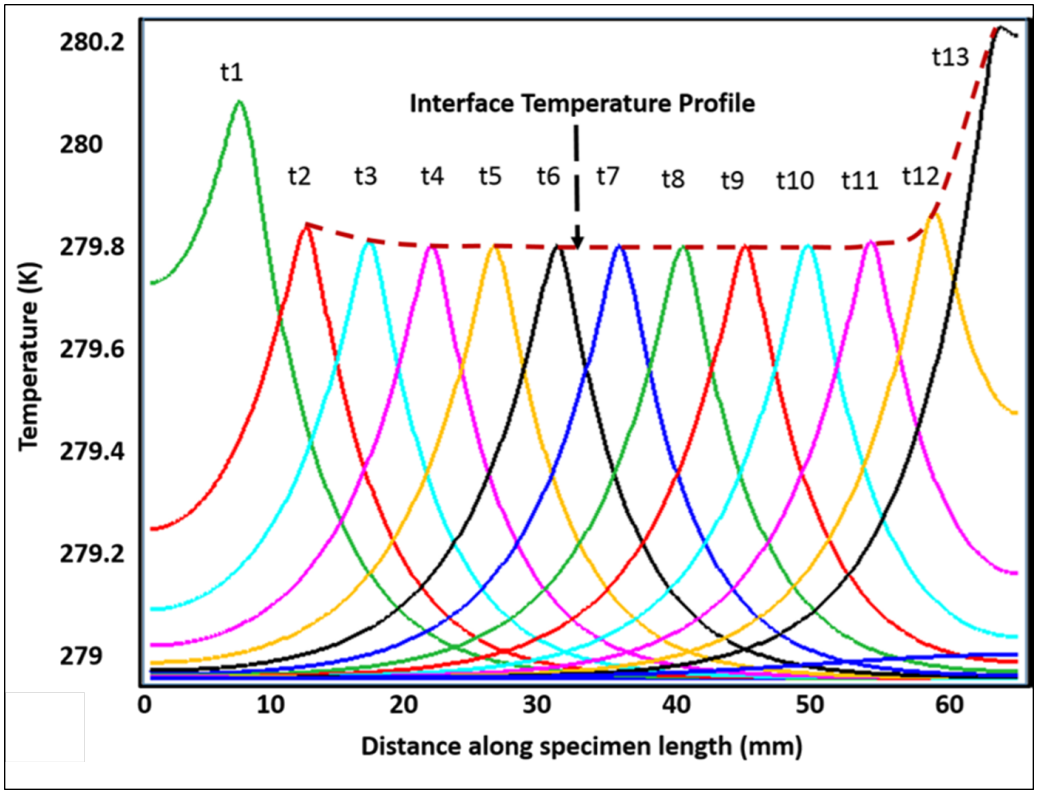

Figure 4.18: Temperature field for constatnt loading rate in Water.(Agboola et al 2015 [109])

towards the end of transformation; the right region has higher temperature. It is important to note that the hardening of SMA or lack thereof depending on ambient media is reflected in the comparison between the stress-strain reponse during inelastic deformation and the temperature field. The dashed red lines of Figures 4.17 and 4.18 shows that the fields are similar to that of the inelastic portion of the stress-strain plots for air and water ambient medium respectively. The observation corroborate the hypothesis that transformation occur locally at the interface thereby having a different stress-strain field which is commensurate to the temperature field at the interface per time along the specimen.

So, it is obvious that a time scale associate with interface evolution, which re-

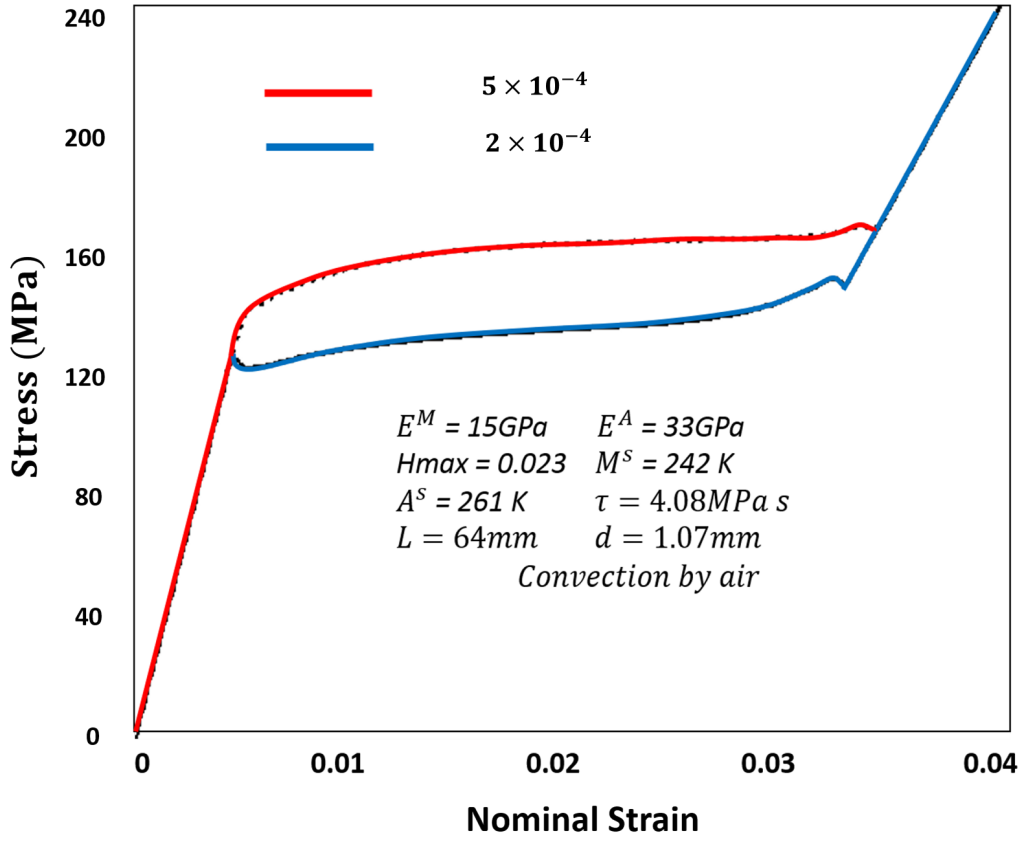

Figure 4.19: Stress-Strain plot under different strain rates in air environment. (Agboola et al 2015 [109])

sult fromt the configurational forces balance, is essential for modeling reliable and controllable SMA response.

4.3.4 Effect of Tensile Loading Rate on SMA Operating in Air Environment

The simulations reported so far is for difference in response of SMA for different environment condition but the same loading rate of 1×10^{-4}. Here simulation in air ambient medium under loading rate of 2×10^{-4} also show thermal hardening, similar to 1×10^{-4}. The reason is the same as that of slower loading rate but the stress-strain response is different as the loading rate is much faster. The faster loading rate

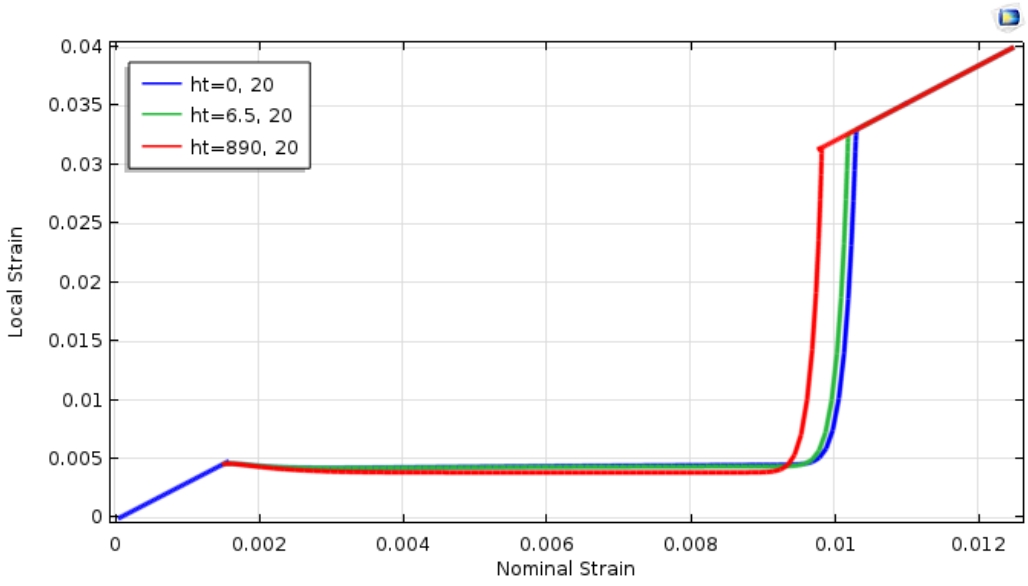

Figure 4.20: Local strain-nominal strain response for different ambient medium under the same mechanical loading condition at $x = 20mm$

does not allow for much time for the heat to be taken out of the material through convection to the ambient medium. Therefore the stress increases much higher than that of 1×10^{-4} since the degree of rise in temperature at the interface is higher. Higher stress value is, therefore, needed to keep martensite as the stable phase. The stress-strain response of figure 4.14and figure 4.19 are different as the loading rate has changed from 1×10^{-4} to 2×10^{-4} and then to 5×10^{-4}. Although the rate at which heat is being exchanged with the ambient medium (simulated by the heat transfer coefficient of air) is the same, the loading rate increase result in different critical stress and the value of the stress during inelastic strain accumulation is increased with the loading rate.

Another feature which is consistent with experimental observation is the vanishing of the strain softening as the loading rate increases. So far, simulation shows that the macroscopic stress strain response of given polycrystalline NiTi SMA, at the

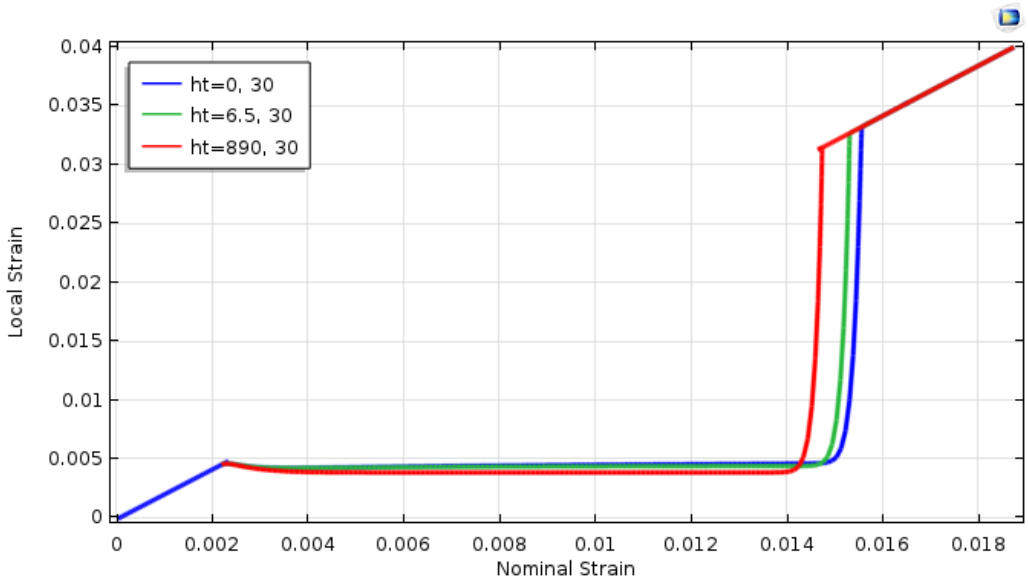

Figure 4.21: Local strain-nominal strain response for different ambient medium under the same mechanical loading conditionat $x = 30mm$

minimum depends on complex interaction between the phase transition kinetics, the external loading rate (mechanical work rate), the speed of heat convection and that of heat conduction away from the interface. Experimentalists have reported similar conclusion.

4.3.5 Nominal Strain-Local Strain Response

The fact that SMA transform by the propagation of a boundary between fully austenite and fully martensite phases, which result in localization of strain, the local strain and the nominal strain is expected to be different. This has been observed in experiments [4]. In order to verify that this model actually capture the appropriate phase boundary motion relation, local strain is plotted against the nominal strain at different point the specimen. These results are depicted in figures 4.20, 4.21, 4.22, 4.23 for local strain measured at $20mm$,$30mm$,$40mm$,$64mm$ respectively . The strain fields generated match qualitatively with that of experiment as

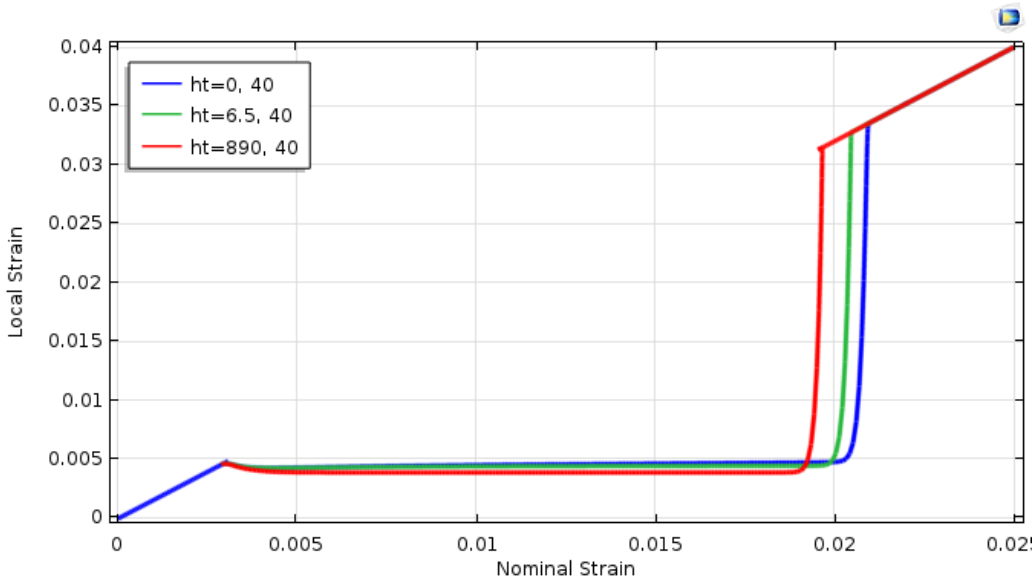

Figure 4.22: Local strain-nominal strain response for different ambient medium under the same mechanical loading condition at $x = 40mm$

seen in figure 7b of [4]. Observe that initially the local (which would represent a local extensometer measurement) and nominal strain(which represents grip displacement divided by specimen length) is the same during elastic deformation of the material for measurement taken at the end of the rod as seen in figure 4.23

Measurement of elastic deformation taken at $20mm$,$30mm$,$40mm$ respectively shows that the nominal strain increases slower than the local strains. At the end of elastic loading, the local strain is 0.005 as seen in the result of figure 4.20 to 4.23 . However, the nominal strain is smaller than the local strain at end of the elastic response stage. The nominal strain is measured as $\frac{u}{L}$, where u is the displacement measured at each point in consideration for the figures. Once the stress reaches the critical isothermal stress level, at the point of nucleation of martensite in austenite; strain localization begins which result in increase in nominal strain as transformation progresses. Observe that once the transformation front reaches the point where field

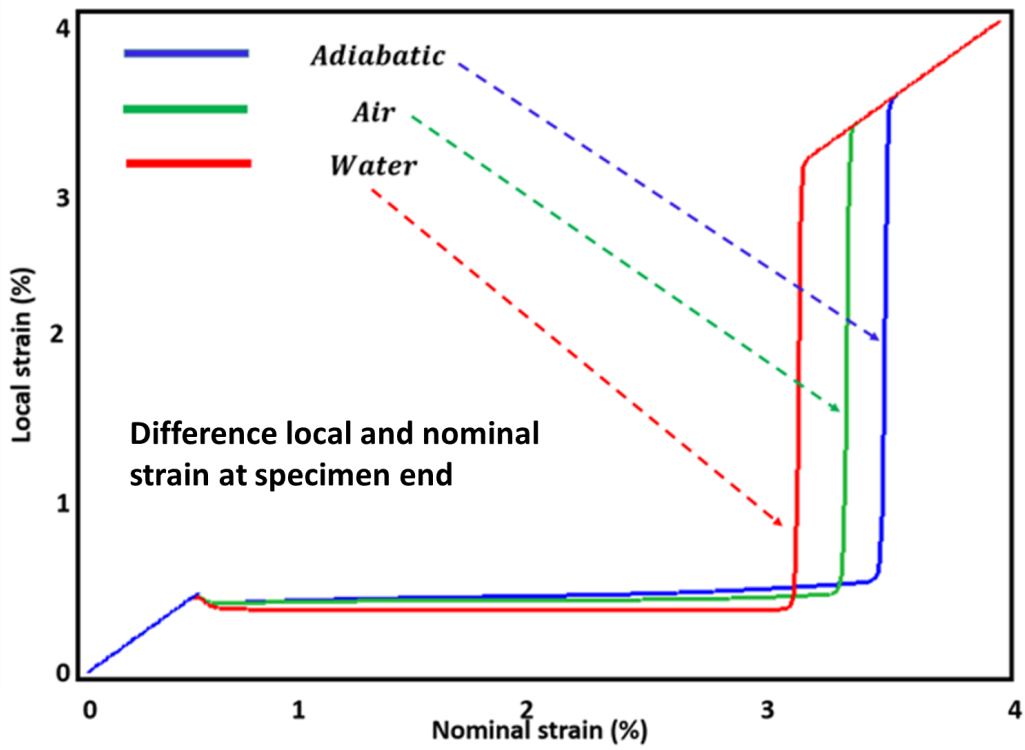

Figure 4.23: Local strain-nominal strain response for different ambient medium under the same mechanical loading condition at rod end $x = L$

s are measured in each of the figures, the local strain experiences a jump in value to increases to that of the Nominal strain. This train field demonstrates as well that not only is the experimental features of the response of this SMA specimen rightly captured but also that the hypothesis of the need to model SMA using transformation by evolving interface is confirmed. For the response of figure 4.23, as the transformation front propagates, inelastic strain is accumulated as the deformation is now inhomogeneous until the entire material is fully transformed. Once the transformation reaches the specimen end, the local and nominal strain becomes the same, which manifest in a jump of strain at the end of the specimen. Subsequent application of load result in elastic deformation of the fully martensite SMA. Another important

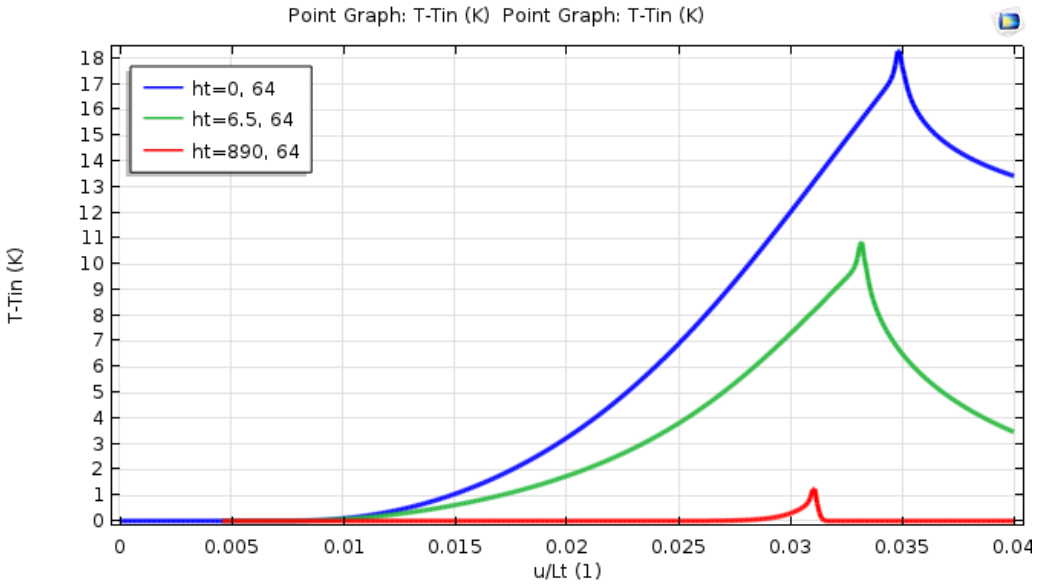

Figure 4.24: Change in temperature-nominal strian response for different ambient medium under the same mechanical loading condition at the end of the rod $x = L$

observation is that the nominal strain level at which the local strain experience jump to match with that of the nominal strain increase as the ambient medium changes from water environment to adiabatic thermal condition for all the results of figures 4.20, 4.21, 4.22, 4.23 .This is because, as explained in earlier section, transformation progresses faster in water than in air and faster in air than in adiabatic condition, manifested by the difference in speed of transformation fronts. The explanation is that due to the level of resistance to transformation by thermal hardening of the materials. A representative plot of change in temperature against nominal strain field at the end of the SMA rod is shown in figure 4.24. Notice that in the figure, the same trend of temperature field across the specimen dimension is shown in the change in temperature against nominal strain. The changes in temperature are higher in ambient medium than in air and higher in air than in water environment. Also looking at the strain level at which the peak in temperature occurs, it is the

same that of the jump in the local strain to increase to that of the nominal strain for the loading in water ambient medium. The temperature peak is also close to the local stain jump for the other local points of measure results. The trend is similar to what was observed in the experimental result by Shaw and kyriakides (1995) (see figure 7b in the paper)

So far, the set of result reported have demonstrated that the macroscopic stress strain response of given polycrystalline NiTi SMA, at the minimum depends on complex interaction between the phase transition kinetics, the external loading rate (mechanical work rate) , the speed of heat convection and that of heat conduction. These observations have been reported in experiment[22]. In addition, and of greater importance the result reported in this work so far demonstrate a strong qualitative and near qualitative agreement between the trend observed in experiment and the simulation. The difference being only in that the properties of the SMA used as compared to that Shaw and Kyriakides (1995) are different but the specimen dimensions are the same. So far, the result of the model suggests strongly that this model promises to be reliable for SMA modeling particularly for thinner devices and components where strong thermo-mechanical interaction with ambient and external mechanical loading rate becomes very significant. This model developed in this work is able to capture experimental features because of the intrinsic rate dependency associated with the phase transition through the introduction of a new interface kinetic time scale along with other time scales of convection, conduction and wave propagation.

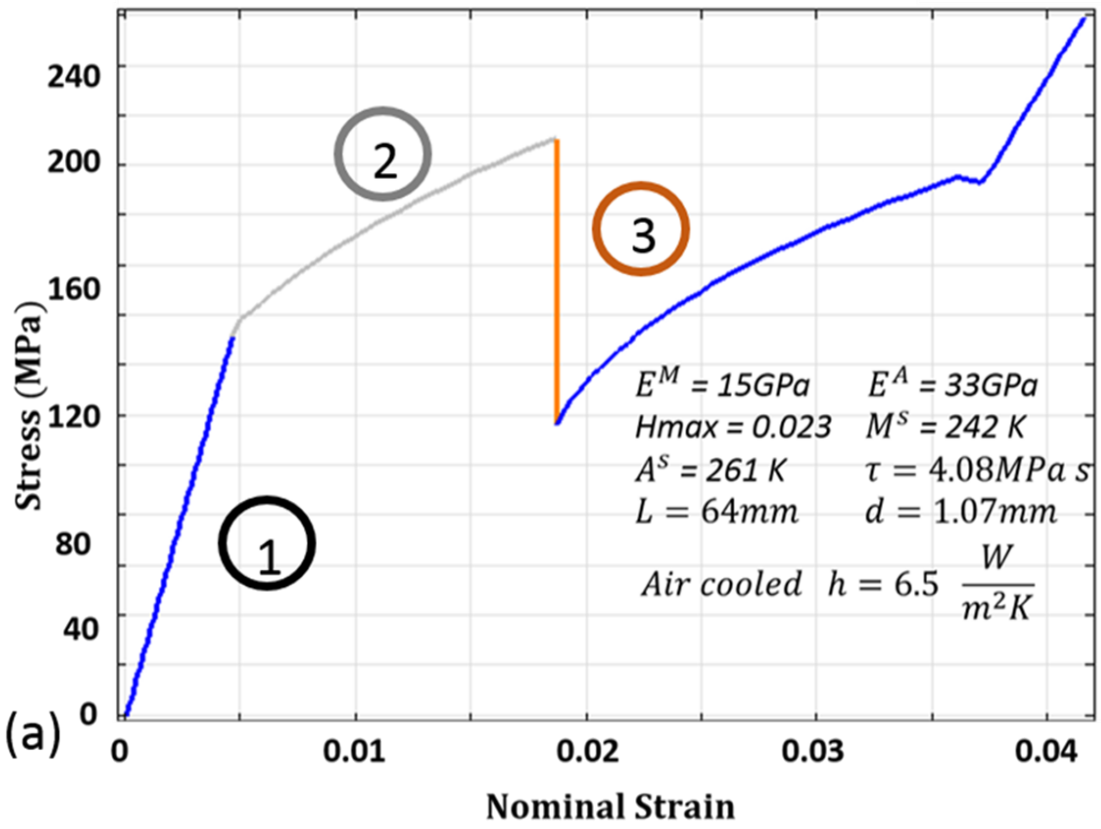

Figure 4.25: Stress relaxation in NiTi SMA within an air ambient medium for representative NiTi parameter in table 4.1 (Agboola et al 2015 [109])

4.4 Mechanically Induced Phase Transformation-Pseudo-Viscoelasticity

Seeming viscoelastic behavior has been reported for shape memory alloy . This behavior includes strain creep at fixed stress and stress relaxation under fixed strain. Simulation of these two phenomena and possible explanation is the focus of this section. The simulations in this work not only show the ability of the model to capture the pseudo-viscous behavior of SMA as claimed by some researcher , and gives scientific explanation for the observed response. There have been two prevalent views on the stress-relaxation and creep observes in SMA near room temperature, which

is appear somewhat anomalous. *Reason being that viscoelasticity is usually observed in Metals at very high temperature based on the mechanism of dislocation.* One view is that the pseudo-creep and stress relaxation in SMA is solely a manifestation of the strong thermomechanical coupling in SMA response. Essentially, that the stress relaxes because temperature drop after the displacement is fixed at the end of the specimen thereby causing the stress needed to sustain phase transformation to also drop. Similarly, it is claimed that the pseudo-creep is a result of the same temperature drop. The other view is that apart from the strong thermomechanical coupling, there is a viscous property of the material that serves to result in these two phenomena of stress relaxation and pseudo-creep. So, to further check my validity of the chosen method that there is the need to use the balance of configurational forces as fundamental to other balance laws of continuum physics to introduce the time scale of phase transformation (consequently how it couples with wave propagation), these seeming anomalous characteristics phenomena are simulated.

4.4.1 Stress Relaxation under Constant Strain in SMA

In addition to the scientific questions on these phenomena in SMA, some researchers such as Russalian and Bhattacharyya [110] have suggested that it is expedient to simulate this behavior under pseudoelastic loading because the ability of model to capture this feature will serve to validate the model as appropriate for SMA design[110]. Initial attempt to simulate the phenomena of stress relaxation in SMA generate the result shown in figure 4.25. The IBVP involve an SMA loaded at a constant stress rate of about $3.3MPa/s$, rather than displacement rate, until a critical stress for transformation is reached based on the $\sigma - T$ phase diagram. At this stress level, martensite is seeded at the left end of the rod. The stress level is produces critical driving force to ensure phase transformation progress. Therefore,

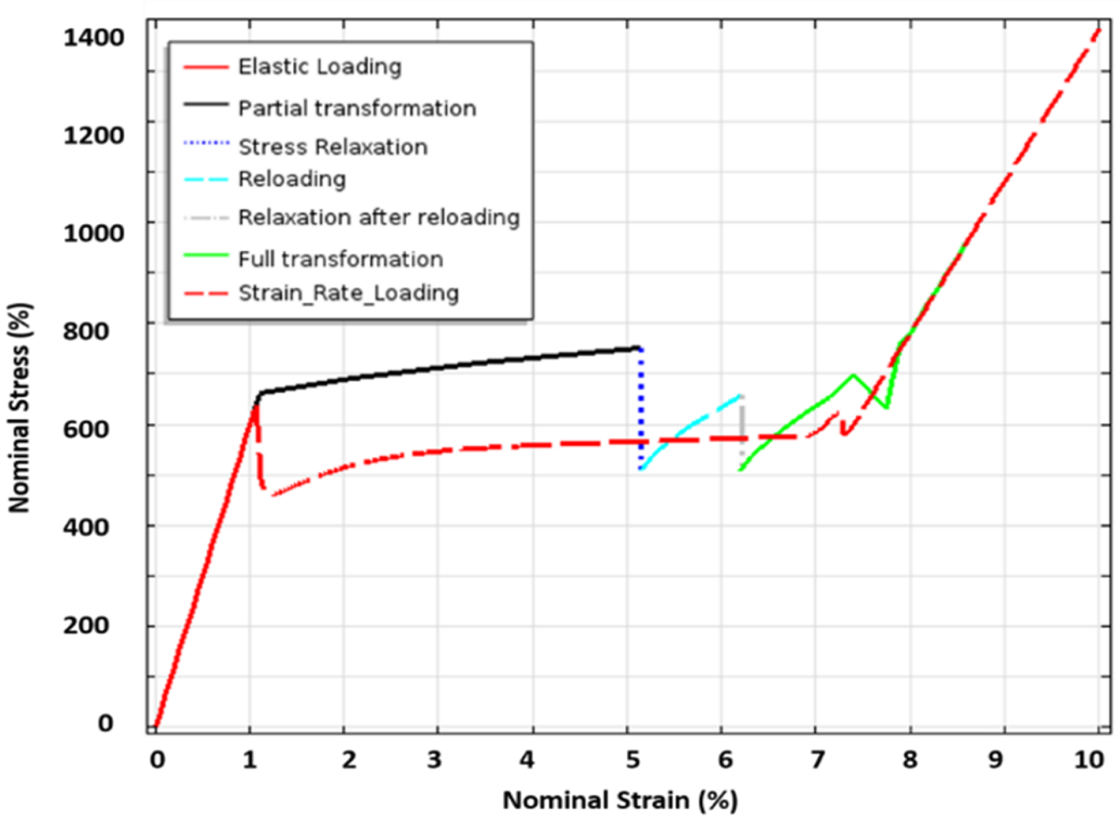

Figure 4.26: Simulated force controlled loading stress-strain response and transformation induced stress relaxation (Agboola et al 2015 [109])

the phase transformation is allowed progress until a point at which the displacement is fixed. The response of the SMA is reported figure 4.25. The figure shows that initial loading of SMA result in elastic homogenous response as shown by stage 1 (blue) of figures 4.25. Once the critical stress is reached, transformation progresses and is shown as stage 2 (gray) in the plot. At this stage the stress continues to increase at constant rate of $3.3MPa/s$ causing accumulation of strain to about $0.018s^{-1}$. The displacement is then fixed at this point to a value of $0.018*L$, where L is the specimen length. The displacement is held constant until about 600s. The stress is observed

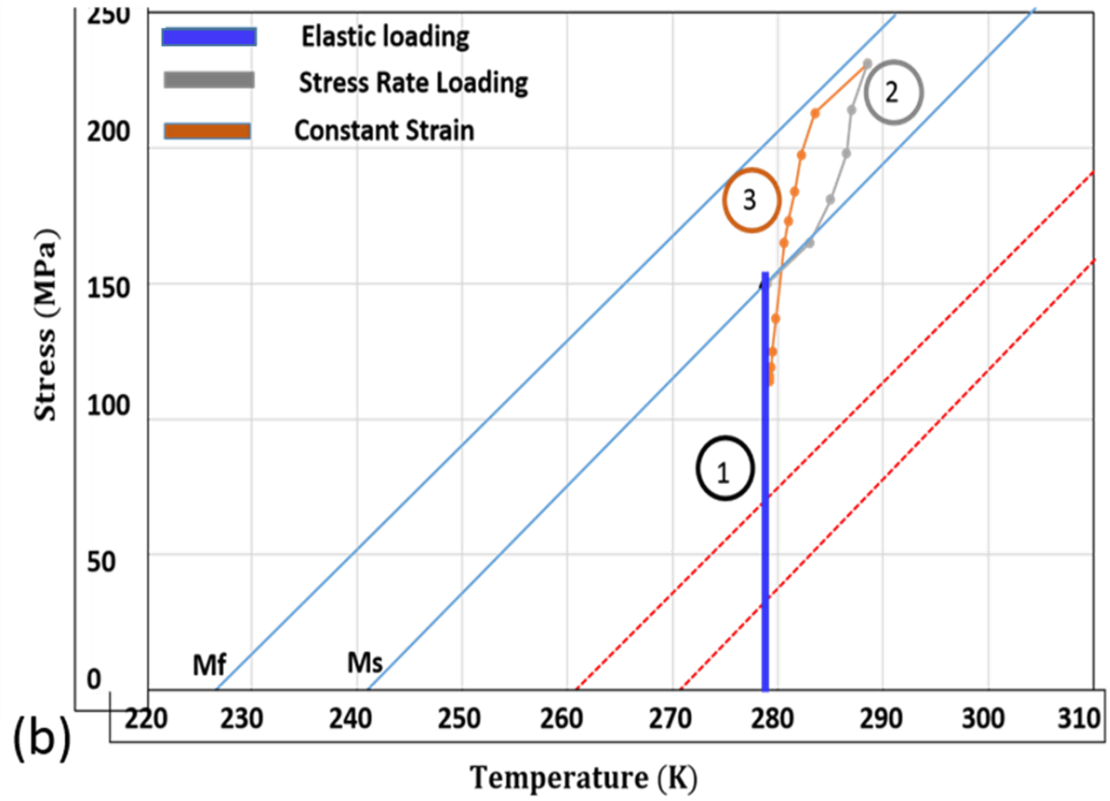

Figure 4.27: Associated stress temperature field for stress relaxation with air ambient medium for parameter in table 4.1 plotted on the stress-temperature phase diagram of the NiTi SMA (Agboola et al 2015 [109])

to drop as indicated by the line labeled 3. Additional energy by through external work on the specimen boundary is required to further transform the SMA after the rest or equilibrium stress is reached. The process of keeping the displacement fixed is often called "strain arrest" by some researcher [110]

It should be noted that the final stress under strain arrest is the value of the plateau stress value needed to propagate the front for an equivalent displaceement rate controlled dloading of the same SMA in water ambient condition (isothermal) as seen in figure 4.26 (see dashed line showing softening). Therefore the result

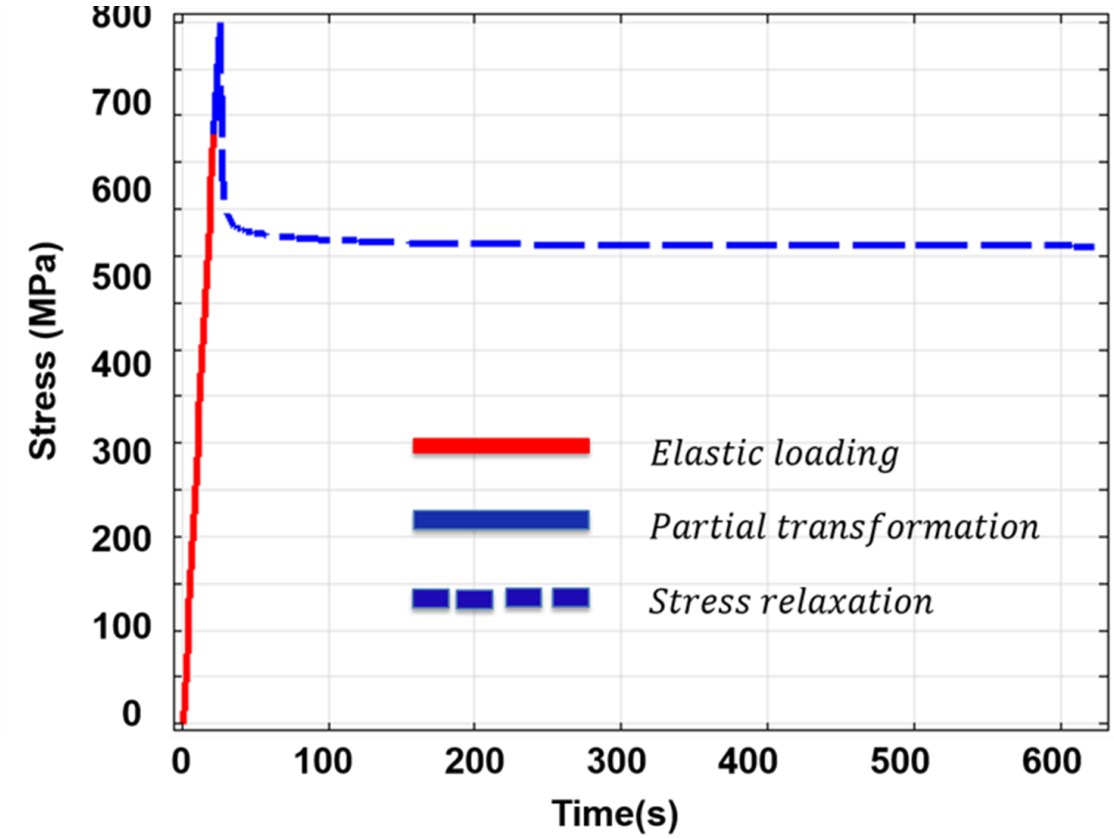

Figure 4.28: Force controlled loading Stress-Strain response and Stress against time during elastic response,partial transformation and stress relaxation.
(Agboola et al 2015 [109])

indicated that the model is able to predict stress relaxation in SMA. A plot of the accompanying temperature profile suggest that during relaxation, the temperature of the interface drops as the system seek to move towards equilibrium (see figure 4.27). The simulation reported in figure 4.25 are all based on properties shown on it. It is important to state here that there is not stress relaxation experimental result for this particular NiTi SMA. So the result is at best qualitative and could not be used to make conclusive statement on the ability of the SMA to simulate stress relaxation. Now based on the loading rate reported by Matsui et al, to see if this relaxation

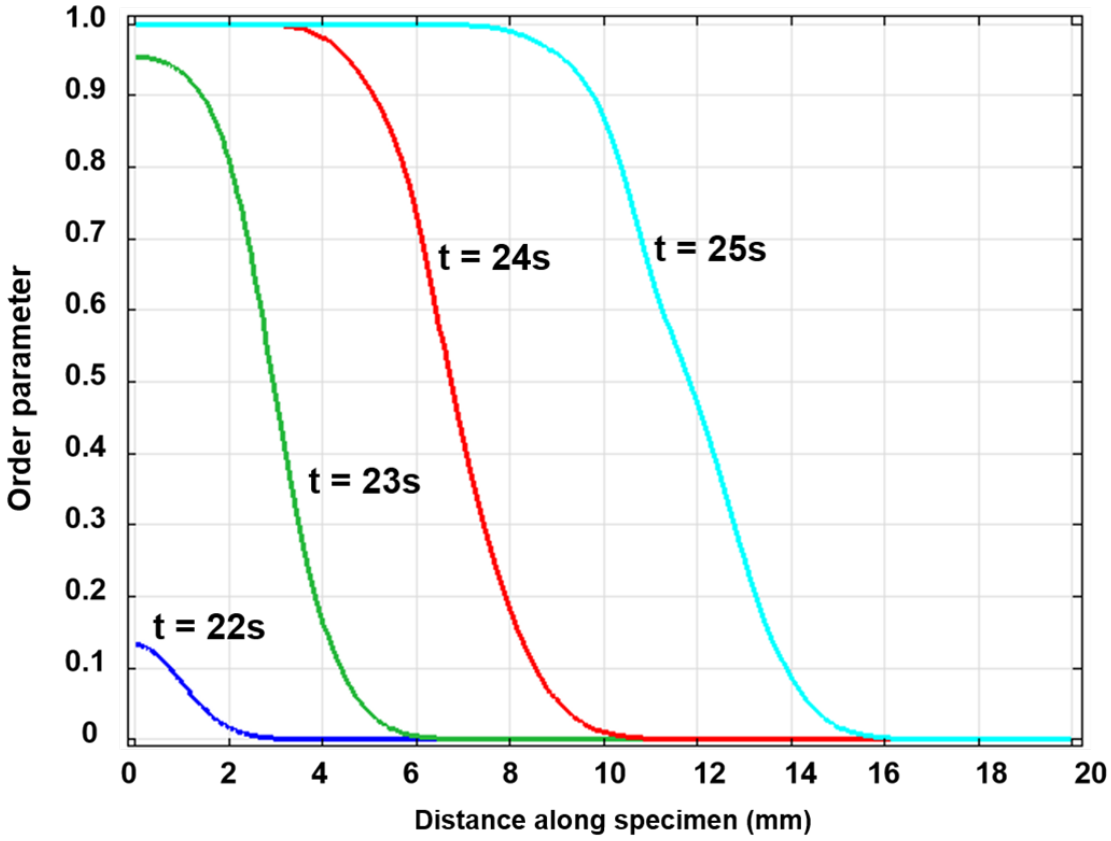

Figure 4.29: Order parameter field showing evolution of transformation front during partial transformation (Agboola et al 2015 [109])

will occur under isothermal condition, simulation using the parameters on figures 4.33 and 4.32. The results are for the response under full thermomechanical loading (i.e. solving the three field equations) and isothermal (i.e. solving balance of configurational forces and balance of linear momentum) respectively. Both result shows obvious relaxation. However, the relaxation final or asymptote stress magnitude is slightly different. These two results indicate that the stress relaxation behavior in SMA is due not only to the strong thermomechanical coupling but also to a possible intrinsic reason that is viscous. At this point, the desires to explain the relaxation phenomena and propose this model as relevant for SMA design necessitate the need

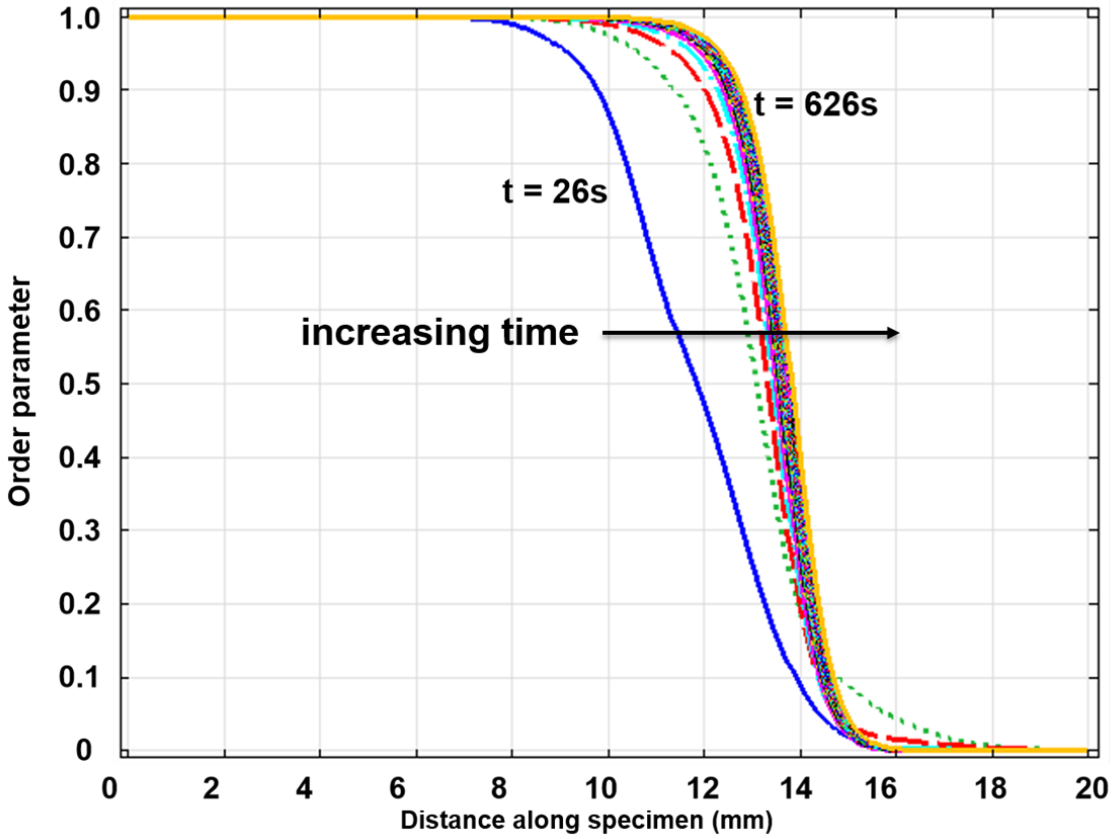

Figure 4.30: Order parameter field showing evolution of transformation front during relaxation (Agboola et al 2015 [109])

to simulate an actual experimental relaxation result with known response and parameters. In 2004, Matsui et al reported experimental results of stress relaxation.These set of result is simulated and the result will be discussed next. The properties of the SMA used by Matsui et al is given in table 4.2 and it is based on the experimental result by Tobushi et al 2004 with the parameter value taken form Tobushi et al 1995 for the same SMA composition. To simulate the response of the SMA, the gradient energy coefficient per unit mass (λ) as well as the kinetic modulus (τ) of the model is calibrated to predict the response of the stress based loading of the SMA, which is shown in figure 4.26 (solid black line and subsequent loading and relaxation). The

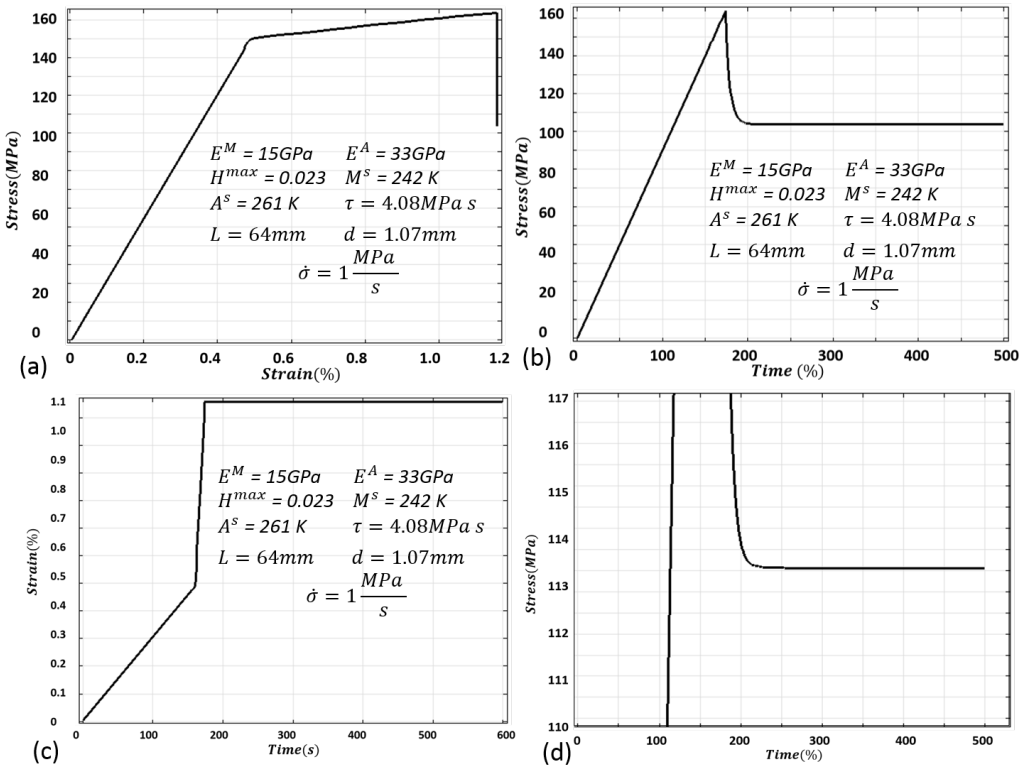

Figure 4.31: Isothermal stress relaxation during constant strain under stress rate of 1 MPa/s

value of the gradient energy coefficient ($\rho\lambda$) and the kinetic modulus (τ) that gave this result are $5N$ and $1 \times 10^7 Pas$ respectively. It should be noted however that for the partial transformation simulation to match with experiment, the value of the heat transfer coefficient is $640W/m^2K$. Once the simulation for the partial transformation (solid black line) and the experiment is the same, the total strain is then arrested. The heat transfer coefficient of $h = 4W/m^2K$ is used to simulate the stress relaxation. The final value of the relaxed stress as predicted by the model matches with that of the experiment for the set of parameters used (see figure 1.12 and 4.28). This value of τ ,$\rho\lambda$ and heat transfer coefficient of $4W/m^2K$ is now used to simulate the experiment for strain rate loading. The result is also in very good agreement

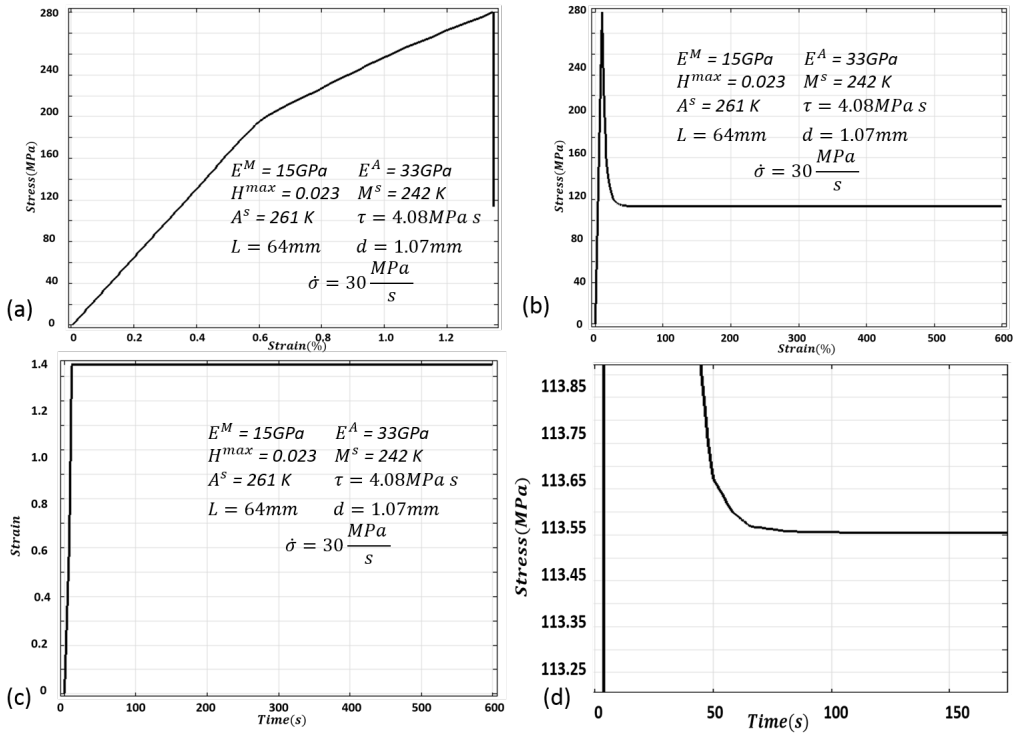

Figure 4.32: Simulated stress relaxation phenomena for coupled isothermal displacement and order parameter field equation under 30 MPa/s sress loading

with the experiment within acceptable discrepancies as seen by comparing figure 1.12 and 4.26 These observations may seem to suggest that the stress relaxation in SMA is solely due to the drop in temperature, whereby the thermal state favors the formation of martensite; therefore less stress is required to ensure further phase transformation due to the thermomechanical coupling. However, this conclusion may be misleading unless the same behavior can be observed under isothermal condition. It is important to note here that the theory that the stress relaxation is due to the drop in temperature during strain arrest has been put forward by some researchers . The question to ask, however, is what our model points towards as the reason for the stress relaxation.

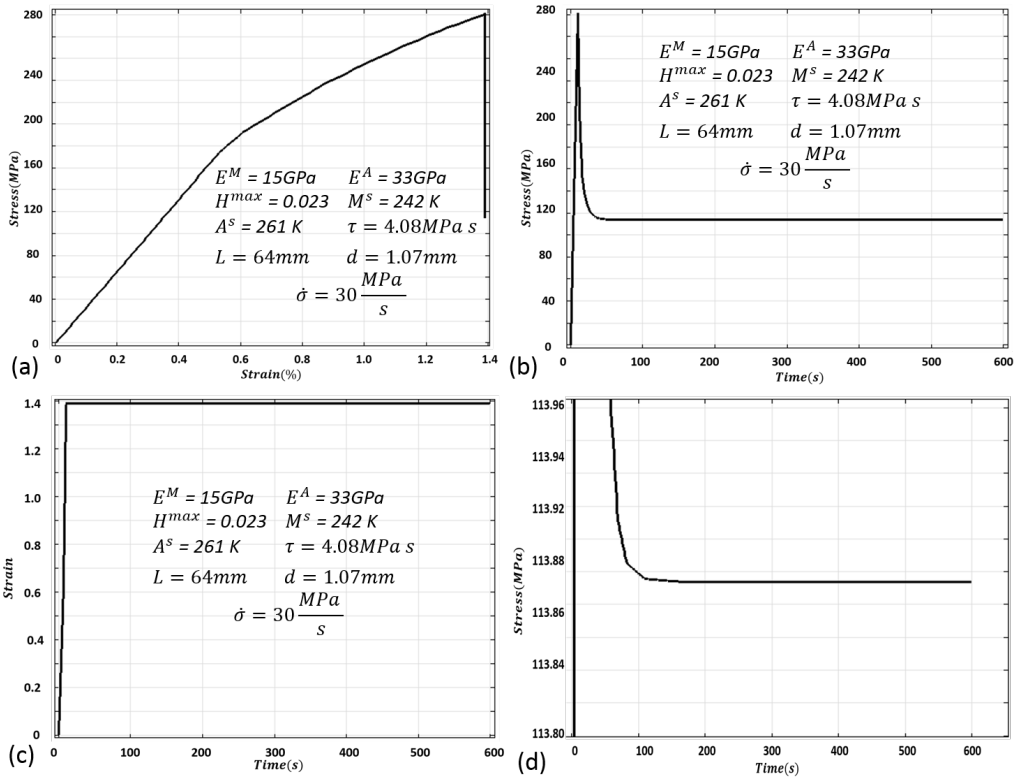

Figure 4.33: Simulated stress relaxation phenomena for fully coupled thermomechanical field equation under 30 MPa/s sress loading

According to the simulation, this relaxation occur due to the further motion of the transformation front which indicates continued phase transformation as the SMA relaxes towards equilibrium (see figure 4.26,4.28,4.29 and 4.30). The model shows that there is a time lag between when the strain was arrested and when the front stops. So, is this further motion of the front (i.e. further transformation) due to drop in temperature or not? To arrive at a solid conclusion, we decided to simulate the relaxation phenomena under isothermal condition using this model. Since there is no thermal effect during relaxation, we expect that if the main reason for the relaxation, due to the motion of the front, is the drop in temperature then we expect that this phenomena should not occur for this isothermal case. On the

contrary, the result of our simulation under isothermal condition does show that transformation front moved during the time that the displacement was fixed and consequently stress relaxation. (See figures 4.31) Therefore, there is reason to belief that apart from thermomechanical coupling, there is an intrinsic explanation for the drop in stress. Since thermal effect is eliminated, we expect that the system move towards a state of equilibrium by minimization of the strain energy and the interfacial energy. Therefore the strain energy stored in the SMA will be expended to move the transformation front. Since the total strain is kept fixed and further inelastic strain accumulate by the further motion of the transformation front, the stress drops so as to maintain the constant strain imposed at the boundary. Noticed that after a given time the stress in the SMA reaches an asymptotic value where the interface stops moving such that for transformation to continue, more energy has to be supplied to perform work in moving that phase transformation front by loading the SMA at the boundary. In addition, to arrive at a solid conclusion, strain arrest under isothermal condition using this model is simulated. Since there is no thermal effect during relaxation, it is expected that if the essential reason for the relaxation resulting from front motion is the drop in temperature then this phenomena should not occur under isothermal condition. The result of our simulation, under isothermal condition, does show the contrary. Stress relaxation and motion of transformation front still occured during strain arrest both for $1MPa/s$ and $30MPa/s$ loading rate as can be seen in figures 4.31 and 4.32. for the $30MPa/s$ loading rate, the corresponding full thermomechanical field equation response is shown in figure 4.33, which strongly show relaxation very close that of teh isothermal. These set of results further corroborates the observation of relaxation under isothermal condition.

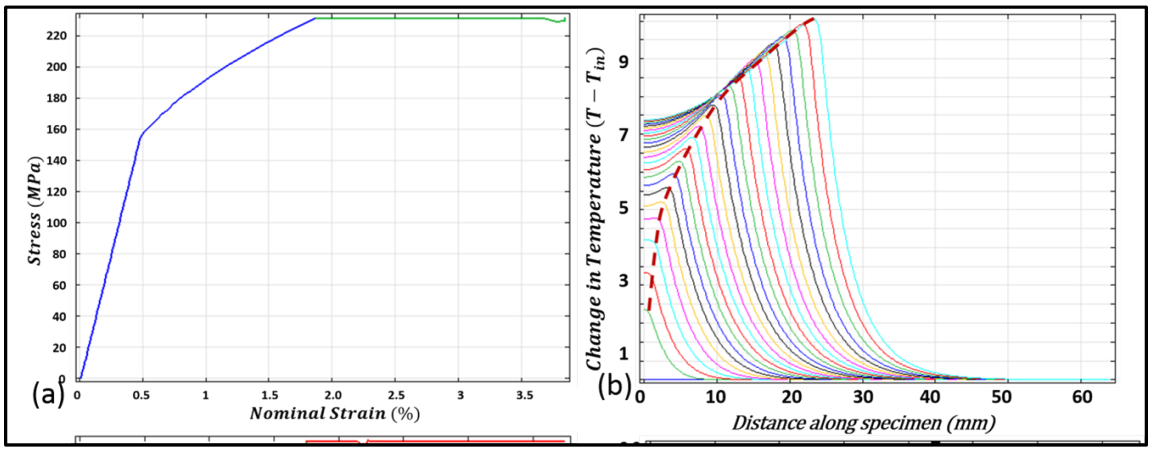

Figure 4.34: (a) Stress strain response during partial transformation and creep in SMA (b) Change in temperature field during partial transformation (Agboola et al 2015 [109])

4.4.2 Transformation Induced Pseudo-Creep

As reported by experiment and shown in figures 1.13 and 1.14, accumulation of strain when stress is constant during transformation is characteristic of pseudoelastic loading of SMAs. In order to validate the versatility and accuracy of this model and its predictions, transformation induced creep behavior of NiTi SMAs is simulated. The simulation is carried out under load and displacement control. Similar to the stress relaxation, the simulation is performed under full thermomechanical coupling and under isothermal condition to corroborate the scientific explanation that the relaxation and creep is not only due to thermomechanical coupling but also an intrinsic viscous like effect resulting fron the evolution of transformation from resulting in isothermal transformation.

4.4.2.1 Transformation Induced Creep under Force Controlled Loading

To simulate the "pseudo-creep" in SMA, the SMA is loaded (using properties in table 4.2) under a stress rate of $3.3MPa/s$ until a strain of about 0.018. At this

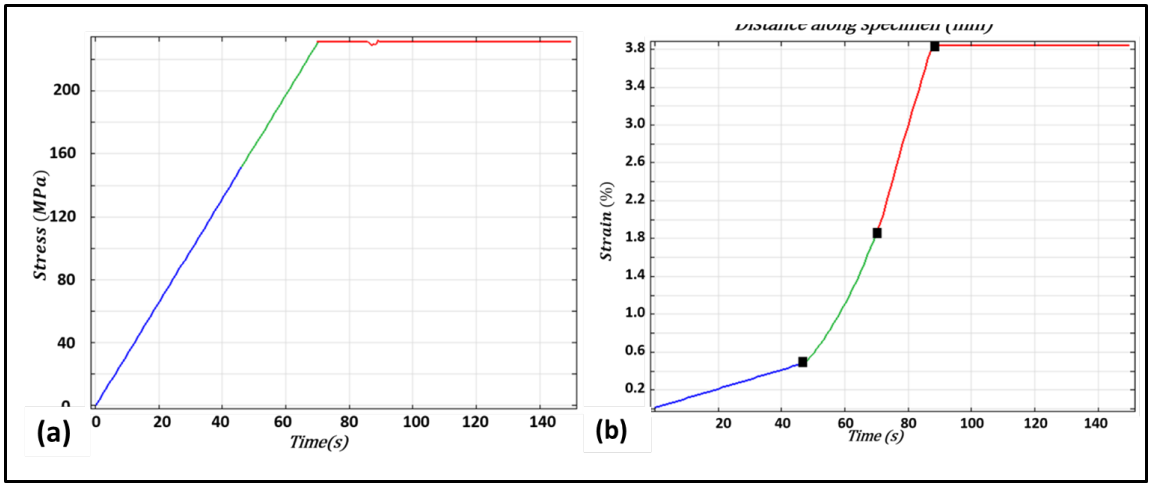

Figure 4.35: (a) Change in stress with time (b) Change in stain with time (Agboola et al 2015 [109])

point the stress is kept constant. The analysis shows, as can be seen in figures 4.34 and 4.35, that strain continues to accumulate until the SMA is fully transformed if the stress is kept constant. This is also due to the fact that the transformation front continues to move as seen in order parameter plot in figure 4.36) as the stress state is above the rest stress associated with mechanical state that allows the two phases to exist in equilibrium. It should however be noted that this simulation was carried in an air ambient medium. Therefore there is going to be heat convection out of the specimen under constant stress, which seem to provide reasonable explanation for the continuous transformation since the lower temperature would favor the stability of austenite over martensite for the same stress level. Since the total strain is not fixed, there is no drop in stress although transformatiion continues as represented by the order parameter evolution, consequently transformation strain. The inelastic or transformation strain continues to accumulate due to the motion of the transformation front until the entire material is fully transformed. It is worth noting that in this case as well, the stress-strain response follows the temperature field as shown in

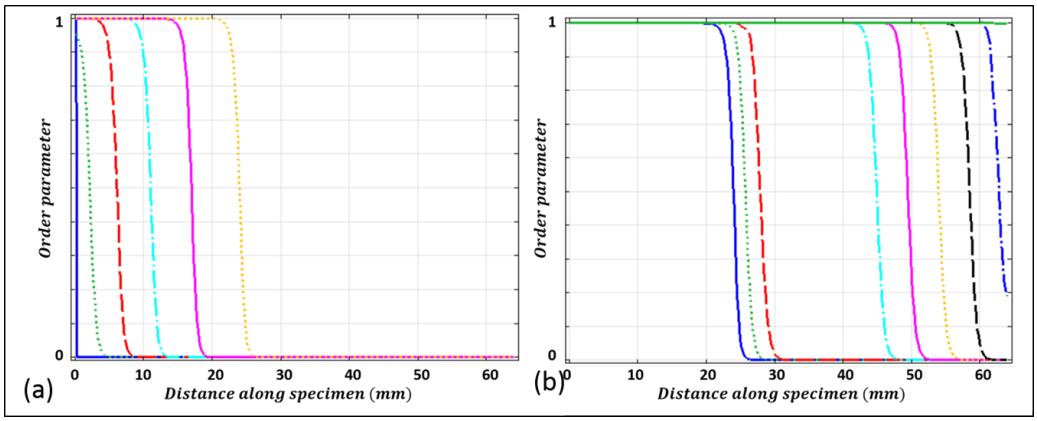

Figure 4.36: Order parameter change showing transformation front evolution during (a) partial transformation and (b) strain accumulation (creep) under stress arrest (Agboola et al 2015 [109])

figures 4.34. Another interesting observation is that the strain-time and stress-time response matches very well with experimentally observed trend.(see figure 4.35 a and b). Figure 4.35a demonstrates that during the strain accumulation the stress in the simulation is actually kept constant. So, there is no doubt that the pseudo-creep actually occurred.Figure 4.35a show the stain plot against time. The result show an initial increase in strain with time at constant rate after which the slope changes because transformation has started at about $46s$. At about $77s$ the stress is kept constant and the strain continues to accumulate until about 90s where the strain no longer increase with time because the entire material has transformed to martensite. The temperature field accompanying the strain accumulation at constant stress is given in figure 4.37a and b. Figure 4.37a represents shows that during the transformation, the temperature field exhibits an increase at the interface as time increases. Once the stress is kept constant, the temperature as shown in figure 4.37b begins to drop with time which favors the formation of martensite at constant stress. So just like that of stress relaxation, there is an obvious thermomechanical reason for the

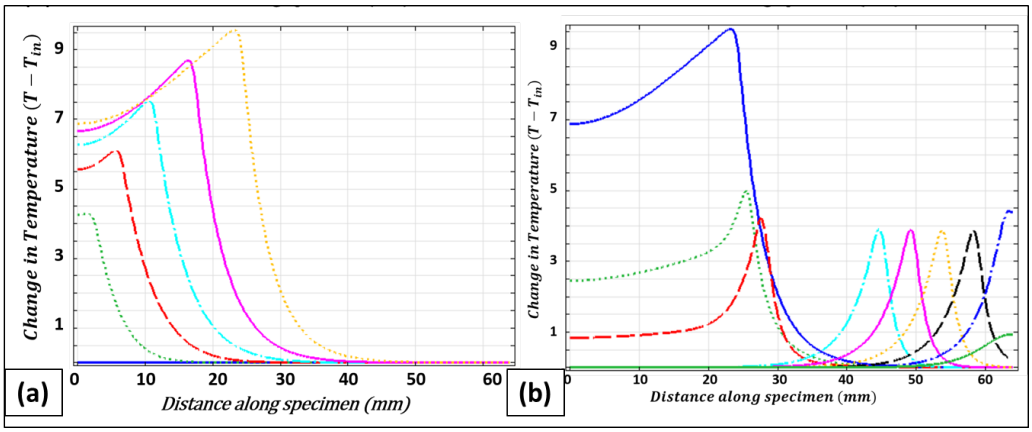

Figure 4.37: Change in temperature accompanying (a) partial transformation and (b) strain accumulation at constant stress (Agboola et al 2015[109])

creep. The question now is if the same behavior will observed under isothermal condition. The answer is yes, the phenomena was observed under isothermal condition. The discussion will be discussed a little later.

4.4.2.2 Transformation Induced Creep under Displacement Controlled Loading

Since the experiment that have been published in the literature does suggest that the accumulation of strain under constant stress is observed even under strain or displacement control [30, 31, 110], simulation of the response of the SMA rod under strain-based loading is simulated. This simulation will be used to show that isothermal transformation does occur under purely mechanical condition. Just like the phenomena of stress relaxation is present in both stress (load) or strain (displacement) controlled loading, figure 4.38 demonstrates that strain (displacement) based loading of SMA exhibits the phenomena of creep accumulation under constant stress. In the result, the SMA is loaded under a strain rate of $10^{-4}s^{-1}$ until the critical stress for transformation begin at an elastic strain of about 0.0048. At which point the seeded martensite nucleus begins to grow and cause the drop in stress but

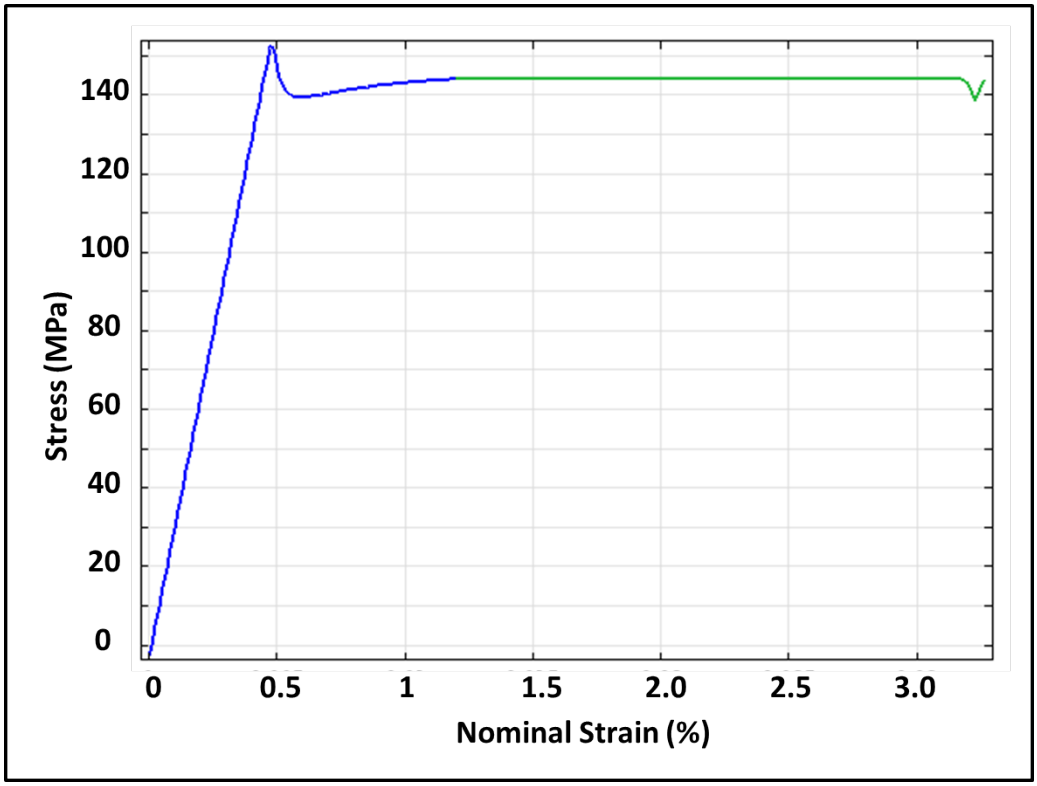

Figure 4.38: Isothermal creep of SMA under constant stress

the transformation front motion result in transformation strain. At about at $120s$ the strain value is now at $0.012s$ and the stress is about $144MPa$ (see Figures 4.39 and 4.39). At this point the stress is held constant at a value of about $144MPa$. What can be observed from the plots is that the strain continues to accumulate until a maximum transformation strain is attained when the entire rod has been transformed. it is important to note that the result presented in figure 4.38 and 4.39, the accumulation of strain under constant stress occurs under isothermal condition. This is trur because when the stress is kept constant, the field equation solved does not include the temperature field equation. Only the balance of configurational forces (for order parameter field) and the balance of linear momentum equations were solved. Therefore, the mechanism behind this phenomenon is not solely thermomechanical

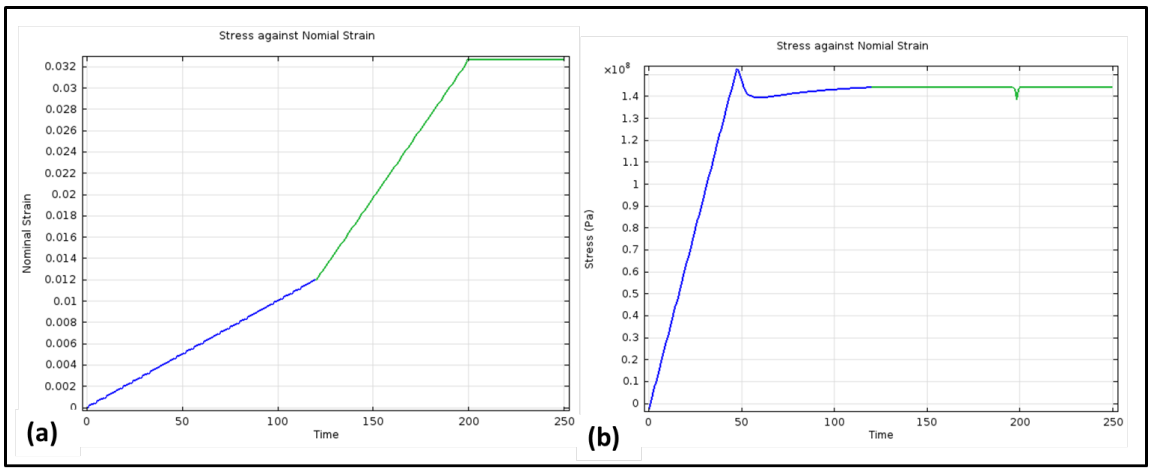

Figure 4.39: (a) Isothermal strain vs time (b) Isothermal stress vs time for creep of SMA under constant stress

effect but also a mechanical reason. Like the stress relaxation result, the explanation I propose is that the elastic energy stored in the material is used to perform work to move the transformation front until the equilibrium is reached where the configuratonal forces are balanced. However, because the displacement of the rod is not fixed at the boundary, the transformation strain generated due to the further transformation (by the motion of the transformation front) continues to add the elastic strain thereby resulting in ana increase in the total strain until the entire material is transformed.

It is important to note the figure 4.39 does show that during the accumulation of the strain ("creep"), the stress is constant. So no external energy is supplied to the material by boundary work by application of stress. This serve to corroborate the explanation that the further transformation is due to stored mechanical energy. In addition, this result shows that apart from thermo-mechanical reasons, whereby the transformation from austenite to martensite is favored because of reduction in temperature, isothermal transformation is possible due mechanical work coming from

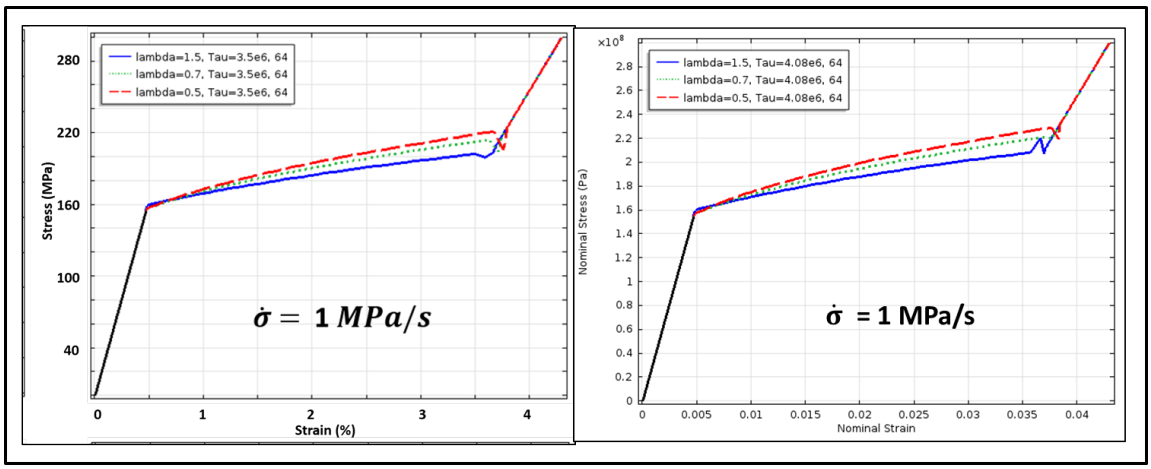

Figure 4.40: Parametric study of effect of gradient energy coefficient (λ) under 1 MPa/s loading

strain energy stored in the material.

Another important insight from the isothermal creep result in addition to the isothermal stress relaxation simulated in this work is that apart from time scale of wave propagation and heat transfer, there is another time scale of phase transformation inherent or characteristic of SMA behavior which results in a viscous behavior. So the hypothesis of this work, that in order to simulate the rate dependent response of SMA, a new time scale associted with phase transformation by interface evolution need to be introduced into SMA modeling, which was introduced using the balance of configurational forces. The results being very representative of experimental findings shows that this model promises to be better suited for SMA design as it can simulate the intrinsic rate dependent response of SMA apart from thermomechanical coupling.

4.4.3 Parametric Study of Kinetic Modulus and Gradient Energy Coefficient

Parametric study of the kinetic modulus τ and the gradient energy coefficients λ is carried out in order to understand their effect and to calibrate the parameter

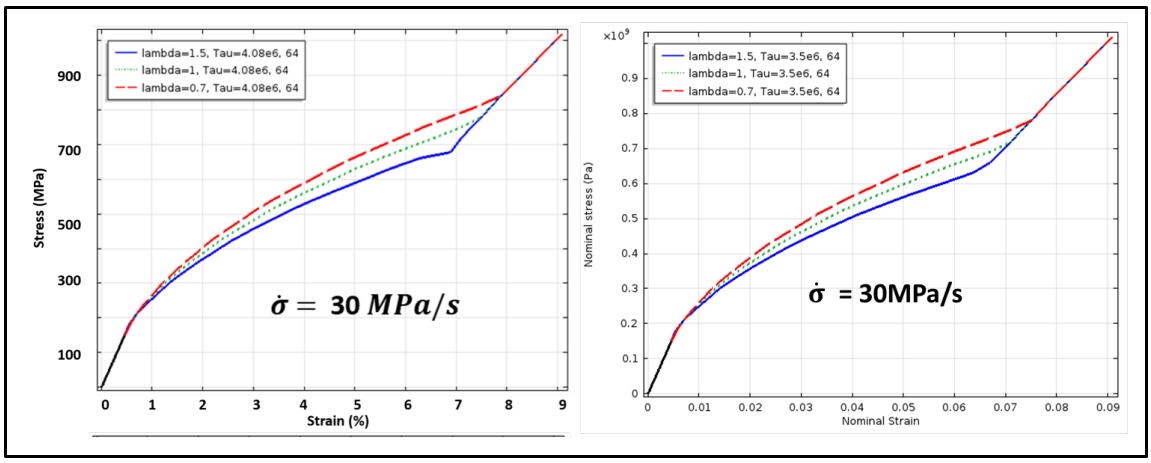

Figure 4.41: Parametric study of effect of gradient energy coefficient (λ) under 30 MPa/s loading

for different SMA. Under a stress rate of $30MPa/s$, the stress-strain response of the SMA is observed to change for different values of τ and λ. As λ increases, the stress corresponding to each strain becomes smaller for the same kinetic modulus. This is suggestive of ability to model interaction between other length scale and the length scale associated with the gradient energy coefficient. As the gradient energy coefficient decreases, which correspond to a thinner interface, a higher stress is needed to generate the same inelastic strain (see Figures4.40,4.41 and 4.42). Since there is an intrinsic length scale associated with the interface width, this model may be improved or calibrated to include the effect of length scales and sizes on the response of the SMA. This may be in the form of inclusion size, interparticle distance, grain size or the actual geometry of the structural material being studied. The kinetic modulus on the other hand has an opposite effect on the stress strain response as compared to the gradient energy coefficient. As the kinetic coefficient increases, the stress corresponding to the same amount of strain increases. This kinetic modulus carries with it an intrinsic time scale and is expected to relate to a characteristic time of

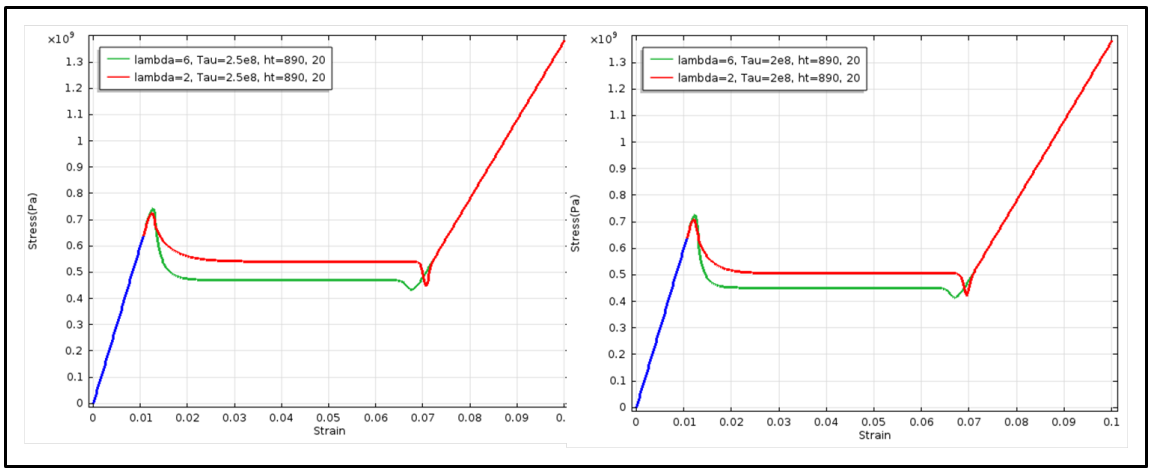

Figure 4.42: Parametric study of effect of gradient energy coefficient (λ) under displacement controlled loading

the SMA phase transformation as shown from the dimensionless parameters and the characteristic time of the thermomechanical model. Since these parameter changes the stress strain response, they are to be calibrated for specific SMA based on material specific characteristic length and time scale as well as thermomechanical properties. Therefore, the specific rate dependent behavior of difference SMA material will result form unique interaction of other time scales with that of phase transformation.

A study of the effect of the kinetic coefficient under displacement and force controlled loading shows that the magnitude of drop between the nucleation and propagation stress reduces with increase in value of the "dynamic viscosity" of the SMA. So, using classical terminology in two phase elastic material modeling, the Maxwell stress increase with increase in the "dynamic viscosity" or "kinetic coefficient" of the SMA as seen in figure 4.43. This effect indicate that higher value of the kinetic coefficient offer less resistance to phase transformation as can be seen in the order parameter field equation (balance of configurational forces) as well. Similar effect can be seen under load control as shown in figures 4.44 and 4.45

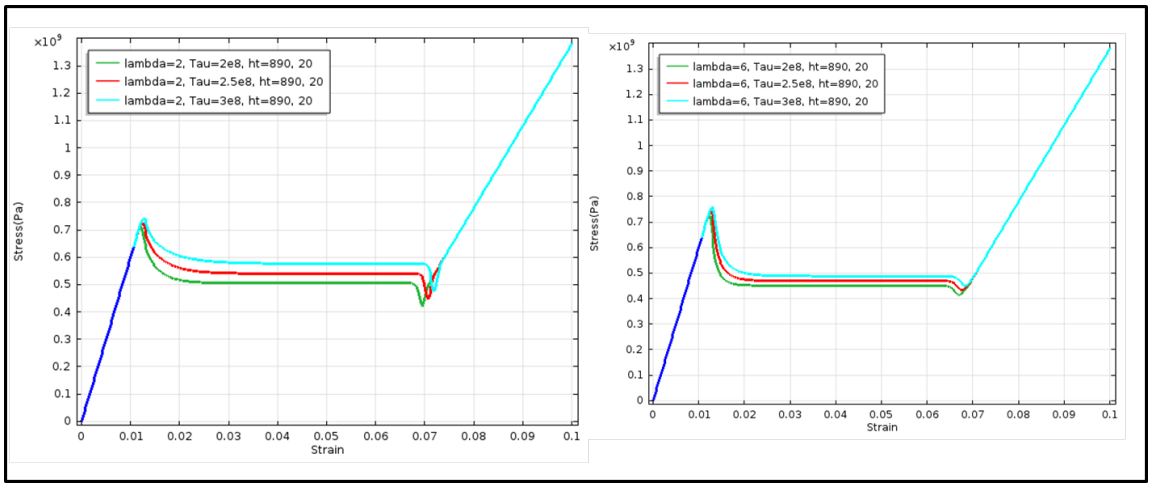

Figure 4.43: Parametric study of effect of Kinetic coefficient (τ) under displacement controlled loading

Similarly, but with opposite variation, increase in the gradient energy coefficient causes the Maxwell stress to decrease. The implication of this is that the gradient energy coefficient introduces high resistance to phase transformation as its magnitude becomes bigger. By implication, these two parameters can be calibrated to capture the relative degree of resistance of various SMA to phase transformation and subsequently the relative speed of response. The dimensionless parameters shows that both parameters depend on $\rho\Delta u_0$ which according to the model represents that latent heat of transformation.

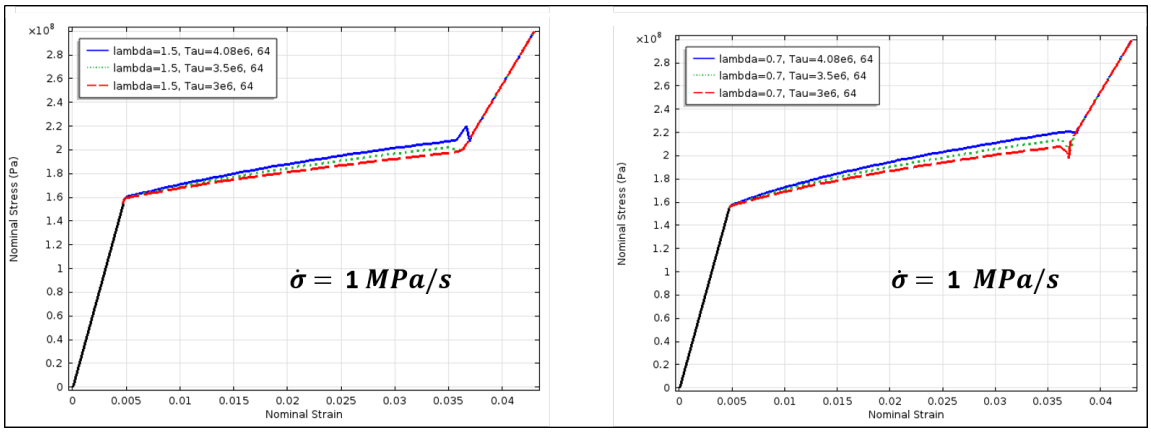

Figure 4.44: Parametric study of effect of Kinetic coefficient (τ) under force controlled loading

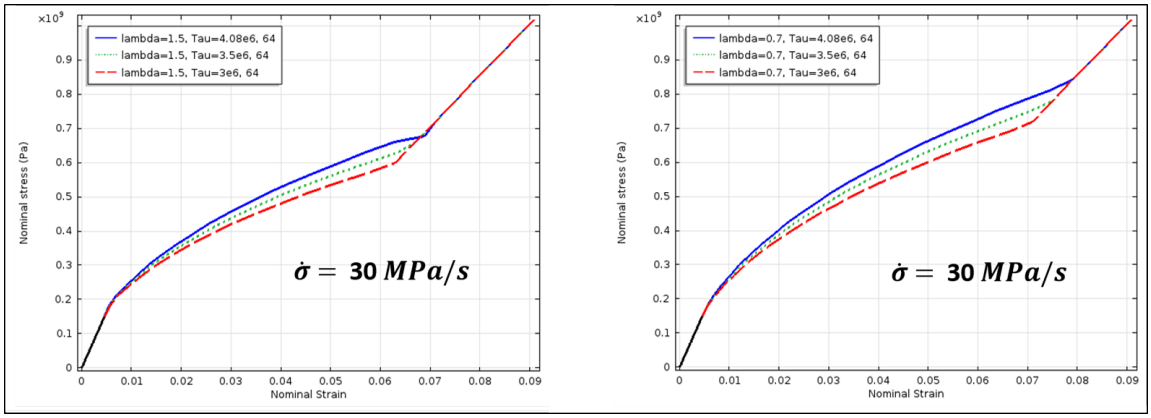

Figure 4.45: Parametric study of effect of Kinetic coefficient (τ) under force control controlled loading

5. THERMALLY INDUCED PHASE TRANSFORMATION USING CPFA

As discussed earlier, one of the manifestation of the shape memory behavior of SMA is a load biased thermally induced phase transformation. In this loading path the SMA transform between austenite and martensite phases under constant load, while temperature is being varied from above A_f to below M_s, and vice versa. As noted earlier, this loading path is very important for the use of SMA as actuators. Other seeming complex path for actuation exists but this is the basic actuation path. The basic question that motivates the result presented in this section is to explore the capability of and scientific insight gained from the model based on the CFPA to simulate challenging experimentally observed responses under thermally induced transformation. Among others, the effect of cooling rate is explored on SMA response as reported from experimental strain-time, strain temperature as well as DSC and DMA result for NiTi and CuNiAl SMA. It is important to model these responses as they will have very strong effect on the SMA response during application in varying cooling environment, particularly in aerospace application where different flight atmospheric flow conditions may exist. Explanation is sought for the reason behind the apparent rate dependent thermal response of SMA. Also, the results are intended to propose experiments that should be carried out to validate this model and get better insight into better testing methods for improved understand of the response of SMA under isobaric thermally induced phase transformation. As noted in the introduction of this dissertation, there are no standards yet for testing and characterizing SMA. Therefore, the ability to use modeling to further aid the design of experiments to characterize, test and understand SMA actuation response is greatly need and would advance the state of scientific knowledge and engineering

design of SMA for various applications. Of particular interest will be in aerospace applications where prevalent remote ambient interaction may not be fully understood experimentally. One interesting application may also be seen in radiative cooling and heating in hypersonic flight vehicle during reentry. Before exploring and analyzing the simulated result of the model, It is important to note that the result of this section are all going to be new in the scientific community for SMA in terms of simulating the dynamic thermo-mechanical response of SMA based on phase front evolution as suggested by experiments for mechanically induced phase transformation. It is this observation that forms the hypothesis that leads to the modeling approach used in this work. It is important to note that the results presented in this chapter are qualitative. More quantitative works and experimentations will be subject of future research. It is known that in the test and application of SMA, heating and cooling rates are concern [115, 10]. Heating and cooling rates are particularly important in bulk SMAs due to prolonged period of heat transfer [116]. Although several work has been conducted on the thermo-mechanical response of SMA, work on the effect of heating and cooling rates are few and far between [116]. In this chapter, thermally induced phase transformation for a load-biased condition is simulated. The transient non-equilibrium character of phase transformation is simulated by incorporating kinetic laws resulting from the configurational forces balance. Probable influence of the gradient energy coefficient (which represents interfacial energy) and the kinetic coefficient (dynamic viscosity) on the forward transformation and by consequence on thermal hysteresis is noted.

5.1 Effect of Cooling Rate on SMA Actuation Response

It is known that the response rate of SMA actuators is the direct result of the combination of their heating and cooling rates [111]. Lohan et al [112, 127] in a

recent set of work studied the heating and cooling rate effects on calorimetric response and martensitic structure on Cu-Zn-Al SMA [112, 127]. In their study, a good correlation between heating rate and reverse martensite transformation temperature, with increasing the heating rate value was found, which was concluded by two variation tendencies experienced by martensite reversion to parent phase: (i) to shift to higher values of critical transformation temperatures and (ii) to become smoother. In particular, in addition to existing studies on the effects of cooling rates (CR) for Ti-Ni, Ti-Ni-Cu, or Ni-Fe-Ga SMA actuators, they studied for Cu-Zn-Al SMA. In addition, Lohan et al (2013)[111] found out that with cooling rate increase, the exothermic peak associated with direct martensitic transformation was observed to increase in intensity with increase in cooling rate, which they attributed to higher amount of parent phase transformed into martensite and therefore causes the transformation temperature to move to lower value. Also, Tadesse et al [10] reported on active cooling of SMA to improve their response time, particularly in embedded condition where heat transfer rate is the controlling factor. The goal was to increase the cooling time so as to improve the response time. The slow speed of the response of SMA due to slowness in dissipation of heat from the SMA has been attributed to the major hindrance to its wide application [113]. So, a model that can help design better actuator with improved understanding of the heat dissipation capability is desired.

Jaeger et al [75] recently published a work where they showed that NiTi SMA exhibits thermal hysteresis which is affected by cooling/heating rates using stress-free thermal analysis. In essence, the apparent transformation temperatures and the hysteresis is said to be affected by the cooling and heating rate. Furthermore they suggested that thermal hysteresis is not only related to interfacial strain energy effects but also effect from the transient character of the transformation process

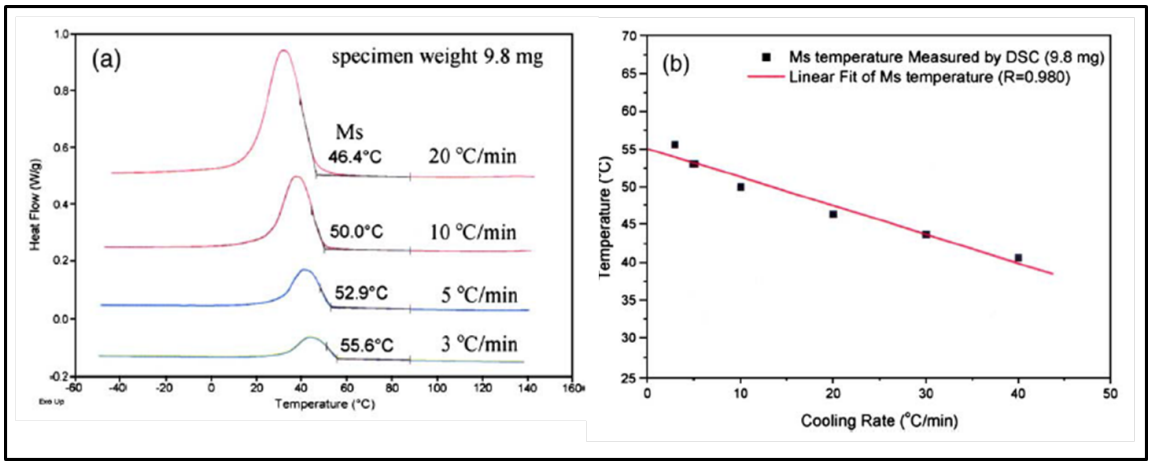

Figure 5.1: DSC Experimental result on the effect of cooling rate on M_s for equiatomic NiTi (S.H. Chang, S.K. Wu 2008 [114])

incorporating specific thermal relaxation times. This two effects will relate to the two coefficients, λ and τ respectively, introduced through the configurational forces balance into the model. [115] studied the effect of heating and cooling rate on the transformation characteristics of TiNiCu SMA alloy using DSC. Their result showed that M_f and A_f depends strongly on the rate of heating and cooling. They observed that M_f decreased and A_f increased with increasing cooling/heating rate. They, however, observed that the M_s and A_s are not sensitive to the cooling rate. Thee observation of Wang et al[115] is different from that of [114] where M_s and A_s depend strongly on heating and cooling rate. Nurveren et al 2008 [116] showed the effect of cooling and heating rate for NiTi SMA annealed below and above certain critical temperature exhibits different effect of cooling and heating rates because of the different number of the stages that transformation has to take. In some cases transformation from austenite to martensite undergoes an $R-phase$ transformation before it undergoes the martensitic transformation (see Otsuka and wren) . Of interest to this work is a single stage transformation from austenite to martensite

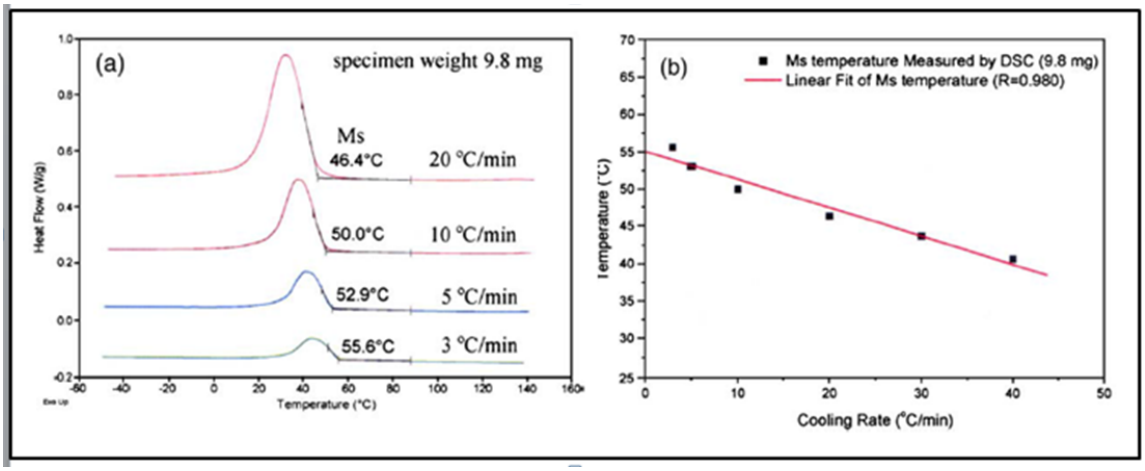

Figure 5.2: DMA Experimental result on the effect of cooling rate on M_s for equiatomic NiTi (S.H. Chang, S.K. Wu 2008 [114]))

and vice versa with single peak of exothermic and single peak of endothermic in DSC thermogram. For the SMA that was annealed above $600°C$, which is more related to the simulation in this chapter, the higher the cooling rate, the lower the start transformation temperatures until a heating/cooling rate of about $10°C/min$ where the transformation temperature remained fairly constant. Austenite finish temperature increases with increase in heating rate after initial decrease from about 1 to $5°C$. However M_f decrease with increase in cooling rate. In addition the heat released and absorbed increases with increase in heating/cooling rate. (See figures 6 and 7 in [116]) In general, experimental works that have been reported so far showed that the transformation temperatures and hysteresis of SMA changes with cooling and heating rate. In stoichiometric NiTi, the martensite start and finish temperatures have been reported to decrease with increase in cooling rate and the austenite start and finish temperature have been reported to increase with increasing cooling rate (see figures 5.1 and 5.2). In some cases like NiTiCu, the martensite and austenite start temperatures have been observed to be independent of the cooling

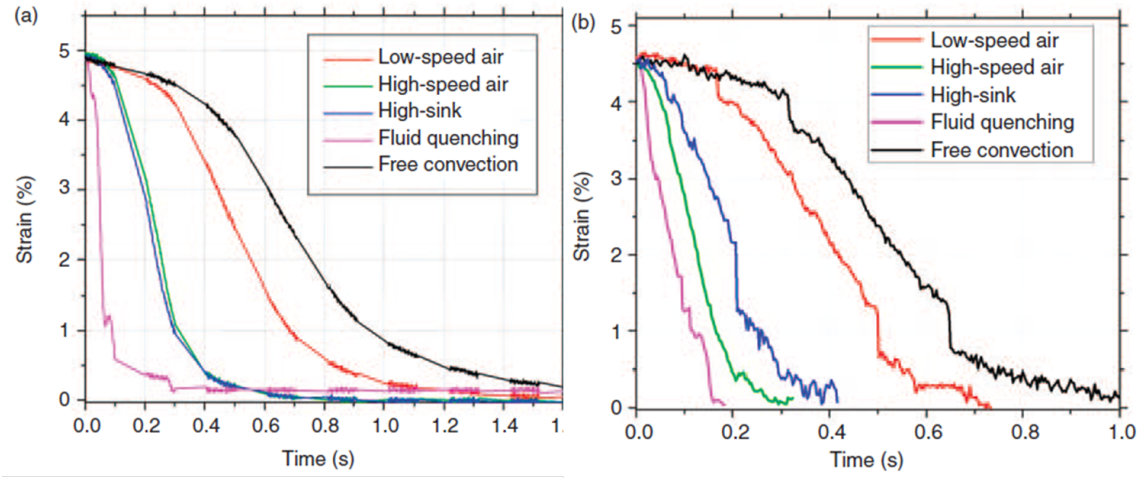

Figure 5.3: Effect of cooling rate on SMA response (Nurveren et al 2009 [116])

or heating rate. But the M_f and A_f are observed to depend on the heating and cooling rates. The disparity between the observation of cooling and heating rates effects on start and finish temperature may be due to other microstructural factors and mechanisms that interplay with the motion of the transformation front. These factors that influence the transformation characteristics in NiTi-based SMAs may include nickel content, ageing after solution treatment to form precipitates, thermo-mechanical treatments, thermal cycling, addition of ternary alloying-elements and processing techniques (see [117, 118, 119, 120, 121, 122, 123]). The effect of cooling and heating rate on the response time of SMA is also known and highly desirable to improve on the limitation of SMA based on narrow bandwidth due to longer response time [10]. Tadassee et al (2009) [10] noted that earlier work studied on SMA motors showed that the problem of achievable velocity is a challenge for SMA application. Change in SMA speed is related to the response time of SMA. Some of the proposed method to achieve a faster response time is to use SMA coupled with fluid cooling system [124, 125], mobile sink [126], running through a metal tube

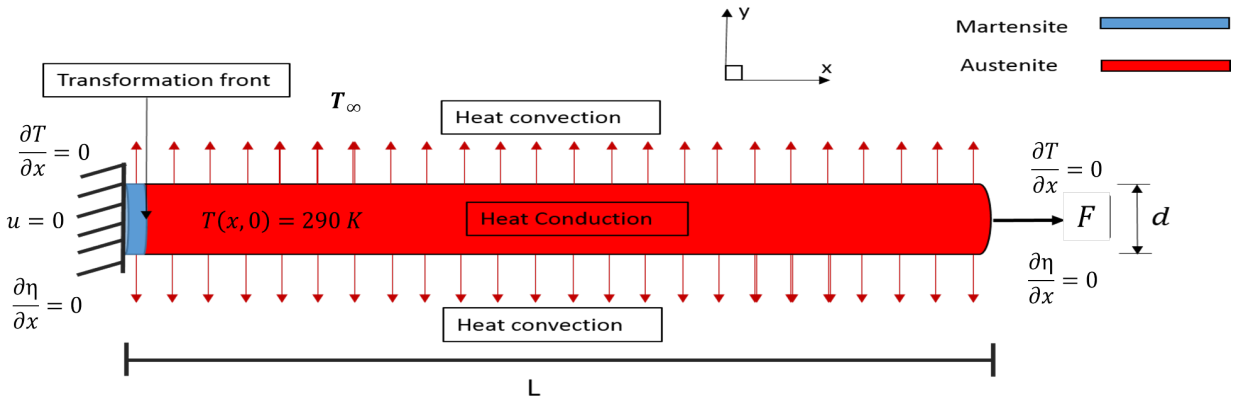

Figure 5.4: IBVP for load biased thermally induced phase transformation (actuation)

filled with silicone grease [113],pneumatic cooling [128]. Figure 5.3a and b shows sets of experiments on the effect of cooling media used for active cooling of SMA. The response is faster for fluid quenching but slower for free convection, resulting in difference in speed of actuator. The effect different cooling media as manifested in different heat transfer coefficient is representative of the effect of cooling rate on the response of SMA. It seems that the effect will be more pronounced as the specimen gets thinner, like wires. Since all the applications mention and described above for SMA as active members depends on cooling and heating rate, it desirable to simulate them with constitutive model in order to aid in their design and active control. All the above stated experimental need and the scientific question of the need for additional balance law to generate kinetic equation to capture intrinsic time scales and consequently rate dependent response of SMA is the reason for the simulation in this chapter. The chapter is with the goal of discussing qualitative demonstration of the capability of the model as well as the insight it offers towards improved application of SMAs, particularly NiTi SMAs.

5.2 Initial Boundary Value Problem

In order to investigate the response of SMA simulation using the SMA model for load-biased thermally induced phase transformation for different cooling rate, an initial-boundary value problem similar to that of the mechanically induced phase transformation is studied. The IBVP is represented on figure 5.4. The boundary conditions are the same as that of the mechanical loading except that the load is constant for all time and the temperature only changes due to convective cooling. In the discussions that follows, the effect of cooling rate, possible test set-up grip effect on the SMA response are elucidated.

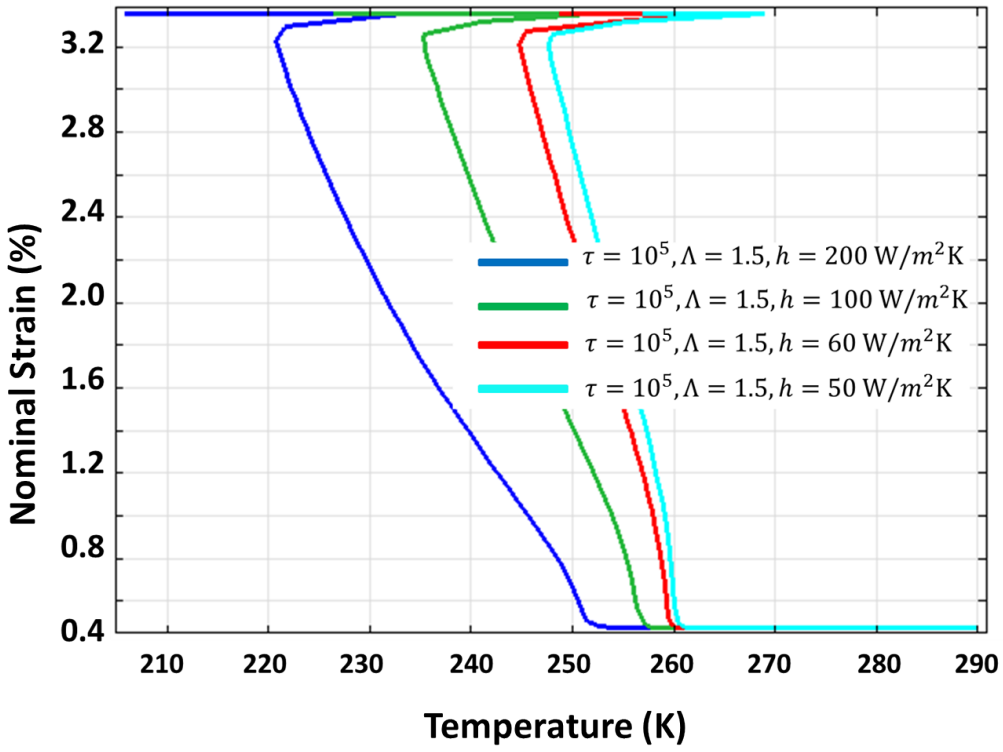

Figure 5.5: Strain-temperature response for single nucleus showing the effect of cooling rate

5.2.1 Simulation of the Effect of Cooling Rate for Single Nucleus and Transformation Front

SMA properties in table 4.1 is used. The SMA rod is initially at a temperature of $290K$, which is above the A_f, is loaded at a stress of $158MPa$. Therefore austenite is the stable phase at this temperature. Now, ambient cooling of the SMA was simulated using the model containing the distributed heat sink. To simulate the effect of cooling rate, the heat transfer coefficient h is varied between several values. The higher the number, the more the degree of convection (consequently cooling rate) as it is obvious from the convective heat transfer boundary condition. At the initial time $t = t_0$, the rod is in the austenite phase with a nucleus of martensite of about $0.02mm$ being seeded at the bottom of the specimen. What this means is that the order parameter will have a value of 0 everywhere in the rod at the beginning of simulation except for the nucleus which has a value of 1, representing austenite and martensite respectively. Figure 5.5 is the nominal strain-temperature response of the rod. It is important to note from the outset that the value of τ and λ will dictate the speed of the response of the SMA. At this point, in order to get a meaningful qualitative response, representative value of 10^5 and 1.5 for τ and $\rho\lambda$ respectively are chosen for the simulation. The value of the $\rho\lambda$ is chosen to match with that used for the mechanical loading simulation for the same SMA used in Chapter 3 for the forward transformation under pseudoelastic loading. The corresponding value of τ that gave qualitatively physically meaningful results is sought. Now from the figure 5.5, the effect of cooling rate does changes the apparent M_s of the SMA as reported in experiment. The faster the cooling rate (represented by higher heat transfer coefficient h), the lower the apparent M_s. The simulation trend matches well with the trends in the DSC and DMA result of figure 5.1 and figure 5.2. So, for

the $h = 200W/m^2K$, the SMA begins to transform at a temperature of about $253K$ and for $h = 100W/m^2K$, the transformation begins at $258K$, both of which are lower than the M_s for the stress value from the phase diagram used for the simulation. As the cooling rate gets slower to about $50W/m^2K$ and $60W/m^2K$, the effect of cooling rate becomes negligible which is in consonance with some experimental observation. These addition slower cooling rate have their apparent transformation temperature at about $260K$ and therefore suggests further that the cooling rate of SMA changes the critical temperature at which transformation begins as well as likely change in the hysteretic response. Another important observation from the plot is that the SMA response deviates from what is often reported classically (see figure 5.5) in that at the end of transformation , the temperature of the SMA rises, unlike what is often reported where the temperature begins to decrease even faster towards the end of transformation. First, the reason for the behavior will be explained shortly after which the possible scientific and engineering implications will be stated. To explain the rise in temperature at the end of transformation, recall that the underlying hypothesis behind the theory. Based on experimental observation, explained in Chapter 1, the idea is that SMA macroscopic response is a result of macroscopic nucleation and propagation of martensitic domain (i.e. phase boundary, interface or transformation front evolution). Therefore, the new time scale associated with phase boundary motion representing phase transformation has to be introduced in SMA model. So, the SMA was originally in austenite, when the simulation begins, the initial nucleus dissolves back to austenite as austenite is the only stable phase at this state of stress and temperature. Once the temperature reaches the apparent M_s depending on the cooling rate, the nucleus suddenly show up again (as it is thermodynamically favored at this state of stress and temperature) since martensite is now the thermodynamically stable phase. The martensitic nucleus begins now to

propagate from the bottom up. Like the mechanical loading of SMA, latent heat is released (forward transformation being exothermic), so the temperature rises locally. However, because of ambient or convective cooling as well as heat conduction in the SMA, the heat is usually quickly transferred out of the SMA transformation front to other part of the specimen. However, once the front reaches the end of the specimen which has a no flux boundary condition for the order parameter and the temperature, the heat released localize at the end of the specimen resulting in a very sudden rise in temperature. The temperature rises considerably as the transformation happens somewhat relatively faster than the cooling rate needed to keep the temperature low in the SMA. Notice that as the convective cooling rate get higher, the amount of rise in temperature gets smaller-corroborating the explanation for the result. This observation has not been reported anywhere from experiment to the best of this author's knowledge and may serve to validate or better improve this model. The trend of cooling rate effect on M_s as shown in the result of the simulation of this chapter is typical of a stoichiometric NiTi , which do not form precipitate, therefore this trend may be characteristics of SMA composition that are not tenable to forming precipitates. Now, for the consequence of this observation, it seems that the testing and characterization of SMA may be affected by the nature of the grip due to the latent heat of transformation. This hypothesis will further examined and discussed in details later. So far, it can be seen that the presented SMA model is able to simulate, not only the forward response of SMA under pseudoelastic loading but also for isobaric thermally induced phase transformation. In addition, new insight to the response of SMA is suggested by the simulation. The implication of these is that, as demonstrated under mechanics loading, the intrinsic time scale of phase transformation introduced to the reported SMA model is the plausible explanation for the reported effect of rate on the SMA response for thermal loading as well.

The transformation time interacts with heat transfer time to result in the complex response. The resulting implication is that SMA macroscopic response should be model as evolving phase boundary in order to capture the realistic response.

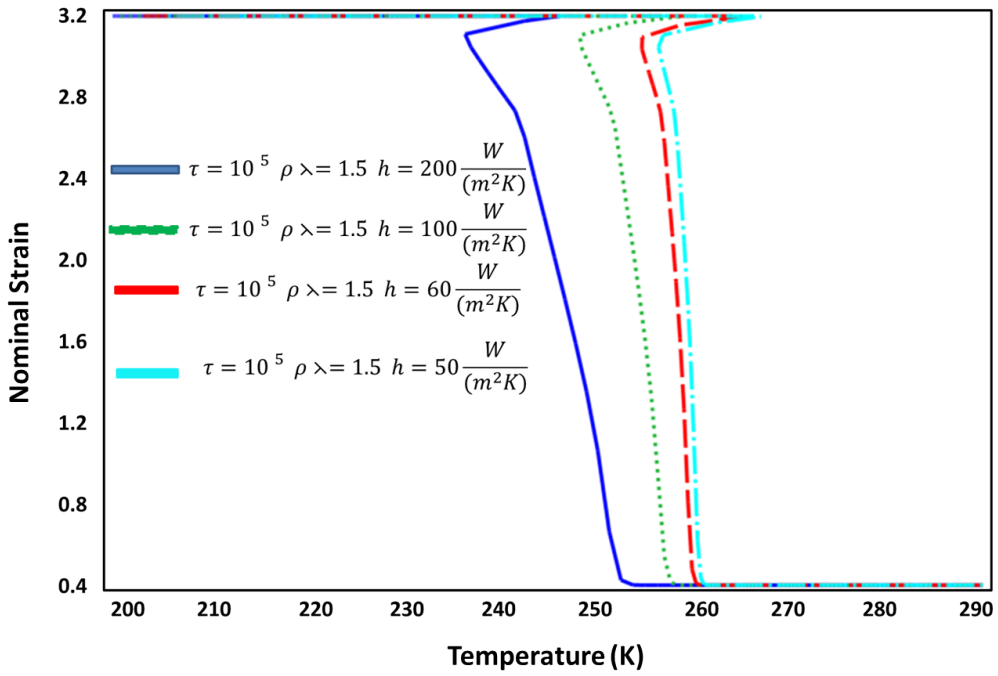

Figure 5.6: Strain-temperature response for SMA response under two nucleation sites intial condition

5.2.2 Simulation of the Effect of Cooling Rate for Two Nucleus and Transformation Fronts

It is expected that the transformation behavior of SMA would involve more than one nucleation site. Investigation of the effect of more than one nucleation site on the SMA response is investigated in this section. The strain-temperature response is given in figure 5.6. In this case as well, the faster the cooling rate lower the apparent M_s. Rise in temperature at the need of transformation is also observed but

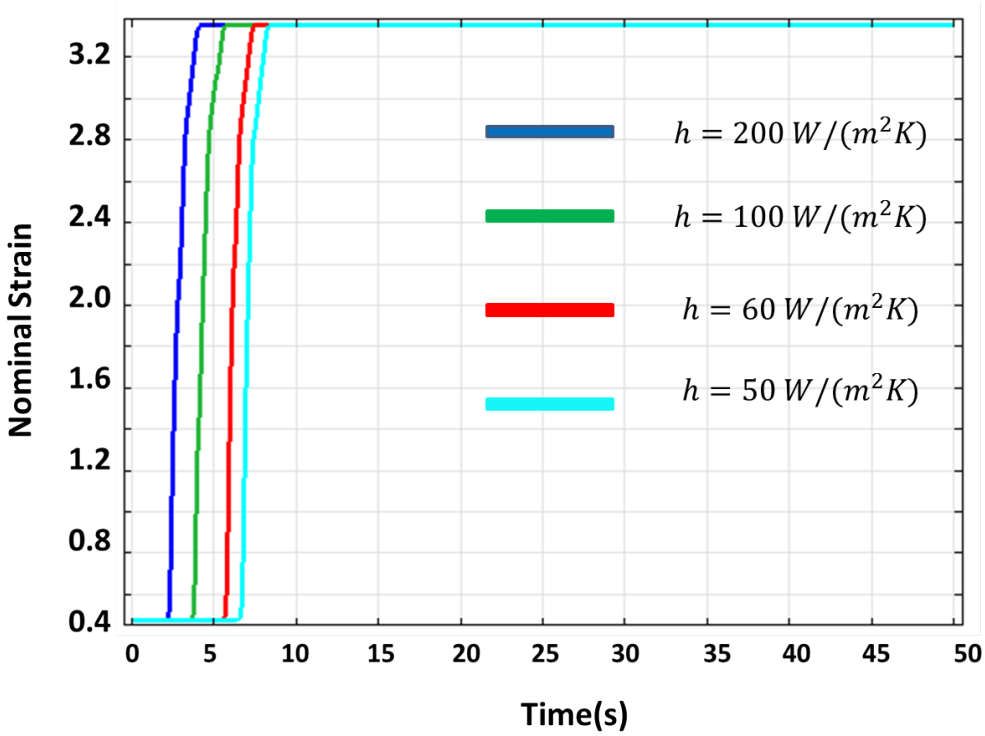

Figure 5.7: Change in response time of SMA based on cooling rate

to a lesser degree in this case. One major observed similarity between the result of single nucleation site (see figure 5.5) and the two nucleation site (see figure 5.6) is that they possess the same apparent M_s for the same cooling rate. However, the apparent M_f temperatures are different because of difference in the hysteretic behavior which may be associated with the amount of latent heat released for the two nucleation site relative to the response with one nucleation site. So the amount of cooling needed to generate the same strain (or actuator) is different in both cases. The single nucleation site result requires more cooling to generate the same actuation or strain that the two nucleation site. Therefore it seems that the response time of an SMA simulated using this model with two nucleation site will be faster than that of the SMA with a single nucleation site for the same ambient condition. If these

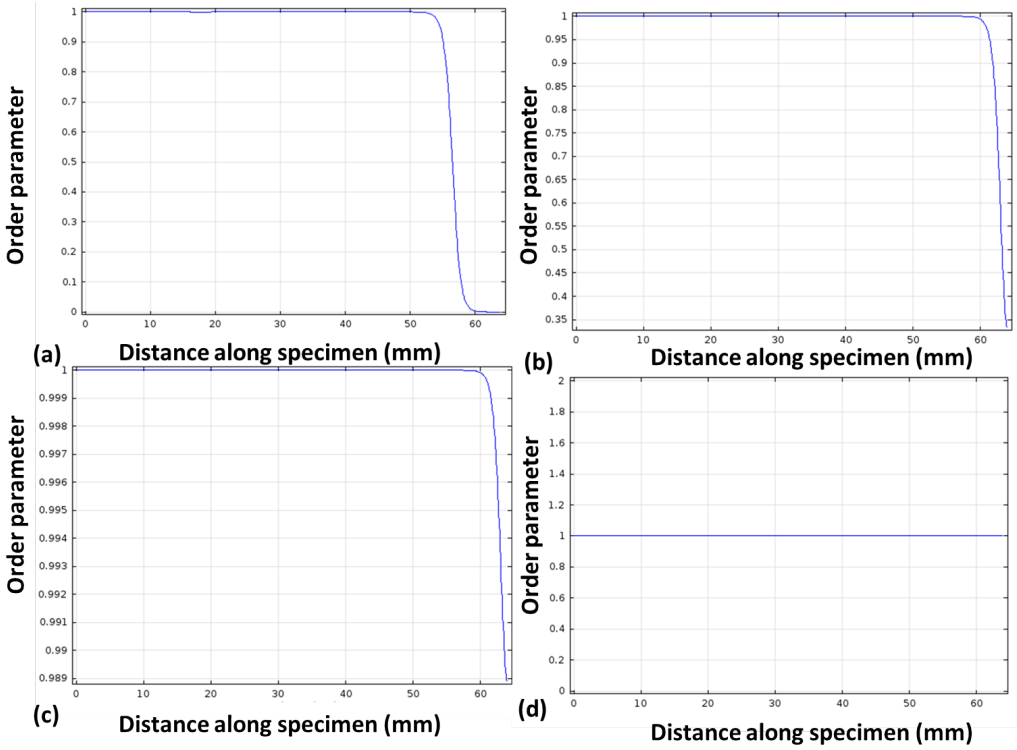

Figure 5.8: Order parameter initial condition-two nucleation sites

findings are physically validated to be true, then it suggests that microstructural manipulation of the SMA to generate more than one nucleation site is desirable for faster actuators. All things being equal, if this finding is true, then it seem that the more propagating macroscopic domain we can generate in an SMA the faster it will respond in different cooling condition. To be able to minimize the design life cycle of producing faster SMA actuators, it is desirable to have a model that can simulate the amount of speed gained with different cooling rate.

Figure 5.7 shows the displacement at the boundary of the rod against time. Cooling rate of the plot decreases from left to right for each strain-time response in figure 5.7.The result demonstrates the change in response time of the SMA depending on the cooling rate, with faster cooling rate resulting in quicker "actuator" response

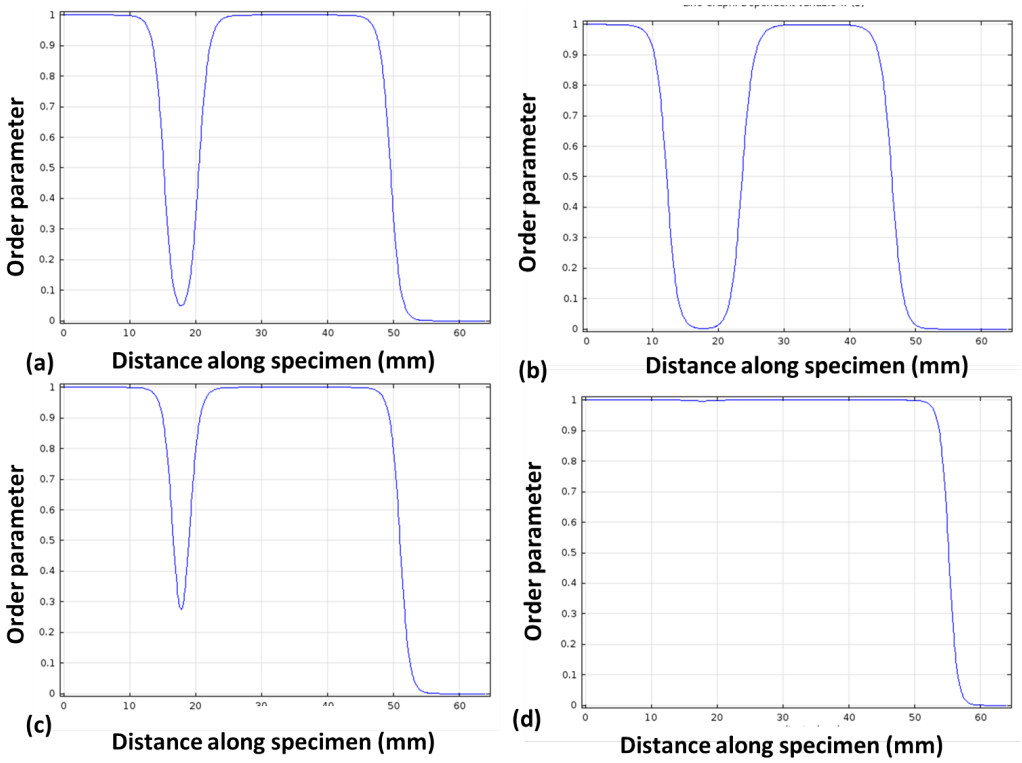

Figure 5.9: Evolution of phase transformation stage 2

time. This result demonstrates that the model developed in this work is very useful to aid the design of better actuators. In addition to change in critical transformation temperature, there is also like change in the hysteretic response as seen in the strain temperature plot difference both under different cooling rate but also when more than one nucleation site is present. So, in order to ensure faster response time of SMA actuators, as noted earlier, method for faster cooling and heating rate should be sought in addition to engineering the microstructure to favor the formation of multiple nucleation site while ensuring inhibiting microstructural effects that suppress multiple nucleation are removed in the microstructural engineering of SMA actuators.

It is important to note that the result presented for the two nucleation result

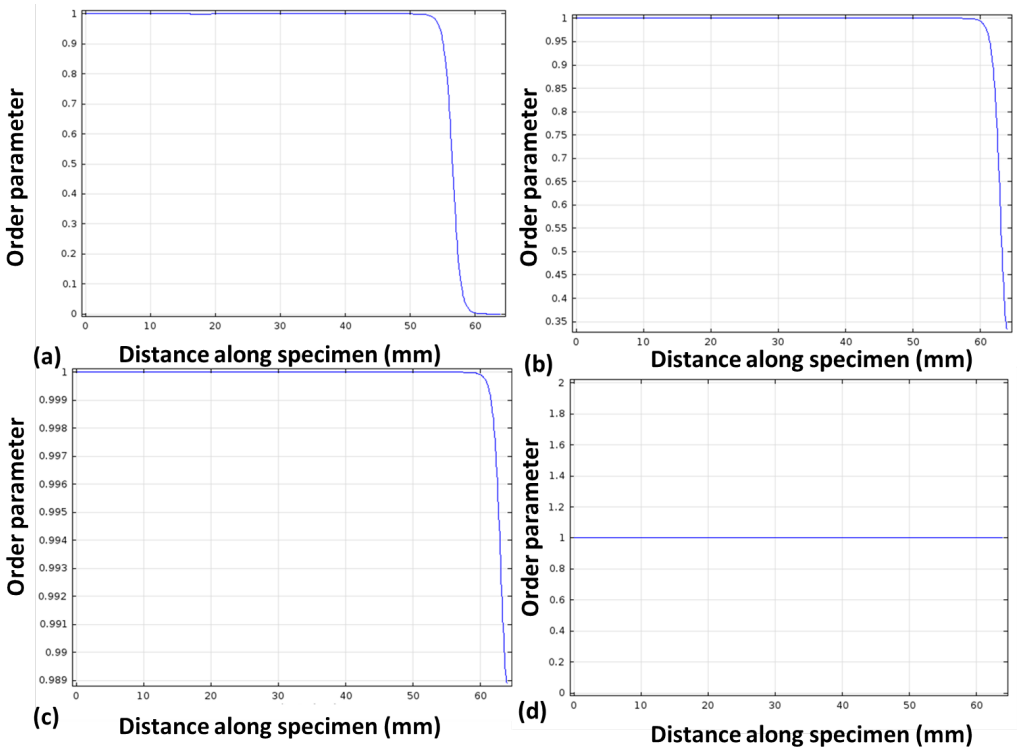

Figure 5.10: Evolution of phase transformation stage 3

comes from more than one initial nucleation site as seen on the evolution of the order parameter plots of figures 5.8, 5.9 and 5.10. This is to demonstrate that the phase transformation front is not elastic wave propagation but an obvious phenomenon of phase transformation front (phase boundary) motion, representing phase transformation, resulting from the kinetic law derived from the configuration forces balance. Figure 5.11 shows the initial condition for two nucleation sites. The nucleus of martensite is first seeded (order parameter η =1) in austenite phase (where order parameter η =0) at two sites. One site is at the left edge and the other is at the center. However, in the plot, the order parameter value went almost to zero but still showed a difference from the rest of the points in the rod as shown by the "bulge" in the field. The reason for the dissolution of the nucleated martensite phase is because

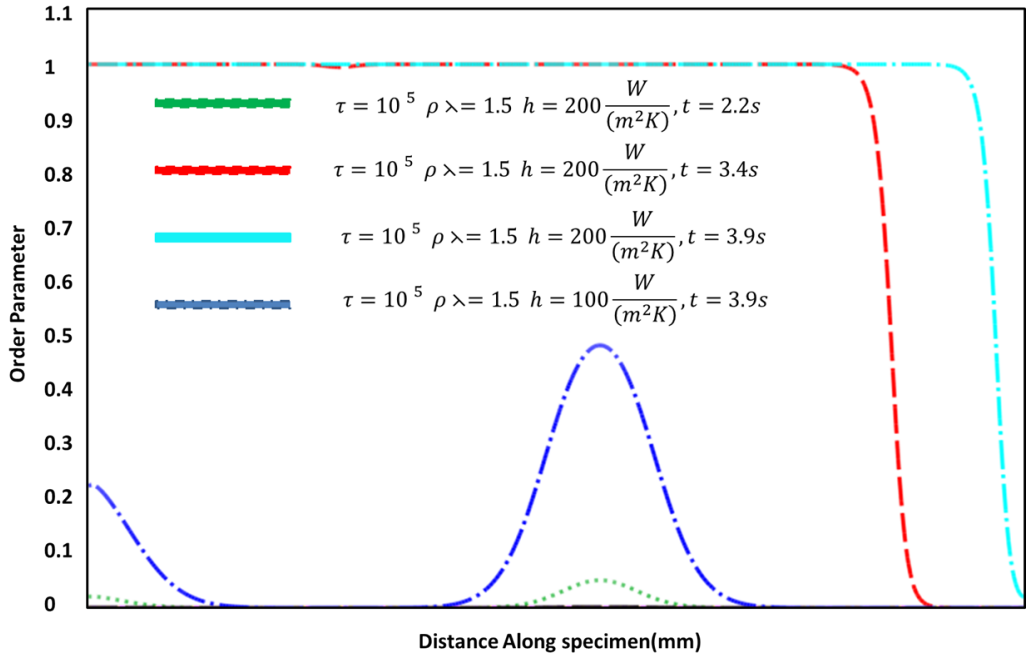

Figure 5.11: Order parameter field representing progress of phase transformation for two nucleation site

the temperature value has not reached a state where the thermodynamic driving force, both local and global, has reached the critical value for the stress state such that it can drive phase transformation. After some time, the driving force reaches the critical value as the temperature drops depending on the cooling rate. What this means in terms of nucleation theory is that the necessary degree of undercooling that favors the nucleation of the martensite phase has been reached. Different cooling rate therefore leads to a different degree of undercooling necessary to nucleate martensite. At this point, the order parameter reaches a value of 1 which indicates the presence of martensite. The transformation front now begins to move on both sides of the nucleus that begins at the center, but move toward the right for the nucleus at the end of the specimen. The transformation continues that way until the entire material is transformed. While transformation fronts are moving, transformation strain

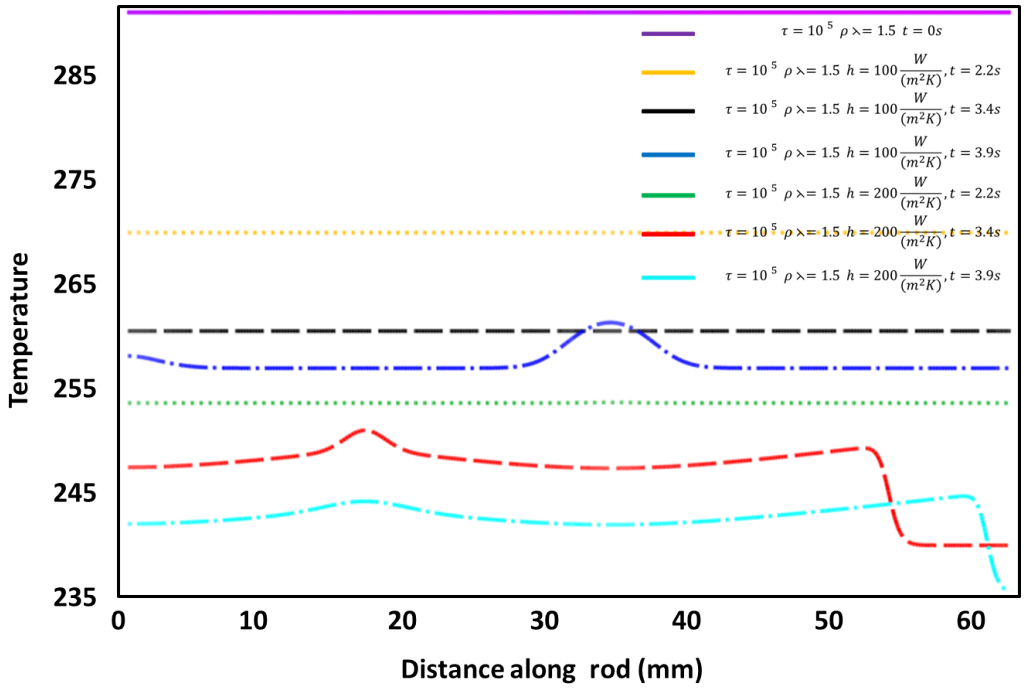

Figure 5.12: Temperature change during cooling of SMA for two nucleation site for different cooling rate

accumulates in the rod, which adds to the elastic strain to increase the total strain of the SMA.

Under different cooling rate for the two nucleation site, the order parameter field shows why there is difference is speed of response. From the figure 5.11the order parameter field for the faster cooling rate with heat transfer coefficient of $h = 200W/(m^2K)$ is almost fully transformed at time $t = 3.9$, while the slower one with heat transfer coefficient $h = 100W/(m^2K)$ is still starting to nucleate at the same time. This explains the effect of cooling rate affecting the apparent M_s due to difference in degree of undercooling that cause different time of nucleation. Also, the difference in time of nucleation and propagation can be seen in figure 5.12 for the temperature field accompanying the order parameter response of figure

5.11. The temperature field clearly supports the explanation provided so far. Notice how the temperature field of $h = 100W/(m^2K)$ at the same time is much higher than that of $h = 200W/(m^2K)$. Initially the temperature field drops uniformly through the rod length. By the time nucleation has occurred as shown by the rise in temperature field for $h = 200W/(m^2K)$ at about time $t = 3.4s$, the temperature field of $h = 200W/(m^2K)$ does not show any rise at all. Only a uniform drop in temperature can be observed.

It is very important to emphasize that the nucleus behaves the way it did and therefore, it is not elastic wave propagation (apart from the obvious fact that the loading is quasi-static and the equilibrium equation is solved for this reported work without inertia effect- second time derivative of the displacement) because it demonstrate that this work is a very fundamental and clear contribution to modeling dissipative materials response such as phase transformation (the theory being extendable to modeling damage, plasticity, fracture and other dissipative mechanism that involves motion of defects, surfaces and interfaces). In addition, the non-dimensionalization of the model shows that the dimensionless parameter resulting from the field equation of the order parameter is orders of magnitude different from that of the displacement field equation containing inertia effect (related to wave propagation). This is one of the major scientific contributions of this work and clearly supports the need for additional fundamental balance law to model phase transition in continuum thermodynamics as used in this work.

5.3 Possible Grip Effect on SMA Response

As noted earlier, it is expected that due to the boundary condition at the end of the specimen, the spike in temperature observed may not be present. The phenomenon is expected to be particularly be more interesting as the specimen becomes

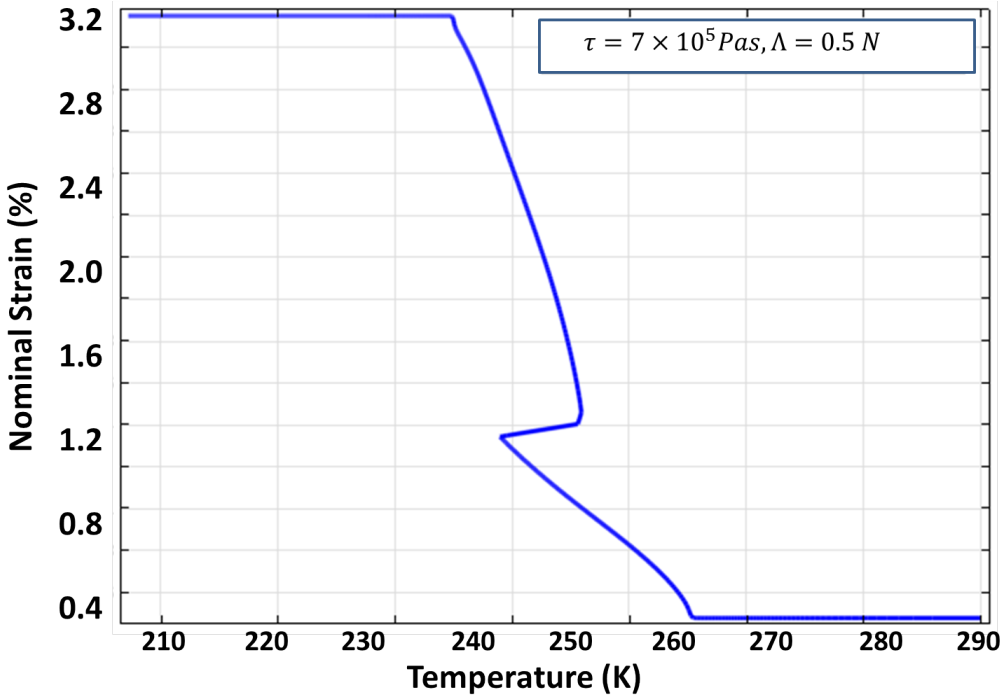

Figure 5.13: Strain-temperature field a new nucleation during transformation due to grip conduction

thinner. So, to prove that the phenomenon is not a numerical error and to eliminate the possible "*grip*" effect, a convective heat transfer boundary condition is applied at the end of the specimen with very high heat transfer coefficient to simulate grip conduction. Notice from figure 5.13 that the spike in the temperature (reported earlier in for example figure 5.6), as the transformation finishes, at the end of the rod is eliminated. The reported temperature is measured at the specimen end. Another important observation, which is non-classical response of the SMA rod is also shown in Figure 5.13. The SMA showed a rise in temperature during partial transformation of the rod. At the end of the rod, temperature rises due to formation of another nucleus because the lower temperature that is close to the end of the specimen due to higher rate of convection (representing grip conduction). The faster heat transfer

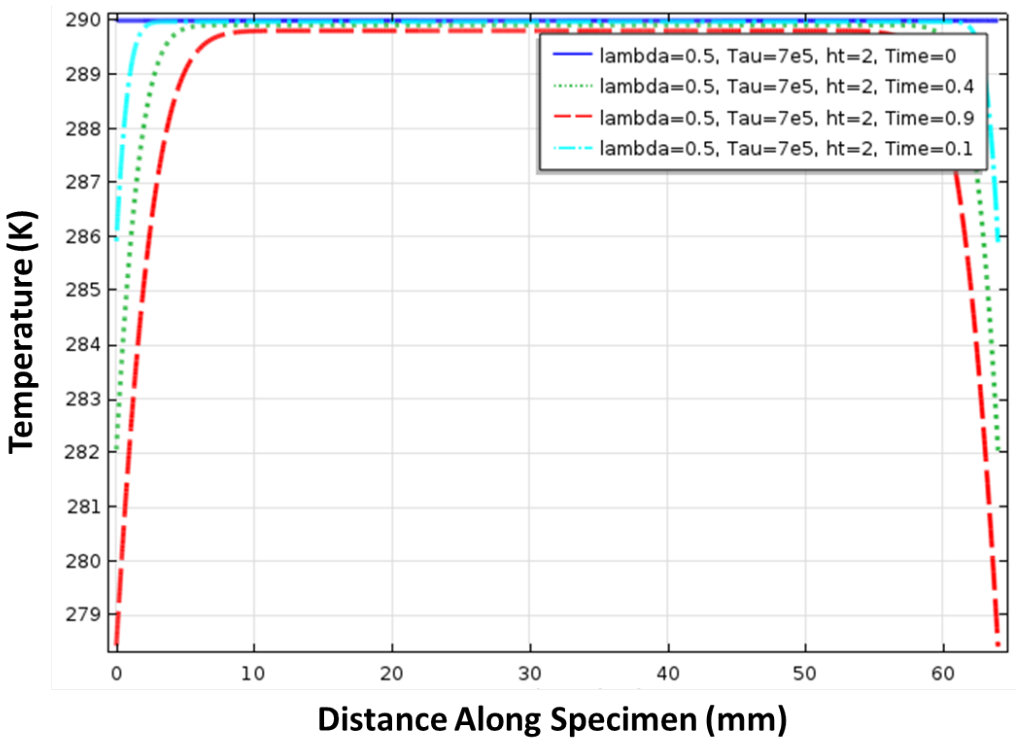

Figure 5.14: Temperature Field accompanying simulation before transformation begins with boundary convection allowed

condition at the end of the rod causes the temperature of the materials close to the SMA rod end to be much lower than the rest of the rod(see figure 5.14, which favor the formation of martensite that subsequently propagates o transform the SMA. Propagation occurs more to the left as can be shown in figure 5.15 as there are more materials to be transformed. Also, because transformation from martensite to austenite is exothermic, there is a rise in temperature at the new interface. Now since there are now two nucleus and two exothermic peaks (see figure 5.13),the response of the material seem to be different. I do not know any experimental work that has reported such a behavior. So, this may be some new insight to the behavior of SMA that this modeling is showing and therefore should be a subject of

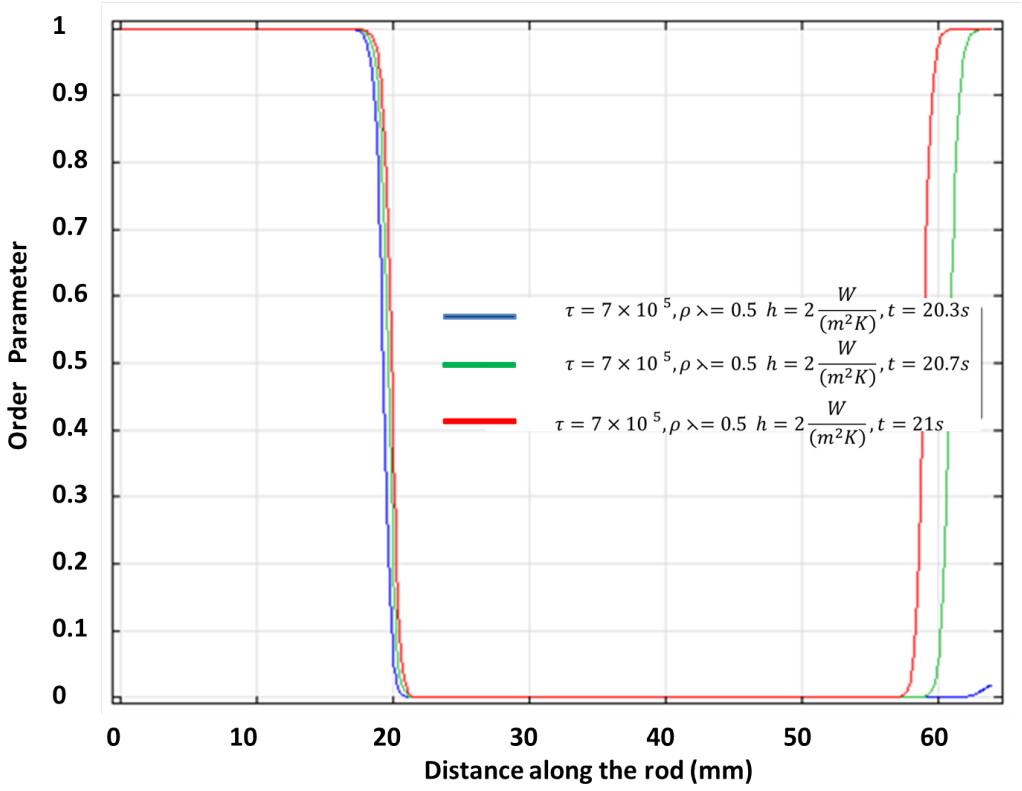

Figure 5.15: Order parameter and new nucleus

future experimental and theoretical investigation. During the phase transformation, when the condition is favorable for the formation of a new martensite nucleus in an originally uniform austenite phase, the temperature field also showed a spike (as represented by the bump in the temperature field to right in figure 5.16 which is the onset of nucleation as can be seen in figure 5.13. The observation could either be a numerical error or an actual constitutive response of the SMA. The result is not numerical since the order parameter field does not show any instability in the response when this spike occur (see figure 5.15). In addition, it seems that such phenomena as was observed in experiment under mechanical loading may occur under thermal loading as well. Just like in mechanical loading case (from experiment), if

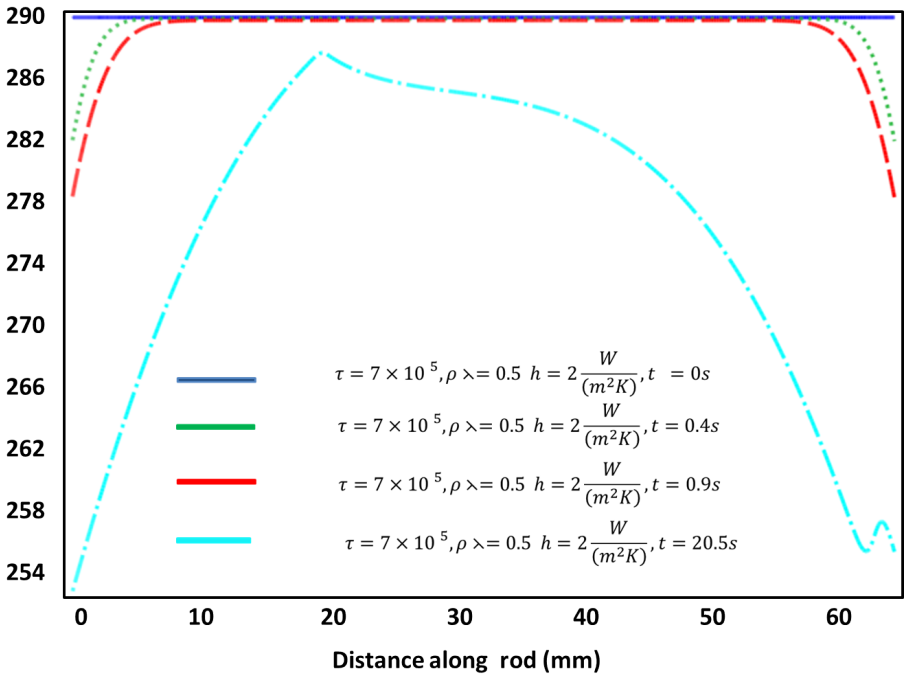

Figure 5.16: Temperature field on the specimen for new nucleation during transformation due to grip conduction

the specimen is cooled from the end and regions that are cooler may result in nucleation as the temperature for nucleation is reached since it is lower than that of other region of the SMA due to the released latent heat. The order parameter field to the left (at the point of the formation of the new nucleus) has the same characteristic features as that of the existing transformation front to the left in (see figure 5.15). Therefore, the rise in temperature is due to the exothermic nature of the forward transformation producing latent heat of transformation, which implies a constitutive response of the material. Now, if an experiment could be carried out using a highly conductive material for the SMA grip, this response may be observed perhaps to a lesser degree. If this behavior is observed, it then serves to not only support the thermodynamic consistency of the model but will become a very strong validation of

the predictive nature of this model. The engineering implication of this anomalous behavior is that the grip used to test and characterize SMA has to represent the thermal conductivity of the material to which the SMA will be connected in application, which point furthermore the complexity that SMA possess to design engineer. On the other hand to see the intrinsic behavior of the SMA for scientific purposes, the experiments need to be carried with the grip being made of very highly insulating material. The take home message from this anomalous behavior is that the SMA macroscopic strain-temperature response could change considerably depending on the thermal condition of the grip used to characterize and the material member it is connected to in application. One important thing to keep in mind is that the observed possible grip effect occurs with values of the kinetic coefficient τ and the gradient energy coefficient $\rho\lambda$ of $7^5 Pas$ and $0.5N$ respectively. So, it is not certain if this phenomenon will be observed for different values of these parameters. Hence it should be the subject of further investigation to ensure that the phenomenon is not limited to this value of SMA parameter-whatever they mean physically.

5.3.1 Possible Experimental Set-up to Validate Grip Effect

To see the effect of cooling rate in SMA as shown by the simulation in this chapter the following experiment is proposed

- An experiment could be designed for a relatively thin SMA wire or rod. The grip of the first test should be insulated from the material to prevent heat transfer between the grip and the SMA rod. To also avoid heat transfer due to contact with thermocouples, a non-contact strain and temperature field measurement such as DIC and IR should be used respectively. The grip displacement should be measured and the nominal strain plotted against the temperature at the end of the specimen. If the simulations of this chapter are physical,

the spike in temperature will be observed at the end of the specimen.

- A second set of experiments should be carried out, if possible, with test grips that are highly conductive. The grips should be varied from those with lower thermal conductivity to those with higher conductivity. The response of each test is expected to be different; if the response observed in this chapter suggesting the effect of the grip is possible, as the cooling due the grip conductivity will drastically change the SMA response.

- A third experiments similar to the first one but with a set up that changes the cooling rate of the SMA rod should be carried out. This is intended to see the effect of ambient cooling on SMA response. The specimen should be placed in a cooling chamber with set up similar to the first test above. These set of experiments should help to validate the thermodynamic consistency and the predictive nature of the reported model.

Finally, to model the heating of the SMA, the appropriate heat source expression representing resistive, radiative as well as inductive heating and cooling should be additional included in the source term of the balance of energy.

6. CONCLUSIONS, FUTURE WORKS AND RECOMMENDATIONS

Thermodynamically consistent, continuum thermodynamic constitutive phase field models using the notion of configurational force balance and order parameters are reported. The first model couples coherency strain energy to diffusion of atomic species and is used to qualitatively simulate precipitate evolution in SMA. Growth and morphology of precipitate in an elastically stressed solid are simulated. The simulation include the effect of elastic inhomogeneity, material anisotropy, concentration depletion around precipitate, precipitate coarsening and ripening in 2-D and 3-D. In essence the capability to simulate coupling between diffusion and coherent elastic effect is developed. The second model is thermo-mechanical and is used to simulate the rate dependent response of SMAs. Two different compositions of NiTi SMA are simulated. The model does couple different time and length scales, which correspond to the different phenomena responsible for the macroscopic response of SMA. The approach used is an extension of continuum thermodynamics by introducing additional balance laws that captures phenomena associated with phase transformation and general phenomena involving boundary motion. Additional balance of configurational forces is introduced along with conventional balance of mass, linear momentum, angular momentum, energy and second law of thermodynamics to derive the thermo-mechanical model. The elasto-diffusion model is also based on incorporation of balance of atomic species mass in addition to configurational forces balance to generate field equation which is a generalization of the classical Cahn-Hilliard equation. The importance of the balance law is demonstrated because, like other balance laws, it resulted in field equations (differential equation). The field equation simulates the evolution of the conserved (concentration) and non-conserved

order parameter, which represents motion of transformation front. Experimentally observed pseudoelastic and constant stress thermally induced phase transformation are simulated. Under pseudoelastic loading, simulation results capture several experimentally observed features of the stress-strain response for forward transformation. The features include

- localized heating at the transformation front or interface, which results in thermal hardening
- Interaction between different ambient medium to determine apparent rate dependent response of SMA. The model simulates the change in response for constant loading rates and different ambient medium as well as for same ambient cooling under different loading rates.
- loading rate dependence of critical stress for phase transformation
- transformation induced stress relaxation; and pseudo-creep in SMA is also simulated with quantitative results

Two additional parameters that introduce intrinsic time and length scales to SMA response are introduced, which are the kinetic coefficient (τ) and the gradient energy coefficient (λ) of SMAs. Different values result in different stress-strain response, which give insight to the fact these parameters will be different for each SMA. Five basic dimensionless parameters are derived for the full thermomechanical SMA model and four time scales of heat conduction, convection, wave propagation and phase transformation are derived. Simulation of thermally induced phase transformation showed that the thermo-mechanical model is able to simulate the rate dependent thermal response in SMA. In particular, the effect of cooling rates on the macroscopic response of SMA such as change in apparent martensite start temperature

and the hysteresis of SMA with cooling rate. This rate dependent response is also shown to be very useful in controlling the speed of SMA actuators. The difference in speed for different cooling rate was observed to be a result of different resistance to transformation front evolution depending on the cooling rate. Therefore the model presented in this work promises to be very useful for controlled actuation application of SMA under strong environmental flow and thermal conditions. Simulations also suggest the effect of testing grip on the response of thin SMA components due to possible conduction for grips that are not properly insulated. To the best of this authors knowledge, the model developed in this work is the first to present the modeling of SMA in a 3-D continuum thermodynamic, constitutive thermodynamically consistent manner; with full thermomechanical coupling based on the propagation of transformation fronts. It is theorized that the stress relaxation behavior of SMA is essentially due to the fact that the macroscopic deformation of SMA components result from the evolution of a phase boundary between fully austenite and fully martensite phases, apart from the thermomechanical coupling. All the different complex interaction resulting in the rate dependent SMA response under pseudoelastic loading and constant stress thermally induced phase transformation converges to interaction with the evolution of a transformation front. Since, the thermo-mechanically coupled model captures rate dependent phenomena in SMA, it should be expected that many design problems that involve complex thermo-mechanical interaction can now be solved. It is concluded that the complex interaction between the loading rate, rate of interface evolution (transformation kinetics), latent heat of transformation, convection and conduction of heat (manifested in temperature change) of the SMA specimen is the reason for the rate dependent response of SMA. This work shows that kinetics of phase transformation in SMA result in characteristic macroscopic properties, and that interaction between time and length scales of prevalent phenomena

with that of phase transformation front evolution has a very definite determinant effect on the rate dependent thermomechanical macroscopic response of SMA. Finally, this work showed that in addition to strong thermomechanical coupling, SMA possess an inherent time scale associated with the transformation front, which result in the pseudo-viscoelastic behavior of SMA viz. stress relaxation and pseudo-creep under constant strain and stress respectively. Furthermore, the similarity of the simulation in comparison to experimental observation gives credibility to the thermo-mechanical model as advancing the state of the art in constitutive modeling of SMA. The model is expected to benefit greatly applications that involve varying loading rates as well as those that involve SMA interacting with solid or fluid media in which they are embedded. Of particular benefit are applications involving thermal interactions in high temperatures aerospace applications. Examples of applications that can be aided by the model include:

- MEMS application of SMA and all form of use of SMA as wires and thin members.
- SMA embedded in polymer for high temperature applications
- Effect of SMA on retention of residual stresses in functionally graded ceramic metal (SMA) composites (GCMeC)
- Aircraft aero-structural morphing members
- Flutter mitigation through the vibration isolation and dampening properties of SMA
- Improved design of SMA torque tube as solid state actuator incorporating the effect of cooling and heating rates.

- Improved design of the variable geometry chevron (VGC) by better incorporating the environmental flow and thermal conditions on SMA response.
- Improved design and control of tensegrity structures with SMA tensile members of deployable space structures.
- Application design of other aircraft morphing structural members and other applications that utilizes SMA as reviewed by Jani et al and the references therein.[1]

As an extension, this work suggests among others, that configurational forces balance may be a fundamental concept necessary in continuum thermodynamics to model material with evolving inhomogeneity, surfaces and interfaces. Combination of this notion with phase field theory (diffuse interface), may lead the scientific community towards modeling several challenging engineering problems involving motion of defects and boundary between distinct phases. Finally, in the light of the limitations of existing models in relation to mechanism reported in experiments for shape memory alloy response, this model is a significant contribution to the state of the art in SMA modeling and by extension a worthwhile contribution to continuum thermodynamics.

6.1 Future Works

There are several works that can be done beyond what is reported in this work using the model developed in this dissertation as well as the framework used. These works include

- Simulation of heating rate effect on load biased thermally induced phase transformation of SMA actuation and structural members.
- Simulation of full hysteretic response of SMA devices.

- Detailed quantitative study the implication of the length scale associated with interface width on SMA response.
- Develop a test set-up to validate the possible effect of grip on SMA response during testing.
- Perform experiment to validate the effect of cooling rate on SMA macroscopic response.
- Improvement of the model to include two or more variants that differentiate tensile and compressive responses in SMA.
- Include transformation induced plasticity to capture irrecoverable strain induced by transformation.
- 2-D and 3-D simulation of SMA macroscopic thermo-mechanical response using the thermo-mechanical model.
- Improvement of the elasto-diffusion model to capture realistic precipitate behavior based on processing condition by incorporating more physical chemical energy.
- Extension of the methodology to coupled thermal, mechanical and diffusion fields for high temperature applications involving thermal migration under mechanical load.
- Linearization of nonlinear field equation to develop a control model for SMA actuator response
- Study the mathematical nature of the set of field equations.

- Develop means of passing predicted precipitate stationary morphology as geometry to analyze SMA macroscopic thermo-mechanical response.
- Develop kinetic model of multiple variants model of SMA using the methodology and their interaction with precipitates.
- Extension of the methodology to couple thermal, mechanical and diffusion fields
- Use model to design tensegrity structures for use in space antennas and general deployable structures
- Simulation of impact problem in SMA using the model to understand the interaction between the transformation front and wave propagation.

6.2 Recommendations

It is recommended that the model developed in this work be verified in details, validated with experimental work that is carefully carried out based on finding from this work. Once the model is verified and refined, attempt should be made to more qualitatively calibrate the kinetic coefficient and the gradient energy coefficient parameters to experiment. Alternatively, map of the Kinetic coefficient and the gradient energy coefficient can be created for several simulated SMA composition. This map may serve to identify some relationship between SMA composition and the numerical range of these parameters. In addition, the dimensionless parameters should be carefully studied for the different SMAs to determine conditions of domination of the different time scales and how they interact. Since this model may be less accurate as the specimen dimensions becomes thicker, analysis should be done to find out what is the range of validity of the model and obvious limitations.

REFERENCES

[1] Jani, J. M., Leary M., Subic A., Gibson M. A., *"A review of shape memory alloy research, applications and opportunities"*, Materials Design, vol 56, 2014 pp. 1078-1113.

[2] Porter, D. A., Easterling, K.E., Sherif, M.Y., *"Phase transformations in metals and alloys"*, (Revised Reprint). CRC press, 2009

[3] Bhattacharya, K., *"Microstructure of martensite-why it forms and how it gives rise to the shape-memory effect"*, vol. 2. Oxford University Press, 2003

[4] Shaw, A. and Kyriakides, K., *"Thermomechanical aspects of NiTi"*, Journal of the Mechanics and Physics of Solids, vol 43, No. 8, 1995 pp. 1243-1281.

[5] Churchill C.B., Shaw J.A., Iadicola M.A., *"Tips and tricks for characterizing shape memory alloy wire: part 2fundamental isothermal responses"*, Experimental Techniques, vol 33, No. 1, 2009 pp. 51-62.

[6] Churchill C.B., Shaw J.A., Iadicola M.A., *"Tips and tricks for characterizing shape memory alloy wire: part 3Localization and Propagation Phenomena"*, Experimental Techniques, vol 33, No. 5, 2009 pp. 70-78.

[7] Shaw, J.A., Churchill C.B., Iadicola M.A., *"Tips and tricks for characterizing shape memory alloy wire: part 1differential scanning calorimetry and basic phenomena"*, Experimental Techniques, vol 32, No. 5, 2008 pp. 55-62.

[8] Reedlunn, B., Churchill, C. B., Nelson, E. E., Shaw, J. A., Daly, S. H. *"Tension, compression, and bending of superelastic shape memory alloy tubes"*, Journal of the Mechanics and Physics of Solids, vol 63, pp. 506-537.

[9] Shaw, A. and Kyriakides, K., *"Initiation and propagation of localized deformation in elasto-plastic strips under uniaxial tension"*, International Journal of Plasticity, vol 43, No. 10, 1998 pp. 837-871.

[10] Tadesse, Y., Thayer, N., and Priya., S.*"Tailoring the response time of shape memory alloy wires through active cooling and pre-stress"*, Journal of intelligent materials systems and structures, vol 21, No. 1, 2009 pp. 19-40.

[11] Choi., J.M., Son., H.M., and Lee, Y.J.,*"Design of Biomimetic Robot-eye system with single vari-focal lens and winding-type SMA actuator"*, In:International Conference on Control, Automation and Systems, 2008 pp. 14-17.COEX Seol Korea

[12] Loh, C.S., Yokoi, H., and Aral., T.,*"Improving heat sinking in ambient environment for the shape memory alloy (SMA)"*, In:Proceedings of IEEE Conference on Intelligent. Robots and Systems, pp. 3560-3565.

[13] Loh, C.S., Yokoi, H., and Aral., T.,*"New shape memory alloy actuator: design and application in the prosthetic hand"*, In:Proceedings of the 27th Annual Conference of the IEEE Engineering in Medicine and Biology, 14, September, Shanghai, China.

[14] Ashrafiuon, H., Eshraghi, M. and Elahinia, M.H.,*"Position control of a three-link shape memory alloy actuated robot"*, Journal of Intelligent Material Systems and Structures, vol 17,2006 pp. 381-392.

[15] Luchetti, T., Zanella, A., Biasiotto, M. and Saccagno, A.,*"Electrically actuated antiglare rear-view mirror based on a Shape Memory Alloy actuator"*, Journal of Materials Engineering and Performance, vol 18,2009. pp. 717-724.

[16] Abeyaratne, R. and Knowles, J. K., *"Evolution of phase transitions- A continuum theory"*, Cambridge University Press, 2006.

[17] Krishnan, R.V., and Brown, L.C., *"SMA single crystal experiments and micromechanical modeling for complex thermomechanical loading"*, Proceedings of SPIE, vol 3992,2000 pp. 516-23.

[18] Gao, X., and Brinson, L.C., *"Pseudo-elasticity and the strain-memory effect in an Ag-45 at.pct, Cd alloy"*, Metallurgical Transaction A vol 4,1973 pp. 689-716.

[19] Leo, P. H., Shield, T.W., and Bruno, O. P., *"Transient heat transfer effects on the pseudoelastic behavior of shapememory wires"*, Acta Metallurgica et Materialia, vol 41, No. 8, 1993 pp. 2477-485.

[20] Churchill C.B., Shaw J.A., Iadicola M.A., *"Tips and tricks for characterizing shape memory alloy wire: part 4 - Thermo-mechanical coupling"*, Experimental Techniques, vol 34, No. 2, 2010 pp. 63-80.

[21] Shaw, A. and Kyriakides, K., *"On the nucleation and propagation of phase transformation fronts in a NiTi alloy"*, Acta Materialia, vol 45, No. 2, 1997 pp. 673-700.

[22] Sun, Q.P., and Li, Z.Q., *"Phase transformation in superelastic NiTi polycrystalline micro-tubes under tension and torsion- from localization to homogeneous deformation"*, Int.J. Solids Struct vol39, 2002pp. 3797-809.

[23] Li, Z.Q., Sun, Q.P.,*"The initiation and growth of macroscopic martensite band in nano-grained NiTi microtube under tension"*, International Journal of Plasticity, vol 18, 2002, pp. 14811498

[24] Mukherjee, K., Sircar, S., Dahotre, N.B., *"Thermal effects associated with stress-induced martensitic transformation in a TiNi alloy"*, Material Science and Engineering, vol 74, 1985 pp. 7584.

[25] Tobushi, H., Endo, M., Ikawa, T., Shimada, D., *"Pseudoviscoelastic behavior of TiNi shape memory alloys under stress-controlled subloop loadings"*, Archives of Mechanics, vol. 55, No. 56,2003 pp. 519-53

[26] Tobushi, H., Endo, M., Ikawa, T., Shimada, D., *"Influence of strain rate on superelastic properties of TiNi shape memory alloy"*, Mechanics of Material, vol. 30, 1998 pp. 141150.

[27] Tobushi, H., Takata, K., Shimeno, Y., Nowacki, W.K., Gadaj, S.P., *"Infuence of strain rate on superelastic behaviour of TiNi shape memory alloy"*, Proceedings of the Institution of Mechanical Engineers, Part L: Journal of Materials Design and Applications, 1999, vol. 213, pp. 93-102

[28] Feng, P., and Q.Sun, *"Experimental investigation on macroscopic domain formation and evolution in polycrystalline NiTi microtubing under mechanical force"*, Journal of the Mechanics and Physics of Solids, vol 54, No. 8, 2010 pp. 1568-1603.

[29] Zhang, X., Feng, P., He, Y., T.You, and Q.Sun, *"Experimental study on rate dependence of macroscopic domain and stress hysteresis in NiTi shape memory alloy strips"*, International Journal of Mechanical Sciences, vol 52, No 12, 2010 pp. 1660-670.

[30] Matsui, R., Tobushi H., and Ikawa T., *"Transformation-induced creep and stress relaxation of TiNi shape memory alloy"*, Proceedings of the Institution

of Mechanical Engineers, Part L: Journal of Materials Design and Applications, vol. 213, No. 2, 2004 pp. 343-353

[31] Takeda, K., Matsui, R.,Tobushi, H., and Pieczyska, E. A., *"Transformation-Induced Relaxation and Stress Recovery of TiNi Shape Memory Alloy"*, Materials, vol 7, 2014 pp. 1912-1926

[32] Lagoudas., D. C., *"Shape memory alloys: modeling and engineering applications"*, 1st ed. New York, Springer, 2010.

[33] Maraldi, M, Molari, L and Grandi D., *"A non-isothermal phase-field model for shape memory alloys:Numerical simulations of superelasticity and shape memory effect under stress-controlled conditions"*, Intelligent Materials Systems and Structures vol 23,No. 10 2012 pp. 1083-092.

[34] Brinson, L.C., Bekker. A., and Hwang S., *"Deformation of shape memory alloys due to thermo-induced transformation"*, Journal of intelligent material systems and structures, vol 7, No. 1, pp. 97-107.

[35] Liang, C., Rogers. C. A.,*"One dimensional thermomechanical constitutive relations for shape memory materials"*, Journal of intelligent materials systems and structures, vol 8, 1997 pp. 285-302.

[36] Lagoudas, D.C., Ravi-Chandar K.,Sarh K., and Popov, P., *"Dynamic loading of polycrystalline shape memory alloys rod"*, Mechanics and Materials vol 35,2003 pp. 423-9.

[37] Takeda, K., Matsui, R.,Tobushi, H., and Pieczyska, E. A., *"Creep and creep recovery under stress-controlled subloop loading in TiNi shape memory alloy"*, Arch. Mech., vol 65, No. 5, 2013 pp. 429444

[38] Guo, W., Steinbach, I., Somsen, C.,Eggeler,G., *"On the effect of superimposed external stresses on the nucleation and growth of Ni_4Ti_3 particles: A parametric phase field study"*, Acta Materialia, vol 59, 2011 pp. 3287-3296.

[39] Efstathiou., C, Sehitoglu., H *"Local transformation strain measurement in precipitated NiTi single crystal"*, Scripta Materialia, vol 59, 2008 pp. 1263-1266.

[40] Zhou, N., Shen,C.,Wagner,M.F.-X.,Eggeler, G., Mills,M.J., and Wang,Y., *"Effect of Ni_4Ti_3 precipitation on martensitic transformation in Ti-Ni "*, Acta Materialia, vol 58, 2010 pp. 6685-6694.

[41] Evirgen,A., Karaman,I., Noebe R.D., Santamarta.R.,and Pons J., *"Effect of precipitation on the microstructure and the shape memory response of the* $Ni_{50.3}Ti_{29.7}Zr_{20}$", $ScriptaMaterialia, vol69, 2013pp.354 - 357$.

[42] Karaca,H.E.,Saghaian,S.M.,Ded,G.,Tobe,H.,Basaran,B.,Maier,H.J.,Noebe,R.D., and Chumlyakov,Y.I., *"Effect of nanoprecipitation on the shape memory and material properties of an Ni-rich NiTiHf high temperature shape memory alloy"*, Scripta Materialia, vol 69, 2013 pp. 354-357.

[43] Santamarta,R., Arroyave,R., Pons J., Evirgen, A.,Karaman I.,Karaca,H.E., Noebe R.D., *"TEM study of structural and microstructural characteristics of a precipitate phase in Ni-rich Ni-Ti-Hf and Ni-Ti-Zr shape memory alloys"*, Acta Materialia, vol 61, 2013 pp. 6191-6206.

[44] Evirgen,A.,Basner,F.,Karaman,I.,Noebe,R.,Pons,J.,Santamarta,R., *"Effect of aging on the martensitic transformation characteristics of A Ni-rich NiTiHf High temperature shape memory alloys"*, Functional Materials letters, vol 5, No. 4 2013 pp. 1250038.

[45] Piotrowski,B., Zineb,T.B.,Patoor,E.,Eberhardtl,A., *"Modeling of niobium precipitates effect on the $Ni_{47}Ti_{44}Zr_9$"*, International Journal of Plasticity, vol 36, 2012 pp. 130-147.

[46] Khalil-Allafi, J., Dlouhy, A., Eggeler,G., *"Ni_4Ti_3 precipitation and its influence on martensitic phase transformations"*, Acta materialia, vol 50, 2002 pp. 4255-4274.

[47] Birman, V., *" Review of mechanics of shape memory alloy structures"*, Applied Mechanics Reviews, vol 50, No. 11, 1997 pp. 645.

[48] . Lagoudas, D.C., Entchev, P.B., Popov, P., Patoor, E., Brinson, L.C., and Gao, X., *" Shape memory alloys Part II: Modeling of polycrystals"*, Mechanics of Materials, vol 38, 2006 pp. 430-462

[49] Patoor, E., Lagoudas, D.C., Entchev, P., Brinson, L.C., and Gao, X., *" Shape memory alloys - Part I: General properties and modeling of single crystals"*, Mechanics of Materials vol 38, No. 5, 2006 pp. 391-429.

[50] Paiva, A., Savi, M. A., *" An overview of constitutive models for shape memory alloys"*, Mathematical Problems in Engineering, 2006 pp. 10.

[51] Bertram, A., *"Thermo-mechanical constitutive equations for the description of shape memory effects in alloys"*, Nuclear Engineering and Design vol 74,1982.

[52] Tanaka, K., *"A thermomechanical sketch of shape memory effect: one-dimensional tensile behavior"*, Res Mechanica vol 18, 1986 pp. 251-63.

[53] Tanaka, K., Kobayashi, S., Sato, Y., *"Thermomechanics of transformation pseudoelasticity and shape memory effect in alloys"*, International Journal of Plasticity vol 2, pp. 59-62.

[54] Boyd, J., Lagoudas, D.C., *"A thermodynamical constitutive model for shape memory materials. Part I: The monolithic shape memory alloy"*, International Journal of plasticity, vol 12, No. 6, 1996 pp. 805-42

[55] Lagoudas, D.C., Bo, Z., Qidwai, M.A., *"A unified thermodynamic constitutive model for SMA and finite element analysis of active metal matrix composites"*, Mechanics of Composite Materials and Structures vol 3, No. 2, pp. 153-79.

[56] Auricchio, F., Petrini, L., *"A three-dimensional model describing stress-temperature induced solid phase transformations: stress-temperature induced solid phase transformations: thermomechanical coupling and hybrid composite applications"*, International Journal for Numerical Methods in Engineering vol 61, 2004 pp. 716-37.

[57] Auricchio, F., Sacco, E.,*"A one-dimensional model for superelastic shape-memory alloys with different elastic properties between austenite and martensite"*, International Journal of Non-Linear Mechanics vol 32, No. 6, 1997 pp. 1101-114

[58] Qidwai, M.A., Lagoudas, D.C., *"On thermomechanics and transformation surfaces of polycrystalline NiTi shape memory alloy material"*, International Journal of Plasticity 16, 2000b pp. 1309-343.

[59] Rajagopal, K.R., Srinivasa, A.R., *"Mechanics of the inelastic behavior of materials. Part I: Theoretical underpinnings"*, International Journal of Plasticity vol 14, No. 10-1, 1998a pp. 945-67.

[60] Rajagopal, K.R., Srinivasa, A.R., *"Mechanics of the inelastic behavior of materials. Part II: Inelastic response"*, International Journal of Plasticity vol 14,No. 10-1, 1998b pp. 969-95.

[61] Savi, M.A., Paiva, A., Baeta-Neves, A.P., Pacheco, P.M.C.L., *"Phenomenological modeling and numerical simulation of shape memory alloys: a thermoplastic-phase transformation coupled model"*, Journal of Intelligent Material Systems and Structures, vol 13, 2002 pp. 261-73.

[62] Popov, P., Lagoudas, D.C., *"A 3-D constitutive model for shape memory alloys incorporating pseudoelasticity and detwinning of self-accommodated martensite"*, International Journal of Plasticity vol 23, No. 10, 2007 pp. 1679-720.

[63] Ziolkowski, A., *"Three-dimensional phenomenological thermodynamic model of pseudoelasticity of shape memory alloys at finite strains"*, Continuum Mechanics and Thermodynamics, vol 19, 2007 pp. 379-98.

[64] Christ, D., Reese, S., *"A finite element model for shape memory alloys considering thermomechanical couplings at large strains"*, International Journal of Solids and Structures, vol 46, No. 20, 2009 pp. 3694-709.

[65] Chemisky, Y., Duval, A., Patoor, E., Zineb, T.B., *"Chemisky, Y., Duval, A., Patoor, E., Zineb, T.B., 2011. Constitutive model for shape memory alloys including phase transformation, martensitic reorientation and twins accommodation"*, Mechanics of Materials vol 43, No. 7,2011 pp. 361-76.

[66] Hackl, K., Heinen, R., Schmahl, W., and Hasan, M., *" Experimental verification of a micromechanical model for polycrystalline shape memory alloys in dependence of martensite orientation distributions"*, Materials Science and Engineering A, vol 481, No. 82, 2008 pp. 347-350

[67] Levitas, V.I., Ozsoy, I.B., *"Micromechanical modeling of stress-induced phase transformations. Part 1. Thermodynamics and kinetics of coupled interface*

propagation and reorientation", International Journal of Plasticity, vol 25, No. 2, 2009a pp. 239-80.

[68] Levitas, V.I., Ozsoy, I.B., *"Micromechanical modeling of stress-induced phase transformations. Part 2. Computational algorithms and examples"*, International Journal of Plasticity, vol 25, No. 3,2009b pp. 546-83.

[69] Petryk, H., Stupkiewicz, S., *" Interfacial energy and dissipation in martensitic phase transformations. Part I: Theory"*, Journal of the Mechanics and Physics of Solids, vol 58 No. 3, 2010 pp. 390-08.

[70] Petryk, H., Stupkiewicz, S., Maciejewski, G., *"Interfacial energy and dissipation in martensitic phase transformations. Part II: Size effects in pseudoelasticity"*, Journal of the Mechanics and Physics of Solids vol 58, No. 3, 373-89.

[71] Abeyaratne, R., and Knowles, J., *"Kinetic relations and the propagation of phase boundaries in solids"*, Archive for rational mechanics and analysis, vol 114, No. 2, pp. 119-54.

[72] Abeyaratne, R., Knowles, J.K.A., *"A continuum model of a thermoelastic solid capable of under- going phase transitions"*, Journal of the Mechanics and Physics of Solids vol 41, 1993 pp. 541-571.

[73] Bruno, O.P., Leo, P.H.,Reitich F., *"Free Boundary Conditions at Austenite-Martensite Interfaces"*, Phys Rev Lett. vol 74, 1995 pp.746-49.

[74] Stoilov, V., Bhattacharyya, A., *" A theoretical framework of one-dimensional sharp phase fronts in shape memory alloys"*, Acta Materialia vol 50, 2002 pp. 4939-952

[75] Jaeger, S., Eggeler, G., and Kastner., O.,*"Modeling thermally induced martensitic transformations in nickel titanium shape memory alloys"*, Continuum Mech. Thermodyn, ,2015 pp.461-481

[76] Rosakis, P., Knowles, J. K.,*"Unstable kinetic relations and the dynamics of solid-solid phase transitions"*, Journal of the Mechanics and Physics of Solids, vol. 45, No. 11, pp. 2055-2081.

[77] Chen, L. Q., *"Phase-fied models for microstructure evolution"*, Annu.Rev.Mater. Res vol 32, 2002 pp. 113-40.

[78] Emmerich .H., *"Advances of and by phase-field modelling in condensed-matter physics"*, Advances in physics, vol 57, No. 1, 2008 pp. 1-87.

[79] Falk, F., *"Model free energy, mechanics, and thermodynamics of shape memory alloys."*, Acta Metallurgica vol 28,No. 12 1980 pp. 1773-1780.

[80] Falk, F., *"Ginzburg-Landau theory of static domain walls in shape-memory alloys."*, Zeitschrift fr Physik B Condensed Matter vol 51,No.2 1983 pp. 177-185.

[81] Falk, F., and Konopka, P., *"Three-dimensional Landau theory describing the martensitic phase transformation of shape-memory alloys"*, Journal of Physics: Condensed Matter vol 2,No.1 1990 pp. 61

[82] Barsch, G. R., and Krumhansl, J. A. *"Twin boundaries in ferroelastic media without interface dislocations"*, Physical Review Letters vol 53,No.11 1984 pp. 1069.

[83] Barsch, G. R., and Krumhansl, J. A. *"Nonlinear and nonlocal continuum model of transformation precursors in martensites."*, Metallurgical Transactions A vol 19,No.4 1988 pp. 761-775

[84] Mamivand, M., Zaeem, M., and Kadiri, H. E., *"A review on phase field modeling of martensitic phase transformation"*, Computational Materials Science, vol 77, No. 2,2013 pp. 304-11.

[85] Abeyaratne, R., Knowles, J.K., *"On the driving traction acting on a surface of strain discontinuity in a continuum"*, J. Mech. Phys. Solids vol 38, 1990 pp. 345-60.

[86] Ericksen, J., *"Equilibrium of bars"*,Journal of elasticity vol 5, No. 3, 1989 pp. 191-201.

[87] Bhattacharya, K., *"Comparison of the geometrically nonlinear and linear theories of martensitic transformation"*, Continuum Mechanics and Thermodynamics, vol 5, No. 3, 1993 pp. 205-42.

[88] Bhattacharya, K., and Kohn, R., *"Symmetry, texture and the recoverable strain of shape-memory polycrystals"*, Acta materialia, vol 44, No. 2, 1996 pp. 529-42.

[89] Bhattacharya, K., and James, R., *"A theory of thin films of martensitic materials with applications to microactuators"*, Journal of the Mechanics and Physics of Solids, vol 47, No. 3, 1999.pp. 531-76.

[90] Shaw, J., *"Simulations of localized thermomechanical behavior in a NiTi shape memory alloy"*, International Journal of Plasticity, vol 16, No. 5, 2000 pp. 541 -562.

[91] Chang, B., Shaw, J., and Iadicola, M., *"Thermodynamics of shape memory alloy wire: modeling, experiments, and application"*, Continuum Mechanics and Thermodynamics, vol 18, No. 1, 2006

[92] He, Y., and Sun, Q., *"Effects of structural and material length scales on stress-induced martensite macrodomain patterns in tube configurations"*, International Journal of Solids and Structures, 2009 46(16), pp. 3045-060.

[93] Berti, V., Fabrizio, M., and Grandi, D., *"Hysteresis and phase transitions for one-dimensional and three dimensional models in shape memory alloys"*, Journal of Mathematical Physics, vol 51, No. 6, 2010 pp. 062901.

[94] Berti, V., Fabrizio, M., and Grandi, D.,*"Phase transitions in shape memory alloys: A non-isothermal ginzburg-landau model"*, Physica D: Nonlinear Phenomena, vol 239, No 1, 2010. pp. 95-02.

[95] Grandi. D., Maraldi, M., and Molari, L., *"A macroscale phase-field model for shape memory alloys with non-isothermal effects: Influence of strain rate and environmental conditions on the mechanical response"*. Acta Materialia, vol 60, No. 1, 2012 pp. 179-91.

[96] Peach, M. O., Koehler *"The forces exerted on dislocations and the stress fields produced by them "*, Physical Review, Vol 80,1951, pp.436-439

[97] Herring. C., *"In The Physics of Powder Metallurgy "*, (ed. W. E. Kingston),1951, McGraw-Hill, New York.

[98] Eshelby, J. D., *"The force on an elastic singularity"*, Philosophical Transactions of the Royal Society of London A: Mathematical, Physical and Engineering Sciences, Vol 244,No. 877,1951, pp 87-112.

[99] Eshelby, J. D., *"In Inelastic Behavior of Solids"*, (eds. M. F. Kanninen, W. F. Alder, A. R. Rosenfield, R. I. Jaffe), 1970,McGraw-Hill, New York.

[100] Eshelby, J. D., *"The elastic energy-momentum tensor"*, Journal of Elasticity, Vol 5, No. 3-4, 1975, pp. 321-335

[101] Gurtin, M. E.,and Struthers, A. *"Multiphase thermomechanics with interfacial structure"*, Physical Review, Vol 112, No. 2., pp.97-160

[102] Gurtin, M., Configurational forces as basic concepts of continuum physics. 2000 Springer.

[103] Gurtin, M.E., *"An introduction to continuum mechanics"*., Mathematics in science and engineering, vol. 158,2003

[104] Gurtin, M.E., Fried, E., and Anand, L., *"The mechanics and thermodynamics of continua"*.,Cambridge University Press, 2010.

[105] Otsuka, K., Ren, X.,*"'Physical metallurgy of TiNi-based shape memory alloys"*, Progress in materials science, vol 50, No. 5,2005 pp. 511-678.

[106] Hu, S. Y., Chen, L. Q.,ı"A phase-field model for evolving microstructures with strong elastic inhomogeneity", Acta materialia, vol. 49, No.11, 2001, pp. 1879-1890.

[107] Jou, H. J., Leo, P. H., Lowengrub, J. S., *"Microstructural evolution in inhomogeneous elastic media"*, Journal of Computational Physics, vol. 131, No.1,(1997),pp. 109-148.

[108] Agboola, B. O., Baxevanis, T., and Lagoudas, D. C.,*"Thermodynamically Consistent Thermomechanical Modeling of Kinetics of Macroscopic Phase Transi-*

tion in SMA Using Phase Field Theory", In ASME Conference on Smart Materials, Adaptive Structures and Intelligent Systems, 2014, pp. V002T02A008-V002T02A008

[109] Agboola, B. O., Lagoudas, D. C.,*"Modeling Rate Dependent Response of Shape Memory Alloys Using a Thermo-Mechanical Continuum Phase Field Approach."*, In 56th AIAA/ASCE/AHS/ASC Structures, Structural Dynamics, and Materials Conference, AIAA Scitech,2015,doi:10.2514/6.2015-1118

[110] Russalian, V.R., and Bhattacharyya A., *"Strain arrest during isothermal uniaxial deformations of nickel-titanium shape memory alloys and rate independent phase diagrams"*, Material science and Technology, vol 20, No. 4, 2013 pp. 400-411.

[111] Lohan, N.M., Pricop, B., Paraschiv, A.L., Suru , M.G., Bujoreanu, L,G .,*"Cooling rate effects on the structure and transformation behavior of Cu-Zn-Al shape memory alloys subjected to differential scanning calorimetry analysis"*, Proceedings of International Conference on Shape Memory and Superelastic Technologies, 2013 pp. 21-22

[112] Lohan, N.M., et al .,*"Heating rate effects on reverse martensitic transformation in a Cu-Zn-Al shape memory alloy"*, lnt.J. Mat. Res., vol 102, No.11, 2011 pp. 1345-1351

[113] Loh, C.S., Yokoi, H., and Aral., T.,*"Natural heat-sinking control method for high-speed actuation of the sma"*, International Journal of Advanced Robotic Systems, vol 3, 2006 pp. 303-312

[114] Chang, S.H., Wu, S.K., *"Effect of cooling rate on transformation temperature measurements of Ti50Ni50 alloy by differential scanning calorimetry and*

dynamic mechanical analysis", Material Characterization, vol 59, 2008 pp. 987-990

[115] Wang, Z.G., Zu, X.T., and Huo., Y.,*"Effect of heating/cooling rate on the transformation temperatures in TiNiCu shape memory alloys"*, Thermochimica Acta 436, 2005 pp. 153-155

[116] Nurveren, K., Akdogan, A., and Huang., W.M.,*"Evolution of transformation characteristics with heating/cooling rate in niti shape memory alloys"*, Journal of materials processing technology, vol 196, 2008 pp. 129-134

[117] Zheng, Y., Cui. L., and Schooten, J.,*"Temperature memory effect of a nickel-titanium shape memory alloy "*, Applied physics Letter, vol 84, 2004 pp. 1-31.

[118] Huang, W. M.,*"Transformation front in shape memory alloy"*, Material Science and Engineering A, vol 392, 2005 pp. 121.

[119] Kurita, T., Matsumoto. H., and Abe, H.,*"Transformation behavior in rolled NiTi "*, J. Alloys Compd, vol 381, 2004 pp. 158-161.

[120] Kurita, T., Matsumoto. H., Sakamoto. H., and Abe, H.,*"Transformation behavior of shock-compressed* $Ni_{48}Ti_{52}$", $J.AlloysCompd, vol400, No.1, pp92-95$.

[121] Liu, Y., Yang. H., Voigt. A.,*"Thermal Analysis of the effect of aging on the transformation behavior of Ti 50.9 at.Ni"*, Material Science and Engineering A, vol 360, 2003 pp. 350

[122] Chrobak, D., Stroz. D., Morawiec. H.,*"Effect of early stages of precipitation and recovery on the multi-step transformation in deformed and annealed near-equiatomic TiNi alloy"*, Scripta Materialia, vol 48, No. 5, 2003 pp. 571

[123] Otsuka, K., Wayman. C.M.,*"Shape Memory Materials"*, Cambridge University Press

[124] Reynaerts, D., Van Brussel. H.,*"Development of a SMA high Performance robotic a"*, In: proceeding of the IEEE conference on advanced robotics, vol 1, 1991 pp.61-66

[125] Bergamasco, M., Salsedo. F., and Dario, P.,*"A linear SMA motor as direct-drive robotic actuator,"*, In: proceeding of the IEEE conference on robotics and automation, vol 1, pp.618-623

[126] Russell, R.A., Gobert, R.B.,*"Improving the response of SMA actuators"*, In: proceeding of the IEEE conference on robotics and automation, vol 3, 1995 pp.2299-2304

[127] Lohan, N.M., et al .,*"Influence of temperature variation rate on calorimetric response during heating and on martensite strusture obtained after subsequent cooling of Cu-Zn-Al shape memory alloy"*, Micro Nano Letters, vol 7, 2012 pp. 540-543

[128] Howe, R.D., Kontarinis, D.A., and Peine, W.J.,*"Shape memory alloy actuator controller design for tactile displays"*, In: proceeding of the IEEE conference on decision and control, vol 4, 1995 pp.3540-3544

APPENDIX

In order to calibrate the free energy to experimental material parameters so that a double well potential that represents stability of austenite and martensite under condition for stress and temperature, the following criterions were imposed on the free energy. The criterions also placed restrictions on the admissible polynomials and are described below

$$G(\eta = 0) = G^{Austenite} \equiv G^{A}, \tag{6.1}$$

$$G(\eta = 1) = G^{Martensite} \equiv G^{M}, \tag{6.2}$$

$$\frac{\partial G}{\partial \eta}(\eta = 0) = 0, \tag{6.3}$$

$$\frac{\partial G}{\partial \eta}(\eta = 1) = 0, \tag{6.4}$$

$$\frac{\partial^2 G}{\partial \eta^2}(\eta = 0) \leq 0, \tag{6.5}$$

$$\frac{\partial^2 G}{\partial \eta^2}(\eta = 1) \leq 0, \tag{6.6}$$

Each of the criterion is to ensure that the free energy is a double well potential with wells at $\eta = 0$ and $\eta = 1$ and that at each state of temperature and stress only a well is minimum and therefore corresponding phase is thermodynamically stable. These criterion will be used to calibrate the free energy to the stress-temperature phase diagram to ensure that forward and reverse transformation behavior are captured for given stress and temperature state and history.

Now, the criteria $G(\eta = 0) = G^{Austenite}$ and $G(\eta = 1) = G^{Martensite}$ implies that the choice of polynomials in the free energy must satisfy the criteria that when $\eta = 0$ they are also zero and when $\eta = 1$, they are also one so that an interpolation between the

free energy of martensite and austenite is ensured. Secondly, the conditions $\frac{\partial G}{\partial \eta}(\eta = 0) = 0$, $\frac{\partial G}{\partial \eta}(\eta = 1) = 0$, $\frac{\partial^2 G}{\partial \eta^2}(\eta = 0) \leq 0$ and $\frac{\partial^2 G}{\partial \eta^2}(\eta = 1) \leq 0$, which represents the stability and instability criteria of the free energy, must be at least twice differentiable with wells and extremum corresponding to the value of $\eta = 0$ and $\eta = 1$. Therefore, $\frac{\partial^2 G}{\partial \eta^2} \geq 0$ correspond to stability condition to ensure a minimum energy for the two values of η. The polynomials in Chapter were selected with these criteria. Some reduction and additions were made to the generic form of the polynomials in order to have a consistent model. Mathematically,

$$G(\eta = 0) = G^A \Rightarrow f(0) = 0, \kappa(0) = 0, m(0) = 0, a(0) = 0, b(0) = 0, \gamma(0) = 0, \quad (6.7)$$

$$G(\eta = 1) = G^M \Rightarrow f(1) = 1, \kappa(1) = 1, m(1) = 1, a(1) = 1, b(1) = 1, \gamma(1) = 1, \quad (6.8)$$

$$\frac{\partial G}{\partial \eta}(\eta = 0) = 0 \Rightarrow \frac{\partial f}{\partial \eta} = 0, \frac{\partial \kappa}{\partial \eta} = 0, \frac{\partial m}{\partial \eta} = 0, \frac{\partial a}{\partial \eta} = 0, \frac{\partial b}{\partial \eta} = 0, \frac{\partial \gamma}{\partial \eta} = 0, \quad (6.9)$$

$$\frac{\partial G}{\partial \eta}(\eta = 1) = 0 \Rightarrow \frac{\partial f}{\partial \eta} = 0, \frac{\partial \kappa}{\partial \eta} = 0, \frac{\partial m}{\partial \eta} = 0, \frac{\partial a}{\partial \eta} = 0, \frac{\partial b}{\partial \eta} = 0, \frac{\partial \gamma}{\partial \eta} = 0, \quad (6.10)$$

represent the conditions for thermodynamic equilibrium and extremum values of the free energy, which the polynomials have to satisfy. The important set of equation that fall out of this conditions are

$$m_0 + m_1 + m_2 + m_3 = 1 \quad (6.11)$$

$$f_0 + f_1 + f_2 = 1 \quad (6.12)$$

$$\kappa_0 + \kappa_1 + \kappa_2 = 1 \quad (6.13)$$

$$2a_0 + a_1 + a_2 = 1 \quad (6.14)$$

$$b_0 + b_1 + b_2 = 1 \quad (6.15)$$

$$\gamma_0 + \gamma_1 = 1. \quad (6.16)$$

Now, the first derivatives of the polynomials w.r.t to η are

$$m^{'} = 2m_0\eta + 3m_1\eta^2 + 4m_2\eta^3 + 5m_3\eta^4, \tag{6.17}$$

$$f^{'} = 2f_0\eta + 3f_1\eta^2 + 4f_2\eta^3, \tag{6.18}$$

$$\kappa^{'} = 2\kappa_0\eta + 3\kappa_1\eta^2 + 4\kappa_2\eta^3, \tag{6.19}$$

$$a^{'} = 2a_0\eta + 3a_1\eta^2 + 4a_2\eta^3, \tag{6.20}$$

$$b^{'} = 2b_0\eta + 3b_1\eta^2 + 4b_2\eta^3, \tag{6.21}$$

$$\gamma^{'} = 2\gamma_0\eta + 3\gamma_1\eta^2 + \gamma_2\eta^3. \tag{6.22}$$

where $()^{'}$ and $()^{''}$ in this appendix represent the first and second derivatives with respect to *eta* respectively. Also, the important set of equation that result from this conditions are

$$2m_0 + 3m_1 + 4m_2 + 5m_3 = 0 \tag{6.23}$$

$$2f_0 + 3f_1 + 4f_2 = 0 \tag{6.24}$$

$$2\kappa_0 + 3\kappa_1 + 4\kappa_2 = 0 \tag{6.25}$$

$$2a_0 + 3a_1 + 4a_2 = 0 \tag{6.26}$$

$$2b_0 + 3b_1 + 4b_2 = 0 \tag{6.27}$$

$$2\gamma_0 + 3\gamma_1 + \gamma_2 = 0. \tag{6.28}$$

Similarly, the second derivatives are

$$m^{''} = 2m_0 + 6m_1\eta + 12m_2\eta^2 + 20m_3\eta^3, \tag{6.29}$$

$$f^{''} = 2f_0 + 6f_1\eta + 12f_2\eta^2, \tag{6.30}$$

$$\kappa^{''} = 2\kappa_0 + 6\kappa_1\eta + 12\kappa_2\eta^2, \tag{6.31}$$

$$a^{''} = 2a_0 + 6a_1\eta + 12a_2\eta^2, \tag{6.32}$$

$$b^{''} = 2b_0 + 6b_1\eta + 12b_2\eta^2, \tag{6.33}$$

$$\gamma^{''} = 2\gamma_0 + 6\gamma_1\eta. \tag{6.34}$$

Furthermore, Austenite (Martensite) is expected to be the stable phase at $T \succ A_s$ ($T \prec M_s$) for zero stress and M_s^σ corresponding to different stress level. Ignoring any difference in thermal expansion between austenite and martensite, the second derivative of the free energy w.r.t to η with conditions that at zero stress for $\eta = 0$ and $\eta = 1$ respectively, austenite (martensite at $M_s(A_s)$ instability should be met. The temperature expression for region of stability of martensite after assuming linear relationship is

$$T \leq \frac{g_0 T_0 - \Delta\epsilon_0\kappa_0}{g_0\Delta c - \Delta s_0 f_0}, \tag{6.35}$$

which implies that

$$M_s = \frac{g_0 T_0 - \Delta\epsilon_0\kappa_0}{g_0\Delta c - \Delta s_0 f_0} \tag{6.36}$$

Now assuming that the heat capacity in austenite and martensite is the same,

$$M_s = \frac{\Delta\epsilon_0\kappa_0}{\Delta s_0 f_0}. \tag{6.37}$$

Similarly for stability of austenite

$$T \geq \frac{\Delta\epsilon_0(\kappa_0 + 3\kappa_1 + 6\kappa_2)}{-\left[(\Delta c(g_0 + 3g_1 + 6g_2) - \Delta s_0(f_0 + 3f_1 + 6f_2)\right]}. \tag{6.38}$$

Therefore

$$A_s = \frac{\Delta\epsilon_0(\kappa_0 + 3\kappa_1 + 6\kappa_2)}{-\left[(\Delta c(g_0 + 3g_1 + 6g_2) - \Delta s_0(f_0 + 3f_1 + 6f_2)\right]}. \tag{6.39}$$

Now assuming that heat capacity is constant between martensite and austenite,

$$A_s = \frac{\Delta\epsilon_0(\kappa_0 + 3\kappa_1 + 6\kappa_2)}{\Delta s_0(f_0 + 3f_1 + 6f_2)}. \tag{6.40}$$

So far the polynomial changes wells at M_s and A_s for stress $\sigma = 0$ under change in temperature. These are the conditions for forward and reverse transformations. However, at different stress level, the transformation start temperatures changes as represented by the Clausius Clapeyron parameters on the phase diagram. In order for the polynomials to change wells appropriately to represent these material conditions, the Clausius Clapeyron parameter expression w.r.t to the free energy parameters is derived by taking the second derivative of the free energy potential. Essentially

$$C_M = \frac{d\sigma}{dT} \tag{6.41}$$

for $\eta = 0$, and

$$C_A = \frac{d\sigma}{dT} \tag{6.42}$$

for $\eta = 1$ Now using the second derivative of the free energy w.r.t to η and ignoring quadratic or nonlinear expressions in axial stress and temperature, m_0 becomes necessarily zero. Now upon manipulation of the expression to make the axial stress the subject of the formula of the equation resulting based on the inequality $\frac{\partial^2 G}{\partial \eta^2}(\eta = 0) \leq 0$ impies that

$$\sigma \geq \frac{\rho\left[\Delta c g_0 T - \Delta c_0 g_0 T_0 - \Delta s_0 f_0 T + \Delta\epsilon_0\kappa_0\right]}{H\gamma_0 + b_0\Delta\alpha_t(T - T_0}. \tag{6.43}$$

Now,at the boundary between region of austenite stability ad isntability the stress is the equaliity of the above expression. Now assuming for simplicity that no change

in coefficient of thermal expansion and heat capacity between the two phases (i.e $\Delta\alpha_t = 0$ and $\Delta c = 0$)

$$\sigma = \frac{\rho\left[\Delta c g_0 T - \Delta c_0 g_0 T_0 - \Delta s_0 f_0 T + \Delta\epsilon_0\kappa_0\right]}{H\gamma_0}. \tag{6.44}$$

Now taking derivative of the above expression w.r.t to temperature, we can determine that

$$C_M = \frac{d\sigma}{dT} = \frac{-\rho\Delta s_0 f_0}{H\gamma_0}. \tag{6.45}$$

Similarly, by using $\frac{\partial^2 G}{\partial\eta^2}(\eta = 1) \leq 0$

$$C_A = \frac{d\sigma}{dT} = \frac{-\rho\Delta s_0(f_0 + 3f_1 + 6f_2)}{H(\gamma_0 + 3\gamma_1)}. \tag{6.46}$$

Now, with these conditions imposed on the free energy to capture the conditions of equilibrium of phases and onset of transformation by changing the wells of the polynomials, we have 17 equation in 17 unknowns that can be solved simultaneously to determine the expressions or values of the coefficient of the polynomials that will satisfy the condition of stability and instability required for phase equilibrium and transformations respectively. For the results presented in this work, since change in heat capacity and thermal expansion is assumed negligible, the set of equations reduces to 13 in 13 unknowns. The equations are summarized below (recall $m_0 = 0$)

$$m_1 + m_2 + m_3 = 1 \tag{6.47}$$

$$f_0 + f_1 + f_2 = 1 \tag{6.48}$$

$$\kappa_0 + \kappa_1 + \kappa_2 = 1 \tag{6.49}$$

$$\gamma_0 + \gamma_1 = 1 \tag{6.50}$$

$$3m_1 + 4m_2 + 5m_3 = 0 \tag{6.51}$$

$$2f_0 + 3f_1 + 4f_2 = 0 \tag{6.52}$$

$$2\kappa_0 + 3\kappa_1 + 4\kappa_2 = 0 \tag{6.53}$$

$$2\gamma_0 + 3\gamma_1 = 0 \tag{6.54}$$

$$M_s = \frac{\Delta\epsilon_0\kappa_0}{\Delta s_0 f_0} \tag{6.55}$$

$$A_s = \frac{\Delta\epsilon_0(\kappa_0 + 3\kappa_1 + 6\kappa_2)}{\Delta s_0(f_0 + 3f_1 + 6f_2)} \tag{6.56}$$

$$C_M = \frac{d\sigma}{dT} = \frac{-\rho\Delta s_0 f_0}{H\gamma_0} \tag{6.57}$$

$$C_A = \frac{d\sigma}{dT} = \frac{-\rho\Delta s_0(f_0 + 3f_1 + 6f_2)}{H(\gamma_0 + 3\gamma_1)}. \tag{6.58}$$

. In this case, which is reported and used for the simulations in this dissertation, the set of equation has 13 unknowns $m_1, m_2, m_3, f_0, f_1, f_2, \kappa_0, \kappa_1, \kappa_2, \gamma_0, \gamma_1, \Delta s_0, \Delta\epsilon_0$ with five material parameters A_s, M_s, C_M, C_A, H which are the austenite start temperature, martensite start temperature, Clausius Clapeyron parameters and the maximum transformation strain under uniaxial loading of SMA respectively. These set of equations are solved simultaneously to give the expressions for the unknowns as described in chapter 2